

# DEVELOPMENT AND EVALUATION OF NANOMATERIAL BASED TARGETED DRUG DELIVERY SYSTEM

## A THESIS

*Submitted in partial fulfilment of the  
requirements for the award of the degree*

*of*

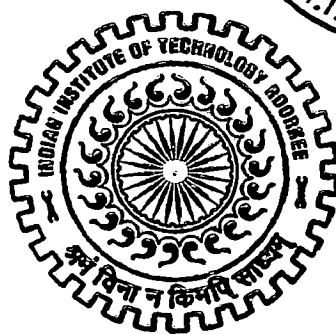
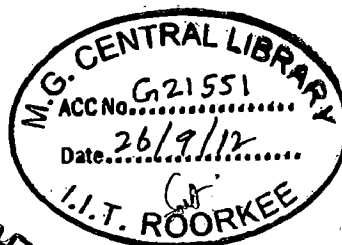
DOCTOR OF PHILOSOPHY

*in*

CHEMISTRY

*by*

**SAURABH SAHU**



DEPARTMENT OF CHEMISTRY  
INDIAN INSTITUTE OF TECHNOLOGY ROORKEE  
ROORKEE-247 667 (INDIA)

DECEMBER, 2011

**©INDIAN INSTITUTE OF TECHNOLOGY ROORKEE, ROORKEE-2011**

**ALL RIGHTS RESERVED**



# INDIAN INSTITUTE OF TECHNOLOGY ROORKEE ROORKEE

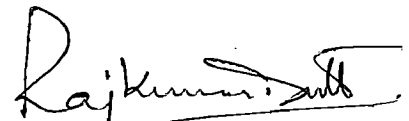
## CANDIDATE'S DECLARATION

I hereby certify that the work which is being presented in the thesis entitled '**Development and evaluation of nanomaterial based targeted drug delivery system**' in partial fulfilment of the requirements for the award of the degree of Doctor of Philosophy and submitted in the Department of Chemistry of the Indian Institute of Technology Roorkee, Roorkee is an authentic record of my own work carried out during a period from July 2007 to December 2011 under the supervision of Dr. Raj Kumar Dutta, Assistant Professor, Department of Chemistry, Indian Institute of Technology Roorkee, Roorkee.

The matter presented in the thesis has not been submitted by me for the award of any other degree of this or any other Institute.

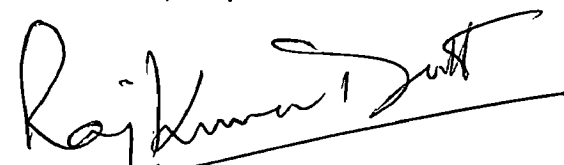
  
(Saurabh Sahu)

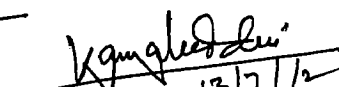
This is to certify that the above statement made by the candidate is correct to the best of my knowledge.

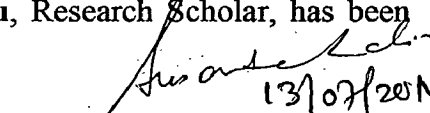
  
(R. K. Dutta)  
Supervisor

Date: 13.12.2011

The Ph.D. Viva-Voice Examination of Mr. Saurabh Sahu, Research Scholar, has been held on 13/07/12.

  
Signature of Supervisor

  
Chairman, SRC

  
13/07/2011  
Professor Susanta Lahiri  
Chemical Sciences Division  
Saha Institute of Nuclear Physics  
1/AF, Bidhannagar, Kolkata - 700 064

External Examiner

  
13-5-12  
Head of Department / Chariman ODC

## ACKNOWLEDGEMENTS

At the outset, I wish to express my deepest sense of gratitude and reverence to my mentor and supervisor Dr. R. K. Dutta for introducing me to this present area of research. His invaluable and meticulous guidance with lots of constructive criticisms have served as a vital source of inspiration for bringing the present work in the final shape. His affectionate treatment and magnanimity made it feasible to bring the present work to conclusion.

I take this opportunity to express my sincere thanks to Prof. V.K. Gupta, present Head of the Department and also to Prof. Kamaluddin and Prof. Ravi Bhushan, previous Heads of the Department, Chemistry for extending all the necessary research facilities. I'd like to thank my Research Committee members Prof. Kamaluddin, Dr. P. Jevanandum and Dr. K. L. Yadav for taking time out of their schedules to advise me on my dissertation. I feel privileged to express unfeigned thanks to Dr. Anil Kumar Head, Centre for Nanotechnology for extending the centre's research facilities. I am also thankful to the staff of the Department of Chemistry for providing countless assistance over these years. Thanks are also to Mr. Abdul Haq, Mr. Madanpal for their technical help. I express my sincere gratitude to Dr. Ramesh Chandra, Mr Sharma and Mr Saini of the Institute Instrumentation Centre of IIT Roorkee for their assistance in using experimental facility.

Further, I am extremely grateful to Dr. A. V. R. Reddy, Head, Analytical Chemistry Division, Bhabha Atomic Research Centre (BARC), Trombay, Mumbai for allowing us to perform instrumental neutron activation analysis. I would also like to extend special thanks to Dr. Ajay K. Gupta, Centre Director, UGC DAE- CSR Centre, Indore, for availing the facilities of the centre. I would like to extend my sincere thanks to Dr. V. Raghendra Reddy and Dr. T. Sripathi Scientist of the Centre, Indore, for helping me perform to Mössbauer and X-ray photoelectron spectroscopy respectively. Further, I express my sincere thanks to staff of ACTERC, Mumbai for conducting in vitro cytotoxicity studies.

It goes without saying that the contribution of friends matters a lot in according such arduous tasks. I express my sincere thanks and regards to my seniors especially Ramswaroop Maharia and Indu Singh for their kind help and motivation round the clock. I convey my heartfelt thanks to all my colleagues, especially, Manviri, Anjaneyulu, Ashok, Himanshu, Bhawani, Ambika, Swati, Mahesh, Debashish, Krishna Rao, Deepika and Aastha without whose uncompromising and relentless cooperation, this work would not have seen

the light of the day in its truest sense. In this chain, how can I forget the immense support from the most loveable friends Mehul, Vineet, Arun, Rahul and his wife Sarita.

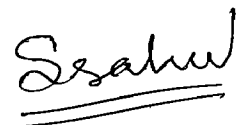
Further, I would like to thank the Almighty, without Him I could do nothing. I want to express my heartfelt gratitude to my parents for their endless love, blessings, support and for always being with me no matter what I also appreciate the love and support from sister, Ms. Sonali Sahu, my brother-in-law Mr. Vikram Sahu, my adorable nephew Divyam and niece Prasiddhi, and my son Shoubhagya who constantly inspired me to achieve this hallmark.

All the words not sum up the pain and hardship that my wife Samiksha, father Satish Kumar and mother Rekha Sahu had to face in my accent for this achievement. Their sacrifice and love has been the guiding principles of my life. Despite the agony and inconvenience, they provided me everything throughout my academics. Their unlimited faith and confidence has made me whatever I am today. Their blessings are the great kinetic force which always lighted my path towards success.

Last but not the least, Ministry of Human Resource and Development (MHRD), India is thankfully acknowledged for awarding fellowship.

IIT Roorkee

Date: 13-12-2011



(SAURABH SAHU)

## ABSTRACT

The advent of nanotechnology has led to exciting applications in various domains of science and technology, including rapid development in nanoscale materials towards developing targeted drug delivery system. Reduction in the sizes of the drug carriers to nanoscale dimension could overcome the biological barriers and can pass through the smallest capillary vessels which could improve in the efficacy and site specificity. As polysaccharides are conventionally used as matrices for carrying drugs, so polysaccharides based nanomaterials have attracted a lot of scientific attention in drug delivery system. In this regard, dextran, chitosan, alginate, starch, pectin etc. have been explored. These drug carriers of nanoscale dimension could be functionalized by various means, *e.g.*, attaching ligands for receptor mediated targeted drug delivery, or by incorporating magnetic materials, *e.g.*, superparamagnetic iron oxide nanoparticles (SPIONs) for guided drug delivery. A few studies have been reported on coating MNPs with chitosan, dextran, polylactic co-glycolic acid (PLGA) and polyvinyl alcohol (PVA) which also facilitated loading of drugs. Among various iron oxide phases, it was noted that the magnetite nanoparticles (MNPs) of about 5–20 nm in diameter were suitable as they exhibit superparamagnetism, high saturation field, biocompatibility and non-cytotoxicity. The synthesized MNPs might require stabilizers to maintain colloidal stability as well as good aqueous dispersion.

In this project, we aimed at developing a novel magnetically responsive hybrid nanomaterial for potential targeted drug delivery system. It comprised of magnetite nanoparticles coated with pectin and were characterized by an array of techniques. Another batch of nanomaterial was synthesized by coating magnetite nanoparticles with pectin reinforced with chitosan and was characterized in similar manner. Here pectin and chitosan were chosen due to its biocompatibility, biodegradability and its low cost. We have evaluated the drug loading efficiencies of diclofenac sodium, 5-fluorouracil (5-FU), oxaliplatin (OHP) in these magnetite coated with polysaccharide nanomaterials. Further we have evaluated their *in vitro* release in different simulated conditions, at different pH. In addition, the cytotoxicity of 5-FU and oxaliplatin loaded nanomaterials were evaluated in various cancer cell lines like HT-29 (colon), HEPG2 (liver) and MIA-PA-CA-2 (pancreas).

The present study comprises six chapters and a brief discussion of each is as follows: In the **first chapter** we have introduced the concept of targeted drug delivery using nanotechnology. A thorough literature survey has been carried out to discuss the various types

of targeted drug delivery systems. We have mainly highlighted polysaccharide based nanomaterials for this purpose. Recent development on superparamagnetic iron oxide nanoparticles (SPIONs) incorporated in polysaccharide nanomaterials for targeted drug delivery is introduced. A detailed literature survey on methods of synthesis of SPIONs is presented. This is followed by aim and scope of the present work.

In **Chapter two**, we have described the experimental methodologies for the fabrication of hybrid nanomaterials of magnetite and pectin (MP) where pectin was cross linked with calcium ions. The formation of these hybrid nanomaterials were characterized by array of techniques. The fabrication conditions were optimized with respect to the concentration of pectin, calcium ions and experimental conditions, namely pH, time. The optimization was based on their morphology and magnetic properties. The magnetite phase was determined from X-ray diffraction (XRD) studies and was confirmed from  $^{57}\text{Fe}$  Mössbauer spectroscopy recorded at room temperature, and at 5 K with and without magnetic field. The average crystallite size was determined to be in the range of 2-8 nm from Debye-Scherrer formula using the most intense peak. Fourier transform infrared (FT-IR) spectroscopy and thermal analysis techniques like thermogravimetry and differential thermal analysis (TG-DTA) were used for interpreting the coating of pectin on magnetite nanoparticles (MNPs). The surface analysis of the pectin coated MNPs by X-ray photoelectron spectroscopy (XPS) studies revealed minimal concentration of Fe on the surface, which indicated that mostly MNPs were incorporated in the calcium pectinate nanomaterials. The morphology of the fabricated nanomaterials was studied by scanning electron microscopy (SEM) and transmission electron microscopy (TEM) and their sizes in dry condition were measured in the range of 100 - 150 nm. While in aqueous medium they were found to be in the range of 300 - 400 nm, as measured by dynamic light scattering (DLS). The increase in size in aqueous medium was attributed to swelling effect. The elemental analysis of the material was determined from energy dispersive X-ray analysis (EDAX) coupled to SEM and the concentration of MNPs was determined by estimating total Fe in the fabricated nanomaterials by instrumental neutron activation analysis (INAA). Zeta potential measurements were used for understanding the nature of interaction among MNPs, pectin, chitosan in the nanomaterials. The magnetic studies were carried out by using superparamagnetic quantum unit interference device (SQUID). The saturation magnetization of these hybrid nanomaterials was 46.21 emu/g, measured at room temperature and applied field of  $\pm 2.5$  T. The field cooled (FC)-zero field cooled (ZFC) measurement studied from

SQUID measurements confirmed superparamagnetic behavior of these materials. These results were corroborated by  $^{57}\text{Fe}$  Mössbauer spectroscopy studies.

In the **third chapter** we have discussed the method of fabricating a targeted drug delivery system by loading diclofenac sodium (DS) drug in magnetite-calcium pectinate nanomaterial. The fabricated system was characterized in the similar manner as mentioned in Chapter 2. Maximum drug loading efficiency was found in the batch fabricated with 1 % pectin solution (w/v). But this composition of pectin led to formation of viscous matrix. On the other hand, the batch prepared with 0.4 % pectin (w/v) resulted in spherical nanomaterials with  $60.6 \pm 1.4$  % encapsulation efficiency. The concentration of the drug loaded in these nanomaterials was found to be  $28.9 \pm 1.6$  % (w/w) on dry weight basis. These drug loaded spherical nanomaterials materials of 100 - 150 nm (in dry condition, as reflected from TEM and SEM studies) exhibited superparamagnetic property as evident from VSM ( $M_s=44.05$  emu/g at room temperature and  $\pm 10$  kOe) and SQUID ( $T_B = 75.4$  K at an applied field of 500 Oe). The *in vitro* release study of the MP-DS was carried out sequentially in simulated gastric, intestinal and colonic fluids by using specific enzymes and by maintaining the pH of the medium. There was negligible release of drug in gastric medium while 88 % of the drug was released rapidly in simulated intestinal fluid. The remaining drug was released in the colonic fluid. On the other hand the MP-DS showed sustained release in phosphate buffer at pH 7.4. The release profile agreed well with the Korsmeyer-Peppas model which satisfied the conditions for non-Fickian transport. This was attributed to swelling effect of calcium pectinate in the aqueous medium which resulted in diffusion based drug release.

In the **chapter four** we reported our studies on enhanced loading of the diclofenac sodium in pectin which was reinforced with chitosan where magnetite nanoparticles were incorporated (MPCh-DS). Notably, here pectin was not cross linked with  $\text{Ca}^{2+}$  ions but was reinforced with chitosan by electrostatic interaction. The methodology for fabrication of the MPCh-DS system was optimized by varying the chitosan concentration, where minimum concentration of chitosan was 0.025 %. The drug loading efficiency was more than 99 %. The formation of the nanomaterials MPCh-DS was confirmed from XRD, FT-IR, TG-DTA,  $^{57}\text{Fe}$  Mössbauer, TEM, SEM, DLS, zeta potential. The sizes of MPCh-DS were in the range of 100 – 150 nm in dry condition and in aqueous medium an average size of 350 nm was measured from SEM, TEM and DLS measurements. The magnetic measurements by VSM revealed a saturation magnetization of 34.40 emu/g (at room temperature and  $\pm 10$  kOe) and the superparamagnetic property was confirmed from SQUID measurement. The *in vitro*



release of the diclofenac sodium from MPCh-DS system was studied in simulated gastric, intestinal and colonic fluids at respective pH. The *in vitro* release study was also carried out in phosphate buffer solution at pH 7.4 to mimic the release of the drug in blood. Similar to the release pattern observed for MP-DS system in the previous chapter, the release of DS from MPCh-DS was negligible in gastric fluid while 68 % of the drug was released rapidly in simulated intestinal fluid. This was followed by 31.5 % drug release in the colonic fluid over a period of 55 h. Overall, 99 % of the drug was released in a sustained manner. Similar to the MP-DS system, the sustained release of drug was better in phosphate buffer (pH ~7.4) and the release profile agreed well the Korsmeyer-Peppas model, satisfying non-Fickian transport. Thus the release mechanism was attributed to swelling effect of pectin reinforced with chitosan in the aqueous medium. This system could be assumed to be suitable for delivering the drug at inflammatory regions, e.g. knee joints if administered intravenously where the drug can be release in a sustained manner over a longer period of time.

In the **chapter five** we have discussed the method of fabricating targeted drug delivery system with anticancer drug 5-FU loaded in magnetite calcium pectinate nanomaterials (MP-5FU). The drug loading efficiency was found to be  $29.8 \pm 3.3$  %. Similar to the previous chapters the fabrication of MP-5FU was confirmed from XRD, FT-IR, TEM, SEM, DLS and zeta potential studies. In aqueous medium, DLS measurement reflected an average size of ~ 300 nm which was attributable to swelling effect of the polymer. The saturation magnetization of these materials was 43.15 emu/g recorded by VSM at room temperature and  $\pm 10$  kOe. The superparamagnetism was confirmed from the FC-ZFC profile recorded from SQUID measurements. The *in vitro* release studies in simulated gastric condition showed 11.8 % release by weight. The release of 5-FU was ~ 40 % in simulated intestinal condition. It was followed by ~ 46 % release of drug in simulated colonic fluid. It accounted for a total release of ~ 98 % over a period of 48 h which exhibited sustained release of the drug in gastrointestinal conditions. Similar to MP-DS system, the *in vitro* release of 5-FU from MP-5FU showed better sustained release in phosphate buffer (pH ~7.4) over a period of 48 h and was in good agreement with swelling controlled drug release mechanisms as discussed in previous chapters. Further the cytotoxicity of the fabricated nanomaterials MP-5FU was studied on HT-29 (colon), HEPG2 (liver), MIA-PA-CA-2 (pancreas) cancer cell lines by SRB assay after 48 h. The % cell viability decreased with increase in the MP-5FU concentration (1-5 mg/mL). The cell viability of MP-5FU at 5 mg/mL was found to be  $60.9 \pm 3.3$  % for HT-29 and  $68.2 \pm 16.1$  % for HEPG2 cancer cell lines. Strikingly, the cell viability for 5 mg/mL

of MP-5FU in MIA-PA-CA-2 pancreatic cancer cell line was  $23.9 \pm 5.1$  % and the corresponding  $GI_{50}$  was 3.7 mg/mL. On the other hand, the  $GI_{50}$  of MP-5FU for HT and HEPG2 was more than 5 mg/mL. The magnetite-pectin system without 5-FU, did not indicate any antiproliferative effect. Therefore decrease in cell viability for MP-5FU was only due to release of the anticancer drug 5-FU from the nanomaterials. These results indicated the successful fabrication of magnetic nanomaterials of pectin for potential delivery of 5-FU.

In **chapter six** we have reported the fabrication of anticancer drug, oxaliplatin (OHP), loaded in the hybrid nanomaterials of magnetite-pectin and in magnetite-pectin reinforced with chitosan. The sizes of these nanomaterials were between 100 - 150 nm in dry condition, confirmed by SEM and TEM. In aqueous medium, DLS measurement reflected an average size of ~330 nm which was attributable to swelling effect of the polymer. The VSM studies revealed high saturation magnetization (45.65 emu/g) at room temperature and  $\pm 10$  kOe. The superparamagnetic property was characterized by SQUID magnetometry. The drug loading efficiency was calculated with respect to platinum (Pt) content by ICPMS, after calibrating the Pt contents in the known concentrations of the drug. The loading efficiencies were  $50.2 \pm 1.5$  % in MPCh-OHP and  $55.2 \pm 1.2$  % in MP-OHP. The *in vitro* release profile of oxaliplatin from MP-OHP in the phosphate buffer pH 5.5 and 7.4 indicated sustained release. On the other hand the release of OHP from MPCh-OHP was rapid. From this we concluded that MP-OHP was a better drug delivery system for sustained release of oxaliplatin and was further studied for its cytotoxicity in MIA-PA-CA-2 (pancreas) and HT-29 (colon) cancer cell line. The % cell viability decreased as the concentration of MP-OHP was increased from 1 mg/mL to 5 mg/mL. However, the  $GI_{50}$  value for MP-OHP in MIA-PA-CA-2 (pancreas) and HT-29 (colon) cancer cell lines was found to be above 5 mg/mL.

Finally we have summarized our work by highlighting the successful fabrication of a novel drug delivery system of nanoscale dimension with sustained release capability of different types of drugs namely DS, 5-FU and oxaliplatin. The additional magnetic property induced due to the presence of superparamagnetic magnetite nanoparticles has enhanced its functionality as a potential magnetically guided targeting ability. It may be interesting to study the *in vivo* applicability of these magnetite-pectin-drug nanomaterials materials for assessing their capacity for magnetically targeted drug delivery system.

# CONTENTS

|   |             |
|---|-------------|
| CANDIDATE'S DECLARATION   | i           |
| ACKNOWLEDGEMENTS  | iii         |
| ABSTRACT  | v           |
| LIST OF TABLES  | xi          |
| LIST OF FIGURES   | xiii        |
| ABBREVIATIONS   | xxiii       |
| <br>  |             |
| <b>CHAPTER - 1 INTRODUCTION: NANOMATERIALS BASED<br/>TARGETED DRUG DELIVERY</b> | <b>1-42</b> |
| 1.1 INTRODUCTION TO NANOSCALE MATERIALS   | 1           |
| 1.2 TYPES OF NANOMATERIALS  | 2           |
| 1.3 NANOMATERIALS FOR DRUG DELIVERY   | 3           |
| <i>1.3.1 Carbon nanotubes (CNTs)</i>  | 4           |
| <i>1.3.2 Nanodiamonds</i>   | 4           |
| <i>1.3.3 Nanoemulsions</i>  | 5           |
| <i>1.3.4 Micelles</i>   | 5           |
| <i>1.3.5 Liposomes</i>  | 6           |
| <i>1.3.6 Solid lipid nanoparticles (SLN)</i>                                    | 6           |
| <i>1.3.7 Dendrimers</i>   | 6           |
| <i>1.3.8 Metallic and metal oxide nanoparticles</i>                             | 7           |
| <i>1.3.9 Polymeric nanoparticles</i>  | 7           |
| 1.4 TARGETED DRUG DELIVERY  | 10          |
| <i>1.4.1 SPIONs for targeting</i>   | 11          |
| 1.5 AIM AND SCOPE   | 20          |
| REFERENCES  | 22          |

|                    |  |              |
|--------------------|--|--------------|
| <b>CHAPTER - 2</b> | <b>NOVEL HYBRID NANOMATERIALS OF<br/>MAGNETITE AND PECTIN</b>                                | <b>43-78</b> |
| 2.1                | INTRODUCTION   | 43           |
|                    | 2.1.1 Objective of the study   | 44           |
| 2.2                | MATERIALS AND METHODS  | 44           |
|                    | 2.2.1 <i>Materials</i>   | 44           |
|                    | 2.2.2 <i>Synthesis of MNPs</i>   | 45           |
|                    | 2.2.3 <i>Synthesis of hybrid nanomaterials of magnetite and<br/>pectin (MP)</i>              | 45           |
|                    | 2.2.4 <i>Characterization</i>  | 46           |
|                    | 2.2.5 <i>Stability of the as-synthesized MP in acidic conditions</i>                         | 49           |
| 2.3.               | RESULTS AND DISCUSSION   | 49           |
|                    | 2.3.1 <i>Optimization conditions and structural studies of<br/>MNPs</i>                      | 50           |
|                    | 2.3.2 <i><sup>57</sup>Fe Mössbauer spectroscopy studies of MNPs</i>                          | 51           |
|                    | 2.3.3 <i>Morphological studies of the MNPs</i>   | 52           |
|                    | 2.3.4 <i>Synthesis of MPs</i>  | 55           |
|                    | 2.3.5 <i>X ray diffraction studies of MPs</i>  | 58           |
|                    | 2.3.6 <i><sup>57</sup>Fe Mössbauer spectroscopy of MP-0.4</i>                                | 59           |
|                    | 2.3.7 <i>Morphological studies of MPs</i>  | 60           |
|                    | 2.3.8 <i>FT-IR analysis</i>  | 63           |
|                    | 2.3.9 <i>Thermal studies</i>   | 64           |
|                    | 2.3.10 <i>Analysis of MNP contents in MP-0.4</i>   | 65           |
|                    | 2.3.11 <i>Zeta potential measurement: Mechanism of the<br/>formation of MP nanomaterials</i> | 67           |
|                    | 2.3.12 <i>Magnetic properties of MP nanomaterials</i>  | 68           |
|                    | 2.3.13 <i>Stability of MP-0.4 in simulated gastric fluid</i>                                 | 70           |
|                    | 2.3.14 <i>Stability studies of MP-0.4 nanomaterials</i>                                      | 71           |
| 2.4                | CONCLUSION   | 74           |
|                    | REFERENCES   | 76           |

|                    |   |               |
|--------------------|---|---------------|
| <b>CHAPTER – 3</b> | <b>DICLOFENAC SODIUM LOADED IN MAGNETITE -<br/>PECTIN NANOMATERIALS</b>   | <b>79-111</b> |
| 3.1                | INTRODUCTION  | 79            |
|                    | 3.1.1 <i>Objective of the study</i>   | 80            |
| 3.2                | MATERIALS AND METHODS   | 80            |
|                    | 3.2.1 <i>Materials</i>  | 80            |
|                    | 3.2.2 <i>Method for fabrication of magnetite-pectin<br/>nanomaterials cross linked with Ca<sup>2+</sup> ions loaded with DS</i> | 83            |
|                    | 3.2.3 <i>Methodology for drug loading analysis</i>  | 84            |
|                    | 3.2.4 <i>Characterization</i>   | 85            |
|                    | 3.2.5 <i>Methodology for in vitro drug release</i>  | 86            |
|                    | 3.2.6 <i>Analysis of in vitro drug release in the respective<br/>simulated fluids</i>   | 87            |
| 3.3                | RESULTS AND DISCUSSION  | 91            |
|                    | 3.3.1 <i>Evaluation of drug loading</i>   | 91            |
|                    | 3.3.2 <i>X-ray diffraction</i>  | 92            |
|                    | 3.3.3 <i>Morphological studies</i>  | 92            |
|                    | 3.3.4 <i>FT-IR analysis</i>   | 94            |
|                    | 3.3.5 <i>Thermal studies</i>  | 96            |
|                    | 3.3.6 <i>Zeta potential measurement: Mechanism of the<br/>formation of nanomaterial of MP-DS</i>                                | 98            |
|                    | 3.3.7 <i>Magnetic studies</i>   | 99            |
|                    | 3.3.8 <i>In vitro drug release studies from MP-DS hybrid<br/>nanomaterial</i>   | 101           |
| 3.4.               | CONCLUSION  | 106           |
|                    | REFERENCES  | 107           |

|                    |  |                |
|--------------------|--|----------------|
| <b>CHAPTER - 4</b> | <b>DICLOFENAC SODIUM LOADED IN<br/>NANOMATERIALS OF MAGNETITE - PECTIN<br/>REINFORCED WITH CHITOSAN</b>                | <b>113-139</b> |
| 4.1                | INTRODUCTION   | 113            |
|                    | <i>4.1.1 Objective of the study</i>  | 113            |
| 4.2                | MATERIALS AND METHODS  | 114            |
|                    | <i>4.2.1 Materials</i>   | 114            |
|                    | <i>4.2.2 Method for fabrication of nanomaterials of magnetite-<br/>pectin- reinforced with chitosan loaded with DS</i> | 114            |
|                    | <i>4.2.3 Methodology for in vitro drug loading analysis</i>  | 115            |
|                    | <i>4.2.4 Characterization</i>  | 116            |
|                    | <i>4.2.5 Methodology for drug release</i>  | 116            |
| 4.3.               | RESULTS AND DISCUSSION   | 116            |
|                    | <i>4.3.1 Evaluation of drug loading</i>  | 116            |
|                    | <i>4.3.2 X-ray diffraction studies</i>   | 117            |
|                    | <i>4.3.3 <sup>57</sup>Fe Mössbauer spectroscopic studies</i>   | 118            |
|                    | <i>4.3.4 Morphological studies</i>   | 119            |
|                    | <i>4.3.5 FT- IR analysis</i>   | 122            |
|                    | <i>4.3.6 Thermogravimetric analysis</i>  | 124            |
|                    | <i>4.3.7 Zeta potential measurement: mechanism of the<br/>formation of nanomaterial of MPCh-DS</i>                     | 126            |
|                    | <i>4.3.8 Magnetic studies</i>  | 128            |
|                    | <i>4.3.9 In vitro release studies of MPCh-DS0.05 nanomaterial</i>  | 131            |
| 4.4                | CONCLUSION   | 135            |
|                    | References   | 137            |

|                    |   |                |
|--------------------|---|----------------|
| <b>CHAPTER - 5</b> | <b>5-FLUOROURACIL LOADED IN NANOMATERIALS<br/>OF MAGNETITE – PECTIN</b>   | <b>141-175</b> |
| 5.1                | INTRODUCTION  | 141            |
|                    | <i>5.1.1 Objective of the study</i>   | 141            |
| 5.2                | MATERIALS AND METHODS   | 142            |
|                    | <i>5.2.1. Materials</i>   | 142            |
|                    | <i>5.2.2 Method for fabrication of nanomaterials of magnetite-<br/>pectin cross linked with Ca<sup>2+</sup> ions loaded with 5-FU</i> | 145            |
|                    | <i>5.2.3 Methodology for drug loading analysis</i>  | 147            |
|                    | <i>5.2.4 Characterization</i>   | 148            |
|                    | <i>5.2.5 In vitro drug release and analysis</i>   | 148            |
|                    | <i>5.2.6 Drug analysis</i>  | 149            |
|                    | <i>5.2.7 Experimental procedure for SRB assay</i>   | 152            |
| 5.3.               | RESULTS AND DISCUSSION  | 154            |
|                    | <i>5.3.1 Evaluation of drug loading</i>   | 154            |
|                    | <i>5.3.2 X-ray diffraction studies</i>  | 155            |
|                    | <i>5.3.3 Morphological studies</i>  | 155            |
|                    | <i>5.3.4 FT-IR analysis</i>   | 158            |
|                    | <i>5.3.5 Zeta potential measurement: mechanism of the<br/>formation of nanomaterial of MP-5FU nanomaterials</i>                       | 159            |
|                    | <i>5.3.6 Magnetic properties of MP-5FU nanomaterials</i>  | 160            |
|                    | <i>5.3.7 In vitro drug release studies from MP-5FU<br/>nanomaterials</i>  | 164            |
|                    | <i>5.3.8 In vitro cytotoxic activity profiles of MP-5FU<br/>nanomaterials</i>   | 168            |
| 5.4                | CONCLUSION  | 170            |
|                    | REFERENCES  | 172            |

|                    |  |         |
|--------------------|--|---------|
| <b>CHAPTER - 6</b> | <b>OXALIPLATIN LOADED IN NOVEL MAGNETIC POLYMERIC NANOMATERIALS</b>  | 177-207 |
| 6.1                | INTRODUCTION   | 177     |
|                    | 6.1.1 <i>Objective of our work</i>   | 178     |
| 6.2                | MATERIALS AND METHODS  | 178     |
|                    | 6.2.1 <i>Materials</i>   | 178     |
|                    | 6.2.2 <i>Method for fabrication of nanomaterials of magnetite-pectin cross linked with Ca<sup>2+</sup> loaded with OHP and magnetite-pectin reinforced with chitosan loaded with OHP</i> | 181     |
|                    | 6.2.2.1 <i>Method for fabrication of nanomaterials of magnetite-pectin cross linked with Ca<sup>2+</sup> ions loaded with OHP</i>  |         |
|                    | 6.2.2.2 <i>Method for fabrication of nanomaterials of magnetite-pectin reinforced with chitosan loaded with OHP</i>  |         |
|                    | 6.2.3 <i>Methodology for drug loading analysis</i>   | 182     |
|                    | 6.2.4 <i>Characterization</i>  | 183     |
|                    | 6.2.5 <i>Methodology for in vitro drug release</i>   | 183     |
|                    | 6.2.6 <i>Drug analysis</i>   | 184     |
|                    | 6.2.7 <i>SRB assay for cytotoxicity studies in cancer cell lines</i>   | 185     |
| 6.3                | RESULTS AND DISCUSSION   | 186     |
|                    | 6.3.1 <i>Drug loading efficiency</i>   | 186     |
|                    | 6.3.2 <i>X-ray diffraction study</i>   | 186     |
|                    | 6.3.3 <i>Morphological studies</i>   | 187     |
|                    | 6.3.4 <i>Zeta potential measurements</i>   | 190     |
|                    | 6.3.7 <i>In vitro cytotoxic activity profiles of MP-OHP</i>  | 191     |
| 6.4                | CONCLUSION   | 202     |
|                    | REFERENCES   | 204     |
|                    | <b>SUMMARY</b>   | 209-214 |
|                    | LIST OF PAPERS PUBLISHED/ ACCEPTED/ SUBMITTED FOR PUBLICATION  | 215     |
|                    | LIST OF PAPERS PRESENTED AT NATIONAL/ INTERNATIONAL CONFERENCES  | 217     |



## LIST OF TABLES

|   |  |     |
|---|--|-----|
| <b>CHAPTER - 2 NOVEL HYBRID NANOMATERIALS OF MAGNETITE AND PECTIN</b>                                       |  |     |
| 2.1   | <sup>57</sup> Fe Mössbauer spectroscopy hyperfine splitting parameters of MNPs   | 52  |
| 2.2   | <sup>57</sup> Fe Mössbauer spectroscopy hyperfine splitting parameters of MP-0.4   | 59  |
| 2.3   | Zeta potential measurements of magnetite nanoparticles (MNPs), pectin solution and MNP coated calcium pectinate hybrid nanomaterials (MPs).  | 67  |
| 2.4   | <sup>57</sup> Fe Mössbauer spectroscopy hyperfine splitting parameters of MP-0.4 after 6 months.   | 72  |
| <b>CHAPTER - 3 DICLOFENAC SODIUM LOADED IN MAGNETITE - PECTIN NANOMATERIALS</b>                             |  |     |
| 3.1.  | Optimization of encapsulation efficiencies and drug loading content in MP-DS hybrid nanomaterial using fixed concentration of MNPs.  | 84  |
| 3.2   | Zeta potential measurements of diclofenac sodium (DS), magnetite calcium pectinate without diclofenac sodium (MP), magnetite calcium pectinate loaded with diclofenac sodium (MP-DS) | 98  |
| <b>CHAPTER - 4 DICLOFENAC SODIUM LOADED IN NANOMATERIALS OF MAGNETITE - PECTIN REINFORCED WITH CHITOSAN</b> |  |     |
| 4.1.  | Optimization of encapsulation efficiencies and drug loading content in MPCh-DS nanomaterials with fixed concentration of MNPs  | 115 |
| 4.2   | <sup>57</sup> Fe Mössbauer spectroscopy hyperfine splitting parameters of MPCh   | 119 |
| 4.3.  | Zeta potential measurements of magnetite nanoparticles (MNPs), pectin solution, chitosan solution, diclofenac sodium solution and nanomaterial MPCh-DS0.05.                          | 127 |
| <b>CHAPTER - 5 5-FLUOROURACIL LOADED IN NANOMATERIALS OF MAGNETITE – PECTIN</b>                             |  |     |
| 5.1.  | Parameters for fabrication of magnetite-pectin-5FU nanomaterials with fixed concentration of MNPs (Protocol I)   | 147 |
| 5.2a  | Optimization of the probe sonication time for fabrication of magnetite-pectin-5FU with 0.1 M 5-FU using different probe sonication time (Protocol II)                                | 147 |

|      |   |     |
|------|---|-----|
| 5.2b | Parameters for fabricating magnetite-pectin-5FU with different concentrations of 5-FU and fixed probe sonication time of 60 min (Protocol II)   | 147 |
| 5.3  | Parameters for fabricating magnetite-pectin-5FU with fixed concentration of MNPs and fixed ultra sonication time of 1 h (Protocol III)  | 147 |
| 5.4. | Zeta potential measurements of magnetite nanoparticles at pH~ 4, calcium pectinate (MP) at pH~ 4, magnetite nanoparticles encapsulated in calcium pectinate nanomaterials loaded with 5-FU (MP-5FU) at pH 4 and 5-FU. | 159 |

**CHAPTER - 6 OXALIPLATIN LOADED  
IN NOVEL MAGNETIC POLYMERIC NANOMATERIALS**

|      |   |     |
|------|---|-----|
| 6.1. | % Encapsulation efficiency (mean $\pm$ SD; SD = standard deviation) measured from triplicate analysis in MP-OHP and MPCh-OHP.   | 182 |
| 6.2. | Zeta potential measurements of oxaliplatin (OHP), magnetite pectin cross lined with Ca <sup>2+</sup> loaded with OHP (MP-OHP) and magnetite pectin reinforced with chitosan loaded with OHP (MPCh-OHP). | 191 |

## LIST OF FIGURES

|   |   |    |
|---|---|----|
| <b>CHAPTER - 1 INTRODUCTION: NANOMATERIALS BASED TARGETED DRUG DELIVERY</b> |   |    |
| 1.1.  | Structures of a monomer unit of chitosan.   | 8  |
| 1.2   | (a) A repeating segment of pectin molecule and functional groups (b) carboxyl (c) ester.  | 10 |
| <b>CHAPTER - 2 NOVEL HYBRID NANOMATERIALS OF MAGNETITE AND PECTIN</b>       |   |    |
| 2.1.  | XRD of the MNPs prepared with different predigestion time (a) predigestion time was 15 min (b) predigestion time was 30 min (c) predigestion time was 45 min.   | 51 |
| 2.2.  | <sup>57</sup> Fe Mössbauer spectra of MNPs recorded at room temperature (300 K) showing superparamagnetically relaxed sextet spectrum. The measurement at 5 K showed typical sextet of magnetic material. The measurement recorded at 5 K and 5 Tesla revealed tetrahedral and octahedral Fe - sites. | 52 |
| 2.3a.   | Scanning electron microscopy (SEM) of clusters of MNPs prepared by using tween-80 as dispersing agent.  | 53 |
| 2.3b.   | Energy Dispersive X-analysis (EDAX) of MNPs using tween-80 as dispersing agent.   | 53 |
| 2.4a.   | Transmission electron microscopy (TEM) of MNPs dispersed with tween 80.   | 54 |
| 2.4b.   | Transmission electron microscopy (TEM) of MNPs dispersed with tween 80 and its corresponding SAED indicating the presence of polycrystalline MNPs.  | 54 |
| 2.5.  | Transmission electron microscopy (TEM) and its corresponding SAED image of MNPs prepared without surfactants.   | 55 |
| 2.6a.   | SEM image showing morphology of MP-0.4 batch synthesized by stirring pectin, MNPs and Ca <sup>2+</sup> for 1 h.   | 56 |
| 2.6b.   | SEM image showing morphology of MP-0.4 batch synthesized by stirring pectin, MNPs and Ca <sup>2+</sup> for 4 h.   | 56 |
| 2.6c.   | SEM image showing morphology of MP-0.4 batch synthesized by stirring pectin, MNPs and Ca <sup>2+</sup> for 6 h.   | 56 |

|        |  |    |
|--------|--|----|
| 2.6d.  | SEM image showing morphology of MP-0.4 batch synthesized by stirring pectin, MNPs and Ca <sup>2+</sup> for 24 h.   | 56 |
| 2.7.   | SEM of nanomaterials synthesized by coating of MNPs with zinc-pectinate.   | 57 |
| 2.8.   | SEM of nanomaterials synthesized by coating of MNPs with magnesium-pectinate.  | 57 |
| 2.9.   | SEM of nanomaterials synthesized by coating of MNPs with manganese-pectinate showing non-uniform rod like shapes of nanomaterials.   | 58 |
| 2.10.  | XRD of the MNPs and various compositions of MPs.   | 58 |
| 2.11.  | <sup>57</sup> Fe Mössbauer spectroscopy measurements of MP-0.4 at room temperature (300 K) showing superparamagnetically relaxed sextet spectrum. The measurement at 5 K showed typical sextet of magnetic material. The measurement recorded at 5 K and 5 Tesla revealed tetrahedral and octahedral Fe – sites. | 60 |
| 2.12a. | Morphology and particle size distribution of MP-0.4 by scanning electron microscopy.   | 61 |
| 2.12b. | EDAX of a selected nanostructure of MP-0.4, marked in the inset illustrated co-localization of Fe and Ca.  | 61 |
| 2.13a. | TEM of spherical shaped MP-0.4 nanomaterial of about 150 nm (as marked).   | 62 |
| 2.13b. | Detailed TEM of a part of MP-0.4 nanomaterials (represented by an arrow in Fig 2.13a) illustrated the presence of polycrystalline MNPs.  | 62 |
| 2.14.  | DLS measurement of MP-0.4 in aqueous solution at pH ~4.  | 63 |
| 2.15.  | FT-IR spectra showing characteristic peaks of MP-0.4, MP-0.6, precursor pectin and calcium pectinate as reference sample.  | 64 |
| 2.16.  | TGA analysis of MNPs, MP-0.4, MP-0.6, pectin and calcium pectinate.  | 65 |
| 2.17a. | Full scan X ray photoelectron spectroscopy (XPS) of MP-0.4.  | 66 |
| 2.17b. | Detailed scan X-ray photoelectron spectroscopy (XPS) of MP-0.4 for Fe analysis.  | 66 |
| 2.18.  | Schematic representation of the proposed mechanism for the synthesis of MP nanomaterials.  | 68 |
| 2.19.  | Magnetization vs field (M-H) curve showing magnetization of MNPs and MPs recorded by SQUID at 300 K.   | 69 |
| 2.20.  | ZFC and FC curve of MP-0.4 recorded at 200 Oe measured by SQUID.   | 70 |

|       |   |    |
|-------|---|----|
| 2.21. | Dissolution profile of Fe release from MNPs (a), MP-0.4 (b) in SGF for a total period of 120 minutes (results are given as mean $\pm$ standard deviation from triplicate analysis). | 71 |
| 2.22. | XRD of MP-0.4 after 6 months showing the characteristic peaks of magnetite.   | 72 |
| 2.23. | <sup>57</sup> Fe Mössbauer spectra of MP-0.4 after storing for 6 months recorded at room temperature, 5 K, 5 K and 5 Tesla.   | 73 |
| 2.24. | Magnetization vs field (M-H) curve of MP-0.4 recorded by SQUID after 6 months of storage.   | 73 |

### **CHAPTER - 3 DICLOFENAC SODIUM LOADED IN MAGNETITE - PECTIN NANOMATERIALS**

|       |   |    |
|-------|---|----|
| 3.1.  | Structure of diclofenac sodium.   | 81 |
| 3.2.  | Calibration curve for estimation of diclofenac sodium in Millipore water measured at $\lambda_{\max} = 276$ nm. (Absorbance is given as mean $\pm$ standard deviation of triplicate analysis).  | 89 |
| 3.3.  | Calibration curve for estimation of diclofenac sodium in SIF without pancreatin measured at $\lambda_{\max} = 276$ nm (Absorbance is given as mean $\pm$ standard deviation of triplicate analysis).                                    | 90 |
| 3.4.  | Calibration curve for estimation of diclofenac sodium in SCF without pectinase measured at $\lambda_{\max} = 276$ nm (Absorbance is given as mean $\pm$ standard deviation of triplicate analysis).                                     | 90 |
| 3.5.  | Calibration curve for estimation of diclofenac sodium in phosphate buffer ph 7.4 measured at $\lambda_{\max} = 276$ nm (Absorbance is given as mean $\pm$ standard deviation of triplicate analysis).                                   | 91 |
| 3.6.  | XRD of the DS, MNPs and MP-DS.  | 92 |
| 3.7.  | Morphology and elemental composition of the marked area of about 100 nm sized MP-DS nanomaterials by SEM-EDAX.  | 93 |
| 3.8a. | Transmission electron microscopy (TEM) of spherical shaped MP-DS hybrid nanomaterials of about 100-150 nm and its corresponding selected area electron diffraction (SAED) image exhibiting the presence of polycrystalline MNPs and DS. | 93 |
| 3.8b. | Detailed transmission electron microscopy (TEM) of one of the nanomaterials of MP-DS.   | 94 |
| 3.9.  | Dynamic Light Scattering (DLS) measurement of MP-DS in aqueous solution at pH ~4.   | 94 |

|        |   |     |
|--------|---|-----|
| 3.10.  | FT-IR spectra of MP, DS and MP-DS hybrid nanomaterials.   | 95  |
| 3.11a. | Thermogravimetric analysis (TGA) of MP-DS, MP (calcium pectinate-magnetite nanoparticles- without drug DS) and pure drug DS.  | 97  |
| 3.11b. | Differential thermal analysis (DTA) of MP-DS, MP and pure drug DS.  | 98  |
| 3.12.  | Schematic representation of mechanism towards formation of the MP-DS hybrid nanomaterials.  | 99  |
| 3.13.  | Magnetization vs field (M-H) curve of MNPs, MP (without drug) and MP-DS measured by VSM at room temperature.  | 100 |
| 3.14.  | ZFC and FC curve of MP-DS recorded at 500 Oe, measured by SQUID.  | 101 |
| 3.15.  | Sequential <i>in vitro</i> release of DS from MP-DS in simulated gastric fluid (SGF pH 1.2) for 2 h, followed by simulated intestinal fluid (SIF pH 6.8) for 3 h and simulated colonic fluid (SCF pH 5.5) up to 48 h. | 103 |
| 3.16.  | <i>In vitro</i> release of DS from MP-DS hybrid nanomaterial in phosphate buffer solution (pH 7.4) for 48 h.  | 104 |
| 3.17.  | Showing linear fit of <i>in vitro</i> release of DS up to 8 h from MP-DS in phosphate buffer solution (at pH 7.4), using Korsmeyer Peppas equation in log scale.  | 105 |

#### **CHAPTER - 4 DICLOFENAC SODIUM LOADED IN NANOMATERIALS OF MAGNETITE - PECTIN REINFORCED WITH CHITOSAN**

|       |  |     |
|-------|--|-----|
| 4.1.  | XRD of the Diclofenac Sodium (DS), MNPs, MPCh, MPCh-DS0.01 and MPCh-DS0.05.  | 118 |
| 4.2.  | <sup>57</sup> Fe Mössbauer spectra of MPCh-DS0.05 recorded at 5 K showing typical sextet of magnetic material and at 5 K and 5 T showing tetrahedral and octahedral sites of Fe <sub>3</sub> O <sub>4</sub> phase. | 119 |
| 4.3.  | SEM of MPCh-DS0.05 showing individual spherical nanomaterials of sizes 100 -150 nm, EDAX analysis showing K-X-ray peaks of Na and Fe indicating the presence of the diclofenac sodium and magnetite in MPCh-DS.    | 120 |
| 4.4a. | TEM showing morphology of MPCh-DS0.05 nanomaterial with size of ~150 nm.   | 120 |
| 4.4b. | TEM showing morphology of MPCh-DS0.05 nanomaterial with size of ~150 nm.   | 121 |
| 4.4c. | Showing detailed TEM image showing aggregation of 100 - 150 nm MPCh-DS0.05 and its corresponding SAED image exhibiting polycrystalline nature of MNPs  | 121 |

|       |   |     |
|-------|---|-----|
| 4.5.  | DLS measurement of MPCh-DS05 in aqueous solution at pH~4.   | 122 |
| 4.6.  | FT-IR spectra of DS, MPCh, MPCh-DS0.01 and MPCh-DS0.05, showing encapsulation of DS in the nanomaterials.   | 123 |
| 4.7a. | TGA plot of MPCh-DS0.05 and MPCh-DS0.01.  | 124 |
| 4.7b. | TGA plot of MPCh and diclofenac sodium (DS).  | 125 |
| 4.8.  | Schematic representation of mechanism towards formation of the MPCh-DS nanomaterials.   | 127 |
| 4.9.  | Magnetization vs field (M-H) curve of MNPs, MPCh, MPCh-DS0.01 and MPCh-DS0.05 measured by VSM at room temperature.  | 129 |
| 4.10. | ZFC and FC curve of MPCh-DS0.05 recorded at 50 Oe, measured by SQUID.   | 130 |
| 4.11. | Sequential <i>in vitro</i> release studies of DS from MPCh-DS0.05 in simulated gastric fluid (SGF pH 1.2) for 2 h, followed by simulated intestinal fluid (SIF pH 6.8) for 3 h and then in simulated colonic fluid (SCF pH 5.5) up to 60 h. | 133 |
| 4.12. | <i>In vitro</i> release studies of DS from MPCh-DS0.05 in phosphate buffer at pH 7.4, for 48 h.   |     |
| 4.13. | Showing linear fit of <i>in vitro</i> release of DS up to 8 h from MPCh-DS0.05 in phosphate buffer solution (at pH 7.4), using Korsmeyer Peppas equation.   | 135 |

## **CHAPTER - 5 5-FLUOROURACIL LOADED IN NANOMATERIALS OF MAGNETITE – PECTIN**

|      |  |     |
|------|--|-----|
| 5.1  | Structure of 5-fluorouracil.   | 143 |
| 5.2. | Calibration curve for estimation of 5-fluorouracil in Millipore water at $\lambda_{\max} = 266$ nm. (Results are given as mean $\pm$ standard deviation, calculated from triplicate analysis)        | 150 |
| 5.3. | Calibration curve for estimation of 5-fluorouracil in SGF without pepsin at $\lambda_{\max} = 266$ nm (Results are given as mean $\pm$ standard deviation, calculated from triplicate analysis).     | 150 |
| 5.4. | Calibration curve for estimation of 5-fluorouracil in SIF without pancreatin at $\lambda_{\max} = 266$ nm (Results are given as mean $\pm$ standard deviation, calculated from triplicate analysis). | 151 |
| 5.5. | Calibration curve for estimation of 5-fluorouracil in SCF without pectinase at $\lambda_{\max} = 266$ nm (Results are given as mean $\pm$ standard deviation, calculated from triplicate analysis).  | 152 |

|        |  |     |
|--------|--|-----|
| 5.6.   | Calibration curve for estimation of 5-fluorouracil in phosphate buffer at $\lambda_{\text{max}} = 266 \text{ nm}$ (Results are given as mean $\pm$ standard deviation, calculated from triplicate analysis).                           | 152 |
| 5.7.   | XRD of the fabricated MP-5FU nanomaterials and the as-synthesized MNPs.  | 155 |
| 5.8.   | Morphology and elemental composition of the 100 nm sized MP-5FU by SEM and EDAX. The X-ray spectrum corresponded to the marked area in the inset.  | 156 |
| 5.9a.  | Transmission electron microscopy (TEM) of MP-5FU showing structure of 100-150 nm, its corresponding SAED image exhibits crystalline nature of the material.  | 156 |
| 5.9b.  | A detailed transmission electron microscopy (TEM) and corresponding selected area electron diffraction (SAED) of the MP-5FU nanomaterial of about 100 -150 nm.   | 157 |
| 5.9c.  | Higher resolution transmission electron microscopy (TEM) of about 100 -150 nm MP-5FU and its corresponding selected area electron diffraction (SAED) showing polycrystalline MNPs.   | 157 |
| 5.10.  | Dynamic Light Scattering (DLS) measurement of MP-5FU nanomaterials in aqueous solution at pH~ 4.   | 158 |
| 5.11.  | FT-IR spectra of MP, 5-FU and fabricated MP-5FU nanomaterials.   | 159 |
| 5.12.  | Schematic representation of mechanism towards formation of the MP-5FU nanomaterials.   | 160 |
| 5.13.  | a) Dispersion of freshly prepared MP-5FU b) showing MP-5FU nanomaterials attracted to the external magnet placed adjacent to sample vial, indicating its magnetic properties.  | 161 |
| 5.14.  | Magnetization vs field (M-H) curve of MNPs and MP-5FU measured by VSM at room temperature.   | 163 |
| 5.15a. | ZFC and FC curves of MP-5FU nanomaterials recorded at 50 Oe, measured by SQUID.  | 163 |
| 5.15b. | ZFC and FC curves of MP-5FU nanomaterials recorded at 500 Oe, measured by SQUID.   | 164 |
| 5.16.  | Sequential <i>in vitro</i> release of 5-FU from MP-5FU nanomaterials in simulated gastric fluid (SGF pH~1.2) for 2 h, followed by simulated intestinal fluid (SIF pH~6.8) for 3 h and simulated colonic fluid (SCF pH~7.4) up to 48 h. | 166 |



|                    |   |     |
|--------------------|---|-----|
| 5.17.              | <i>In vitro</i> sustained release studies of the drug 5-FU for 48 h from MP-5FU nanomaterials in phosphate buffer solution (pH ~7.4)  | 166 |
| 5.18.              | Showing linear fit of <i>in vitro</i> release of 5-FU up to 12 h from MP-5FU nanomaterials in phosphate buffer solution (at pH 7.4), using Korsmeyer Peppas equation in log scale.  | 167 |
| 5.19a.             | <i>In vitro</i> cytotoxic activity profiles of MP-5FU nanomaterials and MP on HT-29 (colon) cancer cell line after 48 h.  | 169 |
| 5.19b.             | <i>In vitro</i> cytotoxic activity profiles of MP-5FU nanomaterials on HEPG2 (liver) cancer cell line after 48 h.   | 169 |
| 5.19c.             | <i>In vitro</i> cytotoxic activity profiles of MP-5FU nanomaterials and MP on MIA-PA-CA-2 (pancreas) cancer cell line after 48 h.   | 170 |
| <br>               |   |     |
| <b>CHAPTER - 6</b> | <b>OXALIPLATIN LOADED IN NOVEL MAGNETIC POLYMERIC NANOMATERIALS</b>   |     |
| 6.1                | Structure of oxaliplatin  | 179 |
| 6.2a.              | Calibration curve showing linear correlation between concentration of oxaliplatin (at pH 7.4) and Pt concentration measured by ICPMS analysis. The results are given as mean $\pm$ SD; (SD = standard deviation calculated from triplicate measurements). | 184 |
| 6.2b               | Calibration curve showing linear correlation between concentration of oxaliplatin (in pH 7.4) and Pt concentration measured by ICPMS analysis. The results are given as mean $\pm$ SD; (SD = standard deviation calculated from triplicate measurements). | 185 |
| 6.3.               | XRD of the MNPs synthesized by coprecipitation method, MP-OHP and MPCh-OHP nanomaterials.   | 186 |
| 6.4a.              | Scanning electron microscopy of MP-OHP nanomaterials.   | 187 |
| 6.4b.              | Scanning electron microscopy energy dispersive X-ray analysis (EDAX) of the marked nanomaterial showing the occurrence of magnetite nanoparticles in MP-OHP nanomaterials.  | 188 |
| 6.5.               | Scanning electron microscopy of MPCh-OHP nanomaterials.   | 188 |
| 6.6.               | TEM of MP-OHP nanomaterials and selected area electron diffraction (SAED) image of MP-OHP showing the presence of polycrystalline MNPs and OHP.   | 189 |
| 6.7.               | TEM of MPCh- OHP nanostructure and selected area electron diffraction (SAED) image of MPCh-OHP showing the presence of polycrystalline MNPs and OHP.  | 189 |

|        |   |     |
|--------|---|-----|
| 6.8.   | DLS measurement of MP-OHP nanomaterials in aqueous solution at pH ~ 4.  | 190 |
| 6.9.   | DLS measurement of MPCh-OHP nanomaterials in aqueous solution at pH ~ 4.  | 190 |
| 6.10.  | Magnetization vs field (M-H) curve of MNPs, MP (without drug) and MP-OHP nanomaterials measured by VSM at room temperature.                                     | 192 |
| 6.11.  | Magnetization vs field (M-H) curve of MNPs, MP (without drug) and MPCh-OHP nanomaterials measured by VSM at room temperature.                                   | 193 |
| 6.12.  | ZFC and FC curve of MP-OHP nanomaterials recorded at 100 Oe, measured by SQUID.   | 193 |
| 6.13.  | In vitro release studies of the drug OHP for 48 h from MPCh-OHP nanomaterials in phosphate buffer solution (pH 5.5)   | 195 |
| 6.14.  | In vitro release studies of the drug OHP for 48 h from MP-OHP nanomaterials in phosphate buffer solution (pH ~5.5)  | 195 |
| 6.15.  | In vitro release studies of the drug OHP for 48 h from MPCh-OHP nanomaterial in phosphate buffer solution (pH ~7.4)   | 196 |
| 6.16.  | In vitro release studies of the drug OHP for 48 h from MP-OHP nanomaterials in phosphate buffer solution (pH ~7.4)  | 196 |
| 6.17.  | Showing linear fit of in vitro release of OHP up to 7 h from MPCh-OHP in phosphate buffer solution (at pH 7.4), using Korsmeyer - Peppas equation in log scale. | 197 |
| 6.18.  | The in vitro release of OHP up to 7 h from MPCh-OHP in phosphate buffer solution (at pH 5.5), using Korsmeyer - Peppas equation in log scale.                   | 198 |
| 6.19.  | Showing linear fit of in vitro release of OHP up to 7 h from MP-OHP in phosphate buffer solution (at pH 7.4), using Korsmeyer - Peppas equation in log scale.   | 198 |
| 6.20.  | Showing linear fit of in vitro release of OHP up to 7 h from MP-OHP in phosphate buffer solution (at pH 5.5), using Korsmeyer - Peppas equation in log scale.   | 199 |
| 6.21a. | <i>In vitro</i> cytotoxic activity profiles of MP-OHP and MP nanomaterials on HT-29 (colon) cancer cell line after 48 h.  | 200 |
| 6.21b. | <i>In vitro</i> cytotoxic activity profiles of OHP on HT-29 (colon) cancer cell line after 48 h.  | 201 |

|        |  |     |
|--------|--|-----|
| 6.22a. | <i>In vitro</i> cytotoxic activity profiles of MP-OHP and MP nanomaterials on MIA-PA-CA-2 cancer cell line after 48 h. | 201 |
| 6.22b. | <i>In vitro</i> cytotoxic activity profiles of OHP on MIA-PA-CA-2 cancer cell line after 48 h.                         | 202 |

## ABBREVIATIONS

|                        |  |
|------------------------|--|
| Bhf                    | Internal magnetization   |
| DLS                    | Dynamic light scattering   |
| DS                     | Diclofenac sodium  |
| DTA                    | Differential thermal analysis  |
| EDAX                   | Energy dispersive X-ray analysis   |
| FC                     | Field cooled   |
| FT-IR                  | Fourier transform infrared spectroscopy  |
| FWHM                   | Full width at half maximum   |
| GI <sub>50</sub>       | Growth inhibition of 50 %  |
| ICPMS                  | Inductively coupled plasma (ICP) mass spectrometry                                   |
| INAA                   | Instrumental neutron activation analysis   |
| M-H curve              | Magnetization vs field curve   |
| MNPs                   | Magnetite nanoparticles  |
| MP                     | Hybrid nanomaterials of magnetite and pectin   |
| MPCh                   | Magnetite nanoparticles: pectin reinforced with chitosan                             |
| MP-OHP nanomaterials   | Nanomaterials of magnetite-pectin cross linked with Ca <sup>2+</sup> loaded with OHP |
| MPCh-OHP nanomaterials | Nanomaterials of magnetite-pectin reinforced with chitosan loaded with OHP           |
| M <sub>s</sub>         | Saturation magnetization   |
| NPs                    | Nanoparticles  |
| O                      | Octahedral   |
| OHP                    | Oxaliplatin  |
| PEG-400                | Polyethylene glycol-400  |
| SAED                   | Selected area electron diffraction   |
| SCF                    | Simulated colonic fluid with enzyme pectinase  |
| SD                     | Standard deviation   |
| SEM                    | Scanning electron microscopy   |
| SGF                    | Simulated gastric fluid with enzyme pepsin   |

|            |  |
|------------|--|
| SIF        | Simulated intestinal fluid with enzyme pancreatin  |
| SLS        | Sodium lauryl sulphate                             |
| SQUID      | Superconducting quantum unit interference device   |
| SRB        | Sulforhodamine B                                   |
| T          | Tetrahedral  |
| $T_B$      | Blocking temperature                               |
| TCA        | Trichloro acetic acid                              |
| TEM        | Transmission electron microscopy                   |
| TGA        | Thermogravimetry analysis                          |
| TG-DTA     | Thermogravimetry and differential thermal analysis |
| UV-visible | Ultraviolet visible spectrophotometry              |
| VSM        | Vibrating sample magnetometer                      |
| XPS        | X-ray photoelectron spectroscopy                   |
| XRD        | X-ray diffraction                                  |
| ZFC        | Zero field cooled                                  |
| 5- FU      | 5- Fluorouracil                                    |

***CHAPTER - 1***

***INTRODUCTION:***

***NANOMATERIALS BASED***

***TARGETED DRUG DELIVERY***

## 1.1 INTRODUCTION TO NANOSCALE MATERIALS

Nanomaterials brought radical changes in the various fields of science and technology. They are considered as futuristic materials for potential wide applications in Physics, Chemistry, Life Sciences, Medicine and Engineering. The striking feature of these nanoscale materials has been increased ratio of surface area to volume which has enabled substantial development in the area of catalysis and sensors. The other key benefit for different types of nanomaterials is the ability to vary their fundamental properties *e.g.*, magnetization [1], optical properties (color) [2, 3], melting point [4], hardness [5], solubility [6] *etc.* as compared to bulk materials without a change in chemical composition. The bulk properties such as melting point and hardness are related to the enhanced surface interactions among nanoparticulates, the size-tunable electronic properties are due to quantum confinement effects. Due to this a new area known as ‘Nanotechnology’ has emerged which offers a common platform to study and explore different types of nanomaterials for their uses ranging from day to day life applications, namely cosmetics, water purifier to advanced technologies in cancer diagnosis and therapy [7-11]. These are materials with morphological features in nanoscale dimensions where generally at least one of the dimensions is less than 100 nm. Such types of materials are found to exhibit extraordinary physico-chemical properties as compared to their bulk ones, which are attributed to their sizes [12]. Though there are evidences of the knowledge and usages of materials of small dimensions in the early days of human civilization, namely nanosized Au (gold) particles were used for body purification in Egyptian civilization [13], or Au and Ag nanoparticles were used in ceramics by Egyptians and Persians in 10<sup>th</sup> century BC for fabrication of ceramic glazes to provide a lustrous or glittering effect [14], but the scientific era of nanoscale materials was believed to have began with the lecture of Nobel laureate, Richard Feynman, in 1959 when he said that “there is plenty of room at the bottom” as discussed by Zhang and Webster [15]. The synthesis of nanomaterials or nanoparticles can be broadly classified as bottom-up approach and top-down approach [16, 17]. The bottom-up approach is usually a chemical method of synthesis where atoms or molecules of certain numbers could congregate to form a particle. On the other hand, the top-down approach is a physical process, where a material can be thought to be milled into an eventual small particle of nanoscale dimension. Stabilizing these nanoparticles has been one of the major challenges in synthesis or fabrication of nanoparticles. This is attributed to the tendency for agglomeration of nanoparticles owing to attractive van der Waals forces. It may be remarked that the basic knowledge of synthesizing

S. Sahul  
13-07-2012

R. Sundar  
13/7/12

nanoscale materials, mainly by chemical route was available since long but their application in nanotechnology was sluggish until the arrival of the sophisticated instrumentations, which made it possible for viewing and manipulating materials on the nanoscale dimension. Development of electron microscopy and more powerful scanning probe microscopy (SPM) during 1980's led to rapid progress in the field of nanotechnology. Since then various methods, namely, chemical methods like co-precipitation, sol-gel, ball milling, chemical vapor deposition, laser pyrolysis, supercritical fluid technology, gamma irradiation *etc.* [18-21] have been developed for synthesizing nanoparticles.

## 1.2 TYPES OF NANOMATERIALS

Broadly nanomaterials fall under two categories: fullerene and inorganic nanoparticles. The carbon nanotubes fall under fullerene group which has been one of the most exciting nanomaterials with large applications ranging between biomedical applications to superconductivity [22, 23]. On the other hand, inorganic nanoparticles comprise of metals, semiconductors and metal oxides are also finding wide application due to their unique optical, magnetic, electrical properties [24-26].

It is found that nanotechnology is developing rapidly in biomedical application, especially in diagnosis and therapy. Most of these reports are based on *in vitro* studies where a wide range of nanoscale materials has been used for suitable applications. For example, emission properties of Au nanoparticles have been extensively studied for imaging cancerous tissues. More interestingly, its quantum size dependent emission property has been tipped to replace the use of conventional fluorescent dye for cellular imaging [27, 28]. In addition, Au nanoparticles were explored for photodynamic therapy. An interesting study has been reported for synthesizing radioactive gold nanoparticles for potential biomedical applications [29]. Similarly, magnetic properties of superparamagnetic iron oxide nanoparticles (SPIONs) were found to be useful in hyperthermia based therapy [30]. Further a lot of attention is being laid on developing multifunctional nanomaterials for higher performance. For example, multifunctional properties provide a tool to achieve imaging, diagnosis and therapy simultaneously [31]. In addition to this, recently there has been growing scientific interest in exploring the opportunities of using polymers of nanoscale dimensions. Notably, polymeric nanomaterials often range in the diameter of 10-1000 nm [12]. For example polyvinyl alcohol, polycaprolactone, polylactic acid, polylactic co-glycolic acid, albumin, gelatin, dextran, alginates, pectinates, chitosan have attracted a great



attention especially in the field of biomedical applications, including imaging, enzyme immobilization and drug delivery [32- 45].

### 1.3 NANOMATERIALS FOR DRUG DELIVERY

Developing efficient drug delivery system of nanoscale dimension has been a major thrust in nanotechnology. This is attributed to some of the advantageous properties of the nanoscale materials namely: (1) small size due to which they can pass through the smallest capillary vessels (2) their ability to penetrate cells and tissue gap to arrive at target organs such as liver, spleen, lung, spinal cord and lymph; (3) their ability to show controlled release properties which is attributed to their biodegradability, pH, ion and/ or temperature sensibility; (4) their ability for localized delivery and thereby reducing toxic side effects. Further, it may be noted that the size ranging from a few nanometers up to tens of nanometers makes them comparable to a virus (20-450 nm), a protein (5-50 nm), or a gene (2 nm wide and 10-100 nm long), which enables them to be in close proximity to a biological entity of interest.

The term 'drug delivery' refers to a method or process of administering a pharmaceutical compound to achieve therapeutic effects in humans or animals. Drug delivery technologies modify drug release profile, absorption, distribution and elimination for the benefit of improving product efficacy and safety, as well as patient convenience and compliance. The most common routes of administration includes peroral (through the mouth), topical (skin), transdermal (skin), transmucosal (nasal, buccal/ sublingual, excretory system), parenteral (intravenous, intra-arterial or intramuscular, intraperitoneal, intrathecal, subcutaneous injection) or implant and inhalation. The parenteral route of administration is associated with various intricacies like general systemic distribution of therapeutic drugs, the lack of drug specificity towards a pathological site, the necessity of a large dose to achieve high local concentration, nonspecific toxicity and other adverse side effects. Therefore to minimize these toxic effects as well as to improve the therapeutic efficacy, delivery of drug only at desirable sites might be favorable. In this regard, it is interesting to know that Paul Ehrlich in 1906 [46] postulated a novel hypothesis of 'magic bullet', which could be targeted to specific location in human body for drug delivery. With the advent of nanotechnology, Ehrlich's hypothesis of magic bullet received a great scientific attention towards developing and understanding the processes involved in drug delivery targeted at cellular and sub-cellular levels.

*S. Sahul*  
13-07-2012

*R. S. Sult*<sup>3</sup>  
13/7/12

Various types of nanoscale materials have been developed for achieving site specific targeted drug delivery. At this stage, it is important to get acquainted with terminologies, like 'host' and 'guest', which are commonly used in targeted drug delivery. Mostly, the substrate material, which is in nanoscale dimension, that holds the drug is referred to as 'host', while the drug is a 'guest'. In certain cases, the 'host' is also referred to as nanocarrier of drug. Some of the host materials of nanoscale dimension were developed for drug delivery.

### **1.3.1 Carbon nanotubes (CNTs)**

Carbon nanotubes, first discovered by Iijima in 1991, consisting of thin graphite sheets rolled up into the shape of a seamless tubular structure were studied for a potential targeted drug delivery system [47, 48]. This structure belongs to the family of fullerenes, which is the third allotropic form of carbon (most common form is C<sub>60</sub>) along with graphite and diamond. These are hollow tubes that are single-walled (0.4 to 2-nm diameter), double-walled (1 to 3.5-nm diameter), or multi-walled (2 to 100-nm diameter). These inner volumes can accommodate bioactive compounds, including drug. Interestingly both hydrophilic and lipophilic drugs can be encapsulated. The targeting and biocompatibility aspects of bioactive loaded CNTs can also be enhanced by effective surface functionalization. It has been reported that more than one drug can be loaded and function as a multidrug therapy system and has been successful in releasing drug over a long period of time, i.e. sustained drug delivery [48].

In spite of these applications CNTs are found to be toxic and due to its tendency to accumulate in major organs, such as lung, liver and spleen, consequent toxicity effect has been a major concern [49, 50].

### **1.3.2 Nanodiamonds**

Nanodiamonds (NDs) are reported to be attractive agents for use in biological and medical applications [51, 52]. This material shows various characteristics such as greater biocompatibility than other carbon nanomaterials, stable photoluminescence, ease of purification, commercial availability, and minimal cytotoxicity [52-54]. Further it can be functionalized and conjugated to a variety of molecules for the purpose of cell labeling and drug delivery [55, 56]. Additionally, by functionalization of nanodiamonds with certain groups like carbonyl oxygen and carboxylic acid (-COOH) functional groups -C(=O)OCH<sub>3</sub>,

-COOH, -NH<sub>2</sub>, or aliphatic moieties, the properties like solubility, specific binding sites on target cells and tissues along with the reduction of the side effects may be observed [57- 58]. This material is suitable for controlled drug delivery applications because of its capability to release drug slowly and consistently as well as excellent drug loading capacity attributed to its large surface area-to-volume ratio. Further, the long-term cytotoxicity and stability of functionalized NDs is still unknown. Additionally these NDs have a tendency to form agglomerates which also hinders its biological applications [51].

### ***1.3.3 Nanoemulsions***

Nanoemulsions are two-phase mixtures of insoluble liquids, with a “continuous phase” surrounding discrete vesicles of the “nanoscale dispersed phase” which are stabilized with a film of surfactant and co-surfactant [59-63]. These emulsions are transparent or translucent systems which have a dispersed-phase droplet size ranging between 20 to 200 nm. They are becoming attractive pharmaceutical formulations due to ease of preparation, thermodynamic stability, and optically transparent nature. Further the nanosize range of the droplets prevent creaming or sedimentation which occurs on storage and droplet coalescence. The rate of drug release from nanoemulsions is affected by their droplet size [64]. Due to long term colloidal stability nanoemulsions can be used as a nanoscale drug carrier and can impart long shelf life of pharmaceuticals. Depending on the nature of the fabrication, namely oil/ water or water/ oil, hydrophobic and hydrophilic drugs respectively can be incorporated. This type of nanoscale drug carrier demonstrated enhanced ability for dermal, transdermal and mucosal transport/ permeation of various drugs [65, 66]. The major limitations of using nanoemulsions are non-suitability for controlled drug release applications, non-palatibility and non-compatibility with other excipients in the case of oral drug delivery.

### ***1.3.4 Micelles***

Micelles which are small (5–100 nm in diameter) colloidal dispersions that are constructed from amphiphilic molecules (possessing both hydrophilic and hydrophobic properties) such as lipids, which contain a hydrophobic core and a hydrophilic head (micellar corona) oriented outwardly. The hydrophilic shell stabilizes the micelle in an aqueous environment for intravenous delivery and the hydrophobic core stores a payload of drug for therapy [67].

### **1.3.5 Liposomes**

Liposomes consist of an amphiphilic phospholipid bilayer which surrounds an aqueous core. They can host both hydrophobic in lipid bilayer as well as hydrophilic drugs in aqueous core respectively. Their size ranges from several nanometers to a few micrometers which depend on the type of the liposome. They are classified as: small unilamellar vesicles (SUV) - ranges from 25–50 nm which is due to the presence of a single lipid layer, large unilamellar vesicles (LUV) - surrounded by a single lipid layer but are larger in size, Multilamellar vesicles (MLV) - surrounded by a multiple layers of a lipid [68, 69]. However, major disadvantage of using liposome for drug delivery has been reported to occur due to processing of synthetic liposomes which is complex as well as involves high cost, while in case of the natural liposomes there is no defined temperature for the transformation of the phase which limits their usage [70]. On the other hand, it has been possible to incorporate magnetic materials in the aqueous core or incorporate magnetized polymers within the lipid bilayer structure of liposomes to prepare magnetic liposome or magnetoliposome [71]. This enables the targeted delivery of therapeutic molecules to a specific site exposed in an external applied magnetic field.

### **1.3.6 Solid lipid nanoparticles (SLN)**

It is a relatively new class of nanoparticles developed for drug delivery. It is also referred to as lipospheres with the size ranging between 50 to 1000 nm. The SLN consists of the lipids which remain in a solid state at room temperature as well as body temperature. Solid lipid nanoparticles consist of a solid lipid core that can carry a hydrophobic drug, which is often stabilized by an external monolayer of steric or charged surfactant. They are made up of a wide variety of lipids including lipid acids, mono-, di-, or triglycerides, glyceride mixtures or waxes, which are stabilized by the suitable biocompatible surfactant(s) of non-ionic or ionic form [72]. For example, this type of carriers exhibited enhancement in antifungal activity of eugenol in immunosuppressed rats through lipid nanocarriers [73].

### **1.3.7 Dendrimers**

These are repetitively branched macromolecules consisting of core, branches, and end groups [74]. It is a promising system for drug delivery owing to its nanometer size range which can be controlled precisely, ease of preparation and functionalization, and their ability to display multiple copies of surface groups for biological reorganization processes.

Dendrimers with hydrophobic core and hydrophilic periphery exhibit micelle-like behavior and have been explored for the encapsulation of hydrophobic compounds and for the delivery of anticancer drugs. Notably majority of the drugs available in pharmaceutical industry are hydrophobic in nature and hence dendrimers are excellent carriers for hydrophobic drugs. The physical characteristics of dendrimers, including their monodispersity, water solubility, encapsulation ability, and large number of functionalizable peripheral groups, are favourable for their usage in drug delivery [75-79]. The major limitation of using dendrimers stems from its high uptake in liver, which can lead to toxicity effect. However, reports have shown that the toxicity can be reduced by surface modification of amine groups [80].

### **1.3.8 Metallic and metal oxide nanoparticles**

A variety of metallic nanoparticles, *e.g.*, Ag, Au *etc.* have been synthesized for several biomedical applications including drug delivery [81-83]. Silver nanoparticles are used to enhance wound healing and for coating plastic catheters. Coated catheters are non toxic and their sustained release of silver reduces infection at the site of the implant because silver is anti-bacterial. Gold nanoparticles (AuNPs) have also been used for cancer cell imaging and targeting. AuNPs are very attractive nanoscale agents as they are biocompatible, may naturally emit radiation, and have high surface reactivity [84]. In addition, use of iron oxide nanoparticles was also found to be significant. Besides their uses as MRI agent for diagnosis, they are also useful for hyperthermia based drug delivery [85]. In addition they are considered to be useful for imparting magnetic property to drug delivery system for magnetic targeting.

### **1.3.9 Polymeric nanoparticles**

In order to overcome the various side effects and other associated problems polymer-based nanoparticles which can effectively carry drugs, proteins, and DNA to target cells and organs have been thoroughly studied [86-88]. Their nanoscale dimension promotes effective permeation through cell membranes and stability in the blood stream. Polymers are very convenient materials for the manufacture of countless and varied molecular designs that can be integrated into unique nanoparticle constructs with many potential medical applications. Polymers, with emphasis on biodegradable ones, are being developed to create delivery systems with excellent drug and protein loading and release properties, a long shelf life, and

little toxicity. Various synthetic polymers, such as polyvinyl alcohol (PVA), poly (lactic co-glycolic acid) i.e. PLGA, poly( $\epsilon$ -caprolactone) *etc.* and their copolymers have been the most extensively studied [32-36]. But due to various associated problems with the synthetic polymers, research has been focused on usages of natural polymers like dextran, alginates, gelatin, albumin, pectin, chitosan, starch [37-45].

Amongst these, chitosan and pectin, due to their ease of availability, low cost, biodegradability, biocompatibility and non-toxicity have been selected for the further discussion. A few important polysaccharide based materials for drug delivery is highlighted below:

### 1.3.9.1 Chitosan

Chitosan is a biodegradable polysaccharide which is produced commercially by deacetylation of chitin, a structural element in the exoskeleton of crustaceans (such as crabs and shrimp *etc.*) and cell walls of fungi. Chitin is a linear copolymer of *N*-acetyl-D-glucosamine and D-glucosamine units which is linked with  $\beta$  - (1- 4)-glycosidic bond, here *N*-acetyl-D-glucosamine units are predominant in the chain of the polymer. The deacetylated form of chitin refers to chitosan (Fig. 1.1) [89]. Generally the average molecular weight of the chitosan lies between 3800 to 20,000 Daltons. Chitin is a copolymer with more than 40 % degree of acetylation (DA) i.e., number of *N*-acetyl-D-glucosamine more than 40% and number of D-glucosamine less than 60 %, which makes it insoluble in dilute acids. In case of chitosan the DA is less than 40 %, i.e., degree of de-acetylation is more than 60 %, which imparts solubility in dilute acids.

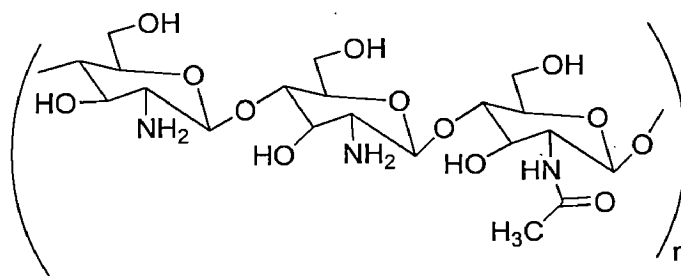


Fig 1.1. Structures of a monomer unit of chitosan.

Further, it may be noted that the amino group in chitosan has a  $pK_a$  value of  $\sim 6.5$ , and hence its charge density due to a protonation in acidic to neutral solution is dependent on pH and the % DA value [90, 91]. This imparts water solubility as well as bioadhesiveness to the chitosan due to which it readily binds to negatively charged surfaces such as mucosal membranes. It also shows strong electrostatic interactions with drugs, genes and MNPs [92-

95]. Further this amino group imparts hemostatic, bacteriostatic, fungistatic, anticancerogen, and anticholesteremic properties. These properties increase the pharmaceutical and medical applications of chitosan. In addition to all these properties chitosan is digested by chitinases, which are secreted by microbes of the colon and is also present in plant ingredients of food, or by lysozymes. The lysozyme in the body degrades chitosan into N-acetyl glucosamine which is followed by its excretion as carbon dioxide via the glycoprotein synthetic pathway. Due to this feature, chitosan has been an excellent material as a carrier for colon specific drug delivery. Lately, methodologies were developed for fabricating magnetic chitosan nanomaterials by blending [96, 97], polymer microgel template [98] and coprecipitation methods [99]. Even MNPs encapsulated by chitosan grafted with copolymers has been reported [95]. Because of reduction of sizes to submicron range and down to 100 – 200 nm sizes, its applicability as drug delivery system has improved tremendously [100, 101]. It is reported that nanosized chitosan loaded with various pharmaceutical compounds and biomolecules e.g. tartrate, 5-fluorouracil, paclitaxel *etc.*, and cyclosporine A, insulin, proteins have been successfully fabricated [102 – 108].

#### 1.3.9.2 Pectin

Pectin is commercially available as a white to light brown powder and is mainly extracted from citrus fruits (peel), but the apple pomace, sugar beet and sunflower are other reported sources [109-111]. Pectin has been used since long in the preparation of jams, jellies, desserts, bakery fillings and toppings, as a stabilizer in milk drinks, protein drink, yogurts, beverages, nutritional and health products [110, 112]. Therefore it may be concluded that the pectin could form a natural part of human diet. Pectin was though found to reduce blood cholesterol levels but it is not effective in adding up to nutrition [113, 114]. It has also been reported that the short-chain fatty acids, which are produced by the microbial degradation of pectin in the colon, have positive influence on health (prebiotic effect). Thus the pectin can be used as a carrier for drug delivery, especially as a controlled release drug delivery, sustained release drug delivery, intragastric drug delivery, colon specific drug delivery, ophthalmic drug delivery, nasal drug delivery, mucosal drug delivery and oral drug delivery [115-124]. Further even the pectin reinforced with the chitosan has also been reported for the delivery of a variety of molecules [125-129]. Furthermore the other reported pharmaceutical applications of pectin comprise gelling agent, thickening agent, binding agent and stabilizer [111].

Basically pectin is a complex heteropolysaccharide which is present in the primary cell walls of terrestrial plants. Mainly it consists of linear polymer which is composed of  $\alpha$ -(1-4)-linked D-galacturonan backbone occasionally interrupted by  $\alpha$ -(1-2)-linked  $\alpha$ -L-rhamnopyranose residues as shown in Fig. 1.2 [130]. Usually a significant part of the galacturonic acid residues of the backbone is methyl esterified. In general pectin contains from a few hundred to about 1000 building blocks per molecule which corresponds to average molecular weights ranging between 50,000 to 150,000 Daltons depending on the source of pectin.

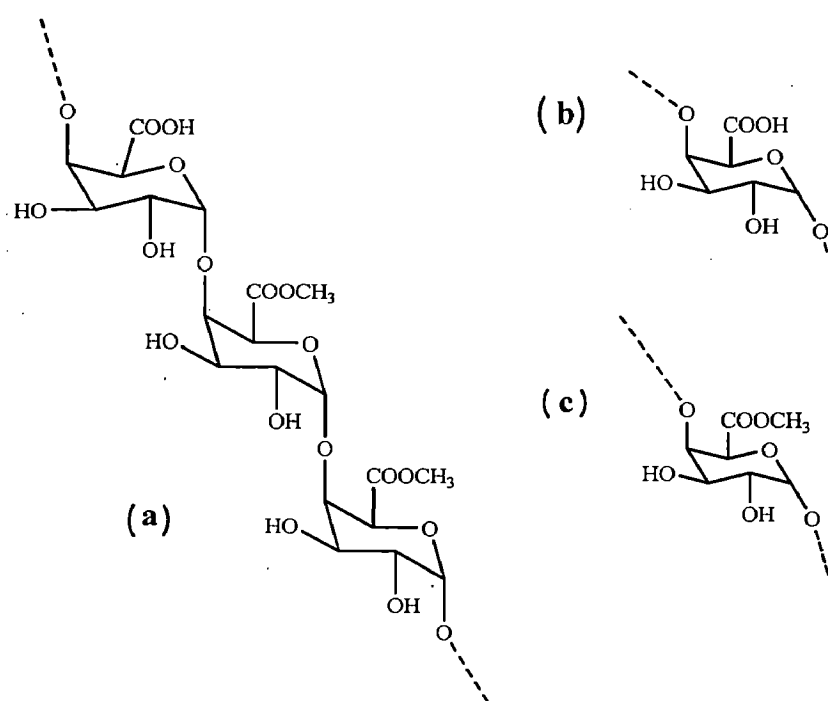


Fig 1.2 (a) A repeating segment of pectin molecule and functional groups, (b) carboxyl, (c) ester.

#### 1.4 TARGETED DRUG DELIVERY

Presently the research on targeted drug delivery has been focused with respect to: (1) the selection of a carrier material or combination of carrier materials to obtain suitable drug release speed; (2) the surface modification or functionalization of nanoparticles to improve their targeting ability; (3) the optimization to increase their drug delivery capability, their application in clinics with the enhancement in the possibility of industrial production; (4) the investigation of *in vivo* dynamic process to disclose the interaction of nanoparticles with blood and targeting tissues and organs.

These problems may be solved by the utilization of nanoparticles with targeting capabilities. If the treatments could be localized, *e.g.*, to the site of a joint, inflammation, or



cancerous tumors then the continuous maintenance of the various potent drugs could be possible. In this regard, the formulation embodying sustained drug release with delivery to a specific organ or location in the body (i.e., targeting), has been a major goal in drug delivery research over the last two decades. The targeting can be achieved either by specific recognition mechanism (ligand- or receptor-mediated targeting) like by use of aptamers, antibody bioconjugation *etc.* or by means of stimuli-sensitive drug carriers [130-134]. The stimuli sensitive carrier delivers drug upon exposure to an external stimulus namely pH, ultrasound, light, enzymes, magnetic fields *etc.* which can also be utilized for the targeted drug delivery [135-143]. In both the cases, minimal systemic distribution of the drug along with its protection from *in vivo* metabolism and elimination has been reported [144]. Besides enhancing the therapeutic efficacy it also minimizes the undesired side effects [144, 145].

Various polymeric nanomaterials have been developed in drug delivery research to effectively deliver drug to a target site and minimize side effects of the drug. But biodegradable polymers are better suited but they alone may not be effective in achieving the targeted drug delivery. Therefore there is still a recognized need for pharmaceuticals to be confined in a selected anatomical site after administration to increase the therapeutic benefit. Incorporation of an additional material, which is sensitive to external or internal stimuli, could be effective in achieving targeting capabilities of the polymeric nanomaterials.

One of the classes of stimuli sensitive drug carriers includes the magnetic materials, especially superparamagnetic iron oxide nanoparticles (SPIONs). SPIONs coated with polymers exhibit various intrinsic advantages such as good biocompatibility, ease of preparation, low cost, high drug loading, enhanced drug stability, low cytotoxicity and protection of the loaded drug molecules.

#### **1.4.1 SPIONs for targeting**

Amongst all these approaches the targeted drug delivery may be obtained by imparting magnetism to a polymeric nanostructured carrier for magnetically guided drug delivery. In this regard, the extensive research has been carried out for the use of superparamagnetic iron oxide nanoparticles (SPIONs) for imaging and drug delivery. The SPIONs of about 5–20 nm in diameter is considered to be a promising material for several biomedical applications *e.g.*, cellular imaging, targeted delivery, targeted chemotherapy, magnetic resonance imaging (MRI), hyperthermia [146-150].

The SPIONs of this size range are sufficiently small so that precipitation due to gravitational force can be avoided. This colloidal stability imparts the stability to SPIONs in water at neutral pH and even in physiological solutions. Furthermore in this size range the particles are expected to have single magnetic domain due to which the magnetization interference from domain wall can be minimum. They exhibit interesting properties such as superparamagnetism, corresponding to particle sizes smaller than 10 nm [15, 34]. They exhibit high field irreversibility, high saturation magnetization, extra anisotropy contributions [151]. Superparamagnetism is induced when the thermal vibration is greater than the magnetic anisotropy energy of the nanoparticle. This anisotropy energy is the potential energy that governs the direction of the spontaneous magnetization. The direction of the spontaneous magnetization in each superparamagnetic particle flips randomly with time, because of the large effect of thermal vibration, which results in the disappearance of the coercivity. Hence, superparamagnetic iron oxide nanoparticles exhibit zero magnetic remanence. Also, the high magnetization response, which is due to the large magnetic moment in the superparamagnetic particles, ensures that movement of the particles can be easily controlled by an external magnetic field. Further due to the phenomenon of superparamagnetism these iron oxide nanoparticles no longer show magnetic interaction after the external magnetic field is removed.

Iron oxide can exist as magnetite ( $\text{Fe}_3\text{O}_4$ ), hematite ( $\alpha\text{-Fe}_2\text{O}_3$ ), beta phase ( $\beta\text{-Fe}_2\text{O}_3$ ), maghemite ( $\gamma\text{-Fe}_2\text{O}_3$ ), epsilon phase ( $\epsilon\text{-Fe}_2\text{O}_3$ ). Amongst these different forms of iron oxides usually magnetite, maghemite and hematite are the three main iron oxides which are included in the category of SPIONs. In magnetite Fe exists as both 2+ and 3+ states, while the Fe in the other iron oxide phases exist as 3+ state. It was though found that various ferrites which are mixed oxides of iron and other transition metal ions like Sn, Co, Mn, and Ni exhibit superparamagnetic behavior [152-156], but due to the biocompatibility and low toxicity only SPIONs have been used thoroughly for various biomedical studies. Further, amongst these SPIONs usually the magnetite nanoparticles (MNPs) are selected due to its superparamagnetic susceptibility, high saturation magnetization, biodegradability, very low toxicity ( $\text{LD}_{50}$  g/kg), relative ease of synthesis and low cost of production. This phase of SPIONs i.e. magnetite has a cubic inverse spinel structure with oxygen forming a face centered cubic closed packing where Fe cations occupying interstitial tetrahedral sites and octahedral sites. The magnetization shown by magnetite is attributed to the hopping of

electrons between  $\text{Fe}^{2+}$  and  $\text{Fe}^{3+}$  ions in the octahedral sites at room temperature. In view of these observations the synthesis of MNPs was carried out in the present work.

Biodegradability and non-toxicity of these nanoscale materials are the major features for their extensive *in vivo* applications. It has been reported that the iron obtained from these nanoparticles is incorporated into red blood cell haemoglobin within 30–40 days [157]. Due to this, accumulation of iron oxide nanoparticles could be perhaps minimized. SPIONs due to their nanometer order sizes would require stabilizing agent for restricting the aggregation phenomenon of nanoparticles of iron oxide. In this regard, it was emphasized that *in situ* synthesis of iron oxide nanoparticles coated with natural polymers could serve two purposes, i.e., stabilizing iron oxide nanoparticles as well as hold the drug for delivery [158]. It is worth mentioning here that the use of iron oxide nanoparticles coated with biopolymers successfully demonstrated magnetic guiding and delivery of drug to a tumor site in lungs by placing a magnet close to chest in order to deliver the anticancer drug only at the tumor site [159].

It must be noted that though the magnetically guided drug delivery has so many advantages but still it also has some of the limitations. The magnetic drug delivery system depends on the strength of the external magnetic field to induce magnetic property in the drug carrier for magnetic transportation and also to control the residence time of the magnetic nanomaterials in the desired area. The drug desorption can also be triggered by suitable magnetic field gradient. But this limitation may be avoided by using external magnetic fields or by implanting internal magnets near to the target by using minimally invasive surgery. In this way for targeted drug delivery using magnetic nanoparticles may also establish a promising strategy [145, 147].

#### 1.4.2.1 Synthesis of magnetite nanoparticles (MNPs)

Synthesis of magnetite nanoparticles (MNPs) is a key feature in the development of magnetic system for targeted drug delivery. Various methods were developed for synthesizing iron oxide nanoparticles. A few selected methods are discussed below:

The MNPs in general may be synthesized by either hydrolytic route or by non-hydrolytic route. Thermal decomposition method is a non-hydrolytic synthetic route which was introduced during the early 21<sup>st</sup> century and developed later on for synthesizing MNPs [160-173]. Monodispersed magnetite ( $\text{Fe}_3\text{O}_4$ ) nanoparticles (MNPs) of sizes below 20 nm were successfully synthesized by thermal decomposition of iron(III) acetylacetonate

(Fe(acac)<sub>3</sub>) [164]. Similarly the precursors of FeOOH and oleic acid were used to prepare MNPs of ~12.5 nm by thermal decomposition method [174]. It was found that higher precursor concentration and operating temperature resulted into formation of larger particles of ~20 to 30 nm sizes with high level of polydispersity [172]. Interestingly, MNPs of different sizes, i.e., 4 nm, 12 nm, and 60 nm could be synthesized by boiling FeCl<sub>3</sub>.6H<sub>2</sub>O in 2-pyrrolidone solution [172]. Further there are more exotic techniques to synthesize MNPs such as laser pyrolysis or chemical vapor deposition [175,176].

On the basis of a series of investigations, it may be commented that the thermal decomposition method is a powerful synthetic route for producing high quality monodispersed and magnetic susceptible nanoparticles with good crystallinity, particle size distribution, and particle size tunability. Despite of all these significant advantages the MNPs synthesized in this process cannot be used directly for biomedical applications. This is attributed to the use of non-biocompatible molecules for stabilizing the iron oxide nanoparticles. For example, coating of the surface of iron oxide nanoparticles with long alkyl chain molecules, namely, oleic acid, oleylamine, 1, 2 - hexadecanediol *etc.*, which are unsuitable for their uses in drug delivery as the coating agents would require organic solvents such as hexane, chloroform, toluene, etc for their dispersion or would require further modification [177]. Therefore, even though the method is based on a simple approach but still it is associated with the disadvantage of the poor dispersibility of the synthesized MNPs around neutral pH or in physiological conditions, and hence limits its *in vivo* applications. Therefore various other methods were also proposed to synthesize MNPs with good aqueous dispersibility. This type of MNPs were prepared by pyrolyzing Fe(acac)<sub>3</sub> in 2-pyrrolidone in the presence of monocarboxyl-terminated poly(ethylene glycol) (MPEGCOOH) [168-170]. Similarly dicarboxyl-terminated PEG (HOOC-PEG-COOH) was also utilized to synthesize biocompatible MNPs [168]. But in both of these cases for delivery of any biomolecules it has to be conjugated covalently to the surface carboxylate residues. Similarly synthesis of MNPs with good aqueous dispersibility was achieved by coating the MNPs with PVP (polyvinyl pyrrolidone) by means of a ‘‘one-pot’’ reaction where Fe(acac)<sub>3</sub> was pyrolyzed in N-vinyl-2-pyrrolidone (NVP) at 200 °C [173]. It was noted that the MNPs which were synthesized by the above mentioned thermal decomposition method though resulted in biocompatible MNPs with good aqueous dispersibility, but these MNPs bear a surface reactive moiety which limits their further modification. Therefore solvent free

thermal decomposition route has been reported for the preparation of SPIONs in powdered form [178].

Further the concept of thermal decomposition was extended to synthesize superparamagnetic iron oxide nanoparticles (SPIONs) using microwave where SPIONs of uniform size and different shapes were produced [179, 180]. But this method was reported to produce MNPs which are unstable in nature. Therefore, other synthetic route of hydrothermal synthesis to prepare monodispersed iron oxide nanoparticles, based on aqueous reactions was carried out by several researchers under high pressure and temperature [181]. This technique was usually used for producing ferrites where phase transferring processes at liquid (ethanol-linoleic acid)/ solid (metal linoleate) and solid/solution (water-ethanol) interfaces was carried out. This process was carried out in combination with reduction reaction which was reported to occur in the vicinity of solid/solution interface and *in-situ* particle surface coating.

Microemulsion technique based on water in oil system has also been reported to synthesize MNPs [182, 183]. This method was accomplished by allowing interaction of aqueous microdroplets in oil (emulsion) as a reaction centre. It may be noted that the iron precursors which are not reactive in the organic phase, formed precipitates of MNPs in aqueous phase and were dispersible in water. In this method size and shape of the MNPs can be varied by modulating parameters such as size and shape of aqueous droplets. Thus this method offered a good control over the size [184, 185]. It may also be noted that due to restricted space in the aqueous microdroplets a low yield of MNPs was obtained by this method. In addition, the removal of excess surfactants after the completion of synthesis, which assisted in the dispersion of MNPs, is a cumbersome process [186].

Further the magnetite nanoparticles with well-defined size, shape (spherical/ ellipsoid), structure and magnetic properties were also reported to be synthesized by sol-gel method [187]. However this method is more appropriate for synthesis of powders of magnetic particles [188]. The gelation step in sol-gel processes generally takes a few days for completion. In addition to this the high temperature required for solvent removal from the gel affects the crystallinity of MNPs [189].

It was interesting to note that the large-scale production MNPs were achieved using supercritical fluid technology. In this regard, rapid thermal decomposition of precursors in solution (RTDS) was utilized effectively [190-193]. Here the precursor iron salt solution is directly brought to a supercritical condition by mixing with another stream of super cooled

H<sub>2</sub>O. This led to the rapid heating rate and high reaction rate to produce MNPs [194]. The high self-dissociation and low dielectric constant of super cooled H<sub>2</sub>O allowed the precipitation of iron oxide without the addition of any strong bases, as otherwise required in conventional precipitation methods [195]. The use of super cooled H<sub>2</sub>O substituted the need of organic solvents and hence the problem of the residual solvent and its removal was absent. Similar to RTDS method, MNPs with size of ~50 nm were successfully synthesized without the addition of strong bases by continuous supercritical hydrothermal synthesis (CSHS) [196]. Sonochemical method was also found to be effective in synthesizing MNPs. In this method, Fe(CO)<sub>5</sub> is used as a precursor which results in a narrow size distribution. But due to inferior particle size tunability the method has not been popular [197, 198].

The current progress in the synthesis of SPIONs is focused towards the use of sonochemical routes [199-201]. In this regard the ultrasonication method is used to prepare monodispersed MNPs. Here a high energy is created by means of the acoustic cavitation which provides localized heat with a temperature of about 5000 K. At this temperature, the collision of bubbles generated by ultrasonication leads to the formation and growth of nuclei of MNPs [201]. Though various shapes of MNPs can be prepared by this method but synthesis at large scale is a challenge.

Similarly reverse precipitation method was developed to prepare uniform sized MNPs (~10 nm) which combined precipitation with the ultrasonic irradiation of FeSO<sub>4</sub>.7H<sub>2</sub>O. Here the sizes and their distributions could be controlled by the feeding conditions of aqueous solution of FeSO<sub>4</sub>.7H<sub>2</sub>O. In the same way under the ultrasonic irradiation, monodispersed magnetite nanoparticles were synthesized by using Fe(OH)<sub>2</sub> precipitate in an ethanol-water solution [202].

Recently, various investigations have also been carried out for the biomimetic synthesis of SPIONs by magnetotactic bacteria using bacteria, fungi, Mms6 protein, or globular protein [203 - 208].

The MNPs ranging between 26 and 38 nm were synthesized by metal-reducing bacterium, *Shewanella sp. strain HN-41*, where a precursor iron oxyhydroxide akaganeite ( $\beta$ -FeOOH) was produced by reducing Fe<sup>3+</sup> ions [209]. Similarly the superparamagnetic MNPs of about 2 to 4 nm were also synthesized efficiently at room temperature using *Haejae-1* and *Shewanella sp.* in the presence of glucose and akaganeite ( $\beta$ -FeOOH) [210]. The MNPs were also produced by *Theroanaerobacter ethanolicus* and *Shewanella* species by reduction of Fe(III) in aqueous medium at pH between 6.5 and 9, with ambient pressure

and temperature below 70 °C [211]. However, by this route of synthesis, the sizes and shapes of MNPs were reported to be inconsistent. Further the large scale production of MNPs is also difficult by this route [212].

Even though so many different methods are developed till date but still the hydrolytic routes to synthesize MNPs is quite popular. Amongst various hydrolytic synthetic routes the co-precipitation is one of the most commonly used method and was first reported in 1925 to produce magnetite by co-precipitating  $\text{Fe}^{2+}/\text{Fe}^{3+}$  ions in aqueous solutions [213]. The method of co-precipitation was further developed in 1956 by partial oxidation of a solution of  $\text{Fe}^{2+}$  ions with  $\text{KNO}_3$  in alkaline solution at 90 °C [214]. Similarly magnetite was also synthesized by partial reduction of  $\text{Fe}^{3+}$  salt under alkaline conditions [215]. The MNPs were synthesized by using of ferrous ammonium sulphate in conjugation with  $\text{FeCl}_3$  at 5 °C and 27 °C in the presence of the stabilizer hexamine [216]. Likewise the stable magnetic colloidal solution can be synthesized in the alkaline solution, and more importantly, in the absence of organic surface capping agents. In addition to these various methods, the influence of other parameters like type of base (ammonia,  $\text{CH}_3\text{NH}_2$  or  $\text{NaOH}$ ), pH, temperature, concentration of cations, *e.g.*,  $[(\text{N}(\text{CH}_3)_4)^+]$ ,  $[\text{CH}_3\text{NH}_3]^+$ ,  $\text{NH}_4^+$ ,  $\text{Na}^+$ ,  $\text{Li}^+$ ,  $\text{K}^+$  and the ratio of  $\text{Fe}^{2+}/\text{Fe}^{3+}$  were meticulously investigated on yield of the coprecipitation reaction to assess different sizes of polydispersed MNPs [217]. It has been observed that under the optimized conditions, the average particle size can be achieved between 4 to 16 nm [218]. Generally the following overall chemical precipitation reaction for the formation of  $\text{Fe}_3\text{O}_4$  may be written as follows:



According to the thermodynamics of the above stated reaction, a complete precipitation of  $\text{Fe}_3\text{O}_4$  is expected between pH 9 and pH 14, while maintaining a molar ratio of  $\text{Fe}^{3+}:\text{Fe}^{2+}$  as 2:1 under a non-oxidizing oxygen free environment. Otherwise,  $\text{Fe}_3\text{O}_4$  might also be oxidized as shown under:



However, during the synthesis of 'bare' magnetic iron oxide particles in alkaline pH (>9) the formation of iron hydroxide impurities may also be observed. Therefore, various types of stabilizing agents, namely like surfactants, polymers or coating with inorganic components, including silica, carbon, precious metals (such as Ag and Au) are used during the synthesis of MNPs. These stabilizers maintain the colloidal stability of iron oxide particles as well as to avoid the formation of unwanted iron hydroxide impurities. It may be

noted that the co-precipitation technique is an intricate approach as the shape and size distribution of the MNPs produced is dependent on various synthetic parameters as well as on the equilibrium of hydrolysis of ferric and ferrous ions [219]. Therefore in general the MNPs prepared via the co-precipitation method are typically characterized by broad size distributions. This may be modulated by particle size-sorting procedures as well as by the use of efficient stabilizing agents [220]. It may further be noted that the synthesis should be performed in controlled atmosphere to avoid unwanted oxidation. In spite of these intrinsic problems the method is still widely used due to the ease of synthesis, possibility of large-scale synthesis with good reproducibility and low cost of production. Further the MNPs obtained by co-precipitation method show high superparamagnetism, moderate size, high crystallinity, large surface areas, high magnetic saturation magnetization, and good dispersibility in aqueous medium [221]. Therefore though the MNPs prepared by organic phase route results in to well-defined monodisperse size but still co-precipitation is preferred, for biomedical applications.

Overall, it may be observed that the preparation of MNPs was very similar to that for bulk magnetite except that the growth of nuclei required effective inhibition so as to obtain particles of nanoscale dimensions. But due to the charge and surface chemistry of SPIONs the Van der Waals attractive forces could lead to the agglomeration of particles. In this regard, electrostatic stabilization and steric stabilization were adopted to prevent the agglomeration to obtain MNPs of desired sizes with good stability [177]. The electrostatic stabilization is attributed to the columbic repulsion between the particles which originates by the electrical double layer formed by adsorbed ions on the particle surface for e.g. in case of iron oxide nanoparticles the citrate ions are used as the reducing agent as well as an electrostatic stabilizer [222]. This stabilization is kinetic in nature which is applicable only to dilute systems. Thus in order to overcome the associated disadvantages, steric stabilization is followed which is due to the coordination of sterically demanding organic molecules, surfactants, and polymers. These molecules sterically stabilize colloidal dispersion of the metals which in turn provides thermodynamic stability to the system. Amongst the various available stabilizers, polymers are considered to be better steric stabilizing agents [177]. The polymer coating offers a protective layer to the encapsulated SPIONs from oxidizing and from any changes in magnetic properties. Furthermore, the polymer coating could also offer a protective layer to SPIONs from leaching in acidic of conditions of stomach [223]. In addition, the polymer coating also allows binding of drugs



by covalent attachment, adsorption or entrapment on the particles. These agents not only impart colloidal stability but also modify the surface of MNPs. It must be noted that as per the concepts of Lewis acid–base as well as that of the hard and soft acids and bases (HSAB), the iron atom on the surface of MNPs is a hard Lewis acid, while compounds containing O or N atoms are soft bases. In this regard various polymers were studied.

#### 1.4.2.2 Polymers for encapsulating MNPs

In general, various biopolymers such as carbohydrates like starch, dextran, chitosan, alginate, gum arabic, proteins like albumin and synthetic polymers such as poly ethylene glycol (PEG), poly vinyl alcohol (PVA), poly methacrylic acids (PMMA), poly lactic co-glycolic acid (PGLA), polystyrene, polyethylene, poly vinyl pyrrolidone (PVP) as well as AB and ABC-type block copolymers containing the fragments of the above stated polymers have been used [223-237]. However, the adsorptions of these polymers on the surface of the MNPs are usually dependent on the pH. This suggests that the electrostatic interaction is a significant factor for the coating of MNPs. Notably, magnetite is an amphoteric solid, with  $\text{pH}_{\text{ZPC}}$  (pH at zero point charge) of  $\sim 6.5$  [238]. Below the  $\text{pH}_{\text{ZPC}}$ , protonation of the surface of MNPs would lead to the formation of  $\text{Fe-OH}_2^+$  moieties, while deprotonation occurring above the isoelectric point which would give rise to  $\text{Fe-O}^-$  surface moieties. This, in turn, would affect the electrostatic interaction between MNPs and various other molecules. Apart from the electrostatic interaction, ligand exchange (surface complexation), hydrophobic interaction, entropic effect, hydrogen bonding, and cation bridging also play important roles in the adsorption of stabilizing agents on the surface of MNPs [177]. Moreover, a detailed investigation on interaction of MNPs with substituted benzoic acids/ phenols of humic and a fulvic acid were reported [239]. The obtained results revealed that the carboxyl functional groups are more active or more important than hydroxyl groups. However, the iron atom forms a mononuclear chelating complex structure simultaneously with hydroxyl groups as well as the carboxyl groups especially when the hydroxyl group is ortho-positioned with respect to the carboxyl groups. Probably this is the reason for the efficient adsorption of carbohydrates, which are abundant in hydroxyl groups, carboxylic groups (in pectin, alginate *etc.*) and amino groups (in chitosan) on the surface of MNPs.

## 1.5 AIM AND SCOPE

SPIONs coated with biodegradable polymers have attracted a great deal of attention for fabricating targeted drug delivery system. This is attributed to their unique capabilities like high stability, high carrier capacity, and feasibility of incorporation of both hydrophilic and hydrophobic substances, along with the possibilities for variable routes of administration. Further, their non-cytotoxicity effect made them suitable material for drug delivery.

Amongst the natural polymers, chitosan and pectin alone and in the combination have gained noteworthy consideration in the field of drug delivery due to their inherent properties like biodegradability, biocompatibility and non-toxicity. In the view of the reports available the present project was focused towards the development of hybrid nanomaterials using pectin, chitosan and in their combination.

Not only there was a scope for exploring synthesis of SPIONs with alternate biodegradable materials, but there was a challenge for reducing the size of such drug carriers to 100 nm or lesser. The available literature mostly corresponded to those of polymeric magnetic micro beads of gels, where the sizes were either in micrometer or sub-micrometer range, even a few reports of their nanomaterials is also available.

The aim of this project is to fabricate and evaluate nanomaterial based drug delivery systems comprising of the following:

- i) To synthesize stable iron oxide nanoparticles, especially the magnetite nanoparticles.
- ii) To fabricate magnetite nanoparticles coated with pectin as a novel magnetic hybrid nanomaterials for drug loading and targeted delivery. Emphasis has been to reduce the size of the carrier to 100 nm. Pectin is chosen as it is not only economical but is biocompatible.
- iii) To study the loading efficiencies of drugs in these nanomaterials. Diclofenac sodium will be used as a model drug for this study. In addition use of anti-cancer drugs, like 5-fluorouracil and oxaliplatin loaded in hybrid magnetic and polymeric nanomaterials would be of prime interest. It would be a challenge to increase the loading efficiency of anti-cancer drugs namely 5-fluorouracil (5-FU) and oxaliplatin in these nano hybrid materials.
- iv) To study the feasibility of enhancement in loading efficiency of diclofenac sodium in magnetite coated with pectin, reinforced with chitosan.

- v) To study the *in vitro* sustained / controlled release patterns of the drug from the nanomaterials in the simulated gastrointestinal fluid, comprising gastric fluid, intestinal fluid and colonic fluid at their respective pH.
- vi) To study the *in vitro* sustained / controlled release patterns of the drug from the nanomaterials in the simulated phosphate buffer solution to mimic drug release in blood.
- vii) To study *in vitro* cytotoxicity of 5-FU loaded and oxaliplatin loaded in magnetite-pectin nanohybrid system in cancer cell lines.

The synthesized nanomaterials at various stages will be characterized by an array of techniques, namely, X-ray diffraction (XRD),  $^{57}\text{Fe}$  Mössbauer spectroscopy, scanning electron microscopy with energy dispersive X-ray analysis (SEM-EDAX), transmission electron microscopy (TEM), Fourier transform infrared spectroscopy (FT-IR), thermal analysis (TG-DTA), dynamic light scattering (DLS), X-ray photoelectron spectroscopy (XPS), vibrating sample magnetometer (VSM), superconducting quantum unit interference device (SQUID), UV-visible spectrophotometry, instrumental neutron activation analysis (INAA) and inductively couple plasma mass spectrometry (ICPMS).

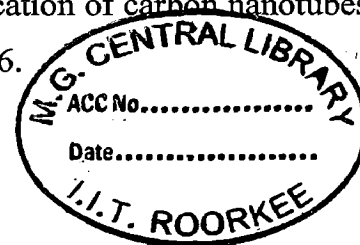
## REFERENCES

1. Huang, C.C.; Chaung, K.Y.; Chou, C.P.; Wu, M.T.; Sheu, H.S., Shieh, D.B.; Tsai, C.Y.; Su, C.H.; Lei, H.Y.; Yeh, C. S. Size-control synthesis of structure deficient truncated octahedral  $\text{Fe}_3\text{-}^{\delta}\text{O}_4$  nanoparticles: high magnetization magnetites as effective hepatic contrast agents. *J. Mater. Chem.*, **2011**, *21*, 7472-7479.
2. Nguyen, D.T.; Kim, D.J.; Kim, K.S. Controlled synthesis and bimolecular probe application of gold nanoparticles. *Micron*. **2011**, *42*, 207-227.
3. Wang, Y.; Qin, Y.; Li, G; Zuolin, C., Zhang, Z. One-step synthesis and optical properties of blue titanium suboxide nanoparticles, *J. Cryst. Growth*. **2005**, *282*, 402-406.
4. Lopeandía, A.F.; Viejo, A.R. Size-dependent melting and supercooling of Ge nanoparticles embedded in a  $\text{SiO}_2$  thin film. *Thermo. Chemica Acta*. **2007**, *461*, 82-87.
5. Sriraman, K.R.; Raman, S.G.S.; Seshdri, S.K. Influence of crystallite size on the hardness and fatigue life of steel samples coated with electrodeposited nanocrystalline Ni–W alloys. *Mater. Lett*. **2007**, *61*, 715-771.
6. Hecq, J.; Deeleeers, M.; Fanara, D.; Vranckx, H.; Amighi, K. Preparation and characterization of nanocrystals for solubility and dissolution rate enhancement of nifedipine. *Int. J. Pharm.* **2005**, *299*, 167-177.
7. Pardeike, J.; Hommoss, A.; Rainer, H.; Müller. Lipid nanoparticles (SLN, NLC) in cosmetic and pharmaceutical dermal products. *Int. J. Pharm.* **2009**, *366*, 170-184.
8. Pradeep, T.; Anshup. Noble metal nanoparticles for water purification. *Thin Solid Films*. **517**, **2009**, 6441-6478.
9. Brigger, C.; Dubernet, P.; Couvreur. Nanoparticles in cancer therapy and diagnosis. *Adv. Drug Delivery Rev.* **2002**, *54*, 631-651.
10. Bhojani, M.S.; Dort, M.V.; Rehemtulla, A.; Ross, B. D. Targeted Imaging and Therapy of Brain Cancer Using Theranostic Nanoparticles. *Mol. Pharmaceutics*. **2010**, *7*, 1921–1929.
11. Kievit, F. M.; Zhang, M. Surface Engineering of Iron Oxide Nanoparticles for Targeted Cancer Therapy. *Acc. Chem. Res.* **2011**, *44*, 853–862.
12. Torchillin. V. P.; *Nanoparticles as drug carriers*, imperial college press, London, **2006**.

13. Mahdihassan, S.; Alchemy. Chinese versus Greek, an etymological approach: a rejoinder, *Am. J. Chin. Med.* **1988**, *16*, 83–86.
14. Brayner, R. The toxicological impact of nanoparticles. *NanoToday*, **2008**, *3*, 348–355.
15. Zhang, L.; Webster, T. Nanotechnology and nanomaterials: Promises for improved tissue regeneration. *J. Nano Today*. **2009**, *4*, 66–80.
16. Venkataraman, S.; Hedrick, J. L.; Ong, Z. Y.; Yang, C.; Rachel, E. L.; Paula, T. H.; Yang, Y. Y. The effects of polymeric nanostructure shape on drug delivery. *Adv. Drug Delivery Rev.* **2011**, *63*, 1228-1246.
17. Wang, Y.; Xia, Y. Bottom-Up and Top-Down Approaches to the Synthesis of Monodispersed Spherical Colloids of Low Melting-Point Metals. *Nano Lett.* **2004**, *4*, 2047–2050.
18. Tartaj, P.; Morales, M. P.; Verdaguer, S.V.; Carreno, T. G.; Serna, C. J. The preparation of magnetic nanoparticles for applications in biomedicine. *J. Phys. D: Appl. Phys.* **2003**, *36*, 182–197.
19. Iwasaki, T.; Kosaka, K.; Watano, S.; Yanagida, T.; Kawai, T. Novel environmentally friendly synthesis of superparamagnetic magnetite nanoparticles using mechanochemical effect. *Mater. Res. Bull.* **2010**, *45*, 481-485.
20. Byrappa, K.; Ohara, S.; Adschiri, T. Nanoparticles synthesis using supercritical fluid technology – towards biomedical applications. *Adv. Drug Deliver. Rev.* **2008**, *60*, 299-327.
21. Roy, K.; Lahiri S. In situ gamma radiation: One step environmentally benign method to produce gold-palladium bimetallic nanoparticles. *Anal. Chem.* **2008**, *80*, 7504-7507.
22. Takesue, I.; Haruyama, J.; Murata, N.; Chiashi, S.; Murayama, S.; Sugai, T.; Shinohara, H. Superconductivity in entirely end-bonded multi-walled carbon nanotubes *Physica C: Superconductivity*, **2007**, 460-462, 111-115.
23. Partha, R.; Conyers, J.L. Biomedical applications of functionalized fullerene-based nanomaterials. *Int. J. Nanomedicine.* **2009**, *4*, 261–275.
24. Kelly, K. L.; Coronado, E.; Zhao, L.L.; Schatz, G.C. The Optical Properties of Metal Nanoparticles: The Influence of Size, Shape, and Dielectric Environment. *J. Phys. Chem. B*, **2003**, *107* (3), 668–677.
25. Gustafsson, S.; Fornara, A.; Petersson, K.; Johansson, C.; Muhammed, M.; Olsson, E. Evolution of Structural and Magnetic Properties of Magnetite Nanoparticles for Biomedical Applications. *Cryst. Growth Des.* **2010**, *10* (5), 2278–2284.

26. Greshnykh, D.; Msdorf, A.F.; Weller, H.; Klinke, C. On the Electric Conductivity of Highly Ordered Monolayers of Monodisperse Metal Nanoparticles. *Nano Lett.* **2009**, *9* (1), 473–478.
27. Zhang, Y.; So, M.K.; Rao, J. Protease-Modulated Cellular Uptake of Quantum Dots. *Nano Lett.* **2006**, *6* (9), 1988–1992.
28. Wu, C.; Bull, B.; Szymanski, C.; Christensen, K.; McNeill, J. Multicolor Conjugated Polymer Dots for Biological Fluorescence Imaging. *ACS Nano*, **2008**, *2* (11), 2415–2423.
29. Roy, K.; Lahiri, S. A green method for synthesis of radioactive gold nanoparticles, *Green Chem.* **2006**, *8*, 1063–1066.
30. Kumar, C. S. S. R.; Mohammad, F. Magnetic nanomaterials for hyperthermia-based therapy and controlled drug delivery. *Adv. Drug Deliv. Rev.* **2011**, *63*(9), 789-808.
31. Arruebo, M.; Fernandez-Pacheco, R.; Ibarra, M.R.; Santamaria, J. Magnetic nanoparticles for drug delivery. *Nano Today*, **2007**, *2* (3), 22-32.
32. Kayal, S.; Ramanujan, R. V. Doxorubicin loaded PVA coated iron oxide nanoparticles for targeted drug delivery. *Mater. Sci. Eng.* **2010**, *30*, 484–490.
33. Barbault, F.S.; Gref, R.; Russo, P.; Guechet, J.; Bochot, A. Design of poly-epsilon-caprolactone nanospheres coated with bioadhesive hyaluronic acid for ocular delivery, *J. Control. Release* **2002**, *83*, 365–375.
34. Suri, S.; Fenniri, H.; Singh, B. Nanotechnology-based drug delivery systems. *J. Occup. Med. Toxicol.* **2007**, 2-16.
35. Acharya, S.; Sahoo, S. K. PLGA nanoparticles containing various anticancer agents and tumour delivery by EPR effect. *Adv. Drug Deliver. Rev.* **2011**, *63*, 170–183.
36. Muthu, M. S.; Rawat, M. K.; Mishra, A.; Singh, S. PLGA nanoparticle formulations of risperidone preparation and neuropharmacological evaluation. *Nanomedicine.* **2009**, *5* (3), 323-333.
37. Kratz, F. Albumin as a drug carrier: Design of prodrugs, drug conjugates and nanoparticles. *J. Control. Release*, **2008**, *132*, 171-183.
38. Gaihre, B.; Khil, M. S.; Lee, D. R.; Kim, H. Y. Gelatin-coated magnetic iron oxide nanoparticles as carrier system: drug loading and *in vitro* drug release study. *Int. J. Pharm.* **2009**, *365* (1-2), 180-189.

39. Aumelas, A.; Serrero, A.; Durand, A.; Dellacherie, E.; Leonard, M. Nanoparticles of hydrophobically modified dextrans as potential drug carrier systems. *Colloids. Surf. B.* **2007**, *59*, 74-80.
40. Yu, C.Y.; Jia, L.H.; Yin, B.C.; Zhang, X.Z.; Cheng, S.X.; Zhuo, R.X. Fabrication of Nanospheres and Vesicles as Drug Carriers by Self-Assembly of Alginate. *J. Phys. Chem.* **2008**, *112*, 16774–16778.
41. Yu, C. Y.; Cao, H.; Zhang, X. C.; Zhou, F. Z.; Cheng, S. X.; Zhang, X. Z.; Zhuo, R. X. Hybrid nanospheres and vesicles based on pectin as drug carriers. *Langmuir.* **2009**, *25*, 11720-11726.
42. Wang, Q.; Zhang, J.; Wang, A. Preparation and characterization of a novel pH-sensitive chitosan-g-poly (acrylic acid)/ attapulgitite/ sodium alginate composite hydrogel bead for controlled release of diclofenac sodium. *Carbohydr. Polym.* **2009**, *78*, 731–737.
43. Gan, Q.; Wang, T. Chitosan nanoparticle as protein delivery carrier-systematic examination of fabrication conditions for efficient loading and release. *Colloids Surf. B.* **2007**, *59 (1)*, 24-34.
44. Jain, A. K.; Khar, R. K.; Ahmed, F. J.; Diwan, P. V. Effective insulin delivery using starch nanoparticles as a potential trans-nasal muco adhesive carrier. *Eur.J.Pharm. Biopharm.* **2008**, *69*, 426-435.
45. Liu, Z.; Jiao, Y.; Wang, Y.; Zhou, C.; Zhang, Z. Polysaccharides-based nanoparticles as drug delivery systems. *Adv. Drug Deliv. Rev.* **2008**, *60 (15)*, 1650-1662.
46. Ehrlich, P. The relations existing between chemical constitution, distribution and pharmacological action, *In: Collected Studies on Immunity*, **1946**, 404–442.
47. Iijima S. Helical microtubes of graphite carbon. *Nature*, **1991**, *354*, 356-358.
48. Zhang, X.; Meng, L.; Lu, Q.; Fei, Z.; Dyson, P.J. Targeted delivery and controlled release of doxorubicin to cancer cells using modified single wall carbon nanotubes. *Biomaterials*, **2009**, *30*, 6041-6047.
49. Sanchez, V.C.; Pietruska, J.R.; Miselis, N.R.; Hurt, R.H.; Kane, A.B. Biopersistence and potential adverse health impacts of fibrous nanomaterials: what have we learned from asbestos. *Nanomed. Nanobiotechnol.* **2009**, *1*, 511–529.
50. Firme, C. P.; Prabhakar, R. B. Toxicity issues in the application of carbon nanotubes to biological systems. *Nanomedicine: NBM.* **2010**, *6*, 245-256.



51. Krueger, A. New carbon materials: Biological applications of functionalized nanodiamond materials. *Chemistry*. **2008**, *14* (5), 1382-1390.
52. Xing, Y.; Dai, L. Nanodiamonds for nanomedicine. *Nanomedicine*. **2009**, *2*, 207–218.
53. Holt, K. B. Diamond at the nanoscale: applications of diamond nanoparticles from cellular biomarkers to quantum computing. *Phys. Eng. Sci.* **2007**, *365*, 2845-2861.
54. Enoki, T.; Takai, K.; Osipov, V.; Baidakova, M.; Vul, A. Nanographene and nanodiamond; new members in the nanocarbon family. *Chem. Asian J.* **2009**, *4*, 796-804.
55. Liu, K. K.; Zheng, W. W.; Wang, C. C.; Chiu, Y. C.; Cheng, C. L.; Lo, Y. S.; Chen, C.; Chao, J. I. Covalent linkage of nanodiamond-paclitaxel for drug delivery and cancer therapy. *Nanotechnology*. **2010**, *21*, 315106.
56. Shimkunas, R. A.; Robinson, E.; Lam, R.; Lu, S.; Xu, X.; Zhang, X. Q.; Huang, H.; Osawa, E.; Ho, D. Nanodiamond-insulin complexes as pH-dependent protein delivery vehicles. *Biomaterials*. **2009**, *30*, 5720-5728.
57. Datta, A.; Kirca, M.; Fu, Y.; To, A.C., Surface structure and properties of functionalized nanodiamonds: a first-principles study. *Nanotechnology* **2011**, *22*, 065706.
58. Chang, I.P.; Hwang, K.C.; Ho, J.A.; Lin, C.C.; Hwu, R.J.R.; Horng, J.C., Facile Surface Functionalization of Nanodiamonds. *Langmuir*, **2010**, *26* (5), 3685–3689.
59. Podlogar, F.; Gasperlin, M.; Tomsic, M.; Jamnik, A.; Rogac, M. B. Structural characterisation of water-Tween 40/Imwitor 308-isopropyl myristate microemulsions using different experimental methods. *Int. J. Pharm.* **2004**, *276*, 115-128.
60. Brime, B.; Frutos, P.; Bringas, P.; Nieto, A.; Ballesteros, M. P.; Frutos, G. Comparative pharmacokinetics and safety of a novel lyophilized amphotericin B lecithin-based oil-water microemulsion and amphotericin B deoxycholate in animal models. *J. Antimicrob. Chemother.* **2003**, *52* (1), 103-109.
61. He, L.; Wang, G. L.; Zhang, Q. An alternative paclitaxel microemulsion formulation: hypersensitivity evaluation and pharmacokinetic profile. *Int. J. Pharm.* **2003**, *250*, 45-50.
62. Seki, J.; Sonoke, S.; Saheki, A.; Fukui, H.; Sasaki, H.; Mayumi, T. A. nanometer lipid emulsion, lipid nano-sphere (LNS), as a parenteral drug carrier for passive drug targeting. *Int. J. Pharm.* **2004**, *273* (1-2), 75-83.



63. Santos, M. N. S.; Pontes, A.; Pereira, V. M.; Caetano, M. N. Colloidal carriers for benzathine penicillin G: nanoemulsions and nanocapsules. *Int. J. Pharm.* **2000**, *208* (1-2), 71-80.
64. Otilia, M.K.; Israel, R.; Hayat, O. Role of nanotechnology in targeted drug delivery and imaging: a concise review. *Nanomedicine: NBM.* **2005**, *1*, 193–212.
65. Puglia, C.; Rizza, L.; Drechsler, M.; Bonina, F. Nanoemulsions as vehicles for topical administration of glycyrrhetic acid: characterization and *in vitro* and *in vivo* evaluation. *Drug Deliv.* **2010**, *17* (3), 123-129.
66. Bielinska, A. U.; Janczak, K. W.; Landers, J. J.; Makidon, P.; Sower, L. E.; Peterson, J. W.; Baker, J. R., Jr. Mucosal immunization with a novel nanoemulsion-based recombinant anthrax protective antigen vaccine protects against *Bacillus anthracis* spore challenge. *Infect. Immun.* **2007**, *75* (8), 4020-4029.
67. Muthu, M. S.; Mishra, A.; Singh, S. Stimulus responses targeted nanomicelles for effective cancer therapy. *Nanomedicine.* **2009**, *4*(6), 657-667.
68. Sessa, G., Weissman, G. J: Formation of artificial lysosome *in vitro*. *J. Clin. Invest.* **1969**, *48*, 76a-77a.
69. Singodia, D.; Verma, A.; Khare, P.; Dube, A.; Mitra, K. and Mishra, P.R. Investigations on feasibility of *in situ* development of amphotericin B liposomes for industrial applications. *J. Liposome Res.* **2011**, doi: 10.3109/08982104.2011.584317
70. Zhang, J. L.; Srivastava, R. S.; Misra, R. D. K. Core-shell magnetite nanoparticles surface encapsulated with smart stimuli-responsive polymer: synthesis, characterization, and LCST of viable drug-targeting delivery system. *Langmuir*, **2007**, *23*, 6343-6351.
71. Zhu, L.; Huo, Z.; Wang, L.; Tong, X.; Xiao, Y.; Ni, K. Targeted delivery of methotrexate to skeletal muscular tissue by thermosensitive magnetoliposomes. *Int. J. Pharm.* **2009**, *370* (1-2), 136-143.
72. Mehnert, W.; Mader, K. Solid lipid nanoparticles Production, characterization and applications. *Adv. Drug Delivery Rev.* **2001**, *47*, 165–196
73. Garg, A.; Singh, S. Enhancement in antifungal activity of eugenol in immunosuppressed rats through lipid nanocarriers. *Colloid Surf. B.* **2011**, *87*, 280–288.

74. Boas, U.; Christensen, J.B.; Heegaard, P.M.H.; Dendrimers in medicine and biotechnology: new molecular tools, **2006**, 1-6.
75. Padilla De Jesus, O. L.; Ihre, H. R.; Gagne, L.; Frechet, J. M.; Szoka, F. C., Jr. Polyester dendritic systems for drug delivery applications: *in vitro* and *in vivo* evaluation. *Bioconjug. Chem.* **2002**, *13*, 453-461.
76. Kihara, F. Arima, H.; Tsutsumi T.; Hirayama, F.; Uekama, Kaneto. Effects of structure of polyamidoamine dendrimer on gene transfer efficiency of the dendrimer conjugate with alpha-cyclodextrin. *Bioconjugate Chem.* **2002**, *13*, 1211–1219.
77. Astruc, D.; Boisselier, E.; Ornelas, C. Dendrimers designed for functions: from physical, photophysical, and supramolecular properties to applications in sensing, catalysis, molecular electronics, photonics, and nanomedicine. *Chem. Rev.* **2010**, *110*, 1857-1959.
78. Tekade, R. K.; Dutta, T.; Gajbhiye, V.; Jain, N. K. Exploring dendrimer towards dual drug delivery: pH responsive simultaneous drug-release kinetics. *J. Microencapsul.* **2009**, *26*, 287-296.
79. Quintana, A.; Raczka, E.; Piehler, L.; Lee, I.; Myc, A.; Majoros, I.; Patri, A. K.; Thomas, T.; Mule, J.; Baker, J. R., Jr. Design and function of a dendrimer-based therapeutic nanodevice targeted to tumor cells through the folate receptor. *Pharm. Res.* **2002**, *19*, 1310-1316.
80. Jevprasesphant, R.; Penny, J.; Jalal, R.; Attwood, D.; McKeown, N. B.; D'Emanuele, A. The influence of surface modification on the cytotoxicity of PAMAM dendrimers. *Int. J. Pharm.* **2003**, *252* (1-2), 263-266.
81. Roe, D.; Karandikar, B.; Bonn-Savage, N.; Gibbins, B.; Rouillet, J. B. Antimicrobial surface functionalization of plastic catheters by silver nanoparticles. *J. Antimicrob. Chemother.* **2008**, *61*, 869-876.
82. Kattumuri, V.; Katti, K.; Bhaskaran, S.; Boote, E. J.; Casteel, S. W.; Fent, G. M.; Robertson, D. J.; Chandrasekhar, M.; Kannan, R.; Katti, K. V. Gum arabic as a phytochemical construct for the stabilization of gold nanoparticles: *in vivo* pharmacokinetics and X-ray-contrast-imaging studies. *Small.* **2007**, *3*, 333-341.
83. Sperling, R. A.; Rivera, G. P.; Zhang, F.; Zanella, M.; Parak, W. J. Biological applications of gold nanoparticles. *Chem. Soc. Rev.* **2008**, *37*, 1896-1908.

84. Patra, C. R.; Bhattacharya, R.; Mukhopadhyay, D.; Mukherjee, P. Fabrication of gold nanoparticles for targeted therapy in pancreatic cancer. *Adv. Drug Deliv. Rev.* **2010**, *62*, 346-361.
85. Kobayashi, T. Cancer hyperthermia using magnetic nanoparticles. *Biotechnol. J.* **2011**, *11*, 1342-1347.
86. Luangtana-anan, M.; Opanasopit, P.; Ngawhirunpat, T.; Nunthanid, J.; Sriamornsak, P.; Limmatvapirat, S.; Lim, L.Y. Effect of chitosan salts and molecular weight on a nanoparticulate carrier for therapeutic protein. *Pharm. Dev. Technol.* **2005**, *10*, 189–196.
87. Prabakaran, M.; Grailer, J. J.; Steeber, D. A.; Gong, S. Stimuli-responsive chitosan-graft-poly(N-vinylcaprolactam) as a promising material for controlled hydrophobic drug delivery. *Macromol. Biosci.* **2008**, *8*, 843-851.
88. Patil, Y.; Panyam, J. Polymeric nanoparticles for siRNA delivery and gene silencing. *Int. J. Pharm.* **2009**, *367*, 195-203.
89. Jayakumar, R.; Menon D.; Manzoor, K.; Nair, S. V.; Tamura, H. Biomedical applications of chitin and chitosan based nanomaterials. *Carbohydr. Polym.* **2010**, *82*, 227-232.
90. Wang, Q.Z.; Chen, X.G.; Liu, N.; Wang, S.X.; Liu, C.S.; Meng, X.H.; Liu, C.G. Protonation constants of chitosan with different molecular weight and degree of deacetylation. *Carbohydr. Polym.* **2006**, *65*, 194-200.
91. Naruphontjirakul, P.; Viravaidya-Pasuwat, K. Development of doxorubicin – core shell O-succinyl chitosan graft pluronic<sup>®</sup>127 copolymer nanoparticles to treat human cancer *IJBBB.* **2011**, *1(2)*, 131-136.
92. Dash, M.; Chiellini, F.; Ottenbrite, R.M.; Chiellini, E. Chitosan A versatile semi-synthetic polymer in biomedical applications. *Prog. Polym. Sci.* **2011**, *36*, 981-1014.
93. Boonsongrit, Y.; Mitrevej, A.; W. Mueller, B. Chitosan drug binding by ionic interaction. *Eur. J. Pharm. Biopharm.* **2006**, *62*, 267-274.
94. Lai, W. F.; Lin M. Nucleic acid delivery with chitosan and its derivatives. *J. Control. Release.* **2009**, *134*, 158-168.
95. Yuan, Q.; Venkatasubramanian, R.; Hein, S.; Misra, R.D.K. A stimulus-responsive magnetic nanoparticle drug carrier: Magnetite encapsulated by chitosan-grafted-copolymer. *Acta Biomaterialia.* **2008**, *4*, 1024–1037.

96. An, X.; Su, Z.; J. Characterization and application of high magnetic property chitosan particles. *Appl. Polym. Sci.* **81**, **2001**, 1175-1181.
97. Jiang, D.; Long, S.; Huang, J.; Xiao, H.; Zhou, J. Immobilization of Pycnopus sanguineus laccase on magnetic chitosan microspheres. *Biochem. Eng. J.* **2005**, *25*, 15-23.
98. Zhang, J.; Xu, S.; Kumacheva, E. Polymer Microgels: Reactors for Semiconductor, Metal, and Magnetic Nanoparticles. *Am. J. Chem. Soc.* **2004**, *126*, 7908-7914.
99. Honda, H.; Kawabe, A.; Shinkai, A.; Kobayashi, T. Development of chitosan-conjugated magnetite for magnetic cell separation. *Ferment. Bioeng.* **1998**, *86*, 191-196.
100. Hwang, H-Y.; Kim, I-S.; Kwon, IC.; Kim, Y-H. Tumor target ability and antitumor effect of docetaxel-loaded hydrophobically modified glycol chitosan nanoparticles. *J. Control. Release*, **2008**, *128*, 23-31.
101. Oh, J. K.; Lee, D. I.; Park, J.M. Biopolymer-based microgels/nanogels for drug delivery applications. *Progress Poly. Sci.* **2009**, 341261-341282.
102. Li, P.; Wang, Y.; Peng, Z.; She, F.; Kong, L. Development of chitosan nanoparticles as drug delivery for 5-fluorouracil and leucovorin blends. *Carbohydr. Polym.* **2011**, *85*, 698-704.
103. Agnihotri, S. A.; Mallikarjuna, N. N.; Aminabhavi, T. M. Recent advances on chitosan-based micro- and nanoparticles in drug delivery. *J. Control. Release*, **2004**, *100*, 5-28.
104. Saboktakin, M.R.; Tabatabaee, R.M.; Maharramov, A.; Ramazanov, M. A. Design and characterization of chitosan nanoparticles-as delivery systems for paclitaxel. *Carbohydr. Polym.* **2010**, *82*, 466-471.
105. Campos, A.M.D.; Sánchez, A.; Alonso, M.J. Chitosan nanoparticles: a new vehicle for the improvement of the delivery of drugs to the ocular surface. Application to cyclosporin A. *Int. J. Pharm.* **224**, 159-168.
106. Wilson, B.; Samanta, M.K.; Santhi, K.; Kumar, K.P.S.; Ramasamy, M.; Suresh, B. Chitosan nanoparticles as a new delivery system for the anti-Alzheimer drug tacrine. *Nanomedicine (NBM)*, **2010**, *6*, 144-152.
107. Makhlof, A.; Tozuka, Y.; Takeuchi, H. Design and evaluation of novel pH-sensitive chitosan nanoparticles for oral insulin delivery. *Eur. J. Pharm. Sci.* **2011**, *42*, 445-451.

108. Grenha, A.; Seijo, B.; Remuñán-López, C. Microencapsulated chitosan nanoparticles for lung protein delivery. *Eur. J. Pharm. Sci.* **2005**, *25* (4-5), 427-437.
109. Mesbahi, G.; Jamalian, J.; Farahnaky A. A comparative study on functional properties of beet and citruspectins in food systems. *Food Hydrocolloids*, **2005**, *19*,731-738.
110. Sorensen, I.; Pedersen, H.L.; Willats, W.G.T. An array of possibilities for pectin. *Carbohydr. Res.* **2009**, *344*, 1872-1878.
111. Rowe, R.C; Sheskey, P. J.; Quinn, M. *Handbook of Pharmaceutical Excipients*; Pharmaceutical Press, Sixth edition, 2009.
112. Tromp, R.H.; de Kruif, C.G.; Eijk, M.V.; Rolin, C. On the mechanism of stabilisation of acidified milk drinks by pectin. *Food Hydrocolloids*, **2004**, *18*, 565-572.
113. Sudheesh, S.; Vijayalakshmi, N. R. Lipid-lowering action of pectin from *Cucumis sativus*. *Food Chem.* **1999**, *67*, 281-286.
114. Cerda, J.J.; Robbins, F.L.; Burgin, C.W.; Baumgartner, T.G.; Rice, R.W. The effects of grapefruit pectin on patients at risk for coronary heart disease without altering diet or lifestyle. *Clin. Cardiol.* **1988**, *11*, 589-594.
115. Liu, L.; Fishman, M. L.; Kost, J.; Hicks, K. B. Pectin-based systems for colon-specific drug delivery via oral route. *Biomaterials*. **2003**, *24*(19), 3333-3343.
116. Ahrabi, S. F.; Madsen, G.; Dyrstad, K.; Sande, S. A.; Graffner, C. Development of pectin matrix tablets for colonic delivery of model drug ropivacaine. *Eur.J.Pharm.Sci.* **2000**, *10* ,43-52.
117. Chambin, O.; Dupuis, G.; Champion, D.; Voilley, A.; Pourcelot, Y. Colon-specific drug delivery: Influence of solution reticulation properties upon pectin beads performance. *Int. J. Pharm.* **2006**, *321*, 86-93.
118. Sriamornsak, P.; Sungthongjeen, S.; Puttipipatkachorn, S. Use of pectin as a carrier for intragastric floating drug delivery: Carbonate salt contained beads. *Carbohydr. Polym.* **2007**, *67*, 436-445.
119. Thirawong, N.; Thongborisute, J.; Takeuchi, H.; Sriamornsak, P., Improved intestinal absorption of calcitonin by mucoadhesive delivery of novel pectin-liposome nanocomplexes. *J. Controlled Release.* **2008**, *125*, 236-245.
120. Maestrelli, F.; Cirri, M.; Corti, G.; Mennini, N.; Mura, P. Development of enteric-coated calcium pectinate microspheres intended for colonic drug delivery. *Eur. J. Pharm. Biopharm.* **2008**, *69*, 508-518.

121. Katav, T.; Liu, L.; Traitel, T.; Goldbart, R.; Wolfson, M.; Kost, J. Modified pectin-based carrier for gene delivery: cellular barriers in gene delivery course. *J. Control. Release.* **2008**, *130*, 183-191.
122. Perera, G.; Barthelmes, J.; Bernkop-Schnurch, A. Novel pectin-4-aminothiophenole conjugate microparticles for colon-specific drug delivery. *J. Controlled Release.* **2010**, *145*, 240-246.
123. Burapapadh, K.; Vollrath, M. K.; Chantasart D.; Sriamornsak, P. Fabrication of pectin-based nanoemulsions loaded with itraconazole for pharmaceutical application. *Carbohydr. Polym.* **2010**, *82*, 384-393.
124. Nguyen, S.; Alund, S. J.; Hiorth, M.; Kjoniksen, A. L.; Smistad, G. Studies on pectin coating of liposomes for drug delivery. *Colloids. Surf. B. Biointerfaces.* **2011**, *88*, 664-673.
125. Hiorth, M.; Tho, I.; Sande, S. A. The formation and permeability of drugs across free pectin and chitosan films prepared by a spraying method. *Eur. J. Pharm. Biopharm.* **2003**, *56*, 175-181.
126. Hagesaether, E.; Hiorth, M.; Sande, S. A. Mucoadhesion and drug permeability of free mixed films of pectin and chitosan: an *in vitro* and *ex vivo* study. *Eur. J. Pharm. Biopharm.* **2009**, *71*, 325-31.
127. José, R. R.; José Ivan X. ; Maria Teresa S. T.; Regina C.M. ; Nágila M.P.S. R; Judith P.A. F. Chitosan-coated pectin beads: Characterization and *in vitro* release of mangiferin. *Food Hydrocolloids.* **2009**, *23*, 2278-2286.
128. Miyazaki, S.; Kubo, W.; Itoh, K.; Konno, Y.; Fujiwara, M.; Dairaku, M.; Togashi, M.; Mikami, R.; Attwood, D. The effect of taste masking agents on *in situ* gelling pectin formulations for oral sustained delivery of paracetamol and ambroxol. *Int. J. Pharm.* **2005**, *297*, 38-49.
129. Giunchedi, P.; Conte, U.; Chetoni, P.; Saettone, M. F. Pectin microspheres as ophthalmic carriers for piroxicam: evaluation *in vitro* and *in vivo* in albinorabbits. *Eur.J.Pharm.Sci.* **1999**, *9*, 1-7.
130. Voragen, A.G.J.; Pilnik, W.; Thibault, J.F.; Axelos, M.A.V.; Renard, C.M.G.C.; Stephen A.M. *Food Polysaccharides and their applications.* **1995**, *21*, 287-339.
131. Cerchia, L.; Franciscis, V. Targeting cancer cells with nucleic acid aptamers. *Trends in Biotechnology*, **2010**, *28*, 517-525.

132. Thomas, A. C.; Campbell, J. H. Conjugation of antibody to cross-linked fibrin for targeted delivery of anti-restenotic drugs. *J. Control. Release.* **2004**, *100*, 357-377.
133. Liu, Y.; Li, K.; Pan, J.; Liu, B.; Feng, S.S. Folic acid conjugated nanoparticles of mixed lipid monolayer shell and biodegradable polymer core for targeted delivery of Docetaxel. *Biomaterials.* **2010**, *31*, 330-338.
134. Veiseh, O.; Jonathan, W.; Gunn, M. Z. Design and fabrication of magnetic nanoparticles for targeted drug delivery and imaging. *Adv. Drug Delivery Rev.* **2010**, *62*, 284-304.
135. He, X.; Hai, L.; Su, J.; Wang, K.; Wu, X. One-pot synthesis of sustained-released doxorubicin silica nanoparticles for aptamer targeted delivery to tumor cells. *Nanoscale.* **2011**, *3*, 2936-2942.
136. Suh, W.; Chung, J.-K.; Park S.H.; Kim S. Wan. Anti-JL1 antibody-conjugated poly (L-lysine) for targeted gene delivery to leukemia T cells, *J. Control. Release.* **2001**, *72*, 171-178.
137. Lu, R.M.; Chang, Y.L.; Chen, M.S.; Wus, H.C. Single chain anti-c-Met antibody conjugated nanoparticles for *in vivo* tumor-targeted imaging and drug delivery. *Biomaterials*, **2011**, *32*, 3265-3274.
138. Negrini, R.; Mezzenga, R.; pH-Responsive Lyotropic Liquid Crystals for Controlled Drug Delivery. *Langmuir*, **2011**, *27*, 5296–5303.
139. Deng, C. X. Targeted drug delivery across the blood-brain barrier using ultrasound technique. *Ther. Deliv.* **2010**, *1*, 819-848.
140. Wu, G.; Mikhailovsky, A.; Khant, H. A.; Fu, C.; Chiu, W.; Zasadzinski, J. A. Remotely triggered liposomal release by near-infrared light absorption via hollow gold nanoshells. *J. Am. Chem. Soc.* **2008**, *130*, 8175–8177.
141. Pedersen, P. J.; Adolph, S. K.; Subramanian, A. K.; Arouri, A.; Andresen, T. L.; Mouritsen, O. G.; Madsen, R.; Madsen, M. W.; Peters, G. H.; Clausen, M. H. Liposomal formulation of retinoids designed for enzyme triggered release. *J. Med. Chem.* **2010**, *53*, 3782-3792.
142. Al-Deen, F.N.; Ho, J.; Selomulya, C.; MaC Coppel R. Superparamagnetic Nanoparticles for Effective Delivery of Malaria DNA Vaccine. *Langmuir.* **2011**, *27*, 3703–3712.

143. Banerjee, S.; Das, T.; Chakraborty, S.; Samuel G.; Korde, A.; Srivastava, S.; Venkatesh, M.; Pillai, M.R.A. Lu-DOTA-lanreotide: a novel tracer as a targeted agent for tumor therapy. *Nucl. Med. Biol.* **2004**, *31*, 753-759.
144. Bawa, P.; Pillay, V.; Choonara, Y. E.; du Toit, L. C. Stimuli-Responsive Polymers and Their Applications in Drug Delivery. *Biomed. Mater.* **2009**, *4*, 022001.
145. Arias, J. L.; López, V. M.; López, V. J.; Delgado, A. V. Development of iron/ethylcellulose (core/shell) nanoparticles loaded with diclofenac sodium for arthritis treatment. *Int. J. Pharm.* **2009**, *382*, 270–276.
146. Bulte, J. W.; Kraitchman, D. L. Iron oxide MR contrast agents for molecular and cellular imaging. *NMR Biomed.* **2004**, *17*, 484-499.
147. Dames, P.; Gleich, B.; Flemmer, A.; Hajek, K.; Seidl, N.; Wiekhorst, F.; Eberbeck, D.; Bittmann, I.; Bergemann, C.; Weyh, T.; Trahms, L.; Rosenecker, J.; Rudolph, C. Targeted delivery of magnetic aerosol droplets to the lung. *Nat. Nanotechnol.* **2007**, *2*, 495-499.
148. Shieh, D. B.; Cheng, F. Y.; Su, C. H.; Yeh, C. S.; Wu, M. T.; Wu, Y. N.; Tsai, C. Y.; Wu, C. L.; Chen, D. H.; Chou, C. H. Aqueous dispersions of magnetite nanoparticles with  $\text{NH}_3^+$  surfaces for magnetic manipulations of biomolecules and MRI contrast agents. *Biomaterials.* **2005**, *26*, 7183-7191.
149. Nigam S., Barick K. C., Bahadur D. Development of citrate-stabilized  $\text{Fe}_3\text{O}_4$  nanoparticles: Conjugation and release of doxorubicin for therapeutic applications. *J. Magn. Mater.* **2011**, *323*, 237–243.
150. Hou, C. H.; Chen, C. W.; Hou, S. M.; Li, Y. T.; Lin, F. H. The fabrication and characterization of dicalcium phosphate dihydrate-modified magnetic nanoparticles and their performance in hyperthermia processes *in vitro*. *Biomaterials.* **2009**, *30*, 4700-4707.
151. Kodama, R.H. Magnetic nanoparticles. *J. Magn. Mater.* **1999**, *200*, 359–372.
152. Liu, F.X.; Li, T. Z. Synthesis and magnetic properties of  $\text{SnFe}_2\text{O}_4$  nanoparticles. *Mater. Lett.* **2005**, *59*, 194-196.
153. Mooney, K. E.; Nelson, J. A.; Wagner M. J. Superparamagnetic Cobalt Ferrite Nanocrystals Synthesized by Alkalide Reduction. *Chem. Mater.* **2004**, *16*, 3155–3161.
154. Nam, J.H.; Kim, W. K.; Park, S. J. Synthesis of nanocrystalline Ni ferrite as a superparamagnetic material. *Phys. Status Solidi A.* **2004**, *20*, 1838–1841.



155. Liu, C.; Zhang, Z. J. Size-dependent superparamagnetic properties of Mn spinel ferrite nanoparticles synthesized from reverse micelles. *Chem. Mater.* **2001**, *13*, 2092–2096.
156. Solis V.T.; Tartaj P., Marban G.; Fuertes A.B. Facile synthetic route to nanosized silica as a hard template. *Nanotechnology*, **2007**, *18*, 145603.
157. Arbab, A. S.; Yocum, G. T.; Kalish, H.; Jordan, E. K.; Anderson, S. A.; Khakoo, A. Y.; Read, E. J.; Frank, J. A. Efficient magnetic cell labeling with protamine sulfate complexed to ferumoxides for cellular MRI. *Blood*. **2004**, *104*, 1217-12123.
158. Tassa, C.; Shaw, S. Y.; Weissleder R. Dextran-Coated Iron Oxide Nanoparticles: A Versatile Platform for Targeted Molecular Imaging, Molecular Diagnostics, and Therapy. *Acc. Chem. Res.*, **2011**, *44*, 842–852.
159. Plank, C. Nanomagnetosols: magnetism opens up new perspectives for targeted aerosol delivery to the lung. *Trends Biotechnol.* **2008**, *26*, 59-63.
160. Rockenberger, J.; Scher, E. C.; Alivisatos, A. P. A New Nonhydrolytic Single-Precursor Approach to Surfactant-Capped Nanocrystals of Transition Metal Oxides *J. Am. Chem. Soc.* **1999**, *121*, 11595-11596.
161. Hyeon, T.; Lee, S. S.; Park, J.; Chung, Y.; Na, H. B. Synthesis of Highly Crystalline and Monodisperse Maghemite Nanocrystallites without a Size-Selection Process. *J. Am. Chem. Soc.* **2001**, *123*, 12798-12801.
162. Hyeon, T. Chemical Synthesis of Magnetic Nanoparticles. *Chem. Commun.* **2003**, *8*, 927-934.
163. Park, J.; An, K.; Hwang, Y.; Park, J. G.; Noh, H. J.; Kim, J. Y.; Park, J. H.; Hwang, N. M.; Hyeon, T. Ultra-Large-Scale Syntheses of Monodisperse Nanocrystals. *Nat. Mater.* **2004**, *3*, 891-895.
164. Sun, S.; Zeng, H. Size-Controlled Synthesis of Magnetite Nanoparticles. *J. Am. Chem. Soc.* **2002**, *124*, 8204-8205.
165. Sun, S.; Zeng, H.; Robinson, D. B.; Raoux, S.; Rice, P. M.; Wang, S. X.; Li, G. Monodisperse  $MFe_2O_4$  (M = Fe, Co, Mn) Nanoparticles. *J. Am. Chem. Soc.* **2004**, *126*, 273-279.
166. Jana, N. R.; Chen, Y.; Peng, X. G. Size- and Shape-Controlled Magnetic (Cr, Mn, Fe, Co, Ni) Oxide Nanocrystals via a Simple and General Approach. *Chem. Mater.* **2004**, *16*, 3931-3935.

167. Cheon, J. W.; Kang, N. J.; Lee, S. M.; Lee, J. H.; Yoon, J. H.; Oh, S. J. Shape evolution of single-crystalline iron oxide nanocrystals . *J. Am. Chem. Soc.* **2004**, *126*, 1950 - 1951.
168. Hu, F.; Li, Z.; Tu, C.; Gao, M. Preparation of Magnetite Nanocrystals with Surface Reactive Moieties by One-Pot Reaction. *J. Colloid. Interface. Sci.* **2007**, *311*, 469-74.
169. Hu, F.Q.; Wei, L.; Zhou, Z.; Ran, Y.L.; Li, Z.; Gao, M.Y. Biocompatible magnetite nanocrystals for *in vivo* magnetic resonance detection of cancer. *Adv. Mater.* **2006**, *18*, 2553-2556.
170. Li, Z.; Wei, L.; Gao, M. Y.; Lei, H. One-Pot Reaction to Synthesize Biocompatible Magnetite Nanoparticles. *Adv. Mater.* **2005**, *17*, 1001-1005.
171. Li, Z.; Chen, H.; Bao, H. B.; Gao, M. Y. One-Pot Reaction to Synthesize Water-Soluble Magnetite Nanocrystals. *Chem. Mater.* **2004**, *16*, 1391-1393.
172. Li, Z.; Sun, Q.; Gao, M. Y. Preparation of Water-Soluble Magnetite Nanocrystals from Hydrated Ferric Salts in 2-Pyrrolidone: Mechanism Leading to Fe<sub>3</sub>O<sub>4</sub>. *Angew. Chem. Int. Ed. Engl.* **2005**, *44*, 123-126.
173. Lu, X.; Niu, M.; Qiao, R.; Gao, M. Superdispersible Pvp-Coated Fe<sub>3</sub>O<sub>4</sub> Nanocrystals Prepared by A "One-Pot" Reaction. *J. Phys. Chem. B.* **2008**, *112*, 14390-14394.
174. Yu, W. W.; Falkner, J. C.; Yavuz, C. T.; Colvin, V. L. Synthesis of monodisperse iron oxide nanocrystals by thermal decomposition of iron carboxylate salts. *Chem. Commun.* **2004**, 2306-2307.
175. Gupta, A. K.; Gupta, M. Synthesis and surface engineering of iron oxide nanoparticles for biomedical applications. *Biomaterials.* **2005**, *26*, 3995-4021.
176. Willard, M.A.; Kurihara, L.K.; Carpenter, E.E.; Calvin, S.; Harris, V.G. Chemically prepared magnetic nanoparticles. *Int. Mater. Rev.* **2004**, *49*, 125-170.
177. Qiao, R.; Yang, C.; Gao, M. Superparamagnetic iron oxide nanoparticles: from preparations to *in vivo* MRI applications. *J. Mater. Chem.* **2009**, *19*, 6274-6293.
178. Maity, D.; Choo, S.G.; Yi, J.B.; Ding, J.; Xue, J.M. Synthesis of magnetite nanoparticles via a solvent-free thermal decomposition route. *J. Magn. Magn. Mater.* **2009**, *321*, 1256-1259.
179. Zhou, H.; Yi, R.; Li, J.; Su, Y.; Liu X. Microwave-assisted synthesis and characterization of hexagonal Fe<sub>3</sub>O<sub>4</sub> nanoplates. *Solid State Sci.* **2010**, *12*, 99-104.
180. Yin, S.; Luo, Z.; Xia, J.; Li, H. Microwave-assisted synthesis of Fe<sub>3</sub>O<sub>4</sub> nanorods and nanowires in an ionic liquid . *J. Phys. Chem. Solids.* **2010**, *71*, 785-788.

181. Kholam, Y.B.; Dhage, S.R.; Potdar, H.S.; Deshpande, S.B.; Bakare, P.P.; Kulkarni, S.D.; Date, S.K. Microwave hydrothermal preparation of submicron-sized spherical magnetite ( $\text{Fe}_3\text{O}_4$ ) powders. *Mater. Lett.* **2002**, *56*, 571–577.
182. Inouye, K.; Endo, R.; Otsuka, Y.; Miyashiro, K.; Kaneko, K.; Ishikawa, T. Oxygenation of ferrous-ions in reversed micelle and reversed micro-emulsion. *J. Phys. Chem.* **1982**, *86*, 1465–1469.
183. Muller, B.W.; Mulle, R.H. Particle-size distributions and particle-size alterations in microemulsions. *J. Pharm. Sci.* **1984**, *73*, 919–922.
184. Munshi, De T. K.; Maitra, A. *J. Colloid. Interface. Sci.* **1997**, *190*, 387-391.
185. Hao, Y. L.; Teja, A. S. Continuous Hydrothermal crystallization of alpha- $\text{Fe}_2\text{O}_3$  and  $\text{Co}_3\text{O}_4$  nanoparticles. *J. Mater. Res.* **2003**, *18*, 415-422.
186. Lu, A. H.; Salabas, E. L.; Schuth, F. A. *Chem. Int. Ed. Engl.* **2007**, *46*(8), 1222.
187. Itoh, H.; Sugimoto, T. Systematic control of size, shape, structure, and magnetic properties of uniform magnetite and maghemite particles. *J. Colloid. Interface. Sci.* **2003**, *265*, 283–295.
188. Xu, J.; Yang, H. B.; Fu, W. Y.; Du, K.; Sui, Y. M.; Chen, J. J.; Zeng, Y.; Li, M. H.; Zou, G. Preparation and magnetic properties of magnetite nanoparticles by sol-gel method *J. Magn. Magn. Mater.* **2007**, *309*, 307-311.
189. Hao, Y. L.; Teja, A. S. Continuous Hydrothermal Crystallization of Alpha- $\text{Fe}_2\text{O}_3$  and  $\text{Co}_3\text{O}_4$  Nanoparticles. *J. Mater. Res.* **2003**, *18*, 415-422.
190. Matson, D. W.; Linehan, J. C.; Bean, R. M. A. S. Continuous hydrothermal crystallization of alpha- $\text{Fe}_2\text{O}_3$  and  $\text{Co}_3\text{O}_4$  nanoparticles. *Mater. Lett.* **1992**, *14*, 222.
191. Matson, D. W.; Linehan, J. C.; Darab, J. G.; Buehler, M. F. Nanophase iron-based liquefaction catalysts synthesis, characterization, and model-compound reactivity. *Energy Fuels.* **1994**, *8*, 10-18.
192. Darab, J. G.; Linehan, J. C.; Matson, D. W. In *enhanced nanoscale catalyst precursor powders generated using a flow-through hydrothermal process*, 29th Intersociety Energy Conversion Engineering Conference, Monterey, CA, August 7-12, **1994**; U.S. Department of Energy, Office of Scientific & Technical Information: Richland, WA, **1994**.
193. Darab, J. G.; Matson, D. W. Continuous Hydrothermal processing of nano-crystalline particulates for chemical-mechanical planarization. *J. Electron. Mater.* **1998**, *27*, 1068-1072.

194. Cote, L. J.; Teja, A. S.; Wilkinson, A. P.; Zhang, Z. J. Continuous hydrothermal synthesis and crystallization of magnetic oxide nanoparticles. *J. Mater. Res.* **2002**, *17*, 2410-2416.
195. Cabanas, A.; Poliakoff, M. The continuous hydrothermal synthesis of nano-particulate ferrites in near critical and supercritical water. *J. Mater. Chem.* **2001**, *11*, 1408-1416.
196. Adschiri, T.; Kanazawa, K.; Arai, K. Rapid and continuous hydrothermal crystallization of metal-oxide particles in supercritical water. *J. Am. Ceram. Soc.* **1992**, *75*, 1019-1022.
197. Abu Mukh-Qasem, R.; Gedanken, A. Sonochemical synthesis of stable hydrosol of Fe<sub>3</sub>O<sub>4</sub> nanoparticles *J. Colloid. Interface. Sci.* **2005**, *284*, 489-494.
198. Cao, X.; Koltypin, Y.; Prozorov, R.; Kataby, G.; J. Preparation of amorphous Fe<sub>2</sub>O<sub>3</sub> powder with different particle sizes. *Mater. Chem.* **1997**, *7*, 2447-2451.
199. Kumar, R.V.; Koltypin, Y.; Xu, X.N.; Yeshurun, Y.; Gedanken, A.; Felner, I. Fabrication of magnetite nanorods by ultrasound irradiation, *J. Appl. Phys.* **2001**, *89*, 6324–6328.
200. Vijayakumar, R.; Koltypin, Y.; Felner, I.; Gedanken, A. Sonochemical synthesis and characterization of pure nanometer-sized Fe<sub>3</sub>O<sub>4</sub> particles. *Mater. Sci. Eng. A.* **2000**, *286*, 101–105.
201. Dang, F.; Enomoto, N.; Hojo, J.; Enpuku, K. A novel method to synthesize monodispersed magnetite nanoparticles, *Chem. Lett.* **2008**, *37*, 530–531.
202. Dang, F.; Enomoto, N.; Hojo, J.; Enpuku, K. Sonochemical synthesis of monodispersed magnetite nanoparticles by using an ethanol-water mixed solvent. *Ultrason. Sonochem.* **2009**, *16*, 649-54.
203. Amemiya, Y.; Arakaki, A.; Staniland, S.S. Tanaka, T.; Matsunaga, T. Controlled formation of magnetite crystal by partial oxidation of ferrous hydroxide in the presence of recombinant magnetotactic bacterial protein Mms6. *Biomaterials.* **2007**, *28*, 5381–5389.
204. Philipse, A.P.; Maas, D. Magnetic colloids from magnetotactic bacteria: chain formation and colloidal stability. *Langmuir.* **2002**, *18*, 9977–9984.
205. Prozorov, T.; Mallapragada, S.K.; Narasimhan, B.; Wang, L.J.; Palo, P.; Nilsen-Hamilton, M.; Williams, T.J.; Bazyliniski, D.A.; Prozorov, R.; Canfield, P.C. Protein mediated synthesis of uniform superparamagnetic magnetite nanocrystals. *Adv. Funct. Mater.* **2007**, *17*, 951–957.

206. Bharde, A.A.; Parikh, R.Y.; Baidakova, M.; Jouen, S.; Hannoyer, B.; Enoki, T.; Prasad, B.L.V.; Shouche, Y.S.; Ogale, S.; Sastry, M. Bacteria-mediated precursor-dependent biosynthesis of superparamagnetic iron oxide and iron sulfide nanoparticles. *Langmuir*. **2008**, *24*, 5787–5794.
207. Roh, Y.; Jang, H.D.; Suh, Y. Microbial synthesis of magnetite and Mn-substituted magnetite nanoparticles: influence of bacteria and incubation temperature. *J. Nanosci. Nanotechnol.* **2007**, *7*, 3938-43.
208. Bharde, A.; Rautaray, D.; Bansal, V.; Ahmad, A.; Sarkar, I.; Yusuf S.M.; Sanyal, M.; Sastry, M. Extracellular biosynthesis of magnetite using fungi. *Small*. **2006**, *2*, 135–141.
209. Lee, J.H.; Roh, Y.; Hur, H.G. Microbial production and characterization of superparamagnetic magnetite nanoparticles by *Shewanella* sp. HN-41. *J. Microbiol. Biotechnology*. **2008**, *18*, 1572-1577.
210. Roh, Y.; Kim, Y.; Lee, S.; Jang, H.; Suh, Y. Microbial production of ultrafine-grained magnetite by fermentation processes at room temperature. *J. Nanosci. Nanotechnol.* **2008**, *8*, 5216-5219.
211. Roh, Y.; Vali, H.; Phelps, T. J.; Moon, J.W. Extracellular synthesis of magnetite and metal-substituted magnetite nanoparticles. *J. Nanosci. Nanotechnol.* **2006**, *6*, 3517–3520.
212. Coker, V.S.; Telling, N.D.; van der Laan, G. ; Pattrick, R.A.D.; Pearce, C.I.; Arenholz, E.; Tuna, F.; Winpenny, R.E.P.; Lloyd, J.R. Harnessing the extracellular bacterial production of nanoscale cobalt ferrite with exploitable magnetic properties. *ACS Nano*. **2009**, *3*, 1922–1928.
213. Welo, L.A.; Baudisch, O. The two-stage transformation of magnetite into hematite. *Philos. Mag.* **1925**, *50*, 399.
214. David.; Welch, A. J. E.; The oxidation of magnetite and related spinels. Constitution of gamma ferric oxide. *Trans. Faraday Soc.* **1956**, *52*, 1642- 1650.
215. Qu, S. C.; Yang, H. B.; Ren, D. W.; Kan, S. H.; Zou, G. T.; Li, D. M.; Li, M. H. Magnetite nanoparticles prepared by precipitation from partially reduced ferric chloride aqueous solutions. *J. Colloid. Interface. Sci.* **1999**, *215*, 190- 192.
216. Bhagwat, S.; Singh, H.; Athawale, A.; Hannoyer, B.; Jouen, S.; Lefez, B.; Kundaliya, D.; Pasricha, R.; Kulkarni, S.; Ogale, S. Low temperature synthesis of magnetite and maghemite nanoparticles. *J. Nanosci. Nanotechnol.* **2007**, *7*, 4294-4302.

217. Kim, J.; Piao, Y.; Hyeon T. Multifunctional nanostructured materials for multimodal imaging, and simultaneous imaging and therapy. *Chem. Soc. Rev.* **2009**, *38*, 372-390.
218. Massart, R.; Cabuil, V. Effect of some parameters on the formation of colloidal magnetite in alkaline-medium-Yield and particle-size control. *J. Chim. Phys. Phys. Chim. Biol.* **1987**, *84*, 967- 973.
219. Massart, R. Atomic and molecular physical chemistry. Preparation of ferrofluids in aqueous surfactant Absensi; behavior as a function of pH and the nature of ions present in solution. *CR Acad. Sci. C. Chim.* Paris 1, **1980**, 291.
220. Massart, R.; Dubois, E.; Cabuil, V.; Hasmonay, E. J. Preparation and properties of monodisperse magnetic fluids *Magn. Magn. Mater.* **1995**, *149*, 1-5.
221. Bandhu, A.; Mukherjee, S.; Acharya, S.; Modak, S.; Brahma, S. K.; Das, D.; Chakrabarti, P. K. Dynamic magnetic behaviour and Mössbauer effect measurements of magnetite nanoparticles prepared by a new technique in the co-precipitation method. *Solid State Commun.* **2009**, *149*, 1790-1794.
222. Munniera, E.; Cohen-Jonathana, S.; Linassiera C.; Douziech-Eyrolles, L.; Marchaisa, H.; Soucéa, M.; Hervéa, K.; Duboisa, P.; Chourpa, I. Novel method of doxorubicin-SPION reversible association for magnetic drug targeting. *Int. J. Pharm.* **2008**, *363*, 170-176.
223. Silva, A.K.A., da Silva, E.L., Oliveira, E.E., Nagashima, T. Jr., Soares, L.A.L., Medeiros, A.C., Ara'ujo, J.H., Ara'ujo, I.B., Carric, A.S., Egito, E.S.T. Synthesis and characterization of xylan-coated magnetite microparticles *Int. J. Pharm.* **2007**, *334*, 42-47.
224. Kim, D.K.; Mikhaylova, M.; Wang, F.H. Starch-coated super paramagnetic nanoparticles as MR contrast agents. *Chem. Mater.* **2003**, *15*, 4343-4351.
225. Griffiths, S. M.; Singh, N. G.; Jenkins, J. S.; Williams, P. M.; Orbaek, A. W.; Andrew, R. B.; Wright, C. J.; Doak, A. S. H. Dextran coated ultrafine superparamagnetic iron oxide nanoparticles: compatibility with common fluorometric and colorimetric dyes. *Anal. Chem.* **2011**, *83*, 3778-3785.
226. Hui-li, M.; Qi, X.; Maitani, Y.; Nagai, T. Preparation and characterization of superparamagnetic iron oxide nanoparticles stabilized by alginate. *Int. J. Pharm.* **2007**, *333*, 177-186.
227. Batalha, I.L.; Hussain, A.; Roque, A.C. Gum Arabic coated magnetic nanoparticles with affinity ligands specific for antibodies. *J. Mol. Recognit.* **2010**, *23*, 462-471.

228. Samanta, B.; Yan, H.; Fischer, N.; Jing Shi, O.; Jerry, D. J.; Rotello V. M. Protein-passivated Fe<sub>3</sub>O<sub>4</sub> nanoparticles: low toxicity and rapid heating for thermal therapy. *J. Mater. Chem.* **2008**, *18*, 1204–1208.
229. Bora, D. K.; Deb, P. Fatty acid binding domain mediated conjugation of ultrafine magnetic nanoparticles with albumin protein. *Nanoscale. Res. Lett.* **2009**, *4*, 138–143.
230. Lutz, J. F.; Stiller, S.; Hoth, A.; Kaufner, L.; Pison, I.; Cartier R. One-Pot Synthesis of PEGylated Ultra small Iron-Oxide Nanoparticles and Their in Vivo Evaluation as Magnetic Resonance Imaging Contrast Agents. *Biomacromolecules.* **2006**, *7*, 3132–3138.
231. Chena, W.; Morupa, S.; Hansenc, M. F.; Banertd, T.; Peuker, U. Mössbauer study of the chemical stability of iron oxide nanoparticles in PMMA and PVB beads. *J. Magn. Mater.* **2008**, *320*, 2099–2105.
232. Lee, S. J.; Jeong, J. R.; Shin, S. C.; Kim, J.C.; Chang, Y. H.; Lee, K. H.; Kim, J. D. Magnetic enhancement of iron oxide nanoparticles encapsulated with poly(D,L-lactide-co-glycolide). *Colloids and Surfaces A.* **2005**, *255*, 19–25.
233. Xu, X.; Friedman, G. Synthesis and utilization of monodisperse superparamagnetic colloidal particles for magnetically controllable photonic crystals *Chem. Mater.* **2002**, *14*, 1249–1256.
234. Chatterjee, J.; Haik, Y. Polyethylene magnetic nanoparticle: a new magnetic material for biomedical applications *J. Magn. Mater.* **2002**, *246*, 382–391.
235. Guowei, D.; Adriane, K.; Chen, X.; Jie, C.; Yinfeng, L. PVP magnetic nanospheres: Biocompatibility, *in vitro* and *in vivo* bleomycin release. *Int. J. Pharm.* **2007**, *328*, 78–85.
236. Oh, J. K.; Park, J. M. Iron oxide-based super paramagnetic polymeric nanomaterials: Design, preparation, and biomedical application. *Prog. Polym. Sci.* **2011**, *36*, 168–189.
237. Talelli, M.; Rijcken, C. J. F.; Lammers, T.; Seevinck, P. R.; Storm, G.; van Nostrum, C. F.; Hennink, W. E. Superparamagnetic Iron Oxide Nanoparticles Encapsulated in Biodegradable Thermo sensitive Polymeric Micelles: Toward a Targeted Nanomedicine Suitable for Image-Guided Drug Delivery. *Langmuir.* **2009**, *25*, 2060–2067.
238. Milonjić, S.K., Ruvarac A.L., Šušić M.V. The heat of immersion of natural magnetite in aqueous solutions, *Thermochim Acta.* **1975**, *11* (3), 261–266.

239. Tombácz, E. E. The effect of humic acid adsorption on pH-dependent surface charging and aggregation of magnetite nanoparticles. *J. Colloid. Interf. Sci.* **2006**, 295(1), 115-123.



***CHAPTER - 2***  
***NOVEL HYBRID***  
***NANOMATERIALS OF***  
***MAGNETITE AND PECTIN***

## 2.1 INTRODUCTION

The nanomaterials of two or more precursors are of tremendous interest in biomedical applications due to their potential synergistic properties that may arise from the combination of these precursors. Two such precursors in the present study are pectin and magnetite nanoparticles (MNPs). Pectin is a biodegradable natural polymer consisting of linear anionic polysaccharide and in general it has been widely explored as a matrix for drug delivery due to its colon specificity [1]. This is mainly attributed to the two reasons: firstly, pectin is resistant to protease and amylase, which are active in upper gastrointestinal (GI) tract [2]. As a result, materials for colon specific delivery, if loaded in pectin could be protected from its dissolution in stomach environment. Secondly, pectin exhibits excellent controlled drug release properties in colon [3, 4]. More over pectin cross linked with  $\text{Ca}^{2+}$  ions forming microbeads of calcium pectinate is reported to be effective formulation for certain colon specific drug molecules [5]. There has been significant advancement towards reducing the size of calcium pectinate to a few hundred nanometers which illustrated efficient loading and delivery of insulin, 5-fluorouracil, and genes [6-8]. The size reduction of the carrier matrix is encouraging as it might facilitate transport properties through biological pathways and barriers to enhance its bioavailability and functionalities. The second precursor, i.e., MNPs exhibits superparamagnetic property [9-11]. Ideally, magnetization interference from domain wall is not expected especially when the particles consist of single magnetic domain in a matrix. In this regard, the MNPs of about 5–20 nm in diameter is considered to be a promising material for several biomedical applications e.g., cellular imaging, targeted delivery, targeted chemotherapy, magnetic resonance imaging (MRI), hyperthermia [12-15]. These are attributed due to its superparamagnetic susceptibility, high saturation magnetization, biocompatibility and non-toxicity [16-18] and also due to their relative ease of synthesis by co-precipitation method [19].

The nanomaterials of pectin and MNPs are thus reckoned to be magnetically responsive and are expected to exhibit the inherent controlled drug release properties. This will allow the investigation of new concepts like magnetic transportation and control release of drug molecules or other suitable substrate for colon specific sites. However, the nanomaterials if administered orally will transit through the stomach where typically the residence time is 2 h [20]. Gastric juice in the stomach consisting of pepsin, mucus and hydrochloric acid (HCl), constitutes pH ~1.2 [21], and are known to favor dissolution of MNPs [22]. Therefore, to retain the magnetic properties of the pectin-MNP nanomaterials

for efficient magnetic targeting to specific sites, namely intestine or colon, it is very important to protect the MNPs of the nanomaterials from acid dissolution in the gastric environment during its transition through stomach.

### 2.1.1 Objective of the study

Drug loaded in pectin nanomaterials have been reported in literature. However, these nanomaterials do not have functionalities for site specific targeting. In view of these observations the current study was focused to develop a novel nanomaterial of pectin with multi-functionalities e.g. efficient drug loading, controlled release and site specific drug delivery. Highly stable formulations are required for usages in the biological systems especially prevention of the loss of the magnetic materials after its exposure to acidic conditions in gastric environment. The present investigation is based on development of a new facile method using co-precipitation and ionotropic gelation techniques for the development of a stable hybrid nanomaterial of pectin with adequate magnetic properties. These hybrid nanomaterials were characterized by an array of techniques e.g. X-ray diffraction (XRD),  $^{57}\text{Fe}$  Mössbauer spectroscopy, scanning electron microscopy (SEM), transmission electron microscopy (TEM), infrared spectroscopy (FT-IR), thermogravimetric analysis (TGA), dynamic light scattering (DLS), zeta potential. The Fe content was measured by instrumental neutron activation analysis (INAA) by relative method and surface Fe content was measured by X-ray photoelectron spectroscopy (XPS). Magnetic properties was measured by superconducting quantum unit interference device (SQUID).

## 2.2 MATERIALS AND METHODS

### 2.2.1 Materials

$\text{Fe}(\text{NO}_3)_3 \cdot 9\text{H}_2\text{O}$ ,  $\text{FeSO}_4 \cdot 7\text{H}_2\text{O}$ , liquid ammonia, anhydrous  $\text{CaCl}_2$ ,  $\text{MgCl}_2$ ,  $\text{MnCl}_2$ ,  $\text{ZnCl}_2$ , tween-80, sodium lauryl sulphate (SLS), polyethylene glycol-400 (PEG-400), 1-10 o-phenanthroline and other reagents (Analytical Grade) were procured for synthesis from Merck, India and were used without further purification. Pectin with 65 to 70% degree of esterification was procured from Hi-Media lab, India. The enzymes pepsin (with an activity of 800-2500 mL units/mg of protein) was procured from Hi-media lab, India. Millipore water (resistivity of  $18.1 \text{ M}\Omega \text{ cm}$  at  $25 \text{ }^\circ\text{C}$ ) was used in all the experiments.

### 2.2.2 Synthesis of MNPs

A molar ratio of 2:1 of  $\text{Fe}(\text{NO}_3)_3 \cdot 9\text{H}_2\text{O}$  and  $\text{FeSO}_4 \cdot 7\text{H}_2\text{O}$  was most suitable for synthesizing MNPs. It agreed well with reported literature [19, 23]. Different batches of mixture were vigorously stirred for 15, 30, and 45 min while maintaining the pH of the mixture at 0.7 [19]. At the time mixing these solutions of  $\text{Fe}(\text{NO}_3)_3 \cdot 9\text{H}_2\text{O}$  and  $\text{FeSO}_4 \cdot 7\text{H}_2\text{O}$  several surfactants like tween-80, SLS, PEG-400 were used. All the batches were characterized by XRD, SEM and TEM to find the optimum condition. Furthermore due to carcinogenic effect of sodium lauryl sulphate (SLS) it was not selected for the further studies. Another batch of MNPs was synthesized in presence of only pectin solution, without any dispersing agent. The excess tween-80 and/ or other impurities like unreacted materials were magnetically separated and washed with Millipore water. It may be noted that a fraction of each of these MNPs were isolated from the respective dispersions for their characterization by SEM, TEM, dynamic light scattering (DLS) and zeta potential measurements. The rest of the synthesized MNPs were either dispersed in the optimum concentration of pectin or were lyophilized. The lyophilized sample was used for their characterization by XRD, TG, SQUID, XPS and  $^{57}\text{Fe}$  Mössbauer spectroscopy.

### 2.2.3 Synthesis of hybrid nanomaterials of magnetite and pectin (MP)

The pectin solutions of 0.2 %, 0.4 %, 0.6 %, 0.8 % and 1.0 % w/v were prepared in Millipore water by continuously stirring for 24 h at room temperature and the pH was maintained at about 4. 25 mL of aqueous dispersion of as-synthesized MNPs with pH adjusted to about 4 with dilute HCl was mixed with 25 mL of pectin solution and the mixture was stirred vigorously for 1 hour at constant pH  $\sim$  4. Then 25 mL of  $\text{CaCl}_2$  solution ( $\text{Ca}^{2+}$ / pectin mass ratio = 2:1) was added drop wise to cross link pectin by ionotropic gelation method [6] along with vigorous stirring for different time intervals ranging from 1-24 h. Similarly cross linking of pectin in the pectin- magnetite system was performed using other divalent ions of  $\text{Mn}^{2+}$ ,  $\text{Mg}^{2+}$  and  $\text{Zn}^{2+}$  by treating pectin at pH  $\sim$  4 with aqueous solutions of  $\text{MnCl}_2$ ,  $\text{MgCl}_2$  and  $\text{ZnCl}_2$ .

Based on the concentration of the pectin solution used (0.2 – 1.0 % w/v), corresponding synthesized magnetite-calcium pectinate nanomaterial were referred to as MP-0.2, MP-0.4, MP-0.6, MP-0.8 and MP-1.0 respectively. After synthesis, the nanomaterials were magnetically separated and washed several times with Millipore water to remove excess of pectin and other unreacted chemicals. Fraction of each of these MPs

were isolated from the respective dispersions for their characterization by SEM, TEM, dynamic light scattering (DLS) and zeta potential measurements. The rest of the synthesized nanomaterials were lyophilized for their characterization by XRD, FT-IR, TG, SQUID, XPS, INAA and  $^{57}\text{Fe}$  Mössbauer spectroscopic studies. In addition, calcium pectinate nanomaterials without MNPs were synthesized by ionotropic gelation method. It was used as a reference sample for confirming the formation of calcium pectinate in the nanomaterials of MPs. The dispersion of the calcium pectinate nanomaterials without MNPs was studied by SEM, TEM, DLS, zeta potential studies. While these dispersed nanomaterials were lyophilized for their characterization by FT-IR and TG analysis.

## 2.2.4 Characterization

### 2.2.4.1 X-ray diffraction and Mössbauer studies

The X-ray diffraction measurements of the as synthesized MNPs and the MP nanomaterials were performed with a powder diffractometer (Bruker AXS D8 Advance) using graphite monochromatized  $\text{CuK}_\alpha$  radiation source, to obtain information about phase of the iron oxide and its crystallite size. The iron oxide phase synthesized by precipitation method was further studied using  $^{57}\text{Fe}$  Mössbauer spectroscopy. The Mössbauer spectra were recorded in transmission mode with  $\sim 30$  mCi  $^{57}\text{Co}$  radioactive source in constant acceleration mode using standard PC-based Mössbauer spectrometer equipped with Weissel velocity drive. The velocity calibration of the spectrometer was done with natural iron absorber at room temperature. The spectra were recorded at 300 K, 5 K (without any applied external magnetic field) and 5 K along with an applied external magnetic field of 5 T (Tesla) applied parallel to the 14.4 keV emitted gamma rays, using JANIS SuperOptiMag superconducting magnet. The recorded Mössbauer spectra were analyzed with NORMOS-SITE/ DIST program.

### 2.2.4.2 Morphology studies

The morphology of the as synthesized MNPs and the MP nanomaterials was studied by the transmission electron microscopy (TEM) FEI Technai-G<sup>2</sup> microscope operated at 200 kV and the field emission scanning electron microscopy (beam resolution of 2 nm) with energy dispersive X-ray analyzer (FESEM – EDAX, FEI-Quanta 200F) operated at 20 kV. The samples for SEM studies were prepared by spraying diluted solution containing nanomaterials on a clean glass plate. It was then dried and coated with thin layer of Au to

impart necessary electrical conductivity for the incident electrons. For TEM studies, the samples were prepared by putting a drop of dispersion of nanomaterials after suitable dilution on a carbon coated 150 mesh copper grid and dried at room temperature. Dynamic light scattering (DLS) experiments were performed by using the Malvern Zetasizer Nano ZS90 instrument with a 4mW He-Ne laser (633 nm wavelength) and a detector at a 173° fixed angle. Size measurements in aqueous condition were performed in triplicate at 25 °C by transferring 1 mL of dust free sample solution into four-clear-size disposable polystyrene cell (Malvern).

In order to find evidence of the formation of MPs nanomaterials, the zeta potential measurements were carried out in triplicate at 25 °C by injecting 0.75 mL of dust free sample solution into disposable folded capillary cells (Malvern). The molecular information of the MPs was obtained by recording FT-IR (Nicolet, Nexus) spectra. Pellets of dried samples were made with KBr and were scanned in the range of 500 - 4000  $\text{cm}^{-1}$ . The cross linked network of pectin coated on MNPs was characterized by thermogravimetric analyses (TGA) using Perkin Elmer, Pyris Diamond. The heating was done under a nitrogen flow (200  $\text{mL min}^{-1}$ ) with a heating rate of 5 °C  $\text{min}^{-1}$  from ambient temperature up to 1000 °C to ensure that the mass loss due to thermal degradation of the coated pectin and to minimize the increase in mass due to oxidation of iron in air.

#### 2.2.4.3 Magnetic studies

A superconducting quantum interference device (SQUID) magnetometer (MPMSXL, USA) was used to analyze the magnetic properties of the as-synthesized nanomaterials. A known amount of lyophilized samples (both MNPs and MP) were packed in a diamagnetic capsule and were inserted in a polyethylene straw as a sample holder. The magnetization measurements were recorded from the hysteresis loop of M-H curve in the range  $\pm 2.5$  T (Tesla) at 300 K using SQUID magnetometer. The field cooled (FC) and zero field cooled (ZFC) measurements were recorded at an applied field of 200 Oe by scanning between 5 and 300 K.

#### 2.2.4.4 Analysis of total Fe content

Conventional elemental analysis techniques like AAS and ICPMS were found to be inefficient for determining total Fe content in magnetite-coated with pectin, due to incomplete acid digestion of these samples. Since instrumental neutron activation analysis

(INAA) does not depend on matrix composition, so this method (relative method of INAA) was used for analyzing Fe content in the MP-0.4 batch from which corresponding magnetite content was derived from its stoichiometric ratio.

#### *Instrumental neutron activation analysis (INNA)*

Accurately weighed 100 mg of the nanomaterials and IAEA soil-5 Reference Materials (RM) were packed separately in aluminum foil. The sealed packets were then marked for identification using waterproof black marker pen. All the packets were sealed in a dust free and clean chamber. These were then collectively packed in a bundle to be fitted in the irradiation container and inserted in the irradiation positions. The samples were irradiated for 6 h using CIRUS reactor at Bhabha Atomic Research Centre, Trombay, Mumbai, India, with a thermal neutron flux of the order of  $10^{13} \text{ cm}^{-2}\text{s}^{-1}$ . The nuclear reaction involved in the analysis was;  $^{58}\text{Fe}(n, \gamma)^{59}\text{Fe}$ . After cooling the irradiated samples for 30 d, the gamma activities of Fe radioisotope produced ( $E_{\gamma} = 1099 \text{ keV}$ ) in the samples and the reference materials were counted using a Compton suppressed HPGe detector of 40 % relative efficiency with respect to 3" x 3" NaI (Tl) detector with 2.0 keV resolution at 1332 keV of  $^{60}\text{Co}$ , coupled to a PC based 8 K MCA in a fixed sample-to-detector geometry. The concentration of Fe in the sample and RM was measured by relative method [24] using the expression:

$$\text{Concn. of element in sample (S}_a\text{)} = \text{Concn. of element in standard (S}_t\text{)} \times \frac{\text{Activity in sample}}{\text{Activity in standard}}$$

Where, activity (A) in the sample (given as counts per second) is measured using the expression:

$$A = N \sigma \phi (1 - e^{-\lambda t_i})$$

Where  $N$  is the number of target atoms of an element in the sample  $\left[ \frac{i \cdot w N_A}{M} \right]$ ,

$i$  = isotopic abundance;  $w$  = mass of an element in grams;  $M$  = Atomic mass of the target atoms in g/mol;  $N_A$  = Avogadro number;  $\sigma$  = thermal neutron absorption cross section in barns ( $1\text{b} = 10^{-24} \text{ cm}^2$ );  $\phi$  = neutron flux ( $\text{cm}^{-2} \text{ s}^{-1}$ ) and  $\lambda$  = the decay constant ( $\text{s}^{-1}$ ) =

$\left( \frac{0.693}{t_{1/2}} \right)$  and  $t_{1/2}$  = half life of the product nucleus (in seconds),  $t_i$  = the irradiation time (in seconds).

The correction of the activity due to cooling given as  $D = (e^{-\lambda t_d})$  was employed, where  $t_d$  = cooling time. The following nuclear data, e.g., isotopic abundance of  $^{58}\text{Fe} = 0.33\%$ , the cross section of the reaction is 1.2 barns and half life of the product nuclide  $^{59}\text{Fe} = 44.6\text{ d}$  were used in the above expression for determining the concentration of Fe. The activities were determined from spectral data analysis using the software PHAST, developed in BARC, Mumbai [25].

#### 2.2.4.5 Analysis of Fe content on the surface of MP

The amount of the MNPs on the surface of the as-synthesized MP batches after lyophilization was determined in terms of Fe contents by X-ray photoelectron spectroscopy (XPS). The XPS measurements were recorded by ESCA VSW scientific instruments Ltd., with  $\text{AlK}_\alpha$  as the source for excitation, operated at 10 kV with an emission current of 10 mA. The sample for XPS characterization was prepared by sprinkling dried lyophilized sample on silver paste applied on copper (Cu) holder. Quantitative analysis of the composition of the sample surface was performed by collecting the integrated intensities of C1s, O1s, Ca2p and Fe2p<sub>3/2</sub> signals using the Wagner's sensitivity factors.

#### 2.2.5 Stability of the as-synthesized MP in acidic conditions

Furthermore, stability of the as-synthesized MP in acidic conditions were determined by the dissolution studies of the MNPs and MPs, conducted as per standard protocol of British Pharmacopoeia in 900 mL of freshly prepared simulated gastric fluid (SGF, pH~1.2) at  $37 \pm 0.1\text{ }^\circ\text{C}$  and 100 rpm for 120 minutes in order to mimic the physiological conditions similar to that of gastrointestinal tract of human body [26]. 5 mL of dissolution fluid was withdrawn at each specified time intervals and replaced with equal volume of fresh medium to mimic the sink conditions of the human body. The withdrawn fluid was filtered and iron content was estimated with Shimadzu 1600 UV Spectrophotometer using 1-10 o-phenanthroline method by recording the absorbance at 510 nm [27].

### 2.3. RESULTS AND DISCUSSION

The strategy to prepare the hybrid nanomaterials of magnetite-pectin (MPs) involved the synthesis of stable MNPs by co-precipitation method followed by its in-situ encapsulation with pectin. The as-synthesized MNPs prepared by co-precipitation method were characterized as follows.



### 2.3.1 Optimization conditions and structural studies of MNPs

The synthesis of nanoscale dimension magnetite required optimization of several experimental parameters. One of these parameters was maintaining of initial pH to  $\sim 0.7$  during mixing of  $\text{Fe}(\text{NO}_3)_3 \cdot 9\text{H}_2\text{O}$  and  $\text{FeSO}_4 \cdot 7\text{H}_2\text{O}$  to achieve small particles. As this pH is reported to be suitable for preparing small particles of MNPs [19]. Furthermore, the time required for mixing the solution of these two iron salts was also critical to synthesize magnetite ( $\text{Fe}_3\text{O}_4$ ). Stirring time of  $\text{Fe}(\text{NO}_3)_3 \cdot 9\text{H}_2\text{O}$  and  $\text{FeSO}_4 \cdot 7\text{H}_2\text{O}$  was varied from 15 to 45 min followed by addition of liquid ammonia to produce magnetite nanoparticles (MNPs). The phase of as-synthesized nanoparticles after lyophilizing was recorded by XRD. Stirring condition of 15 min did not result in the formation of magnetite as evident from its XRD, where characteristic peaks of magnetite were not found (Fig. 2.1 a). The batch prepared by 30 min stirring condition revealed formation of magnetite (Fig. 2.1 b). But the batch synthesized with 45 min stirring time resulted in prominent peak corresponding at 220, 311, 400, 511 and 440 planes indicated the formation of crystalline magnetite phase. This data corroborated well with those of cubic magnetite structures as reported in from the JCPDS 01-11111 data (Fig. 2.1c). The average crystallite size ( $D$ ) of the MNPs was found to be about 2 nm, using the Debye-Scherrer formula i.e.  $D = 0.9\lambda / \Delta \cos\theta$ , where  $\lambda$  is X-ray wavelength,  $\Delta$  is line broadening measured at half-height from the most intense peak of XRD (311 plane) and  $\theta$  is Bragg angle of the particles. Further increase in the pre-digestion time however did not show any improvement in the formation of magnetite phase. Therefore, on the basis of XRD the predigestion time was fixed to 45 min where the  $\text{Fe}_3\text{O}_4$  (cubic) phase matching with JCPDS 01-11111 was observed (Fig.2.1c).

In the above method tween 80 was used as a dispersing agent by using biocompatible surfactant (optimized concentration of 0.2 % v/v, tween-80), for dispersing the as-synthesized MNPs to achieve better particle size distribution.

In addition to avoid the residual chlorides, nitrates and sulphates in the as-synthesized magnetite nanoparticles (MNPs), they were centrifuged and washed repeatedly with Millipore water. In the similar conditions MNPs were also synthesized without dispersing agents.

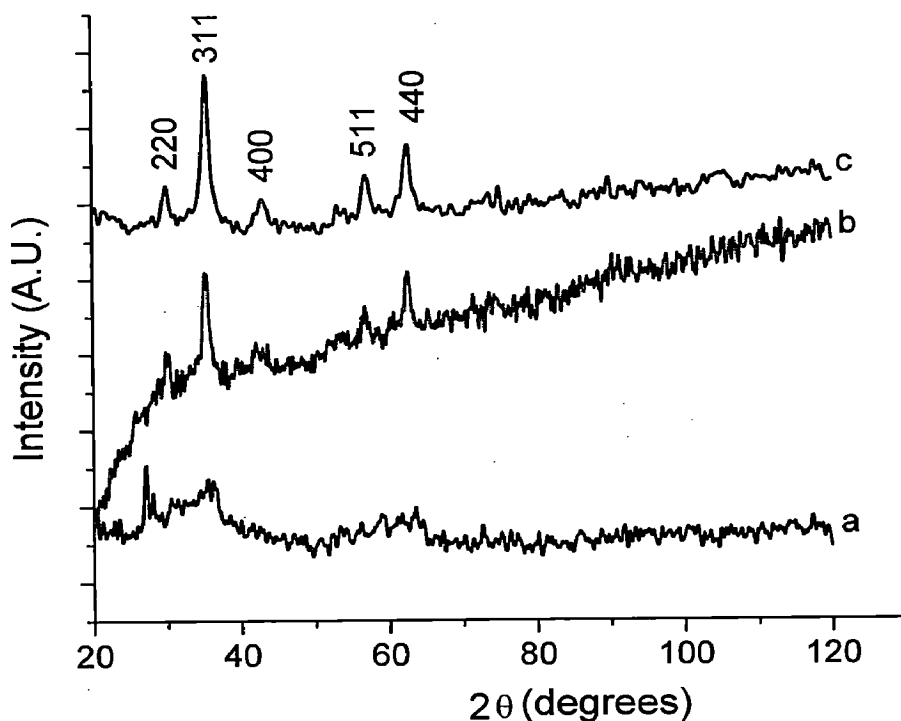
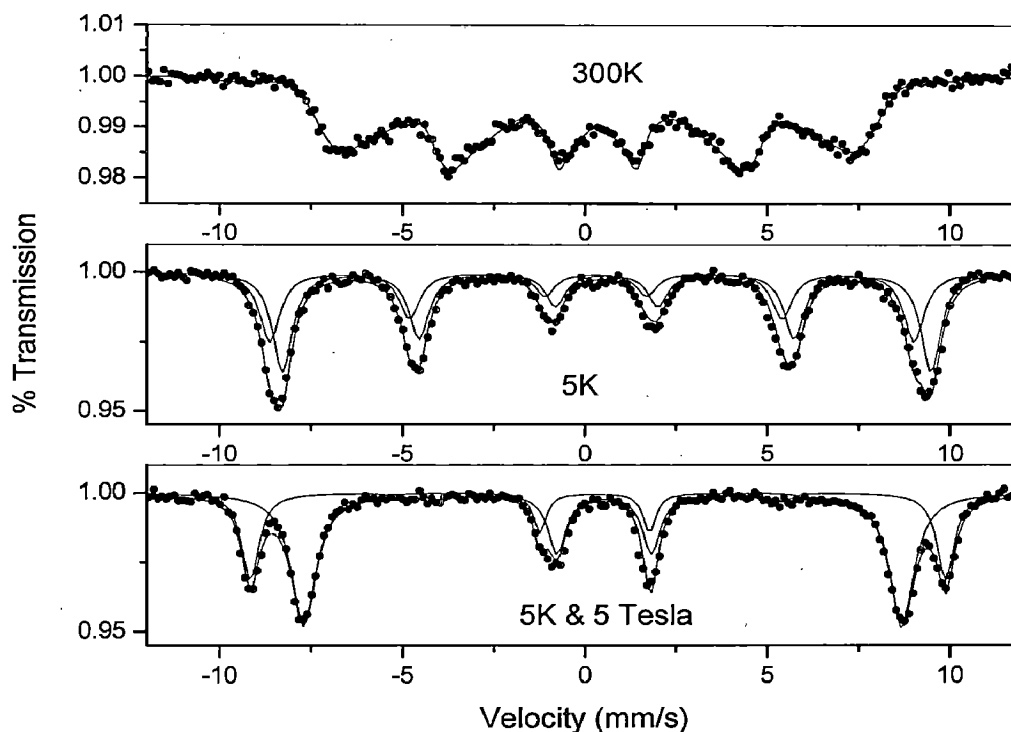


Fig. 2.1. XRD of the MNPs prepared with different predigestion time (a) predigestion time was 15 min (b) predigestion time was 30 min (c) predigestion time was 45 min.

### 2.3.2 $^{57}\text{Fe}$ Mössbauer spectroscopy studies of MNPs

It is essential to perform Mössbauer spectroscopy as the synthesized nanoparticles can be  $\gamma\text{-Fe}_2\text{O}_3$  or  $\text{Fe}_3\text{O}_4$ . The  $^{57}\text{Fe}$  Mössbauer spectroscopy studies of as-synthesized iron oxide nanoparticles recorded at room temperature (RT) showed a relaxed sextet which was typically due to superparamagnetic relaxation effect, attributable to nanoscale dimensions of the particles (Fig. 2.2). At 5 K the relaxation effect was absent as the thermal effect contributing to relaxation was minimized. The broad line width (FWHM) as given in Table 2.1, was perhaps due to overlapping of more than one iron site at 5 K. When the spectrum was recorded at 5 K temperature and in the presence of external magnetic field of 5 Tesla, the octahedral  $\text{Fe}^{2+/3+}$  sites and the tetrahedral sites of  $\text{Fe}^{3+}$  were resolved, which were typically due to magnetite phase. The corresponding hyperfine parameters, namely isomer splitting and quadrupole splitting are presented in the Table 2.1. So from  $^{57}\text{Fe}$  Mössbauer spectroscopy studies, it was confirmed that the synthesized nanoparticles were magnetite and not maghemite. The isomer shift of  $0.319 \pm 0.003$  mm/s corresponds to  $\text{Fe}^{3+}$  at tetrahedral site while that of  $0.512 \pm 0.005$  isomer shift due to octahedral site of  $\text{Fe}^{2+/3+}$ .



**Fig. 2.2.**  $^{57}\text{Fe}$  Mössbauer spectra of MNPs recorded at room temperature (300 K) showing superparamagnetically relaxed sextet spectrum. The measurement at 5 K showed typical sextet of magnetic material. The measurement recorded at 5 K and 5 Tesla revealed tetrahedral and octahedral Fe - sites.

**Table 2.1**  $^{57}\text{Fe}$  Mössbauer spectroscopy hyperfine splitting parameters of MNPs

|        | FWHM<br>(mm/s)    | Isomer shift<br>(mm/s) | Quadrupole<br>splitting (mm/s) | Bhf (Tesla)      | A23              | Area (%) |
|--------|-------------------|------------------------|--------------------------------|------------------|------------------|----------|
| RT     | ND                | ND                     | ND                             | 34.8 (Avg)       | ND               | ND       |
| 5K     | $0.646 \pm 0.018$ | $0.598 \pm 0.009$      | $0.004 \pm 0.007$              | $55.04 \pm 0.03$ | 2.00             | 58.1     |
|        | $0.669 \pm 0.030$ | $0.249 \pm 0.012$      | $-0.105 \pm 0.009$             | $54.69 \pm 0.05$ | 2.00             | 41.9     |
| 5K &   | $0.414 \pm 0.010$ | $0.319 \pm 0.003$      | $0.09 \pm 0.01$                | $59.0 \pm 0.03$  | $0.06 \pm 0.04$  | 31.5 (T) |
| 5Tesla | $0.596 \pm 0.008$ | $0.512 \pm 0.005$      | $-0.041 \pm 0.009$             | $50.77 \pm 0.02$ | $0.122 \pm 0.02$ | 68.5 (O) |

\*ND = not determined, (T): Tetrahedral and (O): Octahedral

### 2.3.3 Morphological studies of MNPs

The scanning electron microscopy (SEM) of the synthesized MNPs dispersed with tween 80 showed formation of large number of agglomerated spherical nanoparticles (Fig 2.3a). Further, the X-ray analysis (EDAX) of a representative magnetite nanoparticle reflected the  $K_{\alpha}$  (6.396 keV),  $K_{\beta}$  (7.007 keV) corresponding to Fe (Fig. 2.3b). In addition, the K X - ray of O peak was observed. The two other peaks corresponded to Au (M-X-ray) due to gold coating on the sample surface and the small intensity of Si K-X-ray came from

the sample holder. The sizes of these MNPs were less than 20 nm evident from TEM studies (Fig. 2.4a, 2.4b). The corresponding selected area electron diffraction (SAED) indicated about the presence of polycrystalline MNPs (Fig. 2.4b).

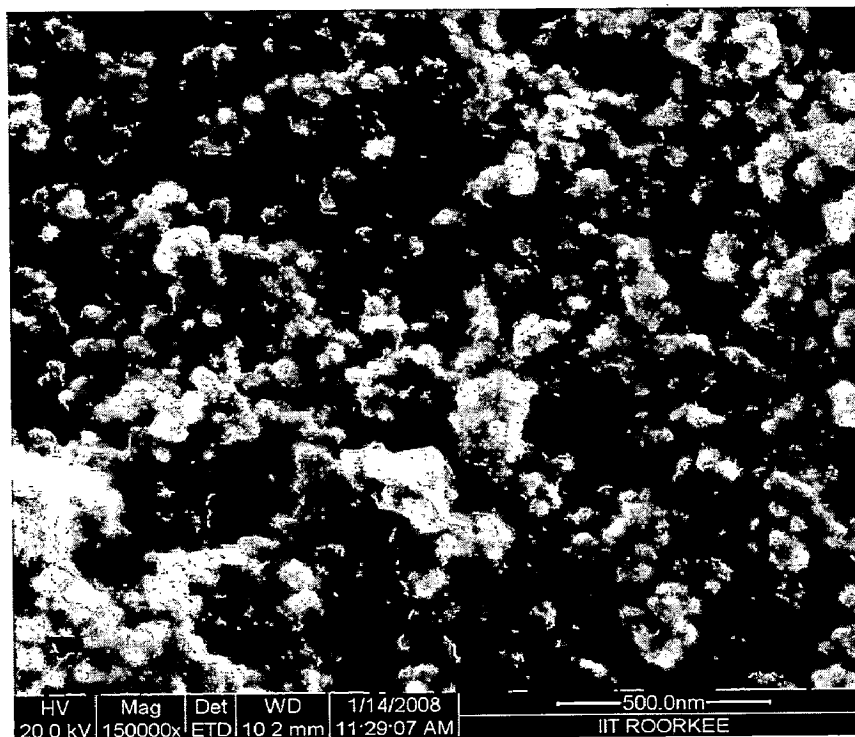


**Fig. 2.3a.** Scanning electron microscopy (SEM) of clusters of MNPs prepared by using tween-80 as dispersing agent.

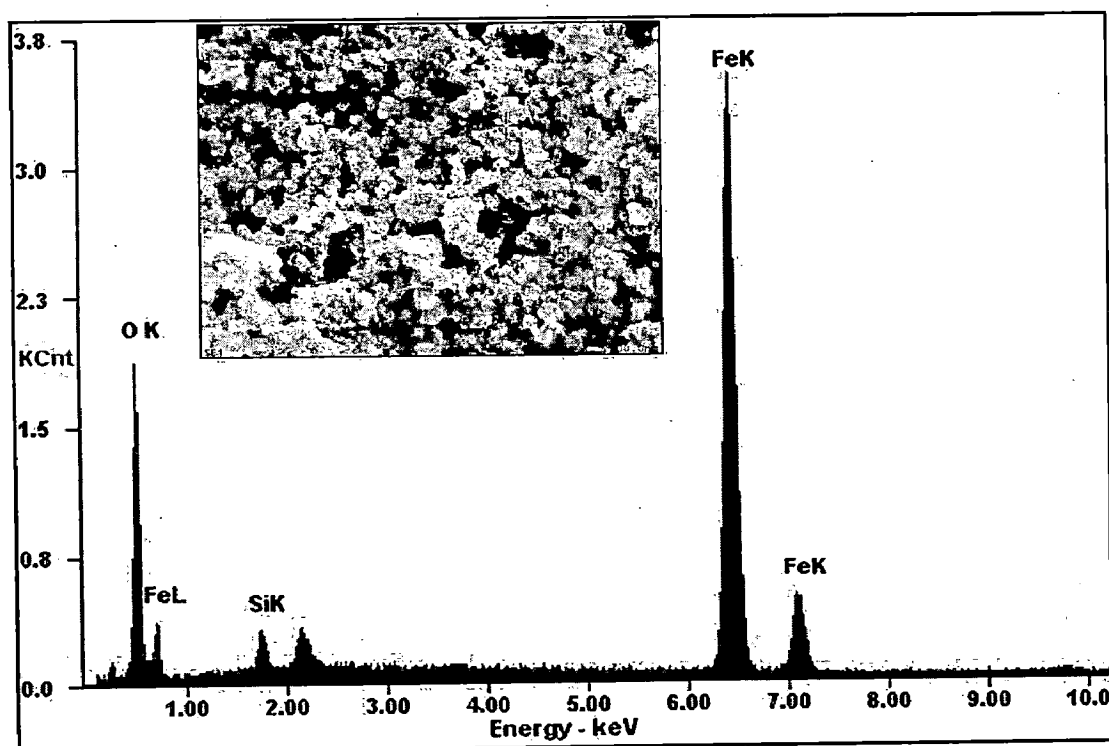


**Fig. 2.3b.** Energy Dispersive X-analysis (EDAX) of MNPs using tween-80 as dispersing agent.

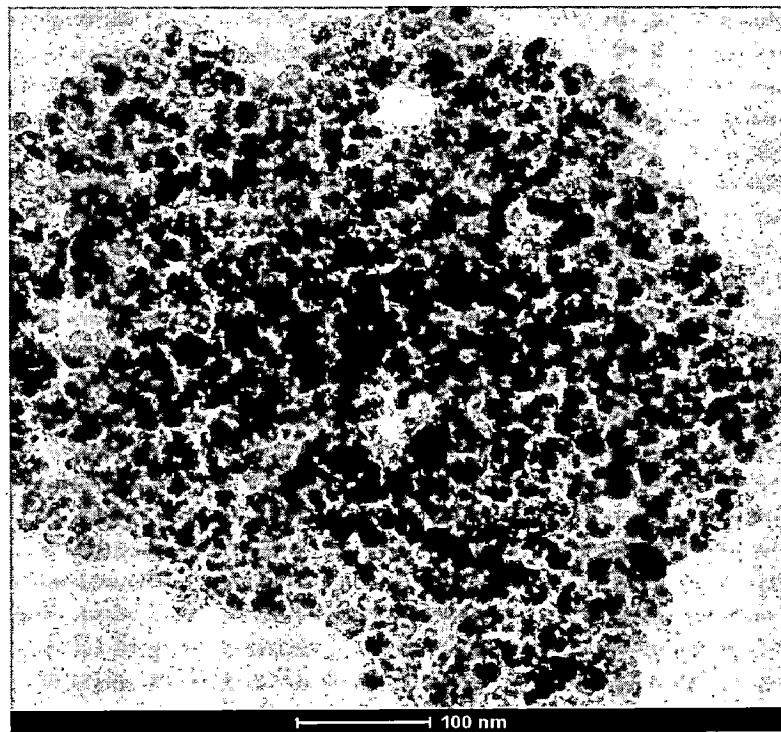


**Fig. 2.4a.** Transmission electron microscopy (TEM) of MNPs dispersed with tween 80.

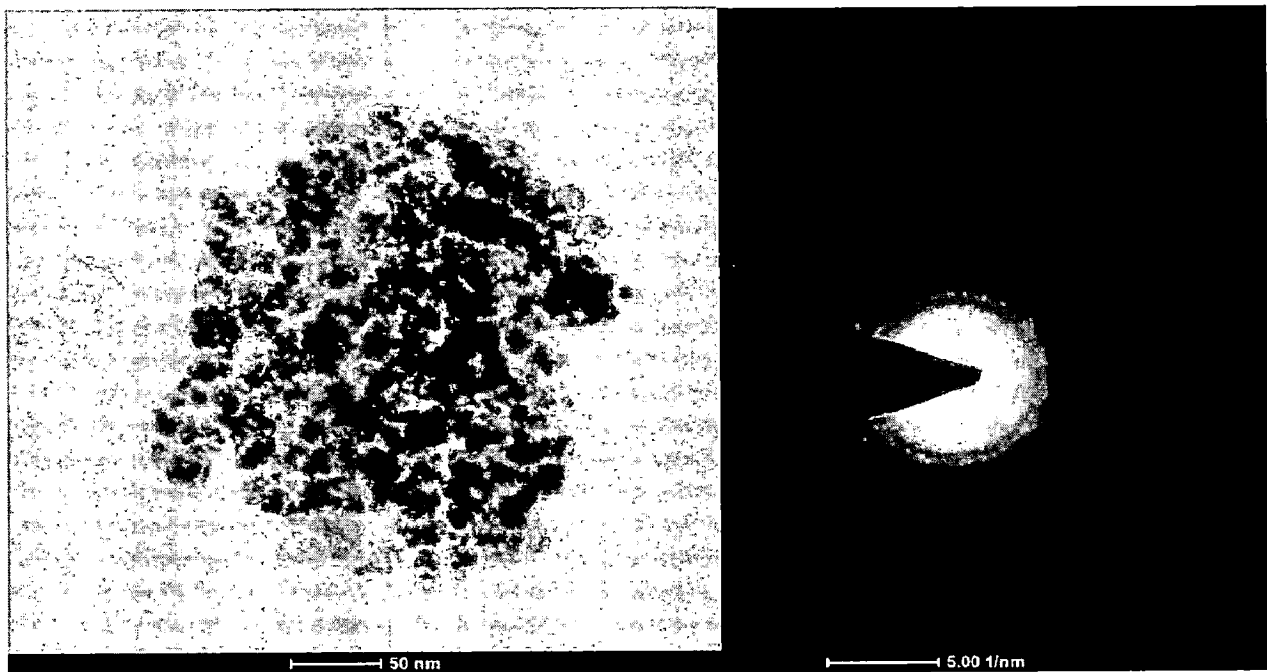


**Fig. 2.4b.** Transmission electron microscopy (TEM) of MNPs dispersed with tween 80 and its corresponding SAED indicating the presence of polycrystalline MNPs.

However, the sizes of these MNPs prepared without surfactants were also found to be less than 20 nm as measured by high resolution TEM (Fig. 2.5). The corresponding SAED image confirmed the presence of polycrystalline MNPs (Fig. 2.5).

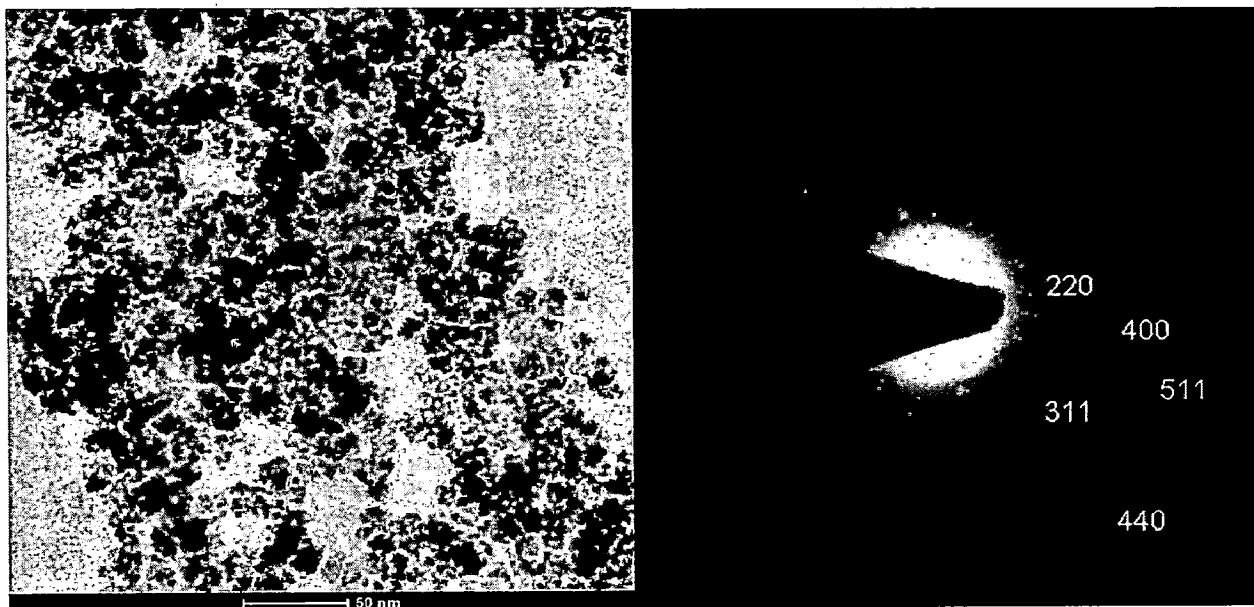


**Fig. 2.5.** . Transmission electron microscopy (TEM) and its corresponding SAED image of MNPs prepared without surfactants.

#### 2.3.4 Synthesis of MPs

The encapsulation of magnetite nanoparticles with pectin was achieved by cross linking pectin with  $\text{Ca}^{2+}$  ions. The above method was optimized to achieve uniform size distribution of these spherical hybrid nanomaterials of magnetite coated with calcium pectinate (which will be referred to as MPs). The key parameters involved in the optimization process were (a) working pH of about 4, (b) pectin precursor concentration (in % w/v),  $\text{Ca}^{2+}$ /pectin mass ratio of 2:1 and (c) vigorous stirring. A fixed amount of as synthesized MNPs were dispersed in pectin where pectin concentration was varied i.e. 0.2 %, 0.4 %, 0.6 %, 0.8 % and 1.0 % w/v. To this dispersion  $\text{CaCl}_2$  solution was added and stirred for 6 h. The trials were taken for different stirring time after adding  $\text{CaCl}_2$  solution to the dispersion of MNPs in pectin, like 1 h, 4 h, 6 h, 8 h, 12 h, 18 h and 24 h. The best result (based on morphology) were obtained for 6 h stirring and thus further synthesis were restricted to 6 h stirring (Fig. 2.6c). It may be observed from the Fig. 2.6c that 6 h showed spherical morphology and beyond 6 h no improvement was observed (Fig. 2.6d). So 6 h stirring was optimum. This experiment was carried out by taking 0.4 % w/v pectin and 0.8 % w/v of  $\text{CaCl}_2$ .



**Fig. 2.6a.** SEM image showing morphology of MP-0.4 batch synthesized by stirring pectin, MNPs and  $\text{Ca}^{2+}$  for 1 h.

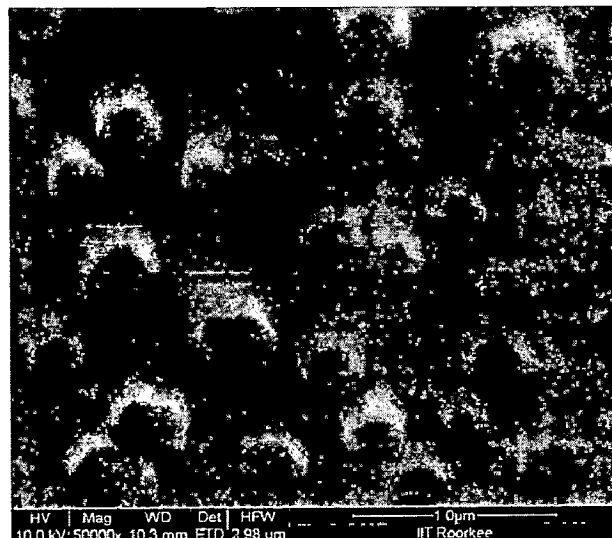


**Fig. 2.6b.** SEM image showing morphology of MP-0.4 batch synthesized by stirring pectin, MNPs and  $\text{Ca}^{2+}$  for 4 h.

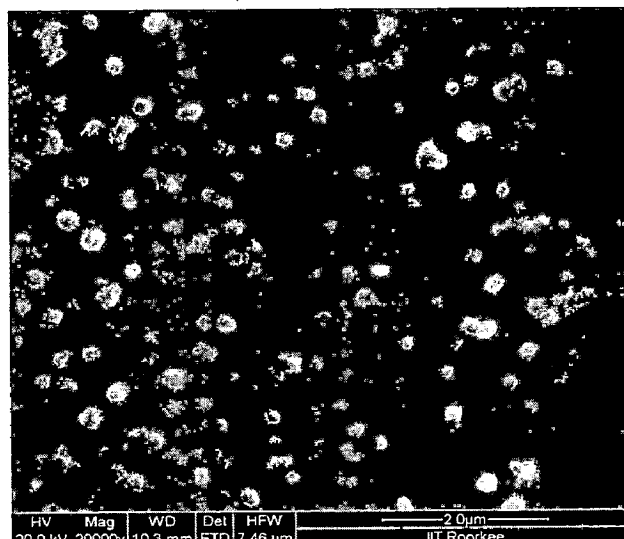


**Fig. 2.6c.** SEM image showing morphology of MP-0.4 batch synthesized by stirring pectin, MNPs and  $\text{Ca}^{2+}$  for 6 h.

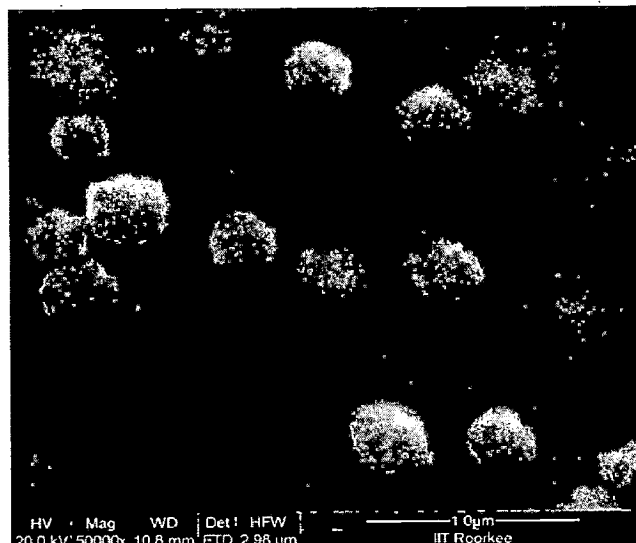


**Fig. 2.6d.** SEM image showing morphology of MP-0.4 batch synthesized by stirring pectin, MNPs and  $\text{Ca}^{2+}$  for 24 h.

Further, the  $\text{Ca}^{2+}$  ions were replaced with other divalent ions, namely,  $\text{Zn}^{2+}$ ,  $\text{Mn}^{2+}$  and  $\text{Mg}^{2+}$ , to evaluate the possibilities of their usage in the synthesis of MNP coated with pectin nanomaterials [8]. The working pH of about 4 and other conditions were kept similar. The use of  $\text{Zn}^{2+}$  led to formation of spherical nanomaterials where pectin was likely to be cross linked with  $\text{Zn}^{2+}$ . The particle size was about 300 nm (Fig. 2.7). On the other hand, the use of  $\text{Mn}^{2+}$  and  $\text{Mg}^{2+}$  resulted in formation of irregular shaped nanomaterials of magnetite-pectin as reflected from their respective SEM images (Fig. 2.8, 2.9). So in our study we focused our mode of synthesis by using  $\text{Ca}^{2+}$  ions for cross linking with pectin.

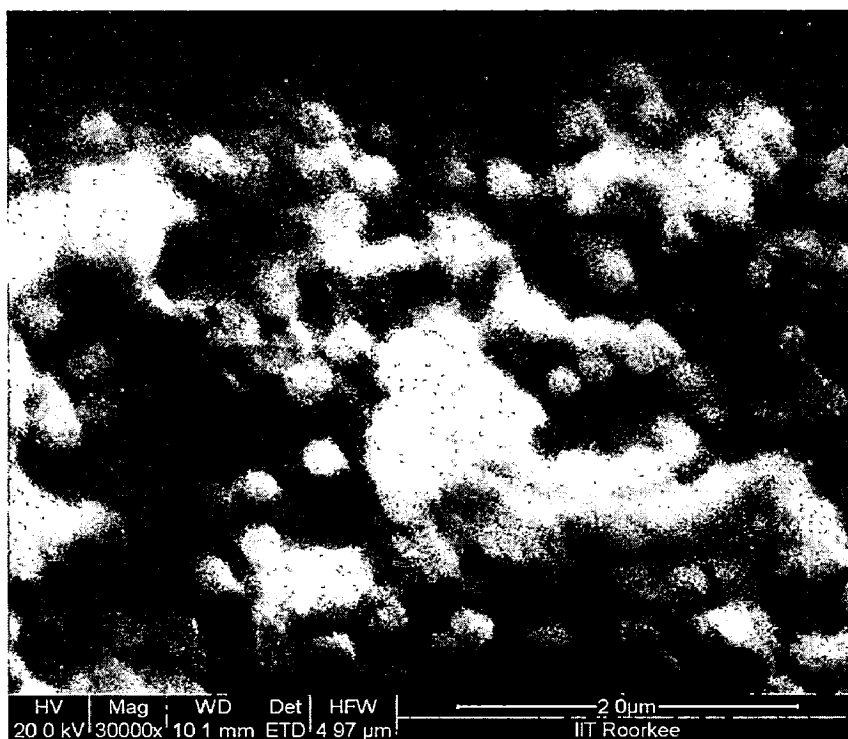


**Fig.2.7.** SEM of nanomaterials synthesized by coating of MNPs with zinc-pectinate



**Fig.2.8.** SEM of nanomaterials synthesized by coating of MNPs with magnesium-pectinate



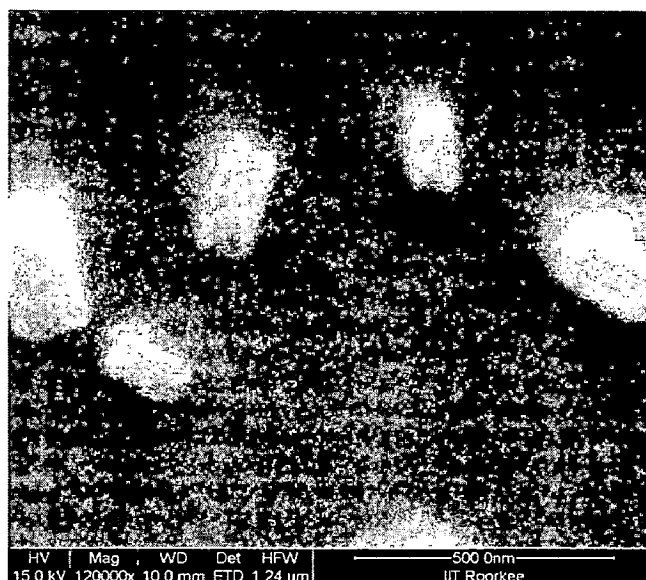


**Fig.2.9.** SEM of nanomaterials synthesized by coating of MNPs with manganese-pectinate showing non-uniform rod like shapes of nanomaterials.

### 2.3.5 X ray diffraction studies of MPs

The magnetite phase was also evident in all the samples of the MPs as supported from observation of the characteristic diffraction patterns at 220, 311, 400, 511 and 440 planes, corroborated to magnetite and well with those of cubic magnetite structures as reported in the JCPDS 01-11111 data (Fig. 2.10). However, in MP-1.0 the magnetite phase was weak, which might be attributed to the matrix effect. The intensity of the characteristic peaks e.g., 311 decreased for the batch prepared with 0.8 % w/v pectin. On increasing pectin concentration to 1.0 % the magnetite phase was weak and the material appears to be amorphous in nature which can be attributed to higher amounts of pectin.

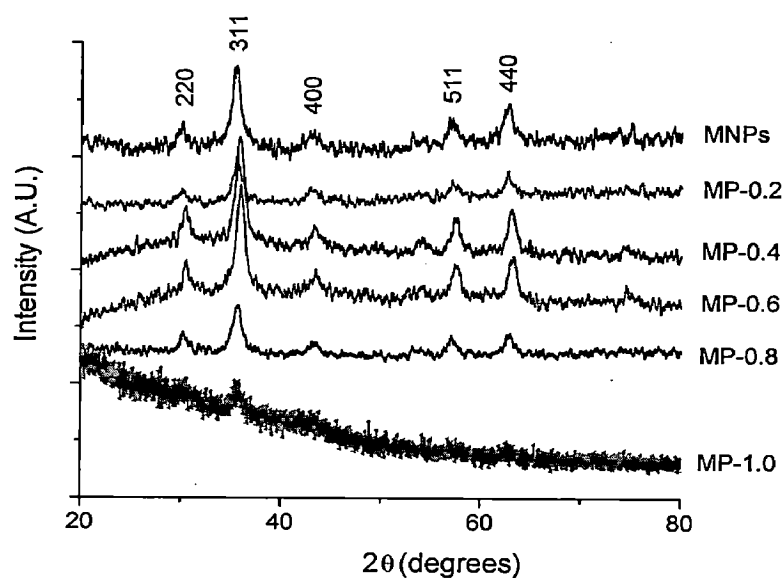


**Fig. 2.10.** XRD of the MNPs and various compositions of MPs.

### 2.3.6 $^{57}\text{Fe}$ Mössbauer spectroscopy of MP-0.4

The  $^{57}\text{Fe}$  Mössbauer spectroscopy of MP-0.4 was studied which showed similar features as observed for MNPs (Fig. 2.11). The spectrum recorded at 300 K showed high superparamagnetic relaxation. The relaxation was more which can be due to lattice contribution of pectin. The spectrum recorded at 5K but with external field showed six line spectrum, when the line width were large. This indicated that most likely two sextets can be fitted as shown in the spectrum. The spectrum recorded at 5 K and 5 T applied magnetic field showed the characteristic tetrahedral ( $\text{Fe}^{3+}$ ) and octahedral ( $\text{Fe}^{2+/3+}$ ) sites of Fe (Fig. 2.11). The hyperfine splitting parameters, e.g., isomer shift and quadrupole splitting corresponding to the two sextets (Fig. 2.11) were similar to that of MNPs which corroborated tetrahedral and octahedral environment.

The corresponding intrinsic magnetic field was measured to be  $58.35 \pm 0.03$  T and  $50.15 \pm 0.02$  T respectively which were in close agreement with the intrinsic magnetic field of MNPs (Table 2.2). The small quadrupole splitting values were attributed to cubic structure of magnetite and corroborated well with the XRD data of these samples. Further, by applying external magnetic field of 5 T, the tetrahedral and octahedral sites of magnetite were resolved where the corresponding A23 parameters (Table 2.2) were small which indicated negligible spin canting in the synthesized MNPs. So from  $^{57}\text{Fe}$  Mössbauer studies it was confirmed that the magnetite phase did not undergo any phase change due to the synthesis of MNP coated with pectin followed by cross linking with  $\text{Ca}^{2+}$  ions in aqueous medium.

**Table 2.2**  $^{57}\text{Fe}$  Mössbauer spectroscopy hyperfine splitting parameters of MP-0.4

|        | FWHM<br>(mm/s)    | Isomer shift<br>(mm/s) | Quadrupole<br>splitting (mm/s) | Bhf (Tesla)      | A23              | Area (%) |
|--------|-------------------|------------------------|--------------------------------|------------------|------------------|----------|
| RT     | ND                | ND                     | ND                             | 27.4 (Avg)       | ND               | ND       |
| 5K     | $0.573 \pm 0.009$ | $0.570 \pm 0.004$      | $0.027 \pm 0.005$              | $54.57 \pm 0.02$ | 2.00             | 57.2     |
|        | $0.536 \pm 0.020$ | $0.262 \pm 0.007$      | $-0.094 \pm 0.007$             | $54.19 \pm 0.03$ | 2.00             | 42.8     |
| 5K &   | $0.476 \pm 0.011$ | $0.323 \pm 0.005$      | $0.06 \pm 0.01$                | $58.35 \pm 0.03$ | $0.08 \pm 0.05$  | 33.2 (T) |
| 5Tesla | $0.592 \pm 0.008$ | $0.495 \pm 0.003$      | $-0.019 \pm 0.007$             | $50.16 \pm 0.02$ | $0.173 \pm 0.02$ | 66.8(O)  |

ND: not determined; (T): Tetrahedral and (O): Octahedral

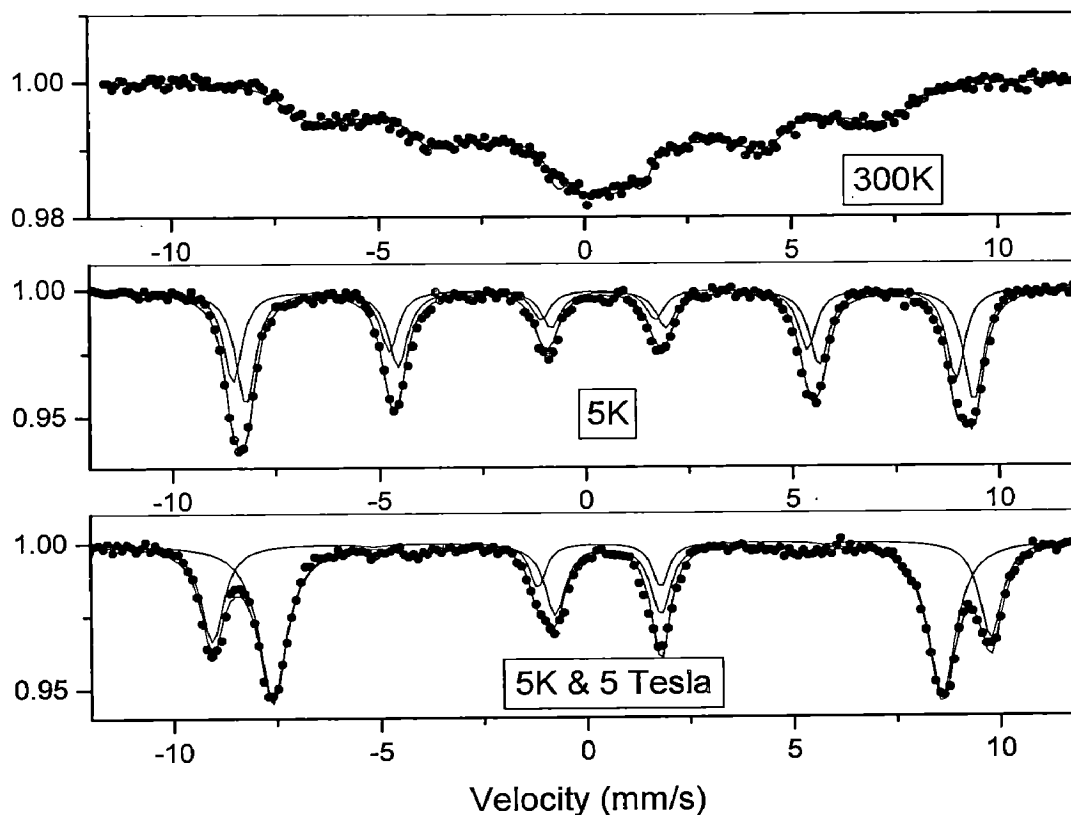


**Fig. 2.11.**  $^{57}\text{Fe}$  Mössbauer spectroscopy measurements of MP-0.4 at room temperature (300 K) showing superparamagnetically relaxed sextet spectrum. The measurement at 5 K showed typical sextet of magnetic material. The measurement recorded at 5 K and 5 Tesla revealed tetrahedral and octahedral Fe - sites.

### 2.3.7 Morphological studies of MPs

#### 2.3.7.1 Scanning electron microscopy (SEM), energy dispersive X-ray analysis (EDAX) studies of MP-0.4

The morphological studies by SEM of the magnetite coated with pectin, cross linked with  $\text{Ca}^{2+}$  are reported for the batches MP-0.4 (0.4% w/v pectin solution) and MP-0.6 (0.6% w/v pectin solution), which were found to be spherical in shape. The sizes of these spherical shaped nanomaterials were in the range of 50 – 200 nm, where most nanomaterials were of sizes 100 – 150 nm (Fig 2.12a), which were also supported from higher resolution SEM image Fig 2.12a (inset). Further the EDAX of a representative nanomaterial showed the characteristic X-rays of Ca and Fe. The co-localization of Fe and Ca in the EDAX analysis of a selected area of a representative spherical nanomaterial (Fig. 2.12b) was characteristic of MNPs and calcium pectinate respectively and thus indicated the formation of MPs.

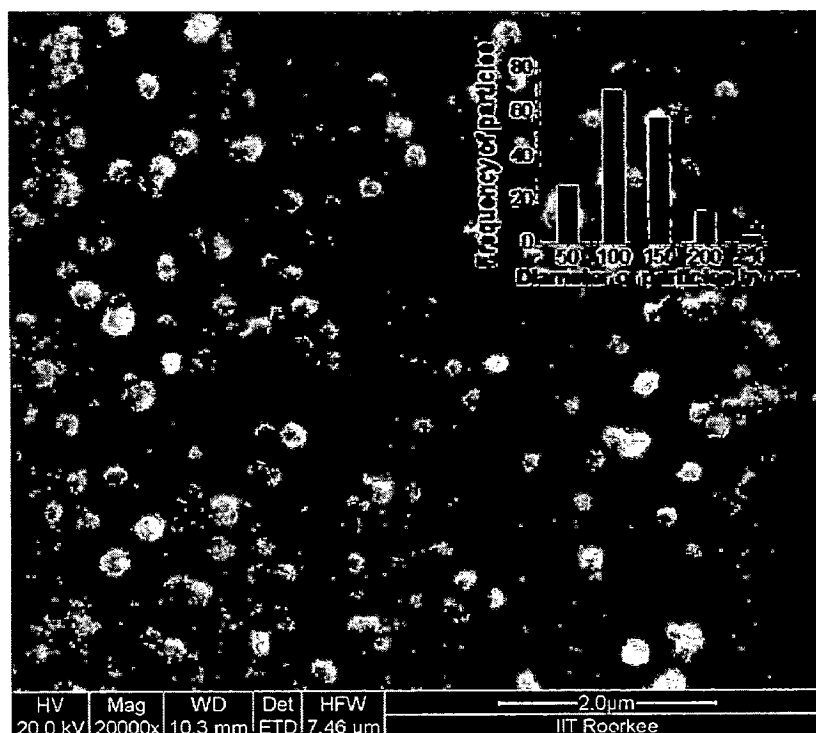


Fig. 2.12a. Morphology and particle size distribution of MP-0.4 by scanning electron microscopy.

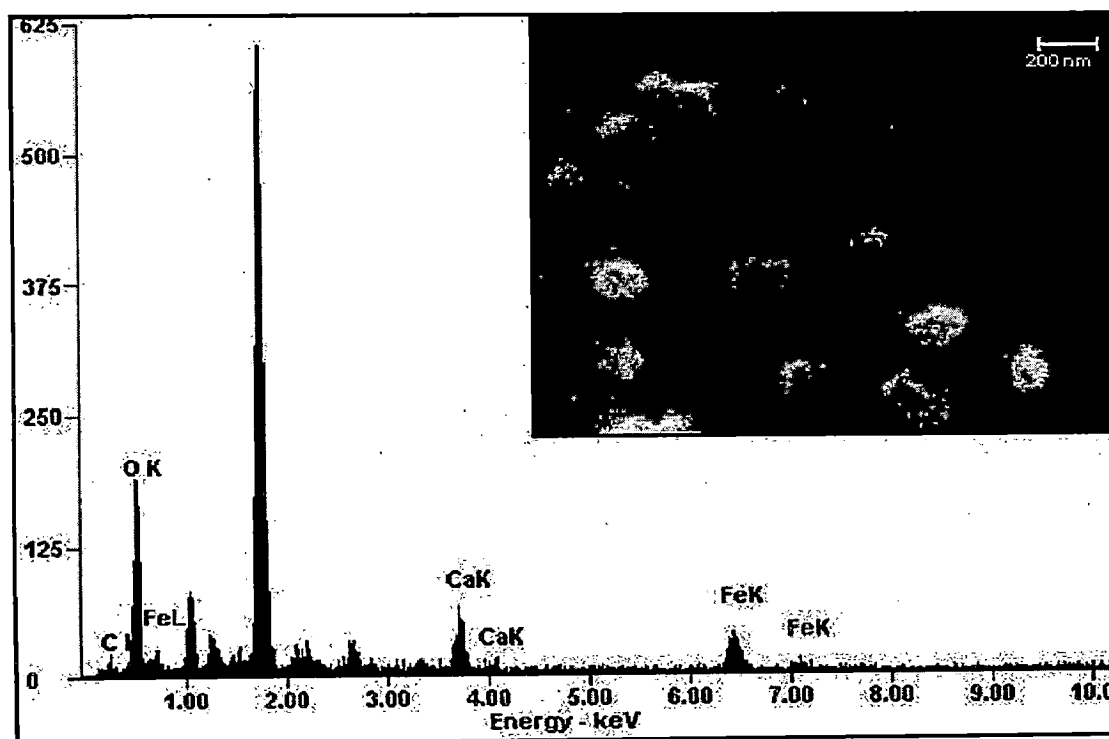
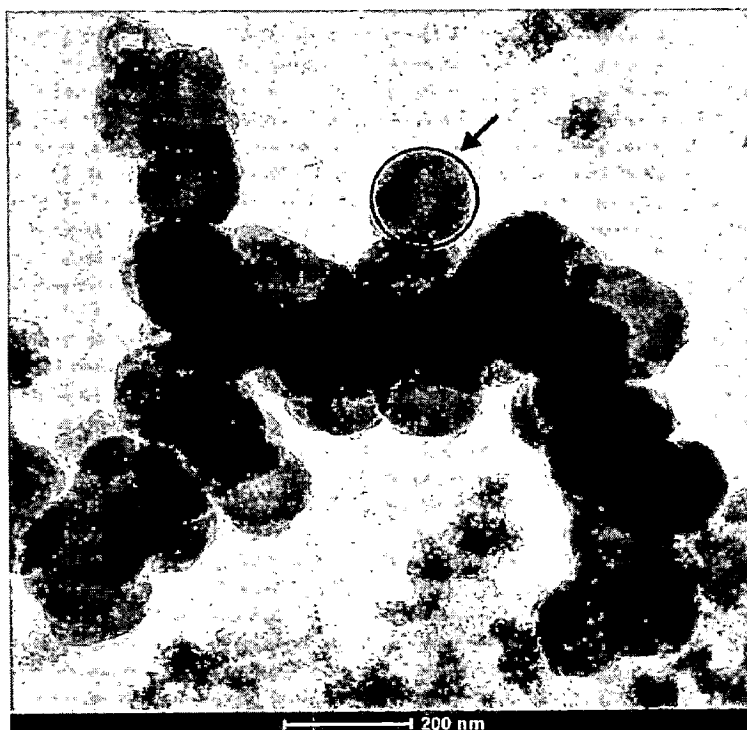


Fig. 2.12b. EDAX of a selected nanomaterials of MP-0.4, marked in the inset illustrated co-localization of Fe and Ca.

### 2.3.7.2 Transmission electron microscopy (TEM) of MP-0.4

The TEM measurements of MP-0.4 nanomaterials revealed synthesis of uniform spherical shaped nanomaterials with sizes of about 100-150 nm and corroborated well with the SEM results (Fig. 2.13a). A higher resolution TEM corresponding to a portion of a

spherical nanomaterial of magnetite-pectin exhibited a large number of encapsulated MNPs. The sizes of these MNPs were measured to be in the range of 2-8 nm (Fig. 2.13b), and the corresponding SAED image indicated its polycrystalline nature (Fig. 2.13b).



**Fig. 2.13a.** TEM of spherical shaped MP-0.4 nanomaterial of about 150 nm (as marked)

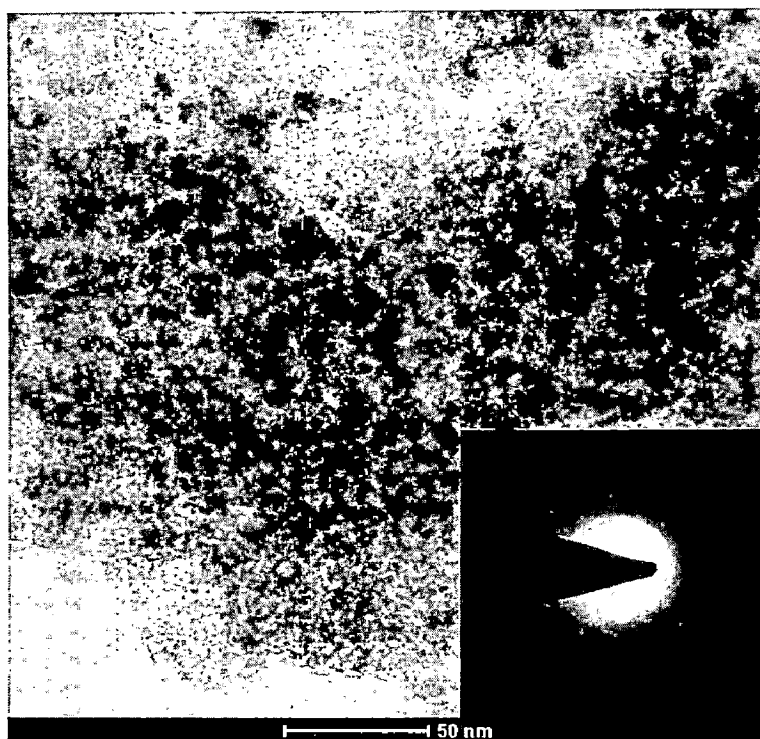


**Fig. 2.13b.** Detailed TEM of a part of MP-0.4 nanomaterials (represented by an arrow in Fig 2.13a) illustrated the presence of polycrystalline MNPs.

### 2.3.7.3 Dynamic light scattering (DLS) of MP-0.4

Furthermore, dynamic light scattering (DLS) measurement of MP-0.4 in aqueous solution at pH ~4 was carried out. The batch MP-0.4 exhibited unimodal size distribution in the range of 230 – 620 nm with maximum intensity at ~ 400 nm (Fig. 2.14). This indicated that the method of synthesis offered a good control over the size of these nanomaterials. It may however be noted that the particle size measured by DLS were larger as compared to those measured by TEM and SEM. The increase in the size in aqueous medium was attributed to swelling effect of calcium pectinate [7].

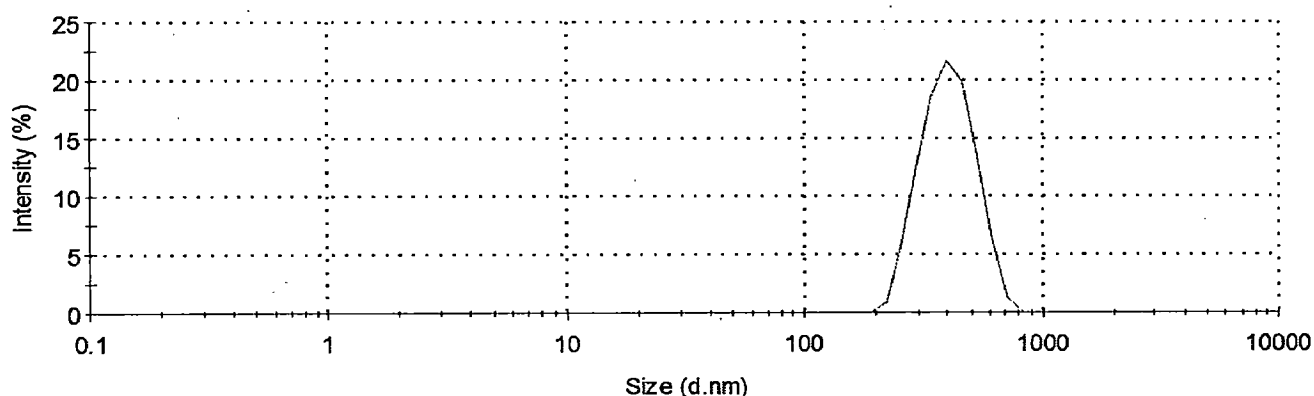


Fig. 2.14. DLS measurement of MP-0.4 in aqueous solution at pH ~4.

### 2.3.8 FT-IR analysis

The formation of MP hybrid nanomaterial was further supported by the FT-IR analyses. The FT-IR spectra (Fig. 2.15) of the pectin showed weak bands at  $1690\text{ cm}^{-1}$  corresponding to COOH group while that of MP-0.4 prepared with tween-80, revealed intense bands at  $1685\text{ cm}^{-1}$ ,  $1395\text{ cm}^{-1}$  and  $1324\text{ cm}^{-1}$  which were characteristic of asymmetric and symmetric stretching of carboxylate groups ( $\text{COO}^-$ ). On the other hand calcium pectinate which was synthesized without any encapsulated MNPs and was used as a reference material for comparing the results of IR and thermal analysis. The IR spectrum of calcium pectinate reference material also showed intense IR bands similar to those observed for MP-0.4 batch. In addition, the IR signatures for pectin and the MPs were found similar in the IR region of  $900\text{--}1250\text{ cm}^{-1}$  which might be due to their similar molecular framework of pectin in both the samples.

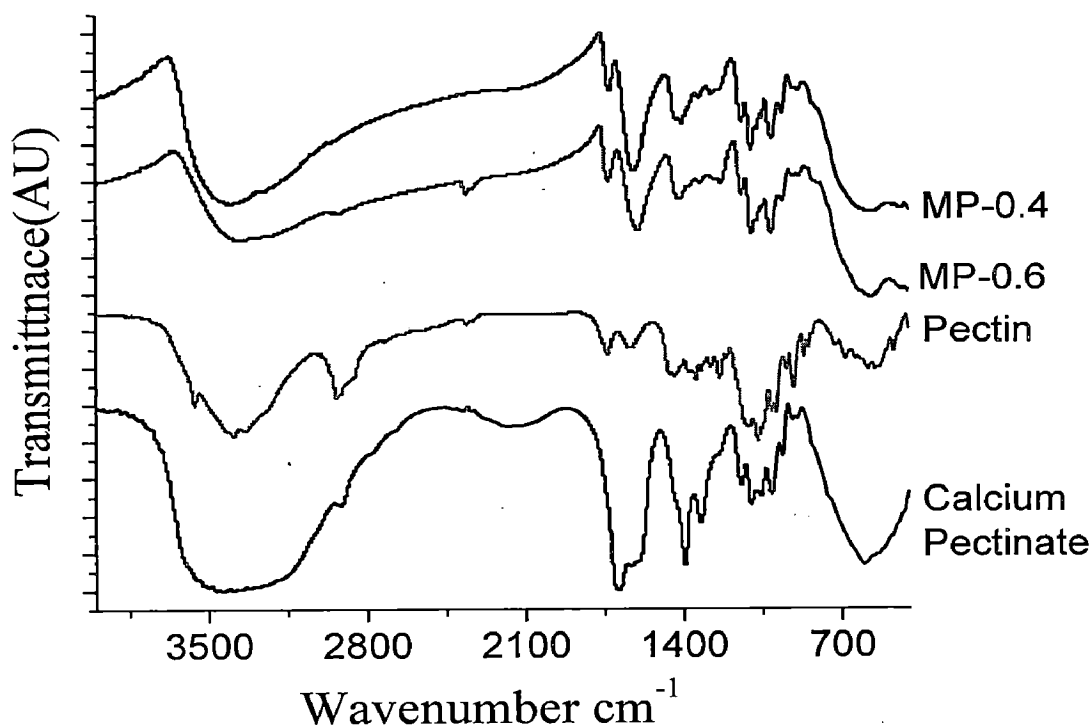


Fig. 2.15. FT-IR spectra showing characteristic peaks of MP-0.4, MP-0.6, precursor pectin and calcium pectinate as reference sample.

### 2.3.9 Thermal studies

The formation of MP-0.4 and MP-0.6 was further confirmed from thermogravimetric analysis (TGA) as exhibited in Fig. 2.16. It illustrated nearly 5 % higher mass loss for MP-0.6 as compared to MP-0.4. This was attributed to higher pectin precursor concentration in MP-0.6 batch. In addition, their TGA thermogram comprised with three distinct thermal events. The first event was recorded in the temperature range between ambient temperature and 110 °C corresponding to a mass loss of about 5 % which was due to desorption of water molecules. The second event showed a gradual mass loss of about 5 % and 8 % in MP-0.4 and MP-0.6 respectively the temperature range of 200-450 °C, which was comparable with the thermal degradation pattern of the calcium pectinate. The third thermal event corresponding to nearly 2 % and 3 % mass loss in MP-0.4 and MP-0.6 respectively the temperature range of 550-775°C did not concur with that of calcium pectinate (without MNP encapsulation), used as a reference material. However, this thermal event appeared to be correlated with the thermal decomposition pattern of precursor pectin corresponding to the temperature range of 320-455°C. From these observations, it may be inferred that the hybrid nanomaterials of MPs contained both non-modified pectin as well as calcium pectinate components. Most likely, calcium pectinate constituted the periphery of the MPs that enclosed pectin interfaced with MNPs. In that situation the thermal decomposition of pectin

would be expected after the thermal degradation of peripheral calcium pectinate. This was perhaps the reason why the onset of thermal decomposition of pectin in the MPs occurred at much higher temperature than that of the precursor pectin [28].

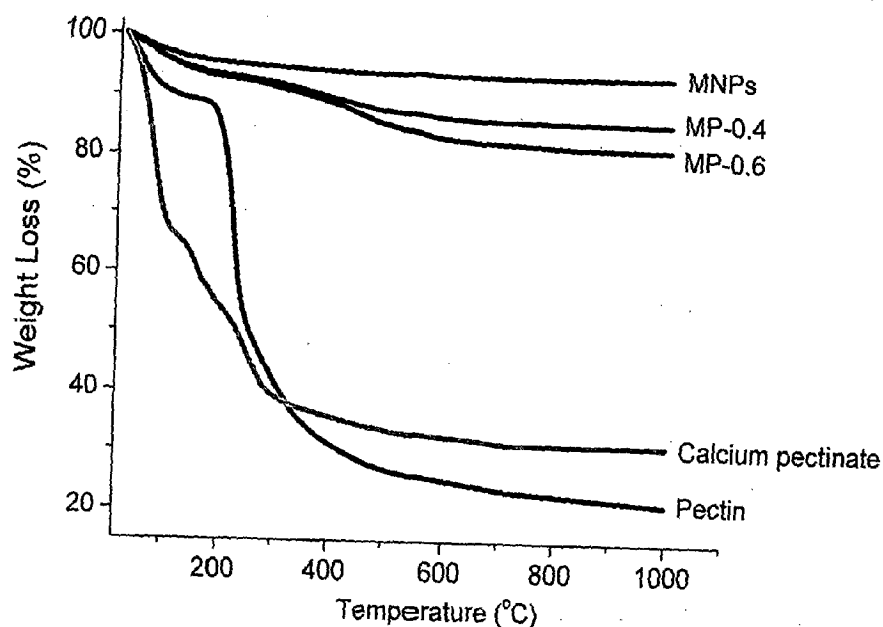


Fig. 2.16. TGA analysis of MNPs, MP-0.4, MP-0.6, pectin and calcium pectinate.

### 2.3.10 Analysis of MNP content in MP-0.4

The Fe content in the MP-0.4, measured by INAA relative method was found to be  $43.3 \pm 2.1$  % (given as mean  $\pm$  standard deviation from triplicate measurements), which corresponded to  $59.6 \pm 2.9$  % of MNPs ( $\text{Fe}_3\text{O}_4$ ) stoichiometrically. The method of analysis was validated by measuring NIST standard reference materials.

Our result was on Fe analysis in MP-0.4 nanomaterials was in good agreement from thermal analysis. From TGA study, calcium pectinate after heating to 1000 °C resulted in weight loss of 68 %, i.e., 32 % was left as residue. Similarly, the batch of MP-0.4 on heating up to 1000 °C, resulted in a weight loss of 16 %. So 84 % of the residual weight of MP-0.4 heated at 1000 °C comprised residual calcium pectinate and MNPs. If we assume 32 % of this weight was due to residual calcium pectinate, which accounted to 26.9 % then the remaining 57.1 % should be MNPs, which was in good agreement with our analysis of MNPs in the batch of MP-0.4 by INAA method.



XPS studies were performed to estimate the presence of MNPs on the surface of MP. It revealed the binding energy of the photoelectron peaks corresponding to C1s, O1s, and Ca2p<sub>3/2</sub>, which were the signatures of calcium pectinate (Fig. 2.17a). The XPS study was more relevant as it exhibited weak binding energy peak corresponding to Fe2p<sub>3/2</sub> (Fig. 2.17b) and the concentration of Fe was calculated to be  $1.6 \pm 0.6$  %. This indicates that the negligible amount of MNPs was present on the surface of MP nanomaterials. From these studies it was concluded that the MNPs were encapsulated by the calcium pectinate.

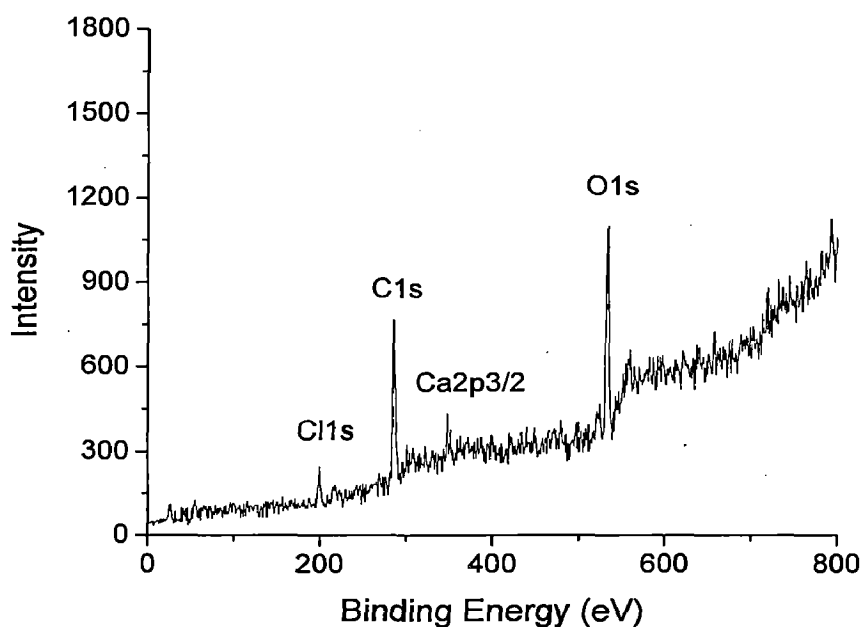


Fig. 2.17a. Full scan X ray photoelectron spectroscopy (XPS) of MP-0.4.

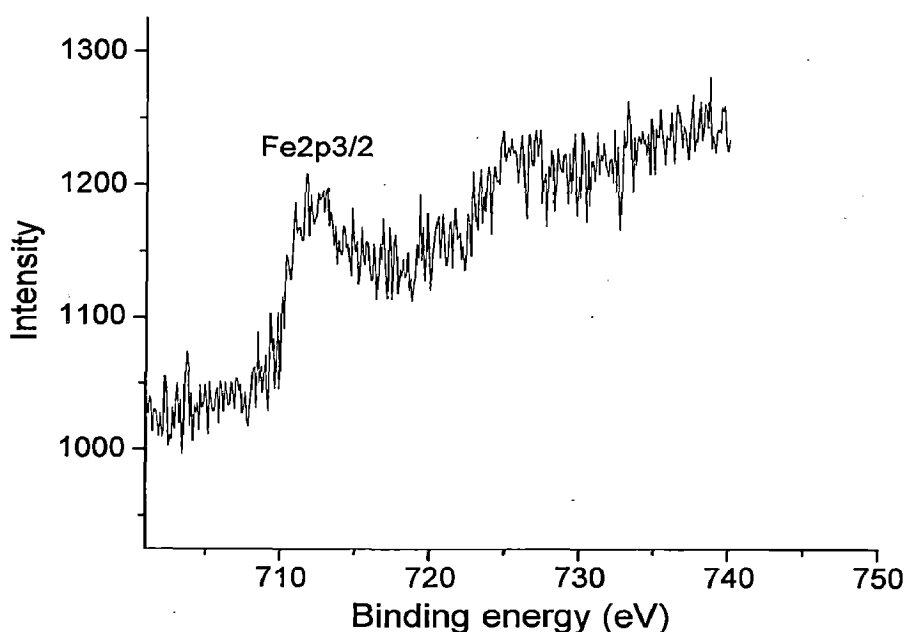


Fig. 2.17b. Detailed scan X-ray photoelectron spectroscopy (XPS) of MP-0.4 for Fe analysis.

### 2.3.11 Zeta potential measurement: Mechanism of the formation of MP nanomaterials

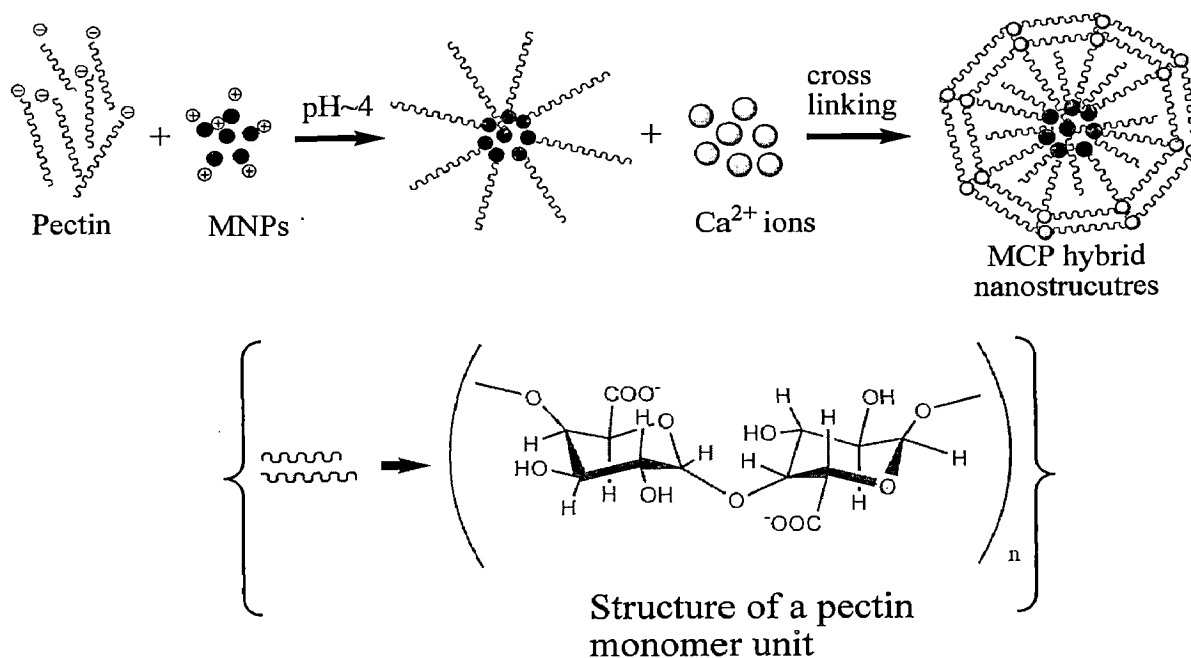
The mechanism towards formation of the MPs is schematically represented in Fig. 2.18, where zeta potential measurements (given in Table 2.3) offered an insight of the proposed mechanism. Firstly, the synthesis of highly stable MNPs at pH ~10, was confirmed from its zeta potential (−41.2 mV) measurement. These MNPs were conditioned at pH~ 4 to interact with pectin. At this pH, the zeta potential of MNPs was found to be +17.1 mV which was considered to be favorable for electrostatic interaction with polyanionic pectin molecules to form an MNP-pectin interface, because the zeta potential of pectin at pH ~4 was recorded to be −35.7 mV. The carboxylic groups of pectin molecules were cross-linked by Ca<sup>2+</sup> ions to form spherical nanomaterials, where the MNPs were encapsulated by calcium pectinate. The likelihood of formation of such spherical shape could be explained in terms of attaining stability by achieving minimum surface energy. The cross linking of pectin might be interpreted from the lowering of zeta potential measurements of MP-0.4 (−17.9 mV), MP-0.6 (−14.7 mV) and MP-1.0 (−14.6 mV) as compared to that of pectin (−35.7 mV). The lowering of zeta potential might be attributed to shielding of charge density on the pectin molecules due to its electrostatic interactions with Ca<sup>2+</sup> ions.

Table 2.3 Zeta potential measurements of magnetite nanoparticles (MNPs), pectin solution and MNP coated calcium pectinate hybrid nanomaterials (MPs).

| Samples        | Measured zeta potential value ( $\zeta$ ) in mV |
|----------------|---|
| MNPs at pH ~10 | − 41.2  |
| MNPs at pH ~4  | + 17.1  |
| Pectin at pH~4 | − 35.7  |
| MP-0.4         | − 17.9  |
| MP-0.6         | − 14.7  |
| MP-1.0         | − 14.6  |

It may be argued that, in order to achieve maximum cross linking it might be desirable to prepare these hybrid nanomaterials at pH > 5.5, where the pectin molecules exhibit very high zeta potential values ( $\zeta = -52$  to  $-56$  mV) [29, 30]. But, onset of depolymerization of pectin occurs at pH greater than 5.5 and thus higher pH values were not used [29, 30]. On the other hand, lower pH (e.g., pH ~2) tends to reduce the zeta potential of pectin [6] and hence may not be suitable for cross-linking with Ca<sup>2+</sup> ions. Besides, lower pH would favor dissolution of the MNPs encapsulated in the nanomaterials of MPs due to weakening of the Fe-O bond by protonation mechanism [31] and might lead towards loss of

magnetic property of the magnetite-pectin (MPs) hybrid nanomaterials. As a compromise, pH ~4 was chosen optimum for synthesis of MPs which offered suitably high zeta potential of pectin ( $\zeta = -35.7$  mV, Table 2.3). Notably, at pH ~4 the zeta potential of MNPs was measured to be +17.1 mV. On the basis of above studies a mechanism was proposed for the formation of magnetite –pectin hybrid nanomaterials as shown in Fig 2.18.



**Fig. 2.18.** Schematic representation of the proposed mechanism for the synthesis of MP nanomaterials.

### 2.3.12 Magnetic properties of MP nanomaterials

The magnetic properties of these MPs were studied by its SQUID measurements. It was noted from SQUID studies that as the precursor pectin concentration was increased from 0.4 to 1.0 % w/v the saturation magnetization ( $M_s$ ) of their corresponding nanomaterials of MP decreased. The measured  $M_s$  at 300 K and 2.5 T were 46.21 emu/g, 38.70 emu/g and 3.05 emu/g for MP-0.4, MP-0.6 and MP-1.0 respectively (Fig. 2.19). These values were however smaller than that of the as-synthesized MNPs (53.9 emu/g) and notably the  $M_s$  reduced significantly, when 1.0 % precursor pectin concentration was used for synthesis of MP-1.0. The drastic reduction of saturation magnetization due to increase in pectin concentration, which could be attributed to various reasons. It might be due to effect of small particle size owing to non-collinear spin arrangement at the surface, or due to the formation of magnetic dead layer by pectin at the domain boundary wall of MNPs [32, 33]. The particle size effect on reduction of  $M_s$  may be ruled out as the same batch of MNPs with

uniform particle size distribution was used for synthesis of different MP compositions. The magnetic moments could however be quenched due to the formation of magnetic dead layer at the domain wall of MNPs. This could hinder the domain wall motion during application of the magnetic field, which might be responsible for the reduction in the saturation magnetization in MPs. In this regard, pectin might form a magnetic dead layer at the surface of MNPs during the formation of the proposed MNP-pectin interface. The reduction in the magnetization for MP-0.6 as compared to those of MP-0.4 was attributed to formation of thicker dead layer of pectin at the domain boundary wall of encapsulated MNPs. It may therefore be inferred that the synthesis of nanomaterials of MPs resulted in pectin-MNP interface with formation of calcium pectinate at the periphery. This system as a whole exhibited superparamagnetic behavior with high magnetization at applied field of 2.5 T but appeared to be influenced by precursor pectin concentration.

It was noted that the magnetization curves (M-H) of different compositions of MPs recorded at 300 K from the hysteresis loop in SQUID measurements were similar to that of the as-synthesized MNPs, and exhibited negligible coercivity and remanence magnetization (Fig. 2.20). This property was attributed to superparamagnetic behavior of magnetite nanoparticles expected for sizes less than 20 nm [34], which further corroborated the ZFC and FC studies.

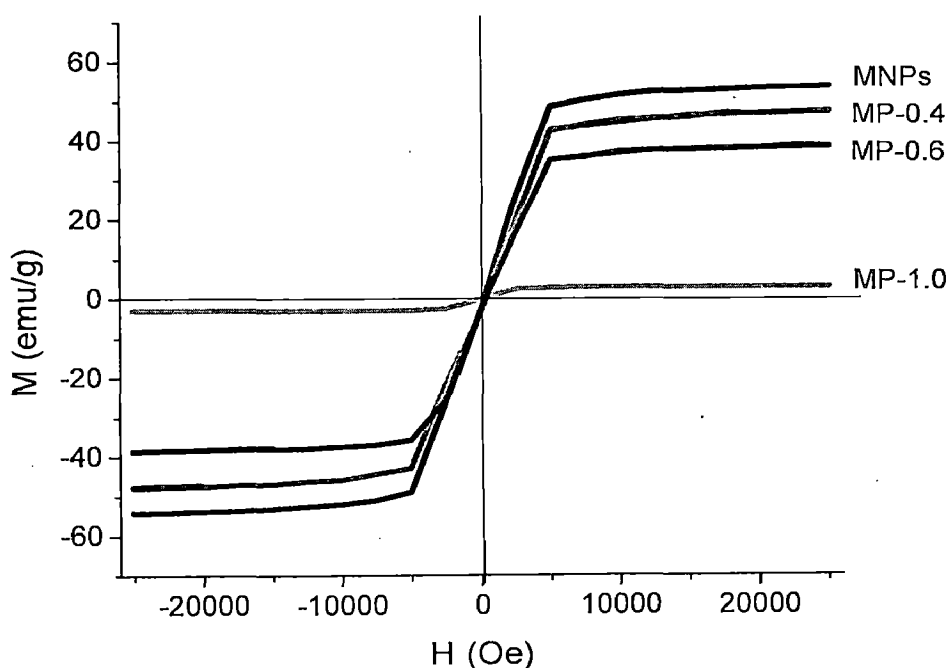


Fig. 2.19. Magnetization vs field (M-H) curve showing magnetization of MNPs and MPs recorded by SQUID at 300 K.

The superparamagnetic behavior of the nanomaterials of MP-0.4 was studied using the temperature dependence magnetization between 5 K and 300 K in zero-field cooling (ZFC) and that of field cooling (FC) in an applied magnetic field of 200 Oe (Fig. 2.20). The ZFC-FC curves were typically due to superparamagnetic MNPs which were encapsulated in MP-0.4. The curves diverged at 93.3 K, characterized as blocking temperature ( $T_B$ ), corresponded to the transition from ferromagnetic to superparamagnetic behavior. In the absence of applied magnetic field and when the sample was cooled the total magnetization was near to zero (as shown in ZFC curve). It was due to the random orientation of the magnetic moments of individual particles. On the other hand, at low temperatures (for FC curve), an externally applied magnetic field energetically favored the reorientation of the individual magnetic moment and hence resulted in the observed magnetization along the direction of the applied field. As the temperature was increased more particles reoriented their magnetic moment (magnetization) along the external applied field [35]. Due to this the magnetization increased till it reached a maximum value of 93.3 K as shown in the ZFC curve (Fig. 2.20). The superparamagnetism observed in MP-0.4 was attributed to the 2-8 nm sized MNPs encapsulated in it. The role of such small particles exhibiting superparamagnetism could be attributed to small magnetic anisotropy energy, proportional to the volume of the particle [34, 35].

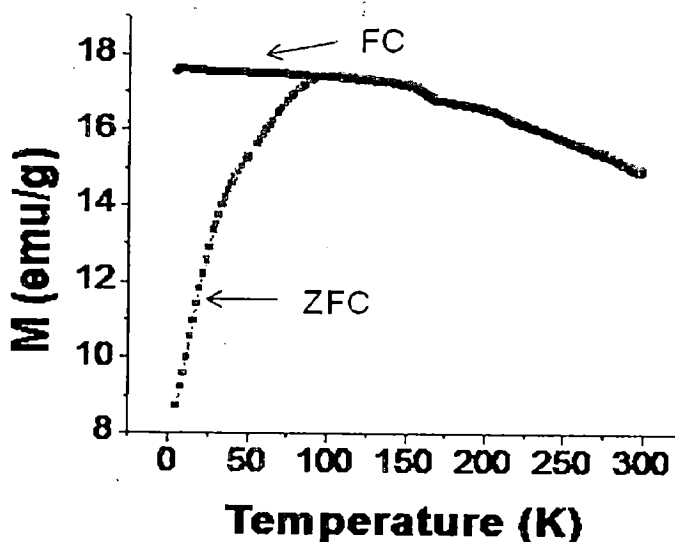


Fig. 2.20. ZFC and FC curve of MP-0.4 recorded at 200 Oe measured by SQUID.

### 2.3.13 Stability of MP-0.4 in simulated gastric fluid

Considering the potential applications of using the nanomaterials of MPs for colon specific delivery via oral administration, it is essential for the MPs to be protected from

Szabud  
13-07-2012

70  
70  
13/7/12

gastric degradation during its transit through stomach (pH~ 1.2) to avoid loss of magnetic materials. The non-degradability of MPs in gastric condition would further ensure protection of loaded materials (e.g., drugs) for colon specific delivery. This aspect was studied by treating MP-0.4 and equivalent amount of MNPs present in MP-0.4 for a total of 120 minutes in simulated gastric fluid (SGF). The cumulative Fe release in SGF from MP-0.4 in sink condition was found to be only 1.9 % for a period of 120 minutes, while that of MNPs was 21.3 % (Fig. 2.21). The low Fe release from MP-0.4 in SGF corroborated well with the Fe concentration at the surface of MP-0.4 calculated from the XPS measurement. This indicated that most of the MNPs were encapsulated within the hybrid nanomaterials of MP and were well protected from gastric environment. Degradation of MPs would have otherwise caused significant release and dissolution of MNPs in SGF. It may therefore be interpreted that the MP-0.4 was impermeable to acidic solution and ensured minimal loss of magnetic materials.

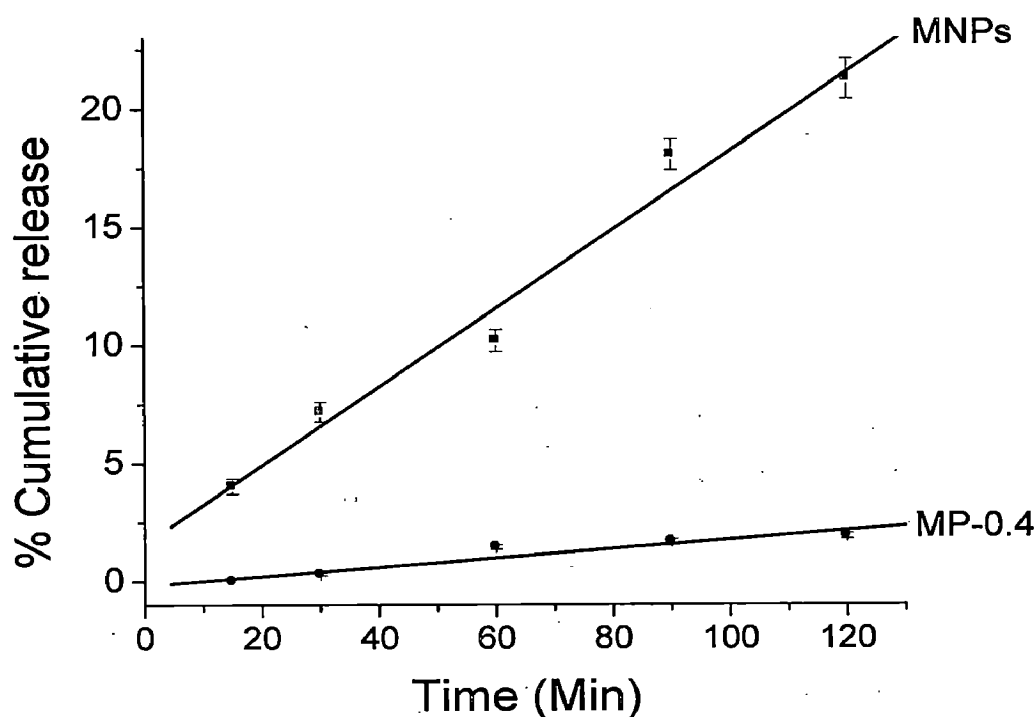


**Fig. 2.21.** Dissolution profile of Fe release from MNPs, MP-0.4 in SGF for a total period of 120 minutes (results are given as mean  $\pm$  standard deviation from triplicate analysis)

#### 2.3.14 Stability studies of MP-0.4 nanomaterials

The stability of the MP-0.4 nanomaterial was studied after its proper storage for 6 months at room temperature. Then, the characterization of this sample was carried out using XRD and Mössbauer spectroscopy. From XRD (Fig. 2.22), it was observed that there was no change in the peaks corresponding to the magnetite which is also indicated by its

corresponding Mössbauer spectra (Fig. 2.23). The  $^{57}\text{Fe}$  Mössbauer spectroscopy studies also showed characteristic tetrahedral ( $\text{Fe}^{3+}$ ) and octahedral ( $\text{Fe}^{2+/3+}$ ) sites of Fe at 5 K and in presence of 5 T externally applied magnetic field (Fig. 2.23). The hyperfine splitting parameters, e.g., isomer shift and quadrupole splitting corresponding to the two sextets (Fig. 2.23) also corroborated tetrahedral and octahedral environment and the corresponding intrinsic magnetic field of the aged MP-0.4 was measured to be quite similar to the freshly prepared one, which were in close agreement with the intrinsic magnetic field of MNPs and MP-0.4 freshly prepared and tested (Table 2.4).

In addition, magnetization of the aged MP-0.4 was measured to be 44.19 emu/gm and was  $\sim 4.5\%$  less than the measured magnetization recorded for freshly prepared MP-0.4 sample (Fig. 2.24). Thus it may be concluded that the system is stable in terms of its structure and magnetization.

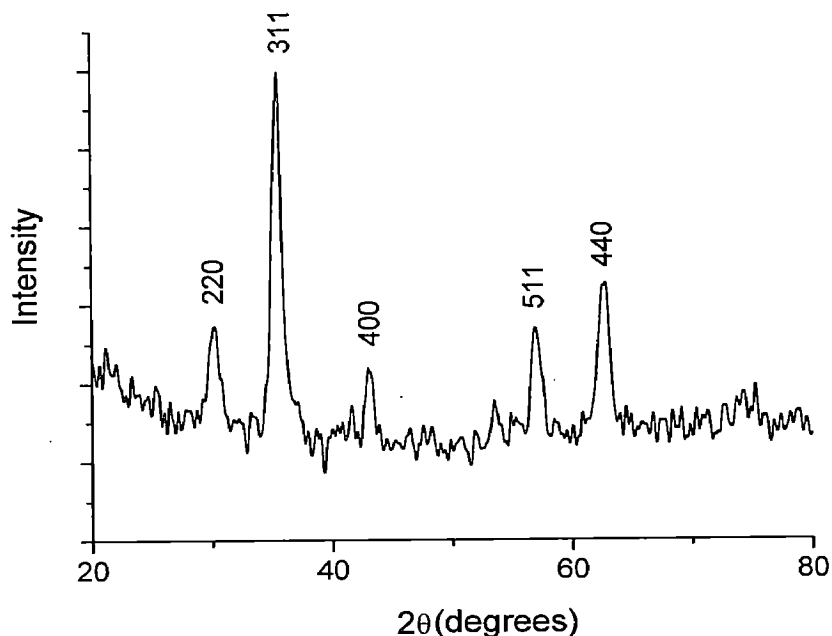


Fig. 2.22. XRD of MP-0.4 after 6 months showing the characteristic peaks of magnetite.

Table 2.4  $^{57}\text{Fe}$  Mössbauer spectroscopy hyperfine splitting parameters of MP-0.4 after 6 months.

|        | FWHM<br>(mm/s) | Isomer shift<br>(mm/s) | Quadrupole<br>splitting (mm/s) | Bhf (Tesla) | A23        | Area (%) |
|--------|----------------|------------------------|--------------------------------|-------------|------------|----------|
| RT     | ND             | ND                     | ND                             | 26.84 (Avg) | ND         | ND       |
| 5K     | 0.663±0.033    | 0.551±0.013            | 0.004±0.011                    | 55.2±0.04   | 2.00       | 70.1     |
|        | 0.608±0.053    | 0.172±0.026            | -0.139±0.026                   | 54.84±0.05  | 2.00       | 29.3     |
| 5K &   | 0.429±0.019    | 0.294±0.007            | 0.102±0.02                     | 58.85±0.04  | 0.05±0.06  | 31.9 (T) |
| 5Tesla | 0.538±0.013    | 0.516±0.006            | -0.06±0.01                     | 50.61±0.03  | 0.186±0.03 | 68.1(O)  |

\*ND = not determined, (T): Tetrahedral and (O): Octahedral

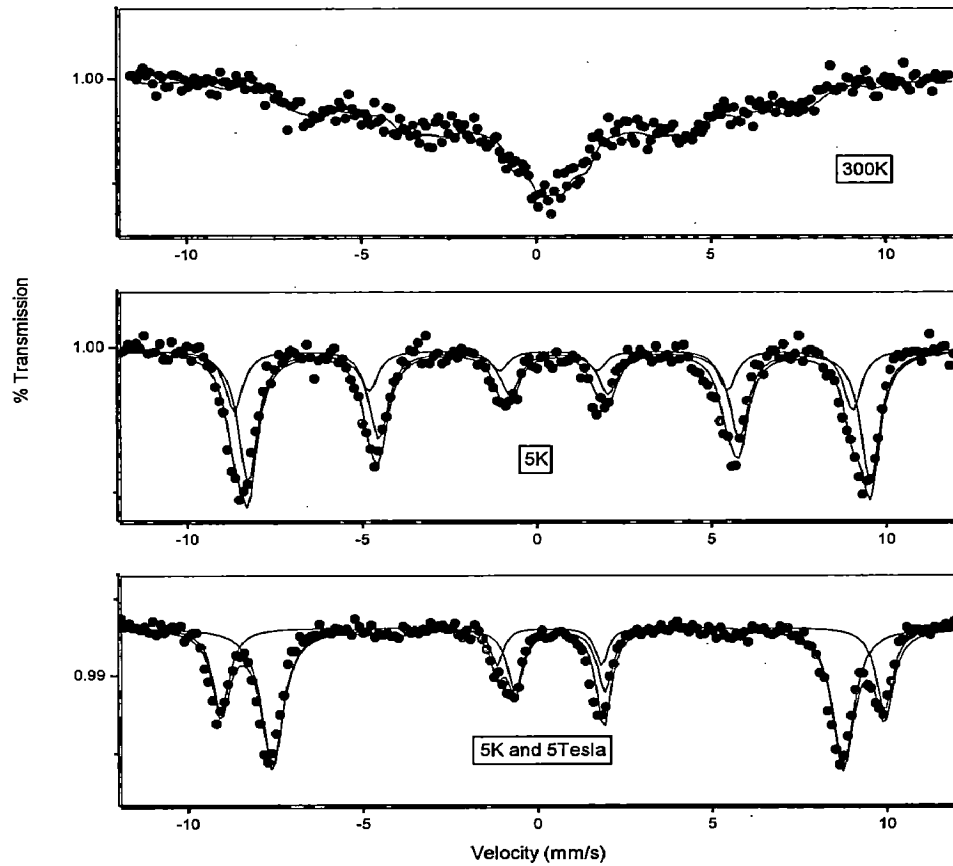


Fig. 2.23.  $^{57}\text{Fe}$  Mössbauer spectra of MP-0.4 after storing for 6 months recorded at room temperature, 5 K, 5 K and 5 Tesla.

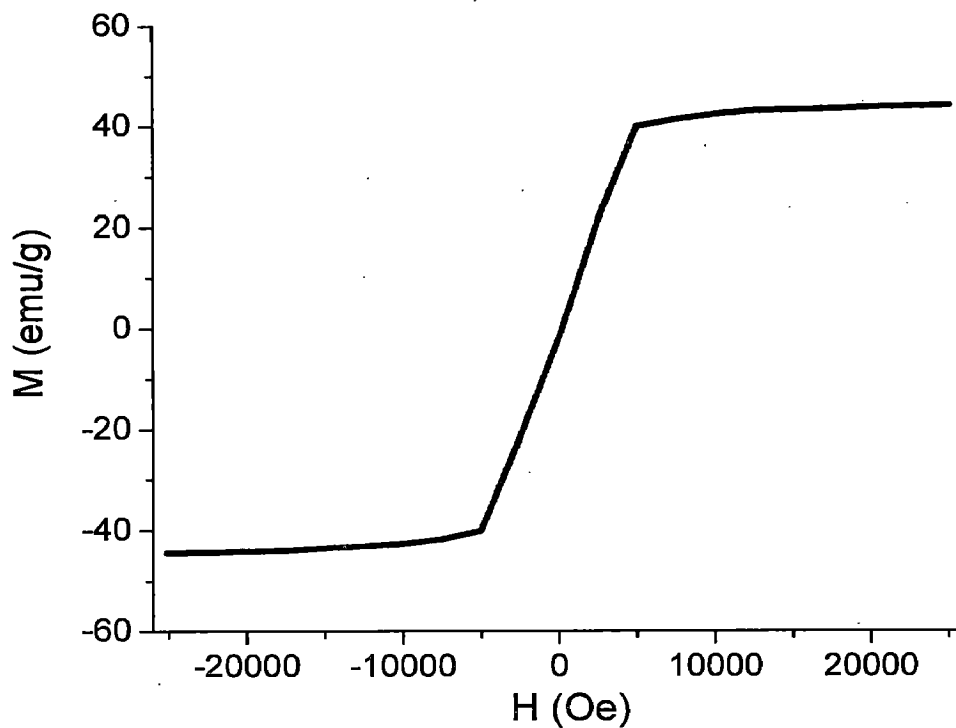


Fig. 2.24. Magnetization vs field (M-H) curve of MP-0.4 recorded by SQUID after 6 months of storage.



## 2.4 CONCLUSION

A facile and an in-expensive method has been developed to synthesize a novel nanomaterial (MP) by completely encapsulating stable superparamagnetic magnetite nanoparticles (MNPs) with pectin followed by cross linking with  $\text{Ca}^{2+}$  ions. The iron oxide nanoparticles were determined to be magnetite by XRD and further confirmed from recording two typical sextets by  $^{57}\text{Fe}$  Mössbauer spectroscopy. The synthesized MPs were spherical in shape with sizes ranging mostly between 100-150 nm in dry condition as evidenced by TEM and SEM. The DLS measurement of representative MP-0.4 nanomaterials showed unimodal size distribution, signifying that the method of synthesizing MPs offered a good control over the size of these nanomaterials. However, the average size of MPs in aqueous solution at  $\text{pH} \sim 4$  was about 400 nm which was due to the swelling of the pectin. Concerning the synthesis of MPs, initially the MNPs of 2-8 nm were synthesized by co-precipitation method with and without dispersing agents. The stability of MNPs was confirmed from its zeta potential measurement. The as-synthesized MNPs were then coated with pectin and formation of MNP-pectin interface was proposed on the basis of their electrostatic interaction at  $\text{pH} \sim 4$ , supported from their respective zeta potentials. Eventually, the MP nanomaterials were achieved by cross linking the carboxylic group of the pectin with  $\text{Ca}^{2+}$  ions to form rigid calcium pectinate structure at the periphery of MP. This was confirmed from reduction of zeta potential of pectin attributed to shielding of its higher charge density by  $\text{Ca}^{2+}$ . The formation of MP nanomaterials was further corroborated by FT-IR, TGA, XPS and its dissolution in SGF. According to our proposed mechanism, most of the MNPs were completely encapsulated within the MP nanomaterials. This was verified from the measurement of Fe content ( $43.3 \pm 2.1$  %) in MP-0.4 by instrumental neutron activation analysis, which corresponded to  $59.6 \pm 2.9$  % of MNPs in MP-0.4. Further, dissolution study of MP-0.4 in SGF which revealed negligible loss of Fe (1.9 %) from the MP-0.4 which correlated well with the surface Fe composition measured by XPS. The MPs were impermeable to acidic solution of SGF and were capable of protecting the encapsulated magnetic nanomaterials. The superparamagnetic nature of the MP-0.4 was confirmed by measuring ZFC-FC profile at an applied field of 200 Oe whose blocking temperature was found to be 93.3 K. Its saturated magnetization was 46.21 emu/g measured at an applied field of 2.5 T, which was lower than that of as-synthesized MNPs (53.9 emu/g at 2.5 T) and it decreased with increasing concentration of the precursor pectin. This property was explained on the basis of magnetic quenching phenomena due to the formation

of magnetic dead layer by pectin at the domain boundary wall of the MNPs which restricted its motion to orient the magnetic moments during externally applied magnetic field. Further the as synthesized system was found to be reasonably stable over a time of 6 months. Therefore, it was concluded that though prior reports on nanomaterials of only calcium pectinate with sizes ~150 nm sizes were available but our method of synthesis could produce magnetically functionalized nanomaterials of the pectin. These nanomaterials could potentially find a wide range of biomedical applications, e.g., targeted delivery of drugs or other biomolecules, imaging by MRI or magnetic fluid hyperthermia.

## REFERENCES

1. Liu, L.; Fishman, M. L.; Kost, J.; Hicks, K.B. Pectin-based systems for colon specific drug delivery via oral route. *Biomaterials*. **2003**, *24*, 3333-3343.
2. Englyst, H.N.; Hay, S.; MacFarlane, G.T. Polysaccharide breakdown by mixed populations of human faecal bacteria. *FEMS Microbiol. Ecol.* **1987**, *95*, 163-171.
3. S.A. Pectin-based oral drug delivery to the colon Expert Opin. *Drug Deliv.* **2005**, *2*, 441-450.
4. Sande, S.A.; Sungthongjeen, S.; Pitaksuteepong, T.; Somsiri, A.; Sriamornsak, P. Studies on petins as potential hydrogel matrices for controlled- release drug delivery *Drug Dev. Ind. Pharm.* **1999**, *25*, 1271-1276.
5. Das, S.; Ng, J. K.Y. Formulation and optimization of zinc-pectinate beads for the controlled delivery of resveratrol. *Pharm. Sci.* **2009**, *99*, 840-860.
6. Cheng, K.; Lim, L. Y. Insulin-loaded calcium pectinate nanoparticles: effects of pectin molecular weight and formulation pH. *Drug Dev. Ind. Pharm.* **2004**, *30* (4), 359-367.
7. Yu, C.Y.; Cao, H.; Zhang, X.C.; Zhou, F.Z.; Cheng, S.X.; Zhang, X.Z.; Zhuo, R.X. Hybrid nanospheres and vesicles based on pectin as drug carriers. *Langmuir*, **2009**, *25*, 11720-11726.
8. Opanasopit, P.; Apirakaramwong, A.; Ngawhirunpat, T.; Rojanarata, T.; Ruktanonchai, U. Development and characterization of pectinate micro/nanoparticles for gene delivery. *Pharm. Sci. Tech.* **2008**, *9* (1), 67-74.
9. Huang, C.C.; Liu, T.Y.; Su, C.H.; Lo, Y.W.; Chen, J.H.; Yeh, C.S. Super paramagnetic Hollow and Paramagnetic Porous Gd<sub>2</sub>O<sub>3</sub> Particles. *Chem. Mater.* **2008**, *20*, 3840-3848.
10. Maenosono, S.; Suzuki, T. ; Saita, S. Superparamagnetic FePt nanoparticles as excellent MRI contrast agents. *J. Magn. Magn. Mater.* **2008**, *320*, L79-L83.
11. Cheng, G.; Romero, D.; Fraser, G.T.; Walker, A.R.H. Magnetic-Field-Induced Assemblies of Cobalt Nanoparticles. *Langmuir*, **2005**, *21*, 12055-12059.
12. Bulte, J.W.; Kraitchman, D.L.; Iron oxide MR contrast agents for molecular and cellular imaging. *Biomed.* **2004**, *17* (7), 484-499.
13. Dames, P.; Gleich, B.; Flemmer, A.; Hajek, K.; Seidl, N.; Wiekhorst, F.; Eberbeck, D.; Bittmann, I.; Bergemann, C.; Weyh, T.; Trahms, L.; Rosenecker, J.; Rudolph, C.

- Targeted delivery of magnetic aerosol droplets to the lung. *Nat. Nanotechnol.* **2007**, 2 (8), 495-499.
14. Shieh, D.B.; Cheng, F.Y.; Su, C.H.; Yeh, C.S.; M.T.; Wu, Y.; Wu, Y.N.; Tsai, C.Y.; Wu, C.L.; Chen, D.H.; Chou, C.H. Aqueous dispersions of magnetite nanoparticles with  $\text{NH}_3^+$  surfaces for magnetic manipulations of biomolecules and MRI contrast agents. *Biomaterials.* **2005**, 26, 7183-7191.
  15. Naruphontjirakul, P.; Viravaidya-Pasuwat, K. Development of doxorubicin – core shell O-succinyl chitosan graft pluronic<sup>®</sup>127 copolymer nanoparticles to treat human cancer *IJBBB.* **2011**, 1(2), 131-136.
  16. Hou, C.H.; Hou, S.M.; Hsueh, Y.S.; Lin, J.; Wu, H.C.; Lin, F.H. The fabrication and characterization of dicalcium phosphate dihydrate-modified magnetic nanoparticles and their performance in hyperthermia processes *in vitro.* *Biomaterials.* **2009**, 30, 4700-4707.
  17. Sestier, C. Z. G. M.; Lacava, L. M.; Lacava, M. F.; Da Silva, R. B.; Azevedo, N.; Buske, C.; Gansau, P. C.; Morais, O; Silva, F.; Pelegri, D.; Sabolovic, D. In vitro toxicity of magnetic fluids evaluated for macrophage cell lines. *J. Magn. Mater.* **2002**, 252, 403-405.
  18. Daniel-da-Silva, A.L.; Trindade, T.; Good fellow, B.J.; Costa, B.F.O.; Correia, R.N.; Gil, A.M. In situ synthesis of magnetite nanoparticles in carrageenan gels. *Biomacromolecules.* **2007**, 8 (8), 2350–2357.
  19. Gnanaprakash, G.; Mahadevan, S.; Jayakumar, T.; Kalyanasundaram, P.; Philip, J.; Raj, B. Effect of initial pH and temperature of iron salt solutions on formation of magnetite nanoparticles. *Mater. Chem. Phys.* **2007**, 103(1), 168-175.
  20. Washington, N.; Washington, C.; Wilson, C.G.; Physiological Pharmaceutics: Barriers to Drug Absorption. *Taylor and Francis.* **2001**.
  21. Sinha, V.R.; Kumria, R. Binders for colon specific drug delivery: an *in vitro* evaluation. *Int. J. Pharm.* **2002**, 249, 23-31.
  22. Schindler, P.W. A solution chemists view of surface chemistry. *Pure Appl. Chem.* **1991**, 63, 1697-1704.
  23. Mikhaylova, M.; Kim, D.K.; Bobrysheva, N.; Osmolowsky, M.; Semenov, V.; Tsakalakos, T.; Muhammed, M. Superparamagnetism of magnetite nanoparticles: dependence on surface modification. *Langmuir*, **2004**, 20, 2472-2477.

24. Sood, D.D.; Reddy, A.V.R.; Ramamoorthy, N. "Fundamentals of Radiochemistry" Indian Association of Nuclear Chemist and allied Scientist, Mumbai, 2000.
25. Mukhopadhyay, P.K. Proceedings of the Symposium on Intelligent Nuclear Instrumentation (INIT-2001) Bhabha Atomic Research Centre, Mumbai. 2001, 307–310.
26. British Pharmacopoeia commission office (BP 2009). Published by the stationary office on behalf of the medicines and healthcare products regulatory agency (MHRA); London., 2009.
27. Christian G.D., *Analytical Chemistry*, sixth ed., John Wiley & Sons, Singapore, 2003.
28. Sahu, S.; Dutta, R.K. Novel hybrid nanostructured materials of magnetite nanoparticles and pectin. *J. Magn. Magn. Mater.* 2011, 323(7), 980-987.
29. Rolin, C.; Nielsen, B.U.; Glaahn, P.E. In: Dumitriu S. (Ed.), Polysaccharides, Marcel Dekker, New York, 1998, 377-432.
30. Grant, G.T.; Morris, E.R.; Rees, D.A.; Smith, P.J.C.; Thom, D. Biological Interactions between Polysaccharides and Divalent Cations: The Egg-Box Model. *FEBS Lett.* 1973, 32, 195-198.
31. Van Oorschot, I.H.M.; Dekkers, M.J. Selective dissolution of magnetic iron oxides in the acid–ammonium oxalate/ferrous iron extraction method. I. Synthetic samples. *Geophys. J. Int.* 2001, 145, 740–748.
32. Shafi, K. V. P. M.; Ulman, A.; Dyal, A.; Yan, X.; Yang, N. L.; Estournes, C.; Fournes, L.; Wattiaux, A.; White, H.; Rafailovich, M. Magnetic enhancement of  $\gamma$ -Fe<sub>2</sub>O<sub>3</sub> nanoparticles by sonochemical coating. *Chem. Mater.* 2002, 14, 1778-1787.
33. Morales, M. P.; Verdaguer, S. V.; Montero, M. I.; Sterna, C. J.; Roing, A.; Casas, L.; Martinez, B.; Sandiumenge, F. Surface and internal spin canting in  $\gamma$ -Fe<sub>2</sub>O<sub>3</sub> nanoparticles. *Chem. Mater.* 1999, 11, 3058-3064.
34. Daou, T. J.; Pourroy, G.; Bégin, C. S.; Grenèche, J. M.; Ulhaq, B. C.; Legaré, P.; Bernhardt, P.; Leuvrey, C.; Rogez, G. Hydrothermal synthesis of monodisperse magnetite nanoparticles. *Chem. Mater.* 2006, 18, 4399–4404.
35. Si, S.; Kotal, A.; Mandal, T.K.; Giri, S.; Nakamura, H.; Kohara, T. Size-controlled synthesis of magnetite nanoparticles in the presence of polyelectrolytes *Chem. Mater.* 2004, 16, 3489-3496.

***CHAPTER - 3***  
***DICLOFENAC SODIUM LOADED***  
***IN MAGNETITE - PECTIN***  
***NANOMATERIALS***

### 3.1 INTRODUCTION

Non-steroidal anti-inflammatory drugs (NSAIDs) are globally the most widely used class of therapeutic drugs and are suitable for development of their sustained and/ or controlled release preparations [1]. The compound 2-[(2, 6-Dichlorophenyl) amino] benzene acetic acid is commonly known as diclofenac sodium (DS), is a drug of NSAID category which has potent anti-inflammatory, analgesic, antipyretic properties and is widely used in the treatment of rheumatoid disorders and other chronic inflammatory diseases [2]. The DS is characterized by a short biological half-life of 1 – 2 h attributed to a very rapid metabolism and elimination, and has high percentage capacity to bind with plasma protein [1, 3]. This necessitates repeated daily dosing during the course of treatment with the drug. Consequently it leads to severe dose-limiting side effects, including cardiac, gastrointestinal, hepatic and renal adverse effects [4]. Therefore, therapy with DS demands sustained/ controlled release formulation for prolonged action at desired sites. In this regard novel drug delivery strategies are required for enhancing the accumulation of DS at the inflammation region to achieve maximum therapeutic efficacy with minimal toxicity. This can be achieved either by specific recognition mechanism, e.g., ligand - or receptor - mediated targeting or by means of stimuli - sensitive drug carriers. The stimuli sensitive carrier delivers drug upon exposure to an external stimulus namely pH, ultrasound, light, enzymes and magnetic field [5-9]. With both the targeting methods, minimal systemic distribution of the drug is achieved which minimizes the undesired side effects and enhances the therapeutic efficacy [10, 11]. Moreover, the dose of the drug required for therapy can be reduced substantially as the non -specific distribution can be minimized. With the advent of nanotechnology, drug formulation can be achieved in the form of nanoparticles (NPs) of desirable size, which promote accumulation of active drug molecules at pathological areas [12, 13]. In this regard, superparamagnetic iron oxide nanoparticles (SPIONs) are promising nanocarriers for magnetically guided transportation of drugs for its delivery at local sites of inflammation especially of the musculoskeletal system. This will provide therapeutic concentrations while minimizing the unwanted side effects [14, 15]. Various types of polymer-iron oxide nanocomposites have been developed for potential targeted drug delivery system [16-18]. Inclusion of SPIONs into polymeric materials does not increase the toxicity, as reported in clinical phase I trials [19]. In this regard, it may be highlighted that the iron oxide NPs coated with chitosan exhibited excellent drug loading and release properties [20]. It is worth investigating on the usages of low cost, biodegradable polymeric materials, for higher drug

loading efficiency, together with sustained or controlled release properties and their ability to exhibit high magnetic susceptibility.

### **3.1.1 Objective of the study**

To fabricate and evaluate a potential targeted drug delivery system comprising of diclofenac sodium loaded in the hybrid nanomaterials of magnetite and calcium pectinate. Cross linking of pectin was required as pectin alone is not capable of shielding the drug due to its water solubility and swelling effect [21, 22]. The formulation parameters were optimized for maximum loading of DS. These nanomaterials of magnetite nanoparticles and pectin loaded with DS were characterized by XRD, SEM-EDAX, TEM, DLS, FT-IR, Thermal studies, zeta potential, SQUID and vibrating sample magnetometer (VSM). The *in vitro* release of DS was studied in simulated gastrointestinal fluids and in phosphate buffer solution.

## **3.2 MATERIALS AND METHODS**

### **3.2.1 Materials**

Chemicals needed for synthesis of MNPs and calcium pectinate, as discussed in Chapter 2, were used. In addition, diclofenac sodium (DS) was procured from Sigma-Aldrich, GmbH, Germany and was also obtained as a gift sample from Piramal Life Sciences Limited Mumbai, India. Phosphate buffer solution was prepared using disodium hydrogen orthophosphate, potassium dihydrogen orthophosphate, sodium hydroxide, sodium chloride, procured from Merck, India. The enzymes pepsin (with an activity of 800-2500 mL units/mg of protein), pancreatin 4NF (from porcine pancreas) and pectinase (polygalacturonase) were procured from Hi-media lab, India. Dialysis membrane made up of regenerated cellulose with MWCO of about 3500 D was procured from Fisher Scientific Pittsburgh PA. Millipore water (resistivity of 18.1 M $\Omega$  cm at 25 °C) was used in all the experiments.

#### **3.2.1.1 Diclofenac sodium**

##### *Physical and chemical properties*

The chemical structure of diclofenac sodium is given in Fig. 3.1. Its molecular weight is 318.13 g/mol. It is an odorless white to off-white colored powder which is crystalline in nature. It is freely soluble in methanol, soluble in ethanol, sparingly soluble in



water, and but is insoluble in chloroform and in dilute acid. Since it is sparingly soluble in water it is included in class II drug as per biopharmaceutical classification system (BCS).

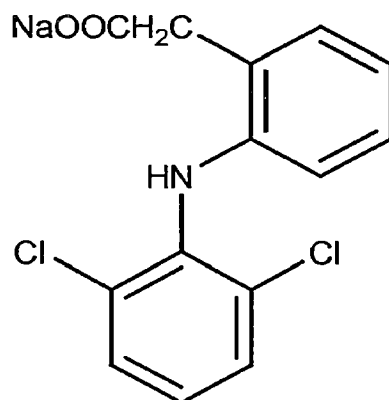


Fig.3.1. Structure of diclofenac sodium.

### Pharmacology

The drug diclofenac sodium (DS) has been reported to exhibit anti-inflammatory (both in acute and subchronic inflammation), analgesic and antipyretic properties. Therefore, it is also used for minor aches, pains, inflammatory disorders and fever associated with common infections. DS can be used against various inflammatory disorders in musculoskeletal system, namely, arthritis, rheumatoid arthritis, polymyositis, dermatomyositis, osteoarthritis, spondylarthritis, ankylosing spondylitis, gout attacks, dental pain, temporomandibular joint and muscle disorders [23]. It is also useful in pain management against kidney stones, gallstones and also in the treatment of acute migraine, in mild to moderate post-operative or post-traumatic pain – particularly when inflammation is also present. It is effective against dysmenorrhea and endometriosis [24]. It also exhibits antiuricosuric properties [25].

### Method of administration

Various routes for administration of DS are adopted namely oral, rectal, intramuscular (IM), intravenous (IV) and topical. Based on the routes of administration a variety of formulations are available for this drug in the national as well as international market. The name of the drug under separate categories of administration is given below along with the name of the company that markets/ manufactures the particular dosage form of the drug:

- a) Oral administration. Tablets of strength 50 mg and 100 mg are available by the commercial name (manufacturer's name in the bracket from India, unless stated): Actfit (BMW), Alefen (Allenge), Diclowin (Wings Pharma), Fensaide (Nicholas),

- Diclofenac DT - dispersible tablet (Blue Cross Laboratories), Dan SR – sustained release tablets (Unison Pharma), Actfit SR (BMW), Voveran SR – sustained release (Novartis), Voltaren XR - extended release tablets (Novartis), Voveran and Voltaren – enteric-coated tablets (Novartis), Diclonac - modified release tablet (Lupin Laboratories).
- b) Intramuscular and intravenous injections: Aclomax (Admac), Actfit (BMW), Adiflam inj (Leben Labs), Agile inj (Ind-Swift), Acnec (Acme), Antiflam inj {75 mg (Prem Pharma)}, Argesic inj {5 mg (Centaur)}, Alefen inj (Allenge) , Movonac (Nicholas Piramal), Diclomol (Win-Medicare) *etc.*
  - c) External gel-based formulation: 3-D (Intas), Alnase gel (Alna Bio), Adiflam gel (Leben Labs), Adgel (Adley), Adiflam gel (Leben Labs), Actfit gel (BMW) *etc.*
  - d) Eye drops e.g. Voltarol ophtha (Novartis Pharmaceuticals, Canada) and Voltaren Ophthalmic (Novartis Pharmaceuticals, Australia).
  - e) Topical lotion e.g. Pennsaid (Nuvo Research Inc. USA).
  - f) Topical patch e.g. Flector patch (King Pharmaceuticals Inc. U.S.A.)

### *Mechanism of action*

DS acts by inhibition of potent enzyme cyclo-oxygenase which reduces the release of arachidonic acid, and enhances its uptake [26]. This results in a dual inhibitory effect on both the cyclo-oxygenase and lipoxygenase pathways.

### *Side effects*

The long-term administration of DS has been reported to result in renal (kidney) papillary necrosis and other renal medullary changes. Usually these adverse renal effects are attributed to the decreased synthesis of renal prostaglandins. Further, this effect is also observed during long-term use in non-sensitive persons and where the resistance to side-effects decreases with age, especially for elderly patients. The reduction in prostaglandin formation decreases the renal blood flow, which may precipitate clear renal decompensation. Therefore in patients with advanced kidney disease, treatment with diclofenac sodium is not recommended [25, 26]. If there is any necessity to initiate NSAID therapy, close monitoring of the patient's kidney function is advisable.

Rarely the liver damage occurs on continuous treatment with DS. Further this damage if occurs is usually reversible. Hepatitis may occur infrequently without any

warning symptoms but it may be fatal. The symptomatic liver disease is developed more commonly in patients with osteoarthritis than those suffering from rheumatoid arthritis. Therefore, the functioning of liver should be monitored regularly during long-term treatment. But it must be noted that, if used for the short-term treatment of pain or fever, diclofenac exhibits less hepatotoxicity than other available NSAIDs. Similarly compared to a variety of NSAIDs available, DS exhibits better tolerance but its long-term use predisposes for peptic ulcer [27]. Prolong treatment with DS might lead to severe side which could lead to upper GI ulcers, gross bleeding, or perforation. This trend if continues, the chances of developing a severe GI complication may occur at some time during the course of therapy. However, even short-term therapy has risk. Therefore, DS should be prescribed with extreme caution in those with a prior history of ulcer disease or GI bleeding [27]. Usually the most impulsive and fatal GI complications are observed in elderly or weak patients and therefore special care should be taken while treating this population.

The drug is a weak and reversible inhibitor of thrombocytic aggregation needed for normal coagulation. In addition, it exhibits bone marrow depression which is though noted infrequently which may progress into leukopenia or agranulocytosis or thrombopenia with / without purpura or aplastic anemia.

#### *Contraindications*

DS is contraindicated for the treatment of perioperative pain in the setting of coronary artery bypass graft (CABG) surgery and in patients with serious gastrointestinal complications. The use of diclofenac sodium in patients with hepatic porphyria should be avoided.

Thus, it was concluded that to minimize these complications, the lowest effective dose of this drug should be used for the shortest possible duration or alternate therapies should be considered. In this regard the targeted therapy is a promising approach. In view of these reports nanoscale targeted drug delivery system loaded with DS in biodegradable polymer is an excellent option.

#### ***3.2.2 Method for fabrication of magnetite-pectin nanomaterials cross linked with $Ca^{2+}$ ions loaded with DS***

MNPs were synthesized by co-precipitation method as discussed in chapter 2 using the optimized conditions. After washing the MNPs, they are redispersed in water and the pH

was adjusted to  $\sim 4$  with dilute HCl. A 25 mL of the dispersion of MNPs were then mixed with 25 mL of 0.4 %, 0.6 % and 1.0 % w/v of pectin solution at pH  $\sim 4$ .

To this dispersion, DS was added, which followed by slow addition of 25 mL of  $\text{CaCl}_2$  solution as given in Table 3.1. For drug loading studies, DS of 0.01 M and 0.05 M concentrations were used. The whole mixture was allowed to stir for 6 h. The concentration of free dissolved drug in the dispersion was determined by the bulk equilibrium reverse dialysis [28].

**Table 3.1.** Optimization of encapsulation efficiencies and drug loading content in MP-DS hybrid nanomaterial using fixed concentration of MNPs.

| Concentration of DS (M) | Pectin (% w/v) | $\text{CaCl}_2$ (% w/v) | Encapsulation Efficiency (%) | Drug loading content (wt %) |
|-------------------------|----------------|-------------------------|------------------------------|-----------------------------|
| 0.01 M                  | 1.0%           | 2.0%                    | $86.0 \pm 0.9$               | ND*                         |
| 0.01 M                  | 0.6%           | 1.2%                    | $59.7 \pm 1.3$               | $29.8 \pm 1.8$              |
| 0.01 M                  | 0.4%           | 0.8%                    | $60.6 \pm 1.1$               | $28.9 \pm 1.2$              |
| 0.05 M                  | 0.4%           | 0.8%                    | $19.4 \pm 2.2$               | ND**                        |

ND\*: Not determined, as 1.0% pectin resulted in polymeric matrix formation,

ND\*\*: Not determined as encapsulation efficiency was poor

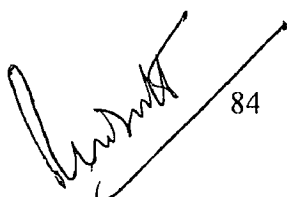
### 3.2.3 Methodology for drug loading analysis

It may be noted that the dispersion obtained after the synthesis of magnetite-pectin nanomaterials cross linked with calcium and treated with DS, comprised free dissolved drug and drug loaded in nanomaterials. Therefore the amount of drug loaded in the nanomaterials would be the difference of total drug taken for fabrication and amount of the free dissolved drug in the dispersion i.e.

Amount of drug loaded (g) = Initial amount of the drug taken – amount of free dissolved drug.

The amount of the free dissolved drug present in the dispersion was determined after performing bulk equilibrium reverse dialysis. The amount of drug was calculated by multiplying concentration of drug with the volume used. Briefly, a dialysis bag of MWCO 3500 D sealed from both ends was immersed in the dispersion of magnetite-pectin nanomaterials cross linked with calcium and loaded with DS and was stirred for 12 h. During this period free dissolved drug in the dispersion diffused into the dialysis bag and attained equilibrium [28]. The concentration of the drug present inside the dialysis bag was

Ssahel  
13-07-2012

  
84

measured by UV visible spectrophotometry at  $\lambda_{\max} = 276$  nm. The detail of drug analysis is discussed in section 3.2.6.

The drug loading content (wt %) in magnetite-pectin nanomaterials cross linked with  $\text{Ca}^{2+}$  and loaded with DS was calculated as follows:

$$\text{Drug loading content (wt \%)} = (a / b) * 100$$

a = amount of the drug loaded in magnetite-pectin nanomaterials loaded with DS.

b = weight of fabricated magnetite-pectin- nanomaterials loaded with DS (in g).

The extent of drug incorporation into magnetite-pectin nanomaterial was expressed in terms of % encapsulation efficiency of DS, which is given as:

$$\% \text{ Encapsulation efficiency} = (a / t) * 100$$

a = amount of the drug loaded in magnetite-pectin nanomaterials loaded with DS.

t = Initial amount of the drug taken.

The advantage of this method is the minimization of processing steps like centrifugation, filtration *etc.* which may lead to the loss of the material during the process. It may also be noted that the % encapsulation efficiency corresponded to the capacity of the drug carrier (nanomaterials of magnetite-pectin cross linked with  $\text{Ca}^{2+}$ ) to load drug. However, it is also important to evaluate the concentration of drug (w/w) in these systems which is given as drug loading content (wt %).

It may be noted here that, the magnetite pectin nanomaterials cross linked with calcium which were fabricated using fixed concentration of the dispersion of MNPs, 0.4 % pectin and 0.8 %  $\text{CaCl}_2$  as discussed in chapter 2, without DS will now be referred to as MP (magnetite nanoparticles: pectin cross linked with  $\text{Ca}^{2+}$ ). Further the batches prepared using same composition as that of MP loaded with 0.01 M DS will now be referred to as MP-DS (magnetite nanoparticles: calcium pectinate: diclofenac sodium).

### 3.2.4 Characterization

The details of the methods used for characterization, namely, XRD, SEM-EDAX, TEM, DLS, TG-DTA, INAA, FT-IR, SQUID, and VSM. The details of techniques other than VSM are as discussed in chapter 2. The VSM (Model 155, Princeton applied research) was used to analyze the magnetic properties of the as-synthesized nanomaterials. A known amount of lyophilized samples (MNPs, MP and MP-DS) were respectively packed in a diamagnetic capsule and were inserted in a polyethylene straw as a sample holder. The

magnetization measurements were recorded from the hysteresis loop of M-H curve in the range  $\pm 10.0$  kOe (Tesla) at room temperature by VSM.

### 3.2.5 Methodology for *in vitro* drug release

It has been reported that after the oral administration of the drug, it passes through stomach (pH  $\sim 1.2 - 3.5$ , transit time  $\sim 1-2$  h) and small intestine (pH  $\sim 5.5 - 6.8$ , transit time  $\sim 3 - 6$  h) before arrival to large intestine i.e. colon (pH  $\sim 6.4 - 7.0$ , transit time  $\sim 12-48$  h) [29]. In addition, in the case of the proximal colon pH values as low as 5.5 – 5.7 have also been reported [29, 30]. Further the optimum pH for the activity of pectinolytic enzyme has been reported to be between 3 and 5 as a compromise pH 5.5 was set for simulated colonic fluid (SCF) with 2.5 % (w/v) of the enzyme pectinase [30, 31]. Therefore, to simulate the gastrointestinal conditions, *in vitro* release studies were carried out sequentially in simulated gastric fluid (SGF) at pH 1.2 for 2 h, in simulated intestinal fluid (SIF) at pH 6.8 for 3 h and in simulated colonic fluid (SCF) at pH 5.5 for the remaining period of 48 h at 37 °C and 100 rpm. In addition to the potential oral administration approach, the drug release from the newly developed nanomaterials of MP-DS via potential intravenous administration approach was estimated by *in vitro* release study in phosphate buffer pH 7.4.

#### 3.2.5.1 Preparation of simulated gastric fluid (SGF) with enzymes

Two grams of sodium chloride (NaCl) and 3.2 g of purified pepsin (with an activity of 800-2500 mL units/mg of protein) were accurately weighed and dissolved in sufficient quantity of Millipore water. Accurately about 80 mL of 0.1 M hydrochloric acid (HCl) was added to the above solution and the volume was made up to 1000 mL using Millipore water. The pH was finally adjusted to 1.2 using 0.1 N HCl / 0.1 N NaOH [32].

#### 3.2.5.2 Preparation of simulated intestinal fluid (SIF) with enzymes

An amount of 6.8 g of monobasic potassium dihydrogen phosphate ( $\text{KH}_2\text{PO}_4$ ) was accurately weighed and dissolved in 250 mL of Millipore water. Seventy seven mL of 0.2 N sodium hydroxide was added to the above solution and the volume was made to 500 mL using Millipore water. Ten grams of purified pancreatin (pancreatin 4 NF from porcine pancreas) was added and the volume was made up to 1000 mL using Millipore water. The pH was finally adjusted to  $6.8 \pm 0.1$  using 0.1 N HCl / 0.1 N NaOH [32, 33].

### 3.2.5.3 Preparation of simulated colonic fluid (SCF) with pectinase

2.5 % w/v solution of pectinase (polygalacturonase) was prepared in phosphate buffer (pH 5.5). The buffer solution was prepared as follows:

Two solutions A and B were prepared.

Solution A: Accurately weighed 13.61 g of potassium dihydrogen orthophosphate ( $\text{KH}_2\text{PO}_4$ ) was dissolved in 1000 mL.

Solution B: Accurately weighed 35.81 g of disodium hydrogen orthophosphate ( $\text{Na}_2\text{HPO}_4$ ) was dissolved in 1000 mL. Then 96.4 mL of solution A was mixed with 3.6 mL of solution B to obtain phosphate buffer of pH 5.5 [32].

### 3.2.5.4 Preparation of phosphate buffer solution (pH 7.4)

To obtain phosphate buffer (pH 7.4), 250 mL of 0.2 M potassium dihydrogen orthophosphate ( $\text{KH}_2\text{PO}_4$ ) was added to 393.4 mL of 0.1 M sodium hydroxide [32].

### 3.2.6 Analysis of *in vitro* drug release in the respective simulated fluids

The dialysis bag diffusion technique was used to study the *in vitro* release of the drug DS from MP-DS nanomaterials [28]. Briefly, the MP-DS nanomaterials fabricated using 0.4 % pectin solution and 0.01 M DS was transferred to a dialysis bag containing 5 mL of freshly prepared simulated gastric fluid (SGF) at pH 1.2, which contained 0.32 % w/v pepsin. This is referred to as donor compartment. This bag with its contents was then transferred to 95 mL of the SGF without enzymes (referred as receptor compartment) to simulate *in vitro* release studies for 2 h at a temperature of  $37.0 \pm 0.1$  °C and at 100 rpm in incubator shaker. This was followed by *in vitro* release studies for 3 h in simulated intestinal fluid (SIF) at pH 6.8 containing 1.0 % w/v pancreatin. Finally the *in vitro* release study in simulated colonic fluid (SCF) containing 2.5 % w/v pectinase at pH 5.5 was performed for a period up to 48 h, to estimate the % cumulative release of DS from MP-DS nanomaterials in SGF, SIF and SCF media to mimic gastrointestinal conditions. In the similar manner % cumulative release was determined in phosphate buffer solution, at pH ~7.4, without enzyme, for 48 h to mimic release condition of the drug DS in blood.

About 1.5 mL of an aliquot was withdrawn from the receptor compartment at each specified time intervals and was replaced with equal volume of fresh medium to mimic the sink conditions of the human body. The aliquot was centrifuged at 15000 rpm for 15

minutes and the supernatant liquid consisting of released drug was estimated with Shimadzu 1600 UV visible spectrophotometer against appropriate blank.

It may be noted that the analysis of drug by UV visible spectrophotometry in the presence of enzymes especially pancreatin, was found to be inaccurate due to turbidity. It is therefore necessary to separate drug from the dispersion. This was achieved by conducting the *in vitro* release studies of DS performed in a dialysis bag containing the enzyme, where the drug released from MP-DS could diffuse out of the dialysis bag while the enzymes of larger molecular weight cannot diffuse out. The estimation of DS released in these media was carried out by UV-visible spectrophotometry.

#### 3.2.6.1 Determination of $\lambda_{\max}$ in Millipore water, SGF, SIF (without pancreatin), SCF and phosphate buffer solution.

The UV-visible absorption spectra of the solution of diclofenac sodium in each of the above medium were recorded to determine the  $\lambda_{\max}$  of DS in the respective media for drug release studies.

10 mg of diclofenac sodium was accurately weighed and transferred to 100 mL volumetric flask, sufficient quantity of Millipore water / SGF without pepsin / SIF without pancreatin / SCF without pectinase was added to dissolve it. The volume was made up to 100 mL with the respective medium to obtain a stock solution of 100  $\mu\text{g/mL}$ . From this stock solution, 1 mL aliquot was taken and diluted to 10 mL. This solution was scanned between 230 to 350 nm on a Shimadzu 1600 double beam UV-Visible spectrometer. The UV spectra exhibited  $\lambda_{\max}$  at 276 nm in all four media and agreed well with the reported values [34]. All measurements were thus carried out at  $\lambda_{\max} = 276$  nm in triplicate, for estimation of the concentration of diclofenac sodium released in these media.

#### 3.2.6.2 Calibration curve for estimation of diclofenac sodium in Millipore water

The calibration curve was prepared by recording absorbance at  $\lambda_{\max} = 276$  nm. The mean value and the standard deviations from triplicate analysis were calculated. The mean values of the absorbance were plotted against the respective concentration of DS ranging between 5 and 40  $\mu\text{g/mL}$  to obtain a calibration curve (Fig. 3.2). A linear fit of the calibration plot ( $R^2 = 0.996$ ) was obtained. The concentration of the drug was calculated from the calibration curve.



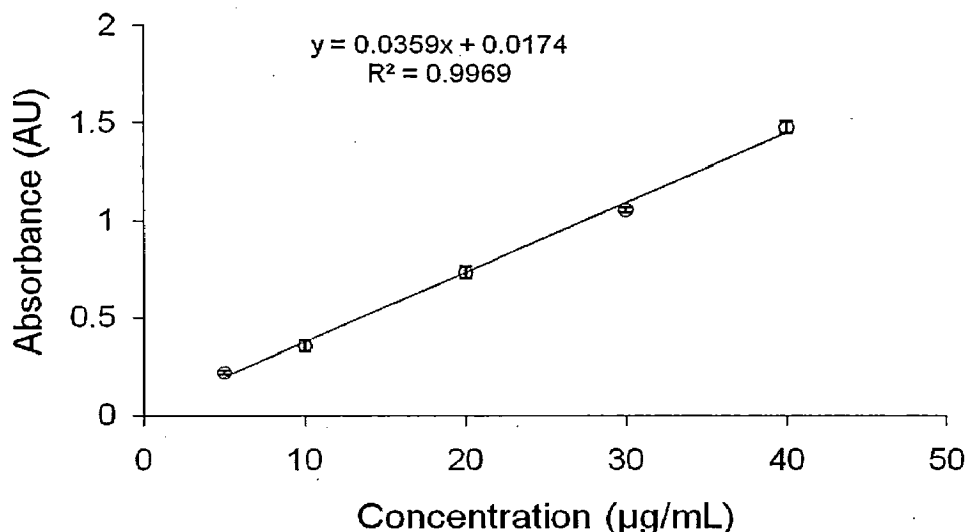


**Fig. 3.2.** Calibration curve for estimation of diclofenac sodium in Millipore water measured at  $\lambda_{\max} = 276$  nm. (Absorbance is given as mean  $\pm$  standard deviation of triplicate analysis)

### 3.2.6.3 Calibration curve for estimation of diclofenac sodium in simulated gastric fluid (SGF)

Since the drug was poorly soluble in SGF thus the equation obtained from the calibration curve corresponding to the different concentrations of DS in Millipore water was used to determine the concentration of the DS in SGF.

### 3.2.6.4 Calibration curve for estimation of diclofenac sodium in simulated intestinal fluid (SIF) at 276 nm

It was noted that by adding pancreatin to solution containing drug in the SIF resulted in turbidity and was thus not-suitable for measuring concentration of drug by UV-visible spectrometry. Therefore the calibration curve was plotted without this enzyme. Further because of this, the protocol given for analysis of released drug was modified (discussed in section 3.2.6). The aliquots from the stock solution of 100  $\mu\text{g/mL}$  were taken and dilutions were made with SIF (without pancreatin) to prepare calibration curve of the DS in the concentration range of 5 to 40  $\mu\text{g/mL}$ . The absorbance of dilutions was measured in triplicate by UV-Visible spectrometry at  $\lambda_{\max} = 276$  nm against SIF (without pancreatin) as blank and the calibration curve was plotted (Fig. 3.3). A linear fit of the calibration curve was obtained ( $R^2 = 0.998$ ). Analysis of *in vitro* release in SIF was performed accordingly.

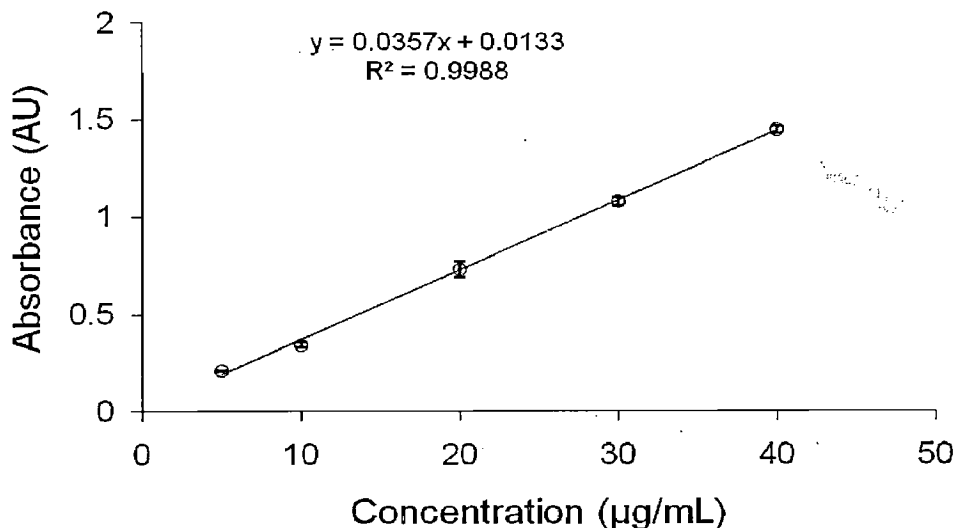


**Fig. 3.3.** Calibration curve for estimation of diclofenac sodium in SIF without pancreatin measured at  $\lambda_{\max} = 276$  nm (Absorbance is given as mean  $\pm$  standard deviation of triplicate analysis)

### 3.2.6.5 Calibration curve for estimation of diclofenac sodium in simulated colonic fluid (SCF)

The aliquots from the stock solution of 100  $\mu\text{g/mL}$  were taken and dilutions were made with SCF without pectinase to prepare sample for calibration in the concentration range of 5 to 40  $\mu\text{g/mL}$ . The absorbance of dilutions was measured by UV-Visible spectrometer at  $\lambda_{\max} = 276$  nm against SCF without pectinase as blank and the calibration curve was plotted (Fig. 3.4). A linear fit of the calibration curve ( $R^2 = 0.997$ ) were obtained.

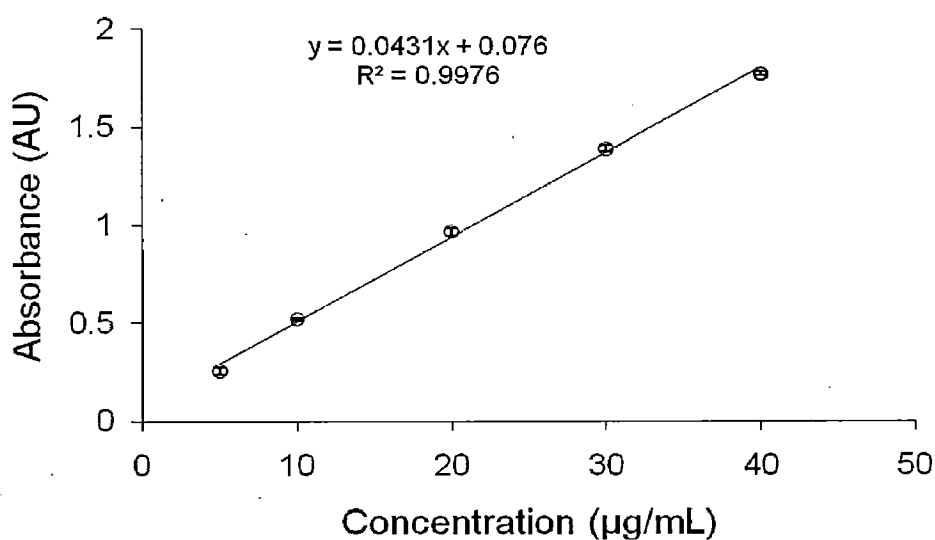


**Fig. 3.4.** Calibration curve for estimation of diclofenac sodium in SCF without pectinase measured at  $\lambda_{\max} = 276$  nm (Absorbance is given as mean  $\pm$  standard deviation of triplicate analysis)

### 3.2.6.6. Calibration curve for estimation of diclofenac sodium in phosphate buffer pH 7.4

The aliquots from the stock solution of 100  $\mu\text{g/mL}$  were taken and dilutions were made with phosphate buffer pH 7.4 to prepare sample for calibration in the concentration range of 5 to 40  $\mu\text{g/mL}$ . The absorbance of the dilutions was measured by UV-Visible spectrometry at  $\lambda_{\text{max}} = 276 \text{ nm}$  against phosphate buffer as blank and the calibration curve was plotted (Fig. 3.5). A linear fit of the calibration curve ( $R^2 = 0.999$ ) was obtained.

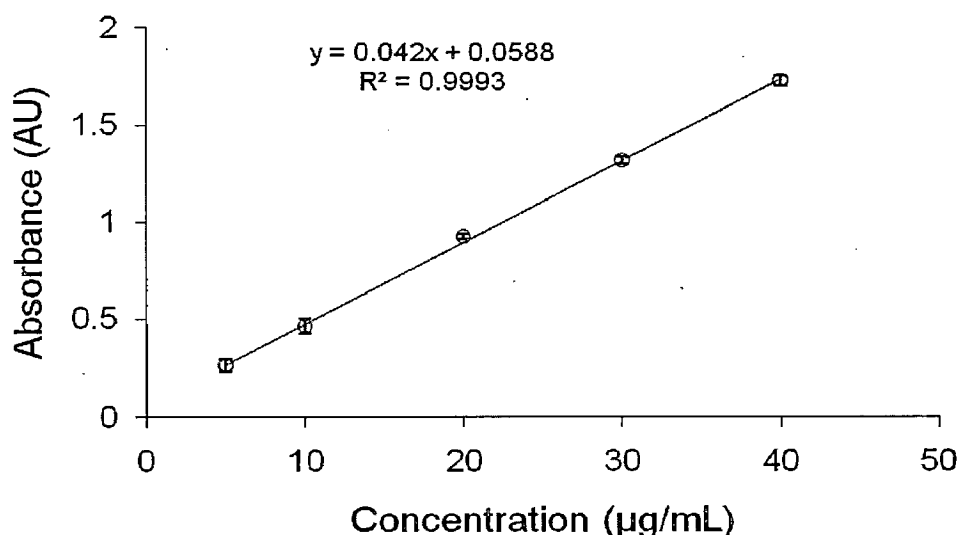


**Fig. 3.5** Calibration curve for estimation of diclofenac sodium in phosphate buffer pH 7.4 measured at  $\lambda_{\text{max}} = 276 \text{ nm}$  (Absorbance is given as mean  $\pm$  standard deviation of triplicate analysis).

## 3.3 RESULTS AND DISCUSSION

### 3.3.1 Evaluation of drug loading

It may be noted from Table-3.1 that the batches synthesized using pectin concentrations of 0.4 % and 0.6 % followed by treatment with 0.01 M DS, resulted in  $\sim 60$  % encapsulation efficiency. On the other hand, the batch synthesized using 1.0 % pectin and 0.01 M DS exhibited higher % encapsulation efficiency (86.0 %). But at such high pectin concentration, viscous polymeric matrix was formed which lead to reduction of saturation magnetization as discussed in chapter 2. Further, by increasing the precursor drug concentration to 0.05 M, the % loading efficiency was found to be only 19.4 %. Increasing the drug concentration did not increase loading efficiency, rather it decreased by three folds. This indicates limiting factor for drug loading capacity by calcium pectinate. From the above results, it was noted that the optimized conditions needed for preparing hybrid nanomaterials of magnetite-pectin-diclofenac sodium were 0.4 % w/v of pectin solution, 0.8 % w/v of  $\text{CaCl}_2$  solution and 0.01 M DS.

### 3.3.2 X-ray diffraction

The formation of as-synthesized stable MNPs in MP-DS was confirmed by recording the position and relative intensities of diffraction patterns at 220, 311, 400, 511 and 440 planes (Fig. 3.6) which corroborated well with those of cubic magnetite ( $\text{Fe}_3\text{O}_4$ ) structures as reported in JCPDS 01-11111 data. Though DS is crystalline in nature as evident from fig 3.6 but the XRD patterns of MP-DS did not reveal any the crystalline nature of DS. (Fig. 3.6). Thus it may be presumed that the DS probably loses its crystallinity after its encapsulation with calcium pectinate.

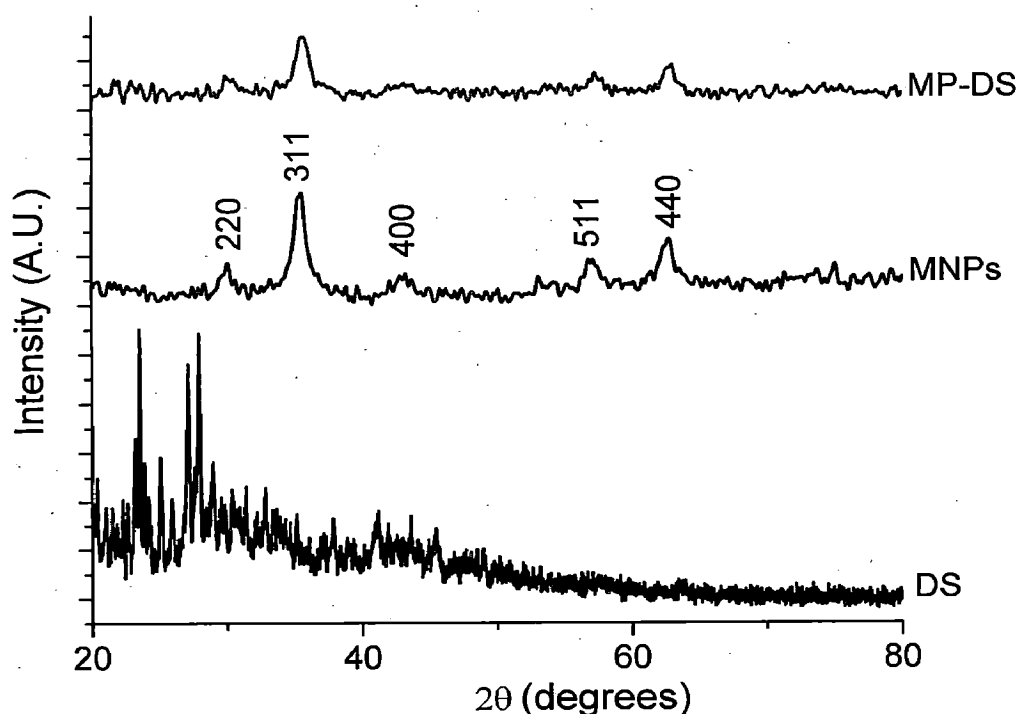


Fig. 3.6. XRD of the DS, MNPs and MP-DS.

### 3.3.3 Morphological studies

The morphology and size distribution of the MP-DS nanomaterial was studied by SEM, TEM and by DLS measurements. The SEM study revealed that the nanomaterials of MP-DS were mostly spherical in shape with sizes in the range of 100 – 150 nm (Fig. 3.7). These were similar to the magnetite – calcium pectinate (MP) nanomaterials as discussed in chapter 2. Further EDAX analysis of a selected area of a representative spherical MP-DS displayed characteristic X-ray peaks of Fe, Na, Ca and corresponding to MNPs, DS and calcium pectinate respectively, which strongly indicated the formation of MP-DS nanomaterial (Fig. 3.7). Further, the TEM analysis of the MP-DS illustrated spherical nanomaterials of ~ 150 nm size (Fig. 3.8a, 3.8b) which corroborated well with our SEM results. Again similar to MP nanomaterials, the TEM study of MP-DS also revealed

encapsulation of a large number of MNPs and its SAED pattern signified polycrystalline nature (Fig. 3.8a).

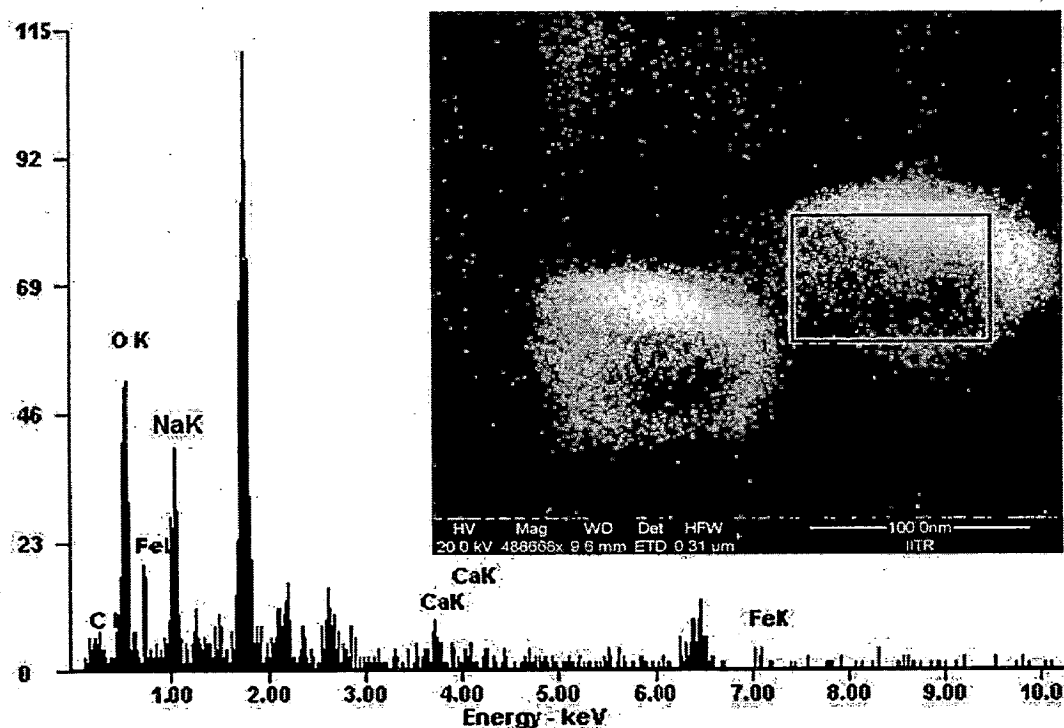


Fig. 3.7. Morphology and elemental composition of the marked area of about 100 nm sized MP-DS nanomaterials by SEM-EDAX.

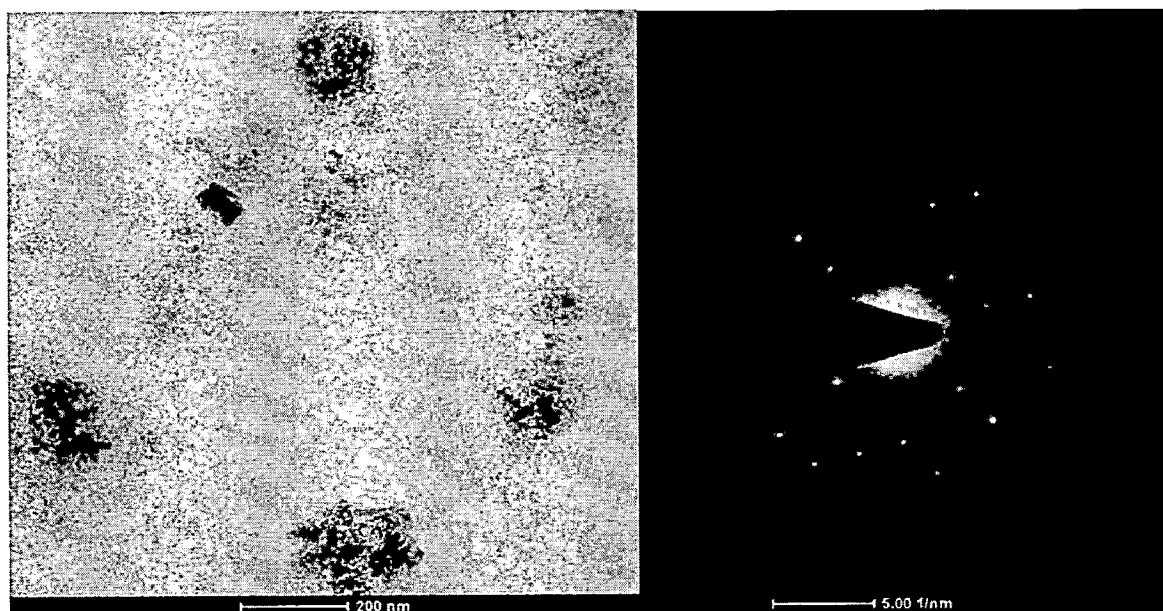


Fig. 3.8a. Transmission electron microscopy (TEM) of spherical shaped MP-DS hybrid nanomaterials of about 100-150 nm and its corresponding selected area electron diffraction (SAED) image exhibiting the presence of polycrystalline MNPs and DS.

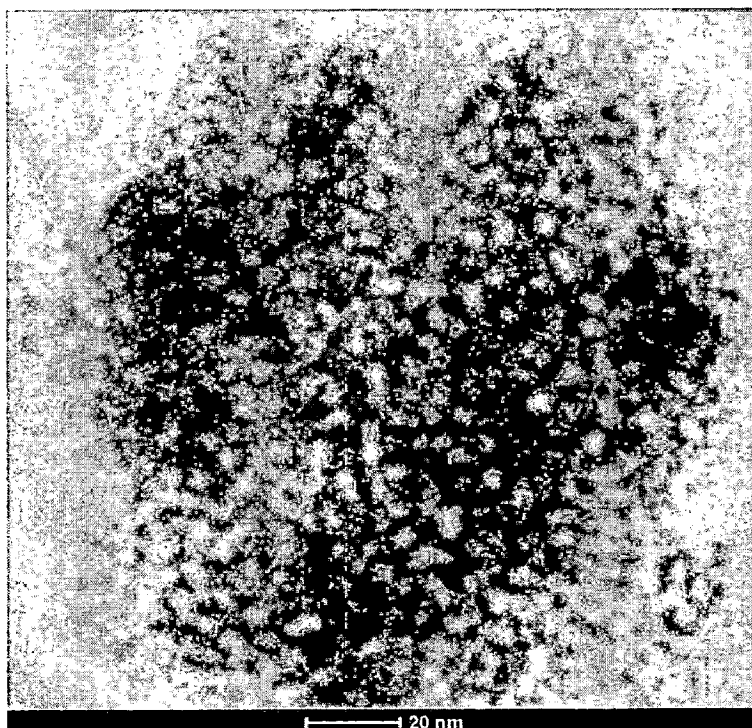


Fig. 3.8b. Detailed transmission electron microscopy (TEM) of one of the nanomaterials of MP-DS.

Furthermore, dynamic light scattering (DLS) measurement of MP-DS in aqueous solution at pH  $\sim 4$  exhibited unimodal size distribution in the range of 220 – 400 nm with maximum intensity at  $\sim 300$  nm (Fig. 3.9), indicating that the method of synthesis of these nanomaterials offered a good control over their sizes. However, the size distribution obtained from DLS measurements were two folds higher than the results from SEM and TEM studies. This can be attributed due to swelling effect of calcium pectinate in aqueous medium as explained by Yu *et al.* [35].

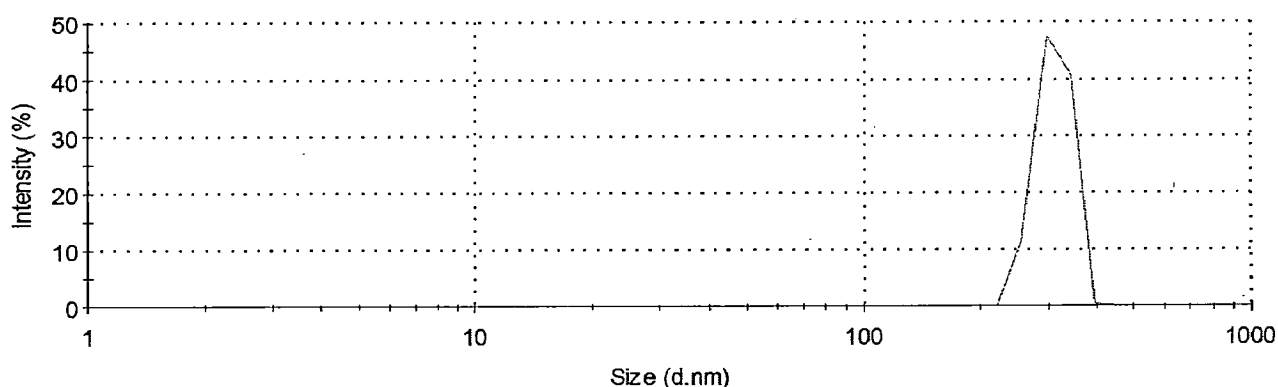


Fig. 3.9. Dynamic Light Scattering (DLS) measurement of MP-DS in aqueous solution at pH  $\sim 4$ .

### 3.3.4 FT-IR analysis

The drug loading in MP-DS hybrid nanomaterial was supported by its FT-IR spectrum (Fig. 3.10). The FT-IR spectrum of MP-DS comprised the characteristic IR peaks

of DS. The DS consists of various functional groups, notably,  $-NH$  and  $COO^-$ , substituted benzene ring and  $C-Cl$ . Similarly, pectin consists of  $-OH$  groups,  $COO^-$ ,  $C-O-C$ , which were studied by IR spectroscopy. The corresponding IR peaks of these groups were identified from literature [36].

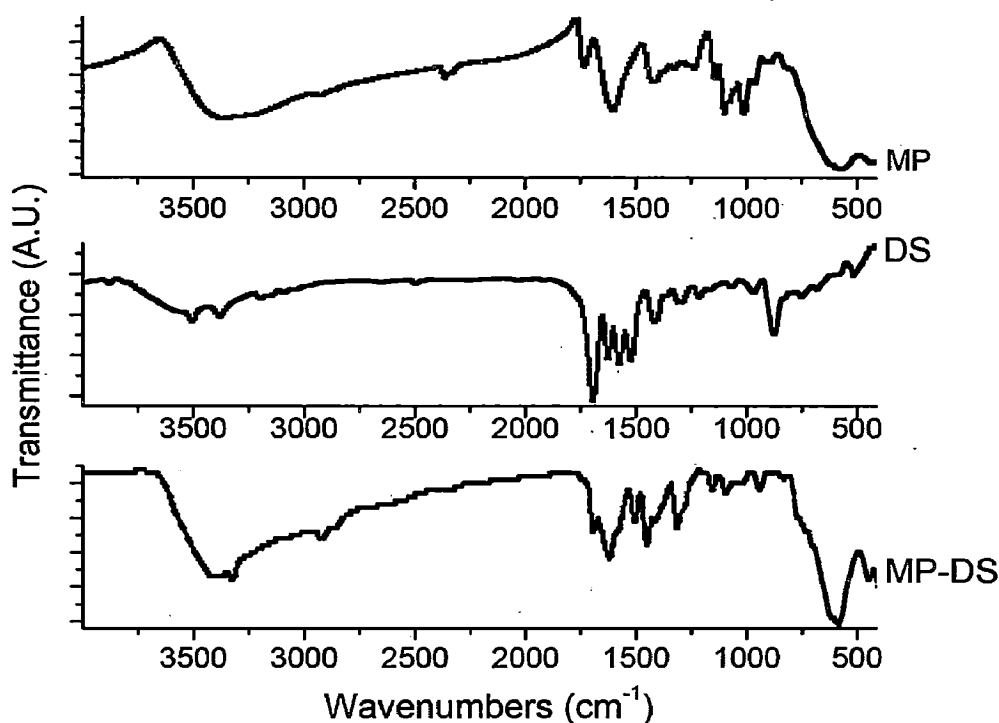


Fig. 3.10. FT-IR spectra of MP, DS and MP-DS hybrid nanomaterials.

The presence of DS encapsulated in magnetite – pectin nanomaterials was evident from the observation of N-H stretching frequency of the secondary amine corresponding to DS at  $3324\text{ cm}^{-1}$  for MP-DS batch, as compared to the N-H stretching frequencies at  $3380\text{ cm}^{-1}$  in the DS (Fig. 3.10). The N-H bending frequency was assigned to the peak recorded at  $1621\text{ cm}^{-1}$ . However, the presence of carboxylate group, in calcium pectinate, would also exhibit IR bands in the region  $1550 - 1650\text{ cm}^{-1}$ , thus the bands observed at  $1650\text{ cm}^{-1}$  in MP-DS were attributable to the presence of carboxylate group. The IR peak at  $1453\text{ cm}^{-1}$  in DS was due to  $-CH_2$  group (in DS) which was also observed in MP-DS at  $1446\text{ cm}^{-1}$ , indicating the loading of DS in the fabricated nanomaterials.

The  $-OH$  group in pectin was evident from the stretching frequencies in the range of  $3200 - 3600\text{ cm}^{-1}$ , and bending frequencies in the range of  $1390 - 1440\text{ cm}^{-1}$ , observed in MP-DS. Notably, due to large number of  $-OH$  groups in pectin, the O-H stretching band was broad and intense.

The peaks were observed at  $1092\text{ cm}^{-1}$ ,  $1156\text{ cm}^{-1}$  and  $1300\text{ cm}^{-1}$  in MP-DS. However in MP nanomaterials the peaks at  $1095\text{ cm}^{-1}$ ,  $1147\text{ cm}^{-1}$  and  $1250\text{ cm}^{-1}$  were

observed, which were attributed to C-O stretching frequencies. The peak at  $1146\text{ cm}^{-1}$  was due to C-O-C stretching frequency and assigned to the C-O-C linking groups in pectin.

The bands in the region of  $1000 - 1300\text{ cm}^{-1}$  were due to C-N group in the DS and MP-DS. The IR peak at  $800 - 1000\text{ cm}^{-1}$ , observed for DS and MP-DS were due to substituted aromatic ring in diclofenac sodium structure. The peak observed at  $590\text{ cm}^{-1}$  was attributable to vibrations of Fe-O bond. As expected, this peak was not observed in the IR spectrum recorded for DS. These observations reflected the formation of MP-DS. Thus from the IR study it was concluded that the fabricated nanomaterial comprised of magnetite nanoparticles, pectin and diclofenac sodium.

### **3.3.5 Thermal studies**

The loading of the DS in the hybrid nanomaterial system of MP-DS was further studied by thermogravimetry analysis (TGA), as given in Fig. 3.11a. The TGA of magnetite nanoparticles encapsulated in calcium pectinate nanomaterial without drug (MP) exhibited 13.5 % mass loss in two stages. The first mass loss about 5% at  $110\text{ }^{\circ}\text{C}$  was due to loss of absorbed water in MP and then further 8.5 % mass loss occurred up to  $750\text{ }^{\circ}\text{C}$  could be attributed to the degradation of calcium pectinate. The stable mass beyond  $750\text{ }^{\circ}\text{C}$  was due to iron oxide and residual calcium pectinate after heating, which accounted for 86.5 % of the MP nanomaterials. This indicated high amount of MNPs were encapsulated in calcium pectinate nanomaterials in MP-DS batch.

However, from this study it was not confirmed whether the amount of drug associated with the MP-DS was completely encapsulated or some fraction of it was bound to the external boundary of the spherical structured calcium pectinate nanomaterials. This was also addressed by the thermal studies of MP-DS, where the thermal events corresponding to the pure drug (DS) did not corroborate with those of the drug encapsulated in hybrid nanomaterials of calcium pectinate-magnetite. In the case of differential thermal analysis (DTA) of pure drug, the major exothermic event was observed at  $650\text{ }^{\circ}\text{C}$  which was associated with a heat release of  $2.53\text{ J/mg}$  (Fig. 3.11b). This was correlated with a mass loss due to thermal degradation as evident from the TG and plot. However in the case of MP-DS batch, the similar exothermic event was not observed at  $650\text{ }^{\circ}\text{C}$  rather it was recorded at  $395\text{ }^{\circ}\text{C}$ , and was associated with a heat release of  $1.69\text{ J/mg}$  (Fig. 3.11b). Such a shift of thermal event towards lower temperature could be thought to be due increase in thermal conductivity of the MP-DS nanomaterial. This phenomenon could be related to structures of nanoscale



dimension. In this regard, it was found in literature that hybrid nanomaterials of 100 nm and less have a tendency to exhibit strikingly different thermal conductivities compared to the bulk materials, where the increase in the thermal conductivity could be attributed to phonon properties [37, 38]. It was discussed from SEM and TEM studies that the sizes of the MP-DS were in the range of 100 – 150 nm, which was therefore favorable for increasing thermal conductivity. Due to this the degradation of drug DS encapsulated in MP-DS nanomaterials was expected to occur at much lower temperature than its bulk drug. The lack of thermal signatures of the pure drug corresponding to its bulk property in the thermal analysis of MP-DS also confirmed that no drug content was outside the nanomaterial. So we concluded that the drug with a loading content (wt %) of ~ 29% was encapsulated within the spherical MP-DS nanomaterials.

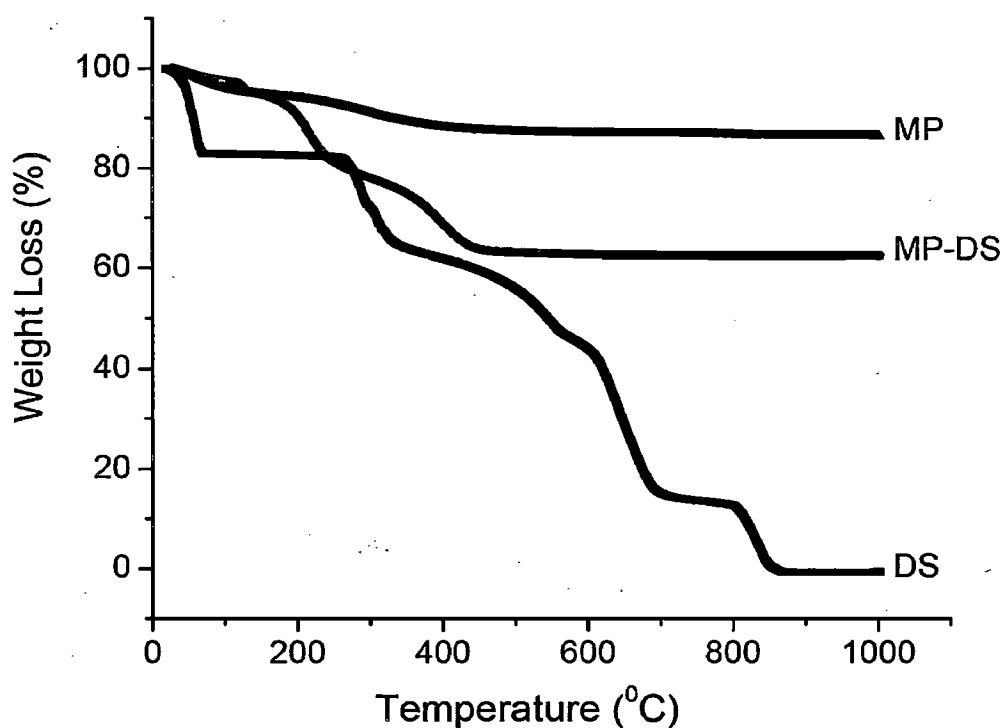


**Fig. 3.11a.** Thermogravimetric analysis (TGA) of MP-DS, MP (calcium pectinate-magnetite nanoparticles- without drug DS) and pure drug DS.

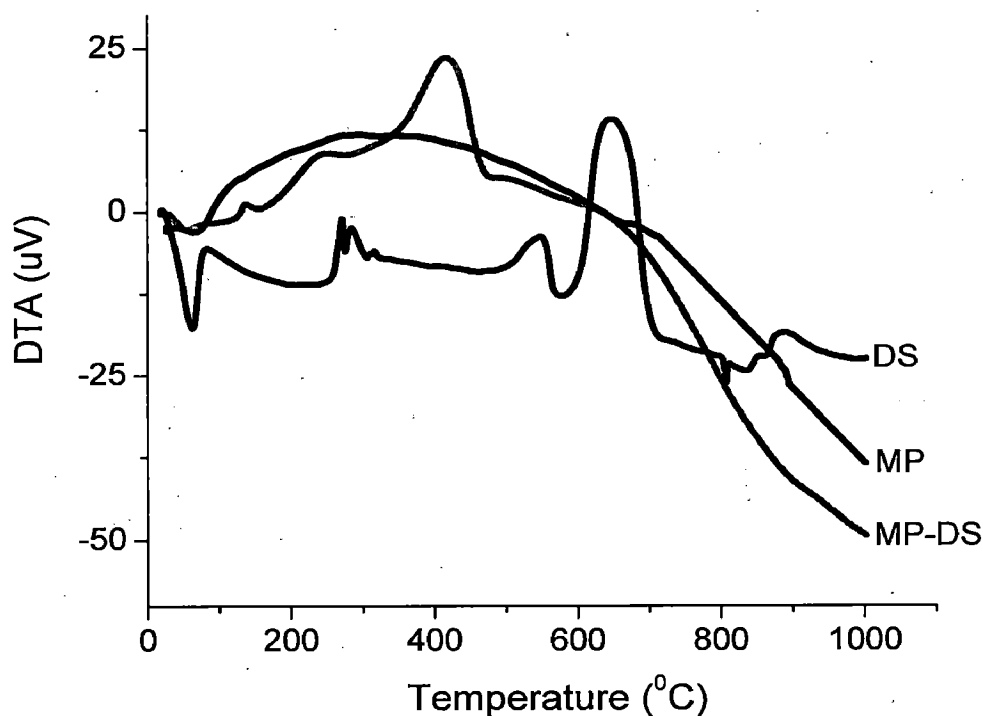


Fig. 3.11b. Differential thermal analysis (DTA) of MP-DS, MP and pure drug DS.

### 3.3.6 Zeta potential measurement: Mechanism of the formation of nanomaterial of MP-DS

The zeta potential measurements (given in Table 3.2) offered an evidence of the stability of MP-DS hybrid nanomaterial as reflected from large zeta potential ( $-47.0$  mV). The zeta potential of diclofenac sodium was measured as  $-110$  mV. In the pectin usually  $\text{Ca}^{2+}$  ion is used for formation of a cross linked network on calcium pectinate. Since both pectin and DS exhibit negative zeta potential ( $-35.1$  mV) so their interaction is less probable. Therefore, it appears that DS is entrapped during the formation of spherical calcium pectinate nanomaterials. Probably due to lack of scope for interaction of pectin with DS, % drug loading was less. In view of the above studies a mechanism towards formation of the MP-DS nanomaterials is proposed as shown in Fig. 3.12.

**Table 3.2** Zeta potential measurements of diclofenac sodium (DS), magnetite calcium pectinate without diclofenac sodium (MP), nanomaterials of magnetite calcium pectinate loaded with diclofenac sodium (MP-DS)

| Samples                | Measured zeta potential value ( $\zeta$ ) in mV |
|------------------------|---|
| Diclofenac Sodium (DS) | $-110$  |
| MP-DS                  | $-47$   |
| MP                     | $-17.6$   |
| Pectin (pH-4)          | $-35.1$   |

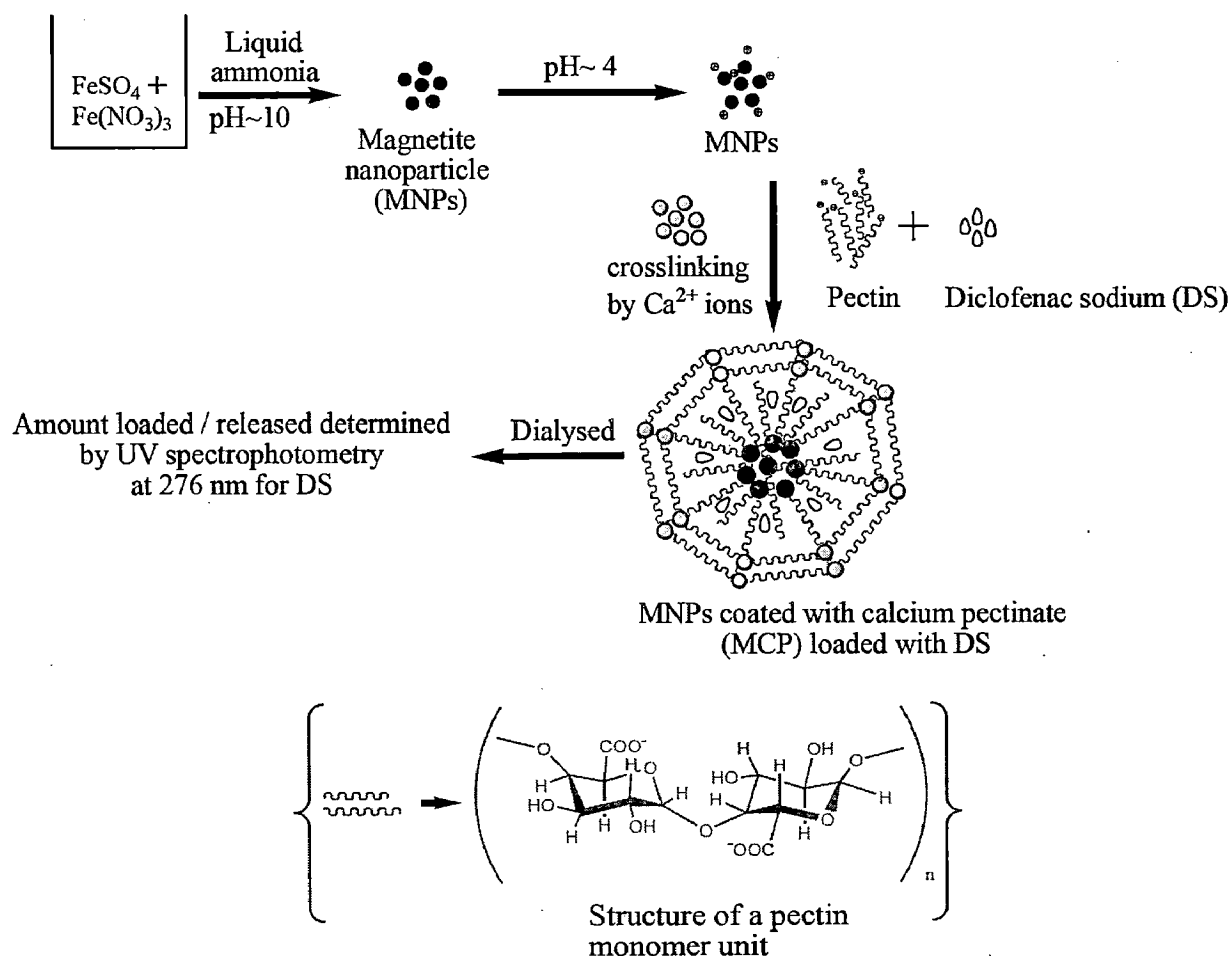


**Fig. 3.12.** Schematic representation of mechanism towards formation of the MP-DS hybrid nanomaterials.

### 3.3.7 Magnetic studies

The magnetic behavior of the MP-DS nanomaterial was studied from its magnetization curve (M-H curve) recorded at room temperature from VSM measurements. The M-H curve for the nanomaterials of MP-DS and MP were similar to that of the as-synthesized MNPs, and exhibited negligible coercivity and remanence magnetization (Fig. 3.13). This phenomenon could be attributed to superparamagnetic behavior of magnetite nanoparticles. The saturation magnetization ( $M_s$ ) measured at room temperature in the range of  $\pm 10$  kOe were 55.93 emu/g, 47.42 emu/g, and 44.05 emu/g for MNPs, MP and MP-DS respectively. The decrease in the saturation magnetization in the calcium pectinate coated MNPs loaded with DS (MP-DS) with respect to MNPs could be attributed due to effect of small particle size owing to non-collinear spin arrangement at the surface, or due to the formation of magnetic dead layer by nonmagnetic material and at the domain boundary wall of MNPs [39, 40]. The particle size effect on reduction of  $M_s$  may be ruled out as the same batch of MNPs with uniform particle size distribution was used for

synthesis of MP. The magnetic moments could however be quenched due to the formation of magnetic dead layer at the domain wall of MNPs, as explained in Chapter 2. In the case of MP-DS, the non magnetic materials, like drug (DS) and calcium pectinate is likely to form magnetic dead layer. This could hinder the domain wall motion during application of the magnetic field, which might be responsible for the reduction in the saturation magnetization in these formulations.

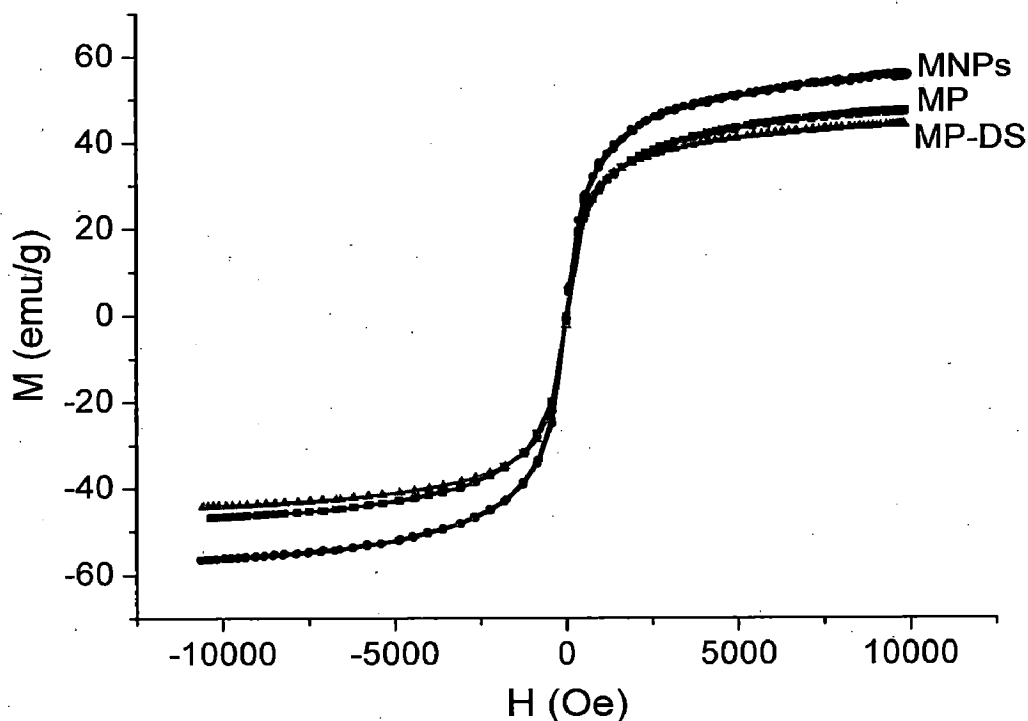


**Fig. 3.13.** Magnetization vs field (M-H) curve of MNPs, MP (without drug) and MP-DS nanomaterials measured by VSM at room temperature.

The superparamagnetic behavior of the MP-DS nanomaterials was studied by SQUID measurement between 5 K and 300 K using zero-field cooling (ZFC) and field cooling (FC) in an applied magnetic field of 500 Oe (Fig. 3.14). The curves diverged at 75.4 K, characterized as blocking ( $T_B$ ) temperature, which corresponded to the transition from ferromagnetic to superparamagnetic behavior. However, the blocking temperature depends on the strength of the applied field during the SQUID measurement. As the applied field in this batch was 500 Oe which was higher than (200 Oe) that used for measuring MP nanomaterials (discussed in chapter – 2), it resulted in lowering of the  $T_B$  value.

In the ZFC curve (Fig. 3.14), without applied magnetic field, when the sample was cooled to 5 K the total magnetization was  $\sim 13.56$  emu/g. Such lower order of magnetization may be attributed to the random orientation of the magnetic moments of individual particles

due to particles less than 20 nm sizes [41]. As the temperature was increased more particles reoriented their magnetic moment (magnetization) along the external applied field. Due to this the magnetization increased till it reached a maximum value of 75.4 K as shown in the ZFC curve. On the other hand, in the FC curve the magnetization measured at 5 K and in the presence of 500 Oe was 21.64 emu/g. The externally applied magnetic field energetically favoured the reorientation of the individual magnetic moment along the direction of the applied field which resulted in the increased magnetization. Such a behavior was characteristic of superparamagnetism typically observed in small ferromagnetic or ferrimagnetic nanoparticles. Below  $T_B$ , the MP-DS nanoparticles exhibited ferromagnetic properties. When the temperature was above the  $T_B$ , the thermal energy becomes higher, which could result in overcoming the anisotropy barrier and randomize the magnetic moment, leading to the superparamagnetic behavior of the nanoparticles [42].

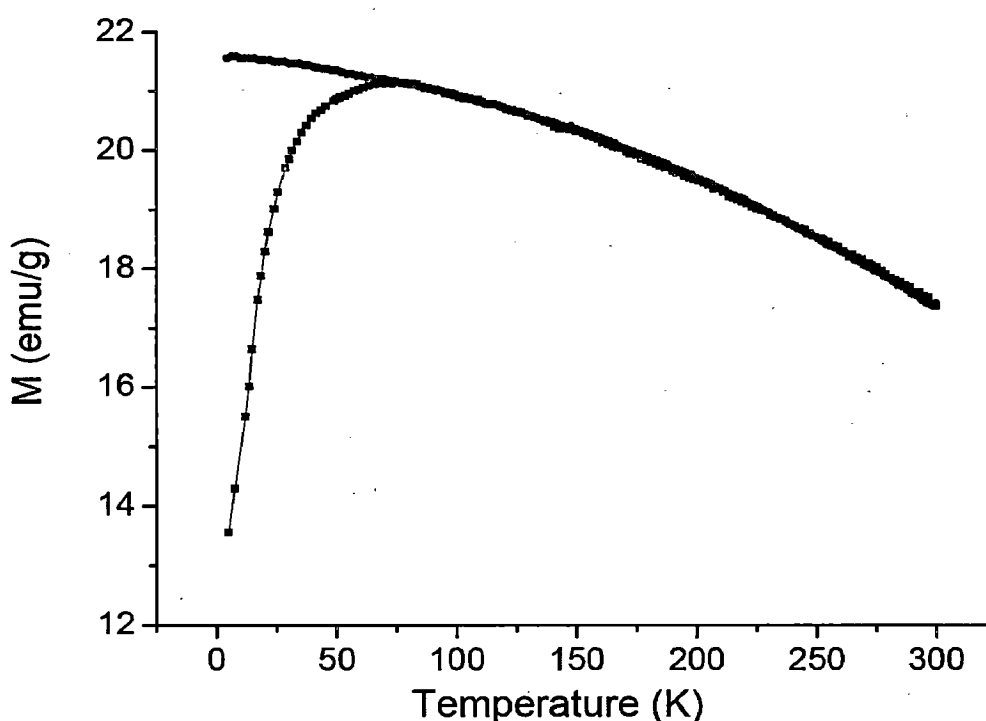


Fig. 3.14. ZFC and FC curve of MP-DS nanomaterials recorded at 500 Oe, measured by SQUID.

### 3.3.8 *In vitro* drug release studies from MP-DS hybrid nanomaterial

It is well-known that the sustained or controlled release of low molecular weight drugs from polysaccharide-based matrices is not trivial. This can be attributed to higher drug solubility due to high water contents in the polysaccharide based matrices. The release rate of drugs from the polysaccharide-based matrices is generally very fast and can be referred to as burst release [35]. Sustained release might be achieved by modifying the polysaccharide

especially by cross-linking in order to hold back the drug in its network structure for sustaining its release. In the case of MP-DS nanomaterial, the pectin was cross-linked with  $\text{Ca}^{2+}$  ions and the nature of release of the drug DS was studied by *in vitro* method by treating MP-DS sequentially in simulated gastric fluid (SGF) followed by its *in vitro* release in simulated intestinal fluid (SIF) and then in simulated colonic fluid (SCF) to mimic the gastrointestinal pathway. In addition, the *in vitro* release study was also carried out in phosphate buffer at pH 7.4 at 37 °C for 48 h to mimic drug release in blood.

### 3.3.8.1 Sequential *in vitro* release in gastrointestinal fluids

The release of drug from a matrix is mostly governed by pH and in certain cases by specific enzymes. It was found that after 2 h only 0.18 % of the drug was released in SGF (showed in Fig. 3.15). Such negligible drug release in SGF indicated significant shielding of the encapsulated drug by calcium pectinate at low pH. This is in good agreement to our previous discussion in chapter 2 where we demonstrated the stability of calcium pectinate in acidic gastric condition. In addition, DS exhibited poor solubility at pH 1.2, which could also affect drug releasing ability in SGF. Our result of poor release of DS at pH 1.2 was in good agreement with the literature report, where electrospun diclofenac sodium loaded Eudragit® L 100-55 nanofibers exhibited *in vitro* release of only 3 % of the loaded drug in 0.1 N HCl in 2 h [43]. Further for such a low release they also attributed to insolubility of Eudragit® L 100-55 in the acidic environment, which probably prevented dissolution of DS. On the other hand, the *in vitro* release of the drug in SIF at pH ~ 6.8 for 3 h was rapid (Fig. 3.15) and agreed well with the literature report [43]. The rapid release in SIF could be attributed to swelling of calcium pectinate nanomaterial due to weakening of calcium pectinate network structure at higher pH. Moreover, the solubility of the drug at this pH was also high. It was noted that about 8 % of the drug loaded in MP-DS nanomaterial was released during the first 2 h in SIF medium, while 80 % of the drug was released during the 3<sup>rd</sup> hour in SIF medium. Such rapid release in the 3<sup>rd</sup> hour perhaps indicated the swelling effect of calcium pectinate. The swelling tendency of calcium pectinate was also corroborated from observation of larger average size of the synthesized MP-DS in DLS measurement as compared to their dried ones measured by SEM and TEM. It may be thought that the hybrid nanomaterials swelled to a maximum level during the 3 h interaction in SIF medium. The swelling of calcium pectinate can be attributed to increase in the concentrations of negatively charged carboxylate groups in pectin at higher pH ( $\text{pK}_a = 2.9$ -

4.1), which however would depend on the degree of esterification [44, 45]. This could lead to repulsion between pectin chains and thus resulted in swelling of pectin. Additionally, DS is a weak acid ( $pK_a = 4.0$ ) with more solubility at neutral pH [46], and thus at pH 6.8 it exhibits rapid release. However, the rate of drug release was again slowed down in simulated colonic fluid (SCF) where the pH was at 5.5 (Fig. 3.15). From these studies, it may be surmised that the MP-DS formulation is very effective for releasing drug in the intestinal region where significant release of the drug (~ 88 %) occurred. While in colonic region, only 11 % drug was released in 43 h at a very slow rate.

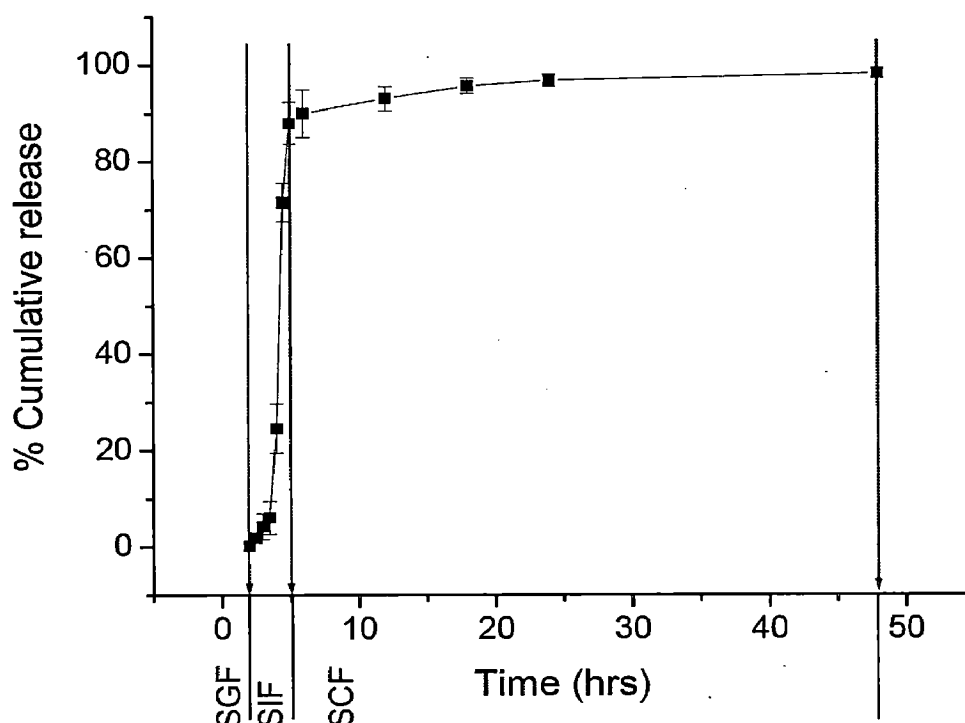


**Fig. 3.15.** Sequential *in vitro* release of DS from MP-DS in simulated gastric fluid (SGF pH 1.2) for 2 h, followed by simulated intestinal fluid (SIF pH 6.8) for 3 h and simulated colonic fluid (SCF pH 5.5) up to 48 h.

### 3.3.8.2 *In vitro* release in phosphate buffer at pH 7.4

The *in vitro* release studies of DS from MP-DS formulation in phosphate buffer solution at pH 7.4 at 37 °C exhibited sustained release where 90 % of DS was released in 8 h (Fig. 3.16). The remaining DS was slowly released during the next 48 h. In the case of ethylcellulose and iron/ ethylcellulose (core/ shell) nanoparticles also sustained release of DS has been reported in phosphate buffer (pH = 7.4) for up to 4 days [11]. In this case slower release of the drug loaded in iron/ ethylcellulose (core/ shell) nanoparticles was reported when compared to that in ethylcellulose. But the overall release rate was much lesser and slower than MP-DS system at this pH. Moreover, cellulose or its derivatives are

non-biodegradable and could be a drawback. On the other hand, our system consists of pectin which is biodegradable. In this regard the polymer PLGA copolymer also reported relatively faster release of DS at this pH which was attributed to the amorphous nature of PLGA copolymer [47]. In this system almost complete drug was released within a time span of 14 h. Further in the case of tailored carboxymethyl guar gum hydrogel with nanosilica for transdermal drug delivery, sustained release of diclofenac sodium was observed for ~20 h where only 70 % of the total drug was released at pH 7.4. The faster release at this pH was attributed to the higher solubility of the DS as supported from its  $pK_a$  value [48].

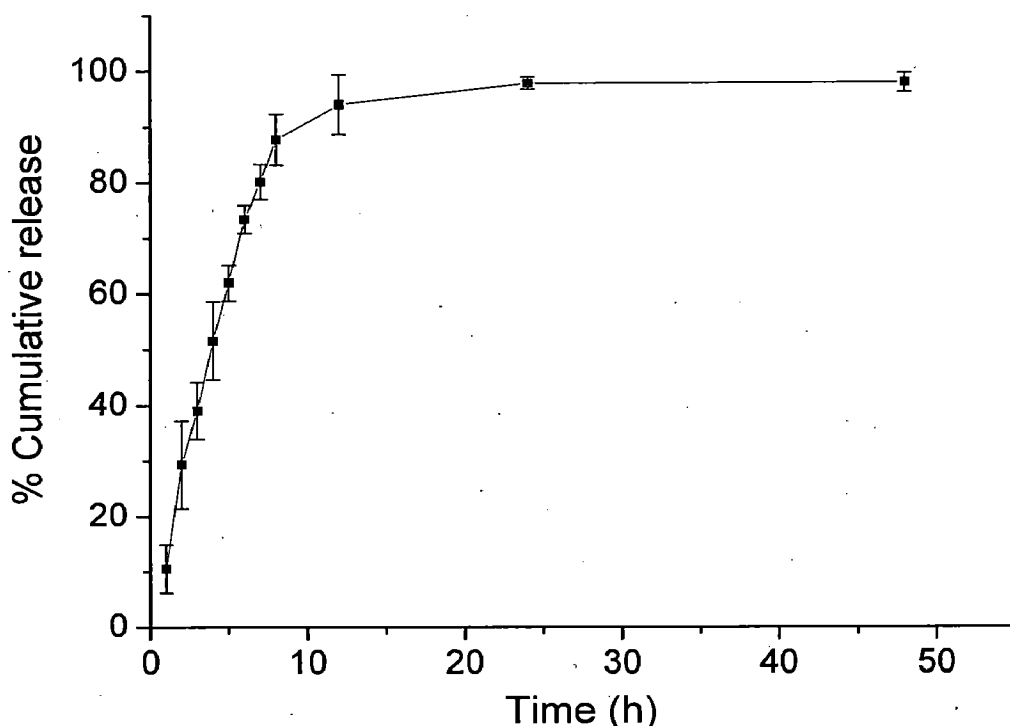


Fig. 3.16. *In vitro* release of DS from MP-DS nanomaterials in phosphate buffer solution (pH 7.4) for 48 h.

### 3.3.8.3 Modeling of drug release

In order to prove the relation of swelling effect on cumulative release the drug release mechanism of the fabricated nanomaterials were studied by simple exponential relation  $(M_t / M_\infty) = kt^n$ , referred to as Korsmayer - Peppas equation [49, 50]. The model is usually used to describe the general solute release behavior from different polymeric materials [50, 51], where  $(M_t / M_\infty)$  is the fractional solute release,  $t$  is the release time,  $k$  is a constant incorporating structural and geometric characteristics of material and  $n$  is the diffusion exponent characteristic of release mechanism. For spheres, the value of  $n < 0.43$  indicates that the drug release from the polymer was due to Fickian diffusion [50, 51]. The value of  $n$  in the range of 0.43 to 0.85 is an indication of both diffusion controlled drug



release and swelling controlled drug release. The values above 0.85 indicate swelling controlled drug release which is related to polymer relaxation during swelling of pectin [52]. The equation of this model was modified in terms of % cumulative release as

$$M_t/M_\infty * 100 = (k*100) * t^n$$

where  $(M_t/M_\infty)*100$  is the experimentally measured % cumulative drug release;  $M_\infty$  corresponded to 100% drug is release,  $M_t$  corresponded to release at time ( $t$ ).

Taking log on both the side we get

$$\log M_t/M_\infty * 100 = \log (k*100) + n \log t$$

The  $\log M_t/M_\infty * 100$  was plotted against  $\log t$  for up to 88 % of cumulative release (Fig. 3.17). The value of  $n$  was obtained from slope and  $(k*100)$  was obtained from the intercept. From the fitted data of release of DS from MP-DS,  $n$  was found to be 0.9868 which indicate the non-Fickian transport of drug release, controlled by swelling effect of calcium pectinate at pH 7.4 [50, 51]. The value of  $k*100$  was found to be 12.43.

On the basis of Korsemeyer - Peppas model we may conclude that the drug release in phosphate buffer pH 7.4 in the case of MP-DS nanomaterials was controlled by the swelling effect of calcium pectinate at this pH which corroborated DLS results.

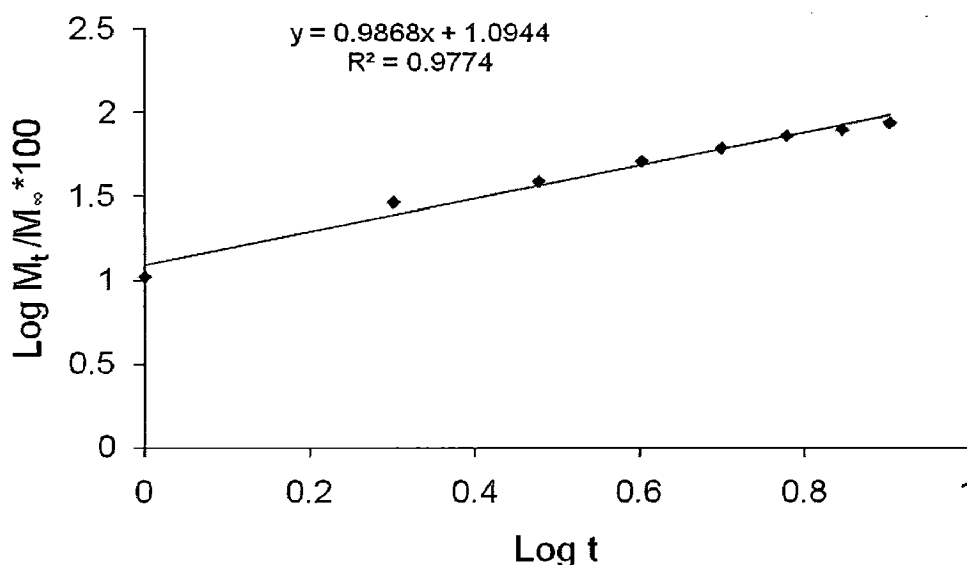


**Fig. 3.17.** Showing linear fit of *in vitro* release of DS up to 8 h from MP-DS in phosphate buffer solution (at pH 7.4), using Korsemeyer Peppas equation in log scale.

Overall, it was noted that unlike polysaccharide matrix for drug carrier which could exhibit burst release property, pectin which is an anionic polysaccharide, was successfully modified to form hybrid nanomaterials of magnetite-calcium pectinate system, capable to load drugs and exhibit sustained release property. Moreover, it also comprised magnetic responsive property for magnetic guiding.

### 3.4 CONCLUSION

Fabrication of a simple, reproducible and novel targeted drug delivery system of 100 - 150 nm size (measured by SEM and TEM) comprising of magnetite nanoparticles, pectin cross linked with calcium ions and the drug diclofenac sodium (MP-DS) has been achieved. The SQUID and VSM studies of MP-DS system confirmed its superparamagnetic nature. Thermal analysis was instrumental in ascertaining that the drug associated with MP-DS was essentially encapsulated in the hybrid nanomaterials. The high  $\zeta$ -potential ( $-47$  mV) indicated the stability of the synthesized drug delivery system. The *in vitro* release studies of DS from hybrid nanomaterial MP-DS system in gastrointestinal fluid was pH dependent. It exhibited poor release in simulated gastric fluid, while about 90% of the drug was released rapidly in simulated intestinal fluid, and thus the colonic release was limited. Therefore, the applicability of this system for colon specific delivery might be limited as it has to pass through intestine before reaching colon so it was thought to be unsuitable for colonic targeting. The *in vitro* release study carried out at pH 7.4 (mimicking blood pH) exhibited sustained release which satisfied non-Fickian release based on Korsmeyer- Peppas model and corresponded to diffusion controlled mechanism. This was attributed to swelling effect of pectin in aqueous medium, also supported by the dynamic light scattering (DLS) measurement which exhibited particle size ranging between 220 – 400 nm.

Overall the sustained drug release at pH 7.4 corresponding to blood pH was encouraging for targeted drug delivery, especially via intravenous administration followed by magnetic guiding to inflammatory site where otherwise the direct drug administration is cumbersome, e.g., knee joints, for its sustained release. This would also minimize the distribution of the drug to other undesirable parts of the body. However this proposal will be further augmented after *in vivo* studies of this formulation.

## REFERENCES

1. Willis, J. V.; Kendall, M. J.; Flinn R. M.; Thornhill, D. P.; Welling, P. G. The pharmacokinetics of diclofenac sodium following intravenous and oral administration. *Eur. J. Clin. Pharmacol.* **1979**, *16*, 405–410.
2. Zuckner, J. International experience with diclofenac in rheumatoid arthritis. *Am. J. Med. Suppl.*, **1986**, *4B*, 39–42.
3. Warner, T. D.; Vojnovic, I.; Bishop-Bailey, D.; Mitchell, J. A. Influence of plasma protein on the potencies of inhibitors of cyclooxygenase-1 and -2. *FASEB J.* **2006**, *20*, 542–544.
4. Carson, J.; Notis, W. M.; Orris, E. S. Colonic ulceration and bleeding during diclofenac therapy. *N. Engl. J. Med.* **1990**, *323*, 135–137.
5. Pedersen.; Negrini, R.; Mezzenga, R. pH-Responsive Lyotropic Liquid Crystals for Controlled Drug Delivery. *Langmuir*, **2011**, *27* (9), 5296–5303.
6. Deng C. X. Targeted drug delivery across the blood-brain barrier using ultrasound technique. *Ther. Deliv.* **2010**, *1*, 819–848.
7. Wu, G.; Mikhailovsky, A.; Khant, H.A.; Fu, C.; Chiu, W.; Zasadzinski, J.A. Remotely triggered liposomal release by near-infrared light absorption via hollow gold nanoshells. *J. Am. Chem. Soc.* **2008**, *130* (26), 8175–8177.
8. Pedersen, P. J.; Adolph, S. K.; Subramanian, A. K.; Arouri, A.; Andresen, T. L.; Mouritsen, O. G.; Madsen, R.; Madsen, M. W.; Peters, G. H.; Clausen, M. H. Liposomal formulation of retinoids designed for enzyme triggered release. *J. Med. Chem.* **2010**, *53* (9), 3782-3792.
9. Al-Deen, F. N.; Ho, J.; Selomulya, C.; Ma, C.; Coppel, R. Superparamagnetic Nanoparticles for Effective Delivery of Malaria DNA Vaccine. *Langmuir*. **2011**, *27*, 3703–3712.
10. Bawa, P.; Pillay, V.; Choonara, Y. E.; Toit, L. C. Stimuli-responsive polymers and their applications in drug delivery. *Biomed. Mater.* **2009**, *4*, 022001.
11. Arias, J. L.; López-Viota, M.; López-Viota, J.; Delgado, A.V. Development of iron/ ethylcellulose (core/ shell) nanoparticles loaded with diclofenac sodium for arthritis treatment. *Int. J. Pharm.* **2009**, *382*, 270–276.

12. Kim, S.; Kim, J. Y.; Huh, K. M.; Acharya, G.; Park, K. Hydrotropic polymer micelles containing acrylic acid moieties for oral delivery of paclitaxel. *J. Control. Release* **2008**, *132*, 222-229.
13. Wei, X. H.; Niu, Y. P.; Xu, Y. Y.; Du, Y. Z.; Hu, F. Q.; Yuan, H. Salicylic acid-grafted chitosan oligosaccharide nanoparticle for paclitaxel delivery. *J. Bioact. Compat. Polym.* **2010**, *25*, 319-325.
14. Saravanan, M.; Bhaskar, K.; Maharajan, G.; Pillai, K. S. Ultrasonically controlled release and targeted delivery of diclofenac sodium via gelatin magnetic microspheres. *Int. J. Pharm.* **2004**, *283*, 71-82.
15. Neuberger, T.; Schöpf, B.; Hofmann, H.; Hofmann, M.; Rechenberg, B. Superparamagnetic nanoparticles for biomedical applications: Possibilities and limitations of a new drug delivery system. *J. Magn. Magn. Mater.* **2005**, *293*, 483-496.
16. Andhariya, N.; Chudasama, B.; Mehta, R. V.; Upadhyay, R. V. Biodegradable thermoresponsive polymeric magnetic nanoparticles: a new drug delivery platform for doxorubicin. *J. Nano. Res.* **2011**, *13(4)*, 1677-1688.
17. Jiang, J. S.; Gan, Z. F.; Yang, Y.; Du, B.; Qian, M.; Zhang P. A novel magnetic fluid based on starch-coated magnetite nanoparticles functionalized with homing peptide. *J. Nano. Res.* **2009**, *11(6)*, 1321-1330.
18. Daniela, P. S.; Ruiz, M. A.; Gallardo, V.; Zanoni, M. V. B.; Arias J. L. Multifunctional antitumor magnetite/chitosan-L-glutamic acid (core/shell) nanocomposites. *J. Nano. Res.* **2011**, *13(9)*, 4311-4323.
19. Lübke, A. S.; Bergemann, C.; Huhnt, W.; Fricke, T.; Riess, H.; Brock, J. W.; Huhn, D. Preclinical experiences with magnetic drug targeting: tolerance and efficacy. *Cancer Res.* **1996**, *56*, 4694-4701.
20. Boonsongrit, Y.; Mitrevej, A.; Mueller, B. W. Chitosan drug binding by ionic interaction. *Eur. J. Pharm. Biopharm.* **2006**, *62*, 267-274.
21. Itoh, K.; Hirayama, T.; Takahashi, A.; Kubo, W.; Miyazaki, S.; Dairaku, M.; Togashi, M.; Mikami, R.; Attwood, D. In situ gelling pectin formulations for oral drug delivery at high gastric pH. *Int. J. Pharm.* **2007**, *335*, 90-96.
22. Sinha, V. R., Kumria, R. Polysaccharides in colon-specific drug delivery. *Int. J. Pharm.* **2001**, *224*, 19-38.
23. Tripathi, K. D.; *Essentials of Medical Pharmacology*, 6<sup>th</sup> Ed.; Jaypee brothers medical Publishers, New Delhi, India, **2008**.

24. Sprato G. R.; *Delmar's Mini Guide to Geriatric Drugs Cengage Learning, Published by Delmar Cengage Learning, New York, 2009*; pp 227-280.
25. Naidoo, V.; Swan, G. E. Diclofenac toxicity in Gyps vulture is associated with decreased uric acid excretion and not renal portal vasoconstriction. *Comp. Biochem. Physiol. C. Toxicol. Pharmacol.* **2008**, *149 (3)*, 269–274.
26. Brater, D. C. Renal effects of cyclooxygenase-2-selective inhibitors. *J. Pain Symptom Manage.* **2002**, *23 (4)*, 15-20.
27. Jeffrey, K. A., *Meyler's Side Effects of Analgesics and Anti-inflammatory Drugs*; Oxford, UK, **2009**.
28. Singh, S.; Muthu, M. S. Preparation and characterization of nanoparticles containing an atypical antipsychotic agent. *Nanomedicine*, **2007**, *2(2)*, 233-40.
29. Liu, L.; Fishman, M. L.; Kost, J.; Hicks, K. B. Pectin-based systems for colon specific drug delivery via oral route. *Biomaterials*. **2003**, *24*, 3333–3343.
30. Yang, L. Biorelevant dissolution testing of colon-specific delivery systems activated by colonic microflora. *J. of Controlled Release*. **2008**, *125*, 77–86.
31. Giselle, F.; Oliveira; Priscileila, C.; Ferrari, Livia, Q.; Carvalho, Raul, C.; Evangelista. Chitosan–pectin multiparticulate systems associated with enteric polymers for colonic drug delivery. *Carbohydr. Polym.* **2010**, *82*, 1004–1009.
32. British Pharmacopoeia commission office (BP 2009). Published by the stationary office on behalf of the medicines and healthcare products regulatory agency (MHRA); London., **2009**.
33. Composition and pharmaceutical dosage form for colonic drug delivery using polysaccharides United States Patent: 6,413,494 Inventors: Lee; Seung Seo (Taejon-si, KR); Lim; Chang Baeg (Taejon-si, KR); Pai; Chaul Min (Taejon-si, KR); Lee; Sujung (Taejon-si, KR); Park; In (Taejon-si, KR); Seo; Moon Gun (Taejon-si, KR); Park; Heenam (Taejon-si, KR) Appl. No.: 318579 Filed: May 25, **1999**.
34. Gonza´lez-Rodríguez, M. L.; Holgado, M. A. ; Sa´nchez-Lafuente, C.; Rabasco, A. M.; Fini, A. Alginate/chitosan particulate systems for sodium diclofenac release. *Int. J. Pharm.* **2002**, *232*, 225–234.
35. Yu, C. Y.; Cao, H.; Zhang, X. C.; Zhou, F. Z.; Cheng, S. X.; Zhang, X. Z.; Zhuo, R. X. Hybrid nanospheres and vesicles based on pectin as drug carriers. *Langmuir*. **2009**, *25*, 11720-11726.

36. Sliverstein, R. M., Webster F. X. *Spectrometric identification of organic compounds*; John Wiley and Sons: Asia, **2002**.
37. Ju, Y. S. Phonon Heat Transport in Silicon Nanostructures. *App. Phys. Lett.* **2005**, *87*, 153106-1-3.
38. Nika, D.; Pokatilov, E.; Askerov, A.; Balandin, A. Phonon thermal conduction in graphene: Role of Umklapp and edge roughness scattering. *Phys. Rev. B*, **2009**, *79*, 1-12.
39. Shafi, K. V. P. M.; Ulman, A.; Dyal, A.; Yan, X.; Yang, N. L.; Estournes, C.; Fournes, L.; Wattiaux, A.; White, H.; Rafailovich, M. Magnetic enhancement of  $\gamma$ -Fe<sub>2</sub>O<sub>3</sub> nanoparticles by sonochemical coating. *Chem. Mater.* **2002**, *14*, 1778-1787. 37.
40. Morales, M. P.; Verdaguer, S. V.; Montero, M. I.; Sterna, C. J.; Roing, A.; Casas, L.; Martinez, B.; Sandiumenge, F. Surface and internal spin canting in  $\gamma$ -Fe<sub>2</sub>O<sub>3</sub> nanoparticles. *Chem. Mater.* **1999**, *11*, 3058-3064.
41. Daou, T. J.; Pourroy, G.; Begin-Colin, S.; Greneche, J. M.; Ulhaq-Bouillet, C.; Legare, P.; Bernhardt, P.; Leuvrey, C.; Rogez, G. Hydrothermal Synthesis of Monodisperse Magnetite Nanoparticles. *Chem. Mater.* **2006**, *18*, 4399-4404.
42. Si, S.; Kotal, A.; Mandal, T.K.; Giri, S.; Nakamura, H.; Kohara, T. Size-controlled synthesis of magnetite nanoparticles in the presence of polyelectrolytes *Chem. Mater.* **2004**, *16*, 3489-3496.
43. Shena, X.; Yu, D.; Zhu, L.; Branford-White, C.; White, K.; Chatterton, N. P. Electrospun diclofenac sodium loaded Eudragit<sup>®</sup> L 100-55 nanofibers for colon-targeted drug delivery. *Int. J. Pharm.*, **2011**, *408*, 200–207.
44. Ofori-Kwakye, K.; Fell, J. T. Biphasic drug release: the permeability of films containing pectin, chitosan and HPMC. *Int. J. Pharm.* **2001**, *226*, 139–145.
45. Ralet, M. C.; Dronnet, V.; Buchholt, H. C.; Thibault, J. F. Enzymatically and chemically de-esterified lime pectins: characterization, polyelectrolyte behavior and calcium binding properties. *Carbohydr. Res.* **2001**, *336*, 117–125.
46. Llinas, A.; Burley, J. C.; Box, K. J.; Glen, R. C; Goodman, J. M. Diclofenac solubility: independent determination of the intrinsic solubility of three crystal forms. *J. Med. Chem.* **2006**, *50* (5), 979–983.
47. Agnihotri, S. M.; Vavia, P. R. Diclofenac-loaded biopolymeric nanosuspensions for ophthalmic application *Nanomedicine (NBM)*. **2009**, *5*, 90–95.

48. Gir, A.; Ghoshb, T.; Pandac, A. B.; Pald, S.; Bandyopdhyaya, A. Tailoring carboxymethyl guar gum hydrogel with nanosilica for sustained transdermal release of diclofenac sodium. *Carbohydr. Polym.* **2011**, doi:10.1016/j.carbpol.2011.09.050
49. Ritger, P.; Peppas, N. A. A simple equation for description of solute release. *J. Control. Release* **1987**, *5*, 23-36.
50. Siepmann, J.; Peppas, N. A. Mathematical modelling of controlled drug delivery. *Adv. Drug Deliv. Rev.* **2001**, *48*, 139–157.
51. Korsmeyer, R. W.; Gurny, R.; Doelker, E.; Buri, P.; Peppas, N. A. Mechanisms of solute release from porous hydrophilic polymers. *Int. J. Pharm.* **1983**, *15*, 25-35.
52. Wang, Q.; Zhang, J.; Wang, A. Preparation and characterization of a novel pH-sensitive chitosan-g-poly (acrylic acid)/ attapulgitite/ sodium alginate composite hydrogel bead for controlled release of diclofenac sodium. *Carbohydr. Polym.* **2009**, *78*, 731–737.

***CHAPTER - 4***  
***DICLOFENAC SODIUM LOADED***  
***IN NANOMATERIALS OF***  
***MAGNETITE - PECTIN***  
***REINFORCED WITH CHITOSAN***



## 4.1 INTRODUCTION

Nanomaterials of polysaccharide based natural polymers have attracted tremendous scientific interest in developing nanoscale targeted drug delivery system. In this regard the chitosan which is a biocompatible, biodegradable and nontoxic cationic polysaccharide has been reported to be used for delivery of various drugs including diclofenac sodium (DS) [1]. Similar to pectin chitosan is a very promising biomaterial for drug delivery system but oral administration is restricted by its fast dissolution in the stomach but has a limitation for controlled drug delivery [2, 3]. Thus to overcome the disadvantages associated with the individual polymer it is usually cross linked with various agents including polyelectrolytes to form a complex network structure of chitosan. Some polymers which were used as cross linking agents are polyvinyl pyrrolidone, chondroitin, xanthan gum, sodium alginate, and pectin etc.; for prolonged drug delivery [3-8]. Advantage of polyelectrolyte complex of chitosan with other polymers includes the avoidance of organic solvents, chemical cross-linking agents which reduces the toxicity and undesirable side effects. These types of materials are though excellent for drug loading and release but they suffer from limitations like targeting ability.

In this regard, we have developed pectin based nanomaterials with magnetite nanoparticles (MNPs) encapsulated in it (discussed in chapter 2) and its potential drug (diclofenac sodium) loading and release capacities, as discussed in chapter 3. However the loading efficiency of the model drug, diclofenac sodium, in 100 – 150 nm magnetite-calcium pectinate nanomaterials was about 60 % and drug loading content (wt %) was 28.9 %. There was a scope for improving the drug loading efficiency. In this regard, it was found from literature reports that microparticles of chitosan exhibits high % entrapment efficiency [9]. In order to improve the drug loading efficiency using pectin, it was thought to explore the conditions of utilizing pectin in combination with chitosan. Our idea was influenced by a similar study on microparticles of sizes 920.48 to 1107.56  $\mu\text{m}$  of pectin re-inforced with chitosan and cross linked with  $\text{Zn}^{2+}$  showed 96.95 – 98.85 % loading of resveratrol as a model drug [10].

### 4.1.1 Objective of the study

Our aim was to reduce the size of the drug carrier and further to use pectin as a major component while chitosan being a minor one, so that the nanomaterial possess mostly the characteristics of pectin. Moreover, use of low cost pectin, as discussed in chapter 2, would

render biocompatibility and biodegradability. Such type of material will be referred to as pectin re-inforced with chitosan. In our method of fabrication of nanomaterials of pectin-chitosan system,  $Zn^{2+}$  or  $Ca^{2+}$  ions were not needed for cross linking pectin, as chitosan was explored to form a cross linked network with pectin by electrostatic interaction. However, the hybrid nanomaterial of pectin-chitosan system lacked magnetic property and there was a scope to incorporate magnetic materials to make it multifunctional. In that case, it could exhibit magnetic responsive property along with drug as carrier ability.

In the present study we report synthesis, characterization and *in vitro* release of diclofenac sodium (DS) from hybrid nanomaterials comprising magnetite-pectin-chitosan system. These type of nanomaterials referred here as MPCh-DS, was characterized by XRD, Mössbauer spectroscopy, SEM-EDAX, TEM, DLS, FT-IR, TG, SQUID and VSM. The *in vitro* release of DS was studied in simulated gastrointestinal fluid and in phosphate buffer solution.

## 4.2 MATERIALS AND METHODS

### 4.2.1 Materials

Chitosan was purchased from Polysciences Inc., Warrington, PA (Molecular Weight ~15,000 with minimum 85% degree of deacetylation). In addition, all the chemicals, except  $CaCl_2$  mentioned in chapter 2 and chapter 3 were used.

Simulated gastric fluid (SGF), simulated intestinal fluid (SIF), simulated colonic fluid (SCF) and phosphate buffer solution were prepared as discussed in chapter 3. The calibration curve of the DS as discussed in chapter 3 was plotted for the determination of the amount of the drug loaded and released in these media by UV-visible spectrophotometry.

### 4.2.2 Method for fabrication of nanomaterials of magnetite- pectin- reinforced with chitosan loaded with DS

MNPs were synthesized by co-precipitation method as discussed in chapter 2 using the optimized conditions. After washing the MNPs, 25 mL of the dispersion of MNPs were mixed with 25 mL of 0.4 % w/v of pectin at pH ~ 4 where pH was controlled by adding dilute HCl.

In another vessel, diclofenac sodium was mixed with 25 mL of chitosan dissolved by adding dilute acetic acid. Here 0.01 M and 0.05 M of DS were respectively stirred with different concentration e.g., 0.00625 % to 0.1 % w/v (Table 4.1). This mix was then added

to the dispersion of MNPs and pectin. The batches of different concentrations of pectin, chitosan and DS used for optimization process of fabrication of MNP encapsulated with pectin re-inforced with chitosan system are presented in Table 4.1. This mixture was then allowed to stir for 6 hrs.

**Table 4.1.** Optimization of encapsulation efficiencies and drug loading content in MPCh-DS nanomaterials with fixed concentration of MNPs

| Concentration of diclofenac sodium | Chitosan (% w/v) | Pectin (% w/v) | % Encapsulation efficiency | Drug loading content (wt %) |
|------------------------------------|------------------|----------------|----------------------------|-----------------------------|
| 0.01 M                             | 0.1%             | 0.4%           | 99.62                      | -                           |
| 0.01 M                             | 0.05%            | 0.4%           | 99.44                      | -                           |
| 0.01 M                             | 0.025%           | 0.4%           | 99.50                      | 46.25 %                     |
| 0.05 M                             | 0.025%           | 0.4%           | 99.49                      | 50.86 %                     |
| 0.05 M                             | 0.0125%          | 0.4%           | 97.40                      | -                           |
| 0.05 M                             | 0.00625%         | 0.4%           | 95.94                      | -                           |

- not analyzed as the nanomaterials of only optimized conditions were studied further. Notably drug encapsulation efficiency was more than 99 % for both 0.01 M and 0.05 M DS, for the same chitosan concentration (0.025% w/v)

#### 4.2.3 Methodology for drug loading analysis

The dispersion of the nanomaterials of magnetite-pectin reinforced with chitosan loaded with DS obtained after the synthesis comprised free dissolved drug and drug loaded in nanomaterials. The drug loaded in these nanomaterials would therefore be difference of total drug taken for fabrication and the amount of free dissolved drug in the dispersion i.e. Amount of drug loaded = Initial amount of the drug taken – amount of free dissolved drug.

The concentration of free dissolved drug in the dispersion was determined by the bulk equilibrium reverse dialysis as discussed in chapter 3. The concentration of the drug present inside the dialysis bag was measured by UV visible spectrophotometry at  $\lambda_{\max} = 276$  nm as discussed in chapter 3.

The drug loading content (wt %) in nanomaterials of magnetite pectin reinforced with chitosan loaded with DS was calculated as:

$$\text{Drug loading content (wt \%)} = (a/b) * 100$$

a = amount of the drug loaded in the nanomaterials of magnetite-pectin reinforced with chitosan loaded with DS.

b = weight of fabricated nanomaterials of magnetite-pectin reinforced with chitosan loaded with DS.

The extent of drug incorporation into nanomaterials of magnetite-pectin reinforced with chitosan was expressed in terms of % encapsulation efficiency of DS, which is given as:

$$\% \text{ Encapsulation efficiency} = (a / t) * 100$$

a = amount of the drug loaded in nanomaterials of magnetite-pectin reinforced with chitosan loaded with DS.

t = Initial amount of the drug taken.

It may be noted here that, the magnetite pectin nanomaterials reinforced with chitosan which were fabricated using fixed concentration of the dispersion of MNPs, 0.4 % pectin, 0.025 % chitosan without DS will now be referred to as MPCh (magnetite nanoparticles: pectin reinforced with chitosan). Further the batches prepared using same composition as that of MPCh loaded with 0.01 M DS will now be referred to as MPCh-DS0.01 and the one prepared using 0.05 M DS as MPCh-DS0.05 respectively.

#### **4.2.4 Characterization**

The details of the methods used for characterization, namely, XRD, FT-IR, DLS, SEM-EDAX, TEM, SQUID, VSM and <sup>57</sup>Fe Mössbauer spectroscopy are discussed in chapter 2 and 3.

#### **4.2.5 Methodology for *in vitro* drug release**

The methodologies used for estimating *in vitro* drug release from MPCh-DS nanomaterials in simulated gastric fluid, simulated intestinal fluid, simulated colonic fluid and in phosphate buffer solution at pH 7.4, were same as discussed in the chapter 3.

### **4.3. RESULTS AND DISCUSSION**

#### **4.3.1 Evaluation of drug loading**

It may be noted from Table 4.1 that the batches of MPCh-DS synthesized using pectin concentrations of 0.4% and chitosan 0.025 % followed by treatment with 0.01 M DS, resulted in ~ 99.50 % encapsulation efficiency. On the other hand, the batch synthesized using 0.01 M DS in 0.05 % chitosan and 0.4% pectin also showed similar encapsulation efficiency. But it was noted that the higher polymer content might reduce the magnetic property of the material as discussed in chapter 2. Further, by increasing the drug concentration to 0.05 M, the encapsulation efficiency was also found to be only ~99.49 %. However, there was about 4 % increase (50%) in the drug loaded content when the initial

drug concentration was 0.05M as compared to the batch of 0.01 M DS. But further decreasing the chitosan concentration to 0.0125 % and 0.00625 % resulted in small decrease in drug loading efficiency. From the above results, it was noted that the optimized conditions needed for preparing hybrid nanomaterials of magnetite-pectin-drug were 0.4 % w/v pectin, 0.025 % w/v of chitosan with 0.01 M and 0.05 M DS ( MPCh-DS0.01 and MPCh-DS0.05 respectively.) In addition, MNP encapsulated with pectin and chitosan but without DS was also synthesized (referred to as MPCh) for comparing the IR and TG data to elucidate drug loading.

The chitosan solution dispersed with various concentrations of DS was then added to crosslink with pectin to form magnetic nanomaterial MPCh-DS. The above method was optimized to achieve uniform size distribution of these spherical nanomaterials. The key parameters involved in the optimization process were pH of about 4, pectin precursor concentration which was taken as 0.4 % in w/v, as optimized in the previous chapters, various concentrations of chitosan (0.1 to 0.00625% w/v) and DS (0.01 M and 0.05 M) followed by vigorous stirring for 6h. The utilization of higher polymer concentrations resulted into the formation of viscous polymeric matrix which might reduce the saturation magnetization of the system [11]. It was found that chitosan concentration of 0.025 % w/v and pectin of 0.4 % w/v with 0.05M DS and 0.01M DS (Table 4.1) was optimum for synthesizing nanomaterial of MPCh-DS which showed ~ 99 % encapsulation efficiency.

#### **4.3.2 X-ray diffraction studies**

The strategy to prepare the magnetic nanomaterial of MPCh-DS involved the synthesis of stable MNPs by co-precipitation method followed by its in-situ encapsulation with pectin. The XRD analysis of MPCh-DS0.05 and MPCh-DS0.01 revealed presence of magnetite phase as supported from the position and relative intensities of diffraction patterns at 220, 311, 400, 511 and 440 planes (Fig. 4.1) which corroborated well with those of cubic magnetite structures as reported in JCPDS 01-11111 data. The average crystallite size ( $D$ ) of the MNPs was found to be about 2 nm, which was calculated using the Debye-Scherrer formula i.e.  $D = 0.9\lambda / \Delta \cos\theta$ , where  $\lambda$  is X-ray wavelength,  $\Delta$  is line broadening measured at half-height from the most intense peak of XRD (311 plane) and  $\theta$  is Bragg angle of the particles. In addition, the diffraction pattern of pure DS was observed in the XRD pattern of MPCh-DS0.05 and MPCh-DS0.01 as shown in Fig. 4.1. The XRD pattern of pure DS

agreed well with the JCPDS data 39-1684. The incorporation of DS was further confirmed from the absence of DS pattern in MPCh (without drug loading).

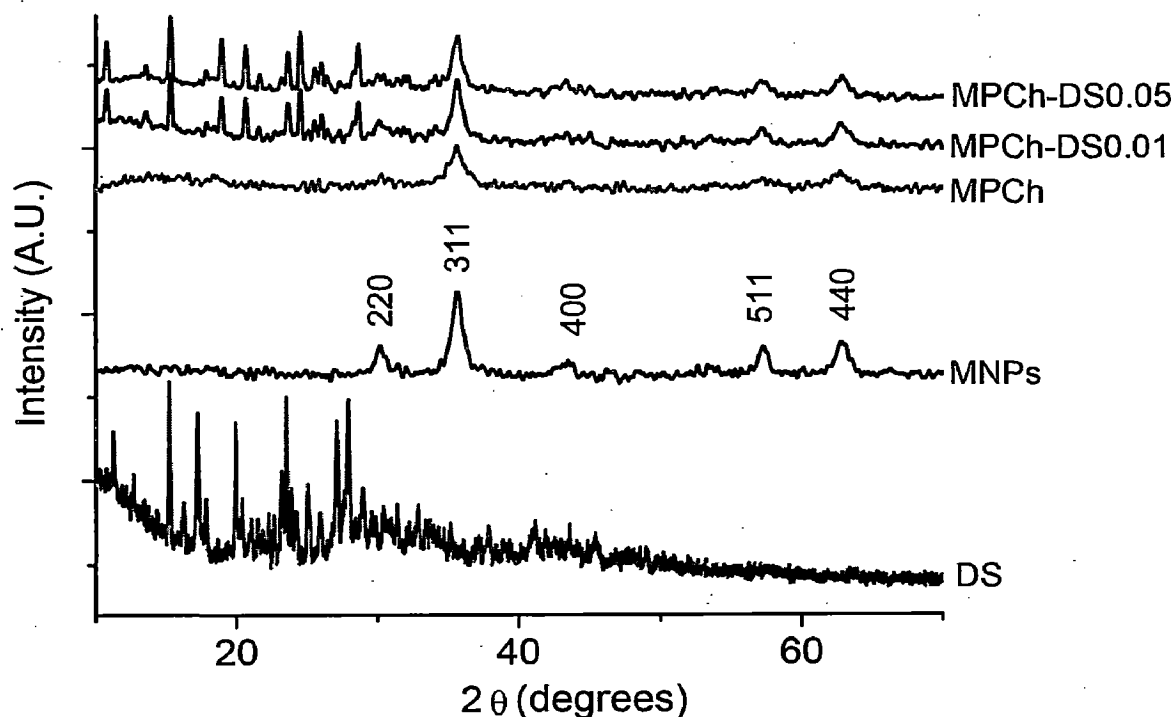
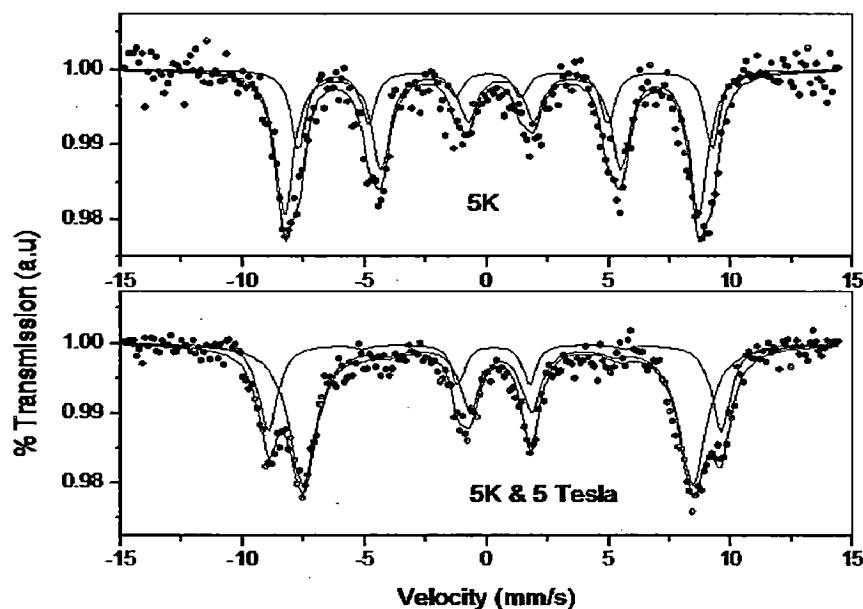


Fig. 4.1. XRD of the Diclofenac Sodium (DS), MNPs, MPCh, MPCh-DS0.01 and MPCh-DS0.05.

#### 4.3.3 $^{57}\text{Fe}$ Mössbauer spectroscopic studies

The formation of magnetite phase in MPCh-DS was also confirmed from the  $^{57}\text{Fe}$  Mössbauer spectroscopy studies of nanomaterials of MPCh-DS0.05 by recording characteristic tetrahedral ( $\text{Fe}^{3+}$ ) and octahedral ( $\text{Fe}^{2+/3+}$ ) sites of Fe at 5 K and in presence of 5T externally applied magnetic field (Fig. 4.2). This study revealed tetrahedral ( $\text{Fe}^{3+}$ ) and octahedral  $\text{Fe}^{2+/3+}$  sites which are typically due to magnetite phase (Fig. 4.2). The corresponding hyperfine splitting parameters, namely, isomer, shift, quadrupole splitting and internal magnetization ( $B_{\text{hf}}$ ) are given in Table 4.2, which were characteristic of magnetite phase. For the batch measure at 5 K and 5 T, isomer shift corresponding to  $\text{Fe}^{3+}$  (tetrahedral) while the isomer shift of 0.5 corresponded Fe shift which is given as  $\text{Fe}^{2+}/\text{Fe}^{3+}$ . Due to the presence of the  $\text{Fe}^{2+}$  the average isomer shift increased. Small order of quadrupole splitting corresponded to cubic structure and hence corroborate with that of magnetite phase. The internal magnetization was found to be 57.49 for tetrahedral site and 49.50 for octahedral site.



**Fig.4.2.**  $^{57}\text{Fe}$  Mössbauer spectra of MPCh-DS0.05 nanomaterials recorded at 5 K showing typical sextet of magnetic material and at 5 K and 5 T showing tetrahedral and octahedral sites of  $\text{Fe}_3\text{O}_4$  phase.

**Table 4.2**  $^{57}\text{Fe}$  Mössbauer spectroscopy hyperfine splitting parameters of MPCh

|                | FWHM<br>(mm/s)    | Isomer shift<br>(mm/s) | Quadrupole<br>splitting (mm/s) | Bhf (Tesla)       | Area (%) |
|----------------|-------------------|------------------------|--------------------------------|-------------------|----------|
| 5K             | $0.730 \pm 0.015$ | $0.409 \pm 0.025$      | $0.064 \pm 0.008$              | $52.50 \pm 0.03$  | 30.8     |
|                | $0.89 \pm 0.012$  | $0.388 \pm 0.022$      | $-0.144 \pm 0.010$             | $52.56 \pm 0.05$  | 69.2     |
| 5K &<br>5Tesla | $0.668 \pm 0.052$ | $0.308 \pm 0.025$      | $0.045 \pm 0.010$              | $57.49 \pm 0.130$ | 30.0 (T) |
|                | $0.971 \pm 0.031$ | $0.514 \pm 0.015$      | $-0.120 \pm 0.018$             | $49.50 \pm 0.010$ | 70.0 (O) |

(T): Tetrahedral and (O): Octahedral

#### 4.3.4 Morphological studies

##### 4.3.4.1 Scanning electron microscopy (SEM), energy dispersive X-ray analysis (EDAX) studies

The SEM study revealed that the fabricated MPCh-DS0.05 nanomaterials were mostly spherical in shape with size distribution in the range of 100 – 150 nm (Fig. 4.3). Further EDAX analysis of a selected area of a representative spherical MPCh-DS nanomaterial exhibited co-localization of sodium (Na) and iron (Fe) as evident from the recorded K-X-rays of Na (1.04 keV) and Fe (6.39 and 7.07 keV) as shown in Fig. 4.3. The detection of co-localized Na and Fe was attributable to those of the diclofenac sodium and MNPs respectively in each spherical nanomaterials and thus indicated the formation of MPCh-DS.

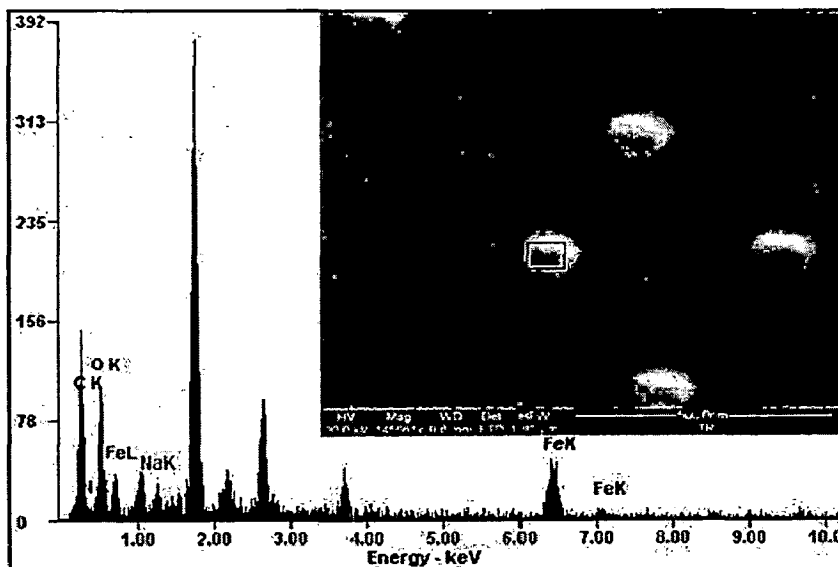


Fig. 4.3. SEM of MPCh-DS0.05 showing individual spherical nanomaterials of sizes 100 -150 nm, EDAX analysis showing K-X-ray peaks of Na and Fe indicating the presence of the diclofenac sodium and magnetite in MPCh-DS.

#### 4.3.4.2 Transmission electron microscopy (TEM)

The TEM analysis of the MPCh-DS0.05 nanomaterials illustrated formation of spherical structures of ~150 nm size which corroborated with the SEM results (Fig. 4.4a, 4.4b). However, some cylindrical shapes structure were also observed which was probably was due to coalescing of two or more spherical nanomaterials. A higher resolution TEM study of a part of a representative nanomaterial of MPCh-DS0.05 revealed encapsulation of a large number of MNPs. (Fig. 4.4c). Its corresponding SAED image revealed polycrystalline nature of the encapsulated MNPs (Fig. 4.4c).

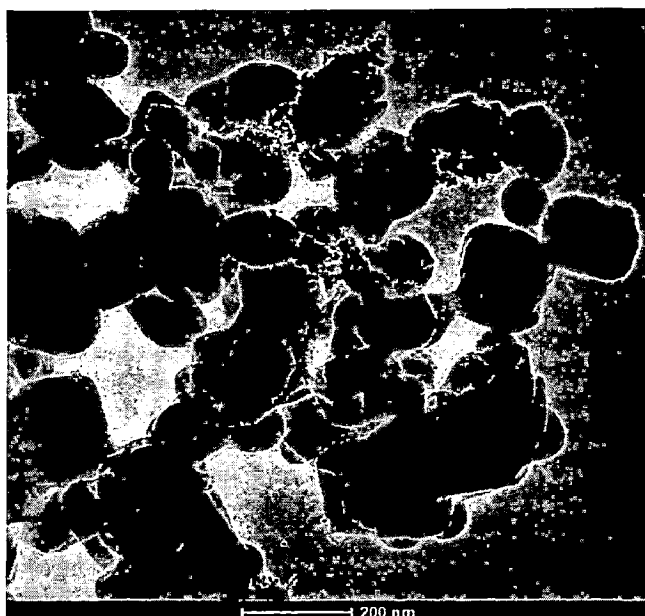
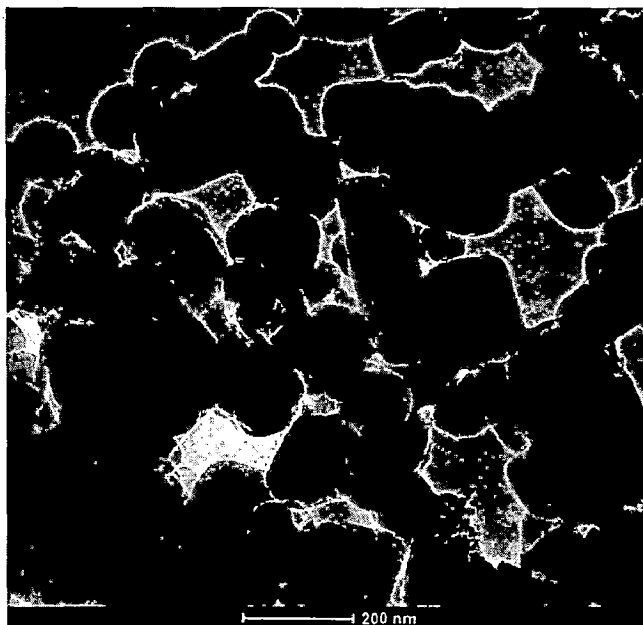
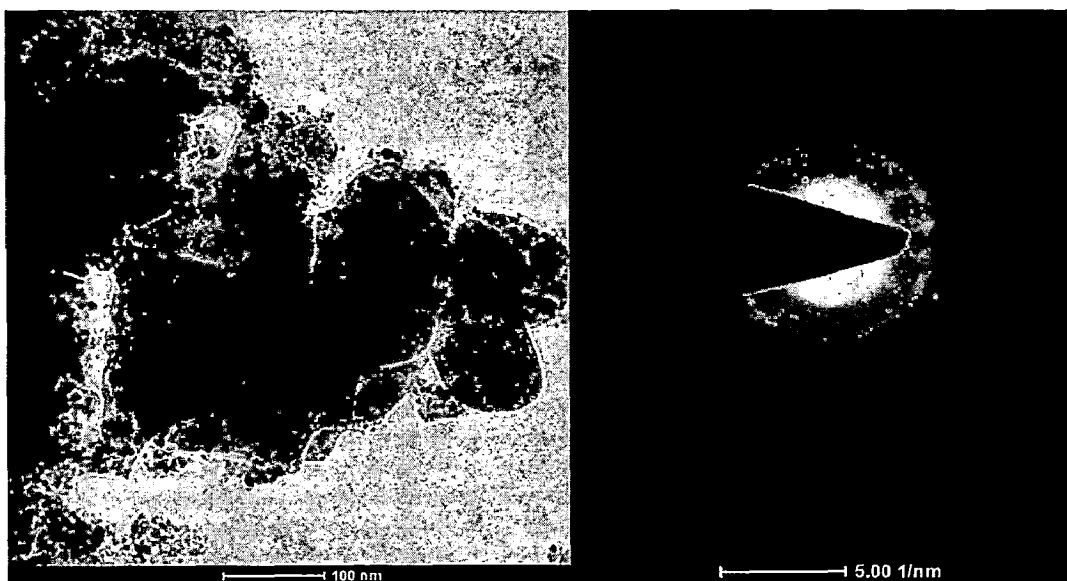


Fig. 4.4a. TEM showing morphology of MPCh-DS0.05 nanomaterial with size of ~150 nm.





**Fig. 4.4b.** TEM showing morphology of MPCh-DS0.05 nanomaterial with size of ~150 nm.



**Fig. 4.4c.** Showing detailed TEM image showing aggregation of 100 - 150 nm MPCh-DS0.05 and its corresponding SAED image exhibiting polycrystalline nature of MNPs.

#### 4.3.4.3 Dynamic light scattering studies

The dynamic light scattering (DLS) measurement of MPCh-DS0.05 in aqueous solution at pH~ 4 exhibited unimodal size distribution in the range of 230 – 520 nm with maximum intensity at ~ 350 nm (Fig. 4.5). This indicated that the method of synthesis offered a good control over the size of these nanomaterials. It may however be noted that the particle size measured by DLS was larger than those measured by TEM and SEM. Primarily, SEM and TEM studies were carried out in dried materials while DLS studies

were carried out in aqueous medium. The increase in the sizes of MPCh-DS0.05 nanomaterials could be attributed to the swelling effect of pectin in aqueous medium [12].

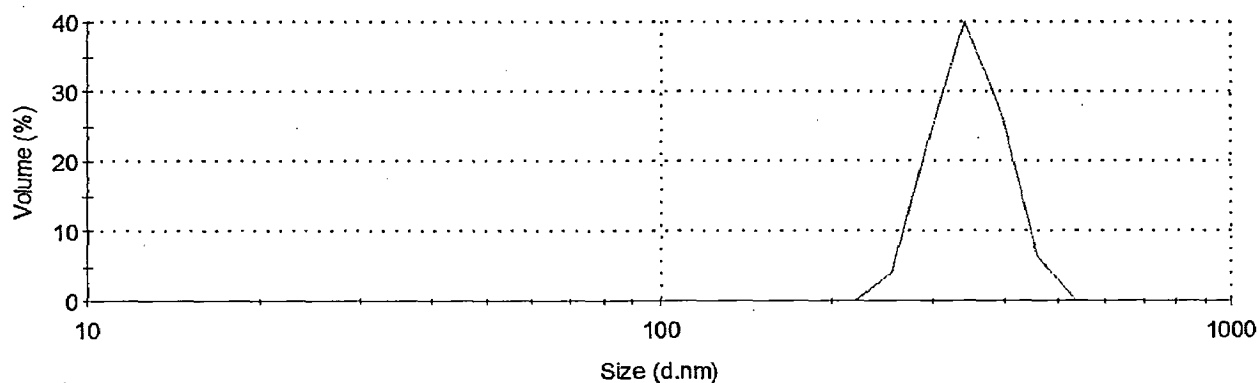
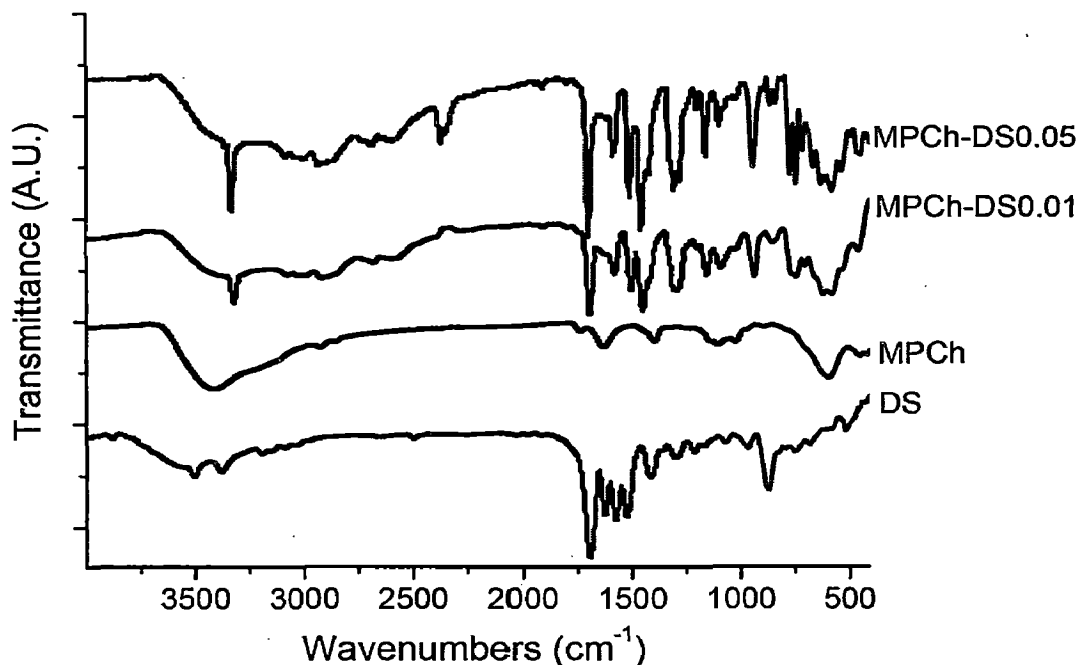


Fig. 4.5. DLS measurement of MPCh-DS05 in aqueous solution at pH~4.

#### 4.3.5 FT- IR analysis

The encapsulation of DS in MPCh-DS was further elucidated by FT-IR analyses. As mentioned in the chapter 3, DS consists of various functional groups, notably, -NH and  $\text{COO}^-$ , substituted benzene ring and C-Cl. Similarly, pectin and chitosan consists of -OH groups,  $\text{COO}^-$ , C-O-C, which were studied by IR spectroscopy. The corresponding IR peaks of these groups were identified from literature [13].

The presence of DS encapsulated in magnetite-pectin-chitosan nanomaterials was evident from observation of characteristic IR peaks of DS in the MPCh-DS batch. The N-H stretching frequency of the secondary amine corresponding to DS at  $3326$  and  $3337\text{ cm}^{-1}$  for the batches MPCh-DS0.01 and MPCh-DS0.05 respectively, as compared to the N-H stretching frequencies at  $3380\text{ cm}^{-1}$  observed in the DS (Fig. 4.6). The N-H bending frequency in these batches was recorded at  $1621\text{ cm}^{-1}$ . However, the presence of carboxylate group, in calcium pectinate, would also exhibit IR bands in the region  $1550 - 1650\text{ cm}^{-1}$ . Thus the bands observed at  $1577$  and  $1579\text{ cm}^{-1}$  in MPCh-DS0.01 and MPCh-DS0.05 were attributable to the presence of carboxylate group. The bands in this region were also observed for magnetite-pectin-chitosan system indicating carboxylate group contributed from MPCh as similar bands were observed in MPCh batch. The IR peak recorded at  $1453\text{ cm}^{-1}$  in DS was due to  $-\text{CH}_2$  group of aromatic ring (in DS) which was also recorded in MPCh-DS0.01 and MPCh-DS0.05 batches.



**Fig. 4.6.** FT-IR spectra of DS, MPCh, MPCh-DS0.01 and MPCh-DS0.05, showing encapsulation of DS in the nanomaterials.

The -OH group in pectin and chitosan were evident from the stretching frequencies in the range of 3200 – 3600  $\text{cm}^{-1}$ , and bending frequencies in the range of 1390 – 1440  $\text{cm}^{-1}$ , observed in MPCh, MPCh-DS0.01 and MPCh-DS0.05. Notably, due to large number of -OH groups in chitosan and also in pectin, the O-H stretching band was broad and intense. As a result, the N-H stretching frequency peak due to  $-\text{NH}_2$  group in chitosan was masked. The IR peaks recorded at 1017  $\text{cm}^{-1}$ , 1094  $\text{cm}^{-1}$ , 1147  $\text{cm}^{-1}$ , 1290  $\text{cm}^{-1}$  were observed in MPCh, MPCh-DS0.01 and MPCh-DS0.05, which were attributable to C-O stretching frequencies. The peak at 1146 was due to C-O-C stretching frequency corresponding to the C-O-C linking groups in pectin. The IR peak at 773  $\text{cm}^{-1}$ , observed for DS, MPCh-DS0.01 and MPCh-DS0.05 were due to substitute aromatic ring in diclofenac sodium structure. The peaks occurring at 773  $\text{cm}^{-1}$  and 745  $\text{cm}^{-1}$  are likely to be due to di-substituted benzene ring in the DS structure. So from the above IR studies, where the peaks of DS agreed well with those of MPCh-DS indicated the formation of MPCh-DS0.05 and MPCh-DS0.01. The peak observed at 590  $\text{cm}^{-1}$  was attributable to vibrations of Fe-O bond. As expected, this peak was not observed in the IR spectrum recorded for DS. So from the above IR studies, peaks of DS agreed well with those of MPCh-DS indicated the formation of MPC-DS0.05 and MPCH-DS0.01. Furthermore, the absence any peak in the region 1680-1630  $\text{cm}^{-1}$  in MPCh-DS0.05, MPCh-DS0.01 and MPCh indicated that the amide bond formation did not occur due to interaction of pectin and chitosan. This indicated that the formation of these nanomaterials was perhaps based on the electrostatic interaction between DS, pectin and

chitosan. These observations reflected the formation of MPCh-DS0.05 and MPCh-DS0.01. Thus from the FT-IR study it was concluded that the fabricated nanomaterial comprised of magnetite nanoparticles, pectin, chitosan and diclofenac sodium.

#### 4.3.6 Thermogravimetric analysis

The encapsulation of DS in MPCh-DS was studied by thermogravimetric (TG) analysis as shown in Fig. 4.7a. The TG plot of DS exhibited step wise degradation (Fig 4.7b). Initial weight loss of ~ 17 % was observed till 80 °C. The DS was thermally stable up to 250 °C. Beyond that the drug started decomposing, first rapidly between 250 °C – 290 °C where about 18 % of the drug decomposed and then gradual thermal decomposition occurred between 300 °C and 685 °C corresponding to in 50 % mass loss. Finally (~15 % of DS decomposed in the range of 840 °C – 870 °C.

The thermal analysis of the as-synthesized nanomaterial of magnetite – pectin – chitosan (MPCh) exhibited 29.8 % mass loss at ~ 800 °C and then it was thermally stable (Fig. 4.7b).

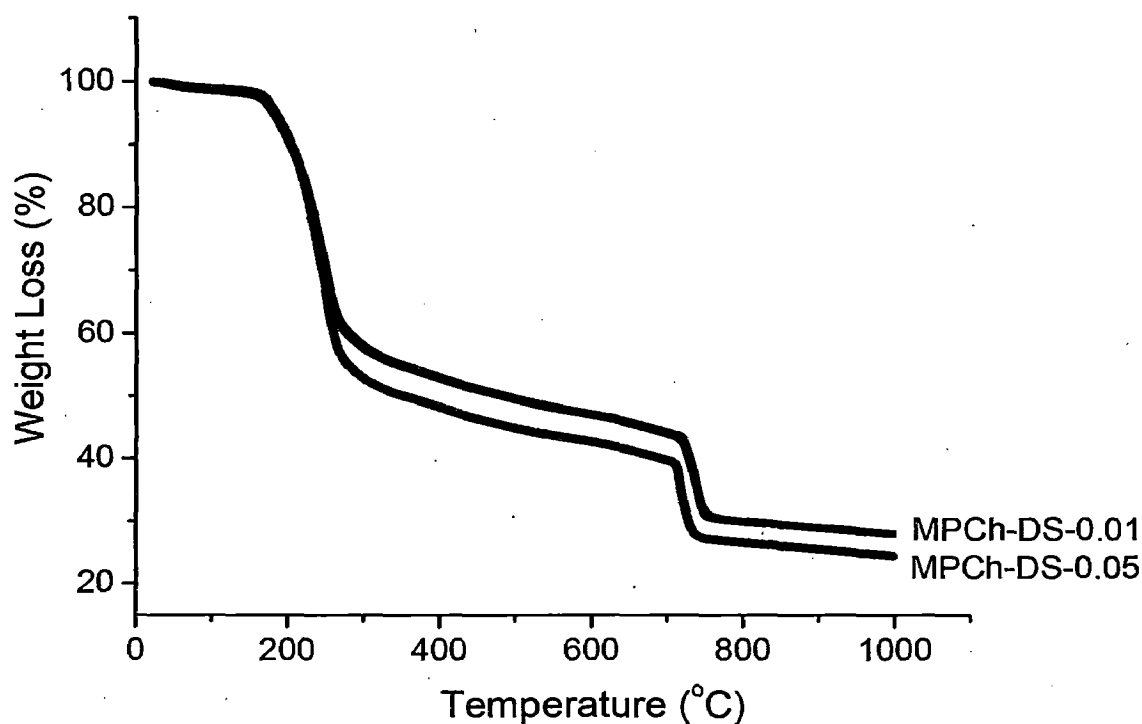


Fig. 4.7a. TGA plot of MPCh-DS0.05 and MPCh-DS0.01.

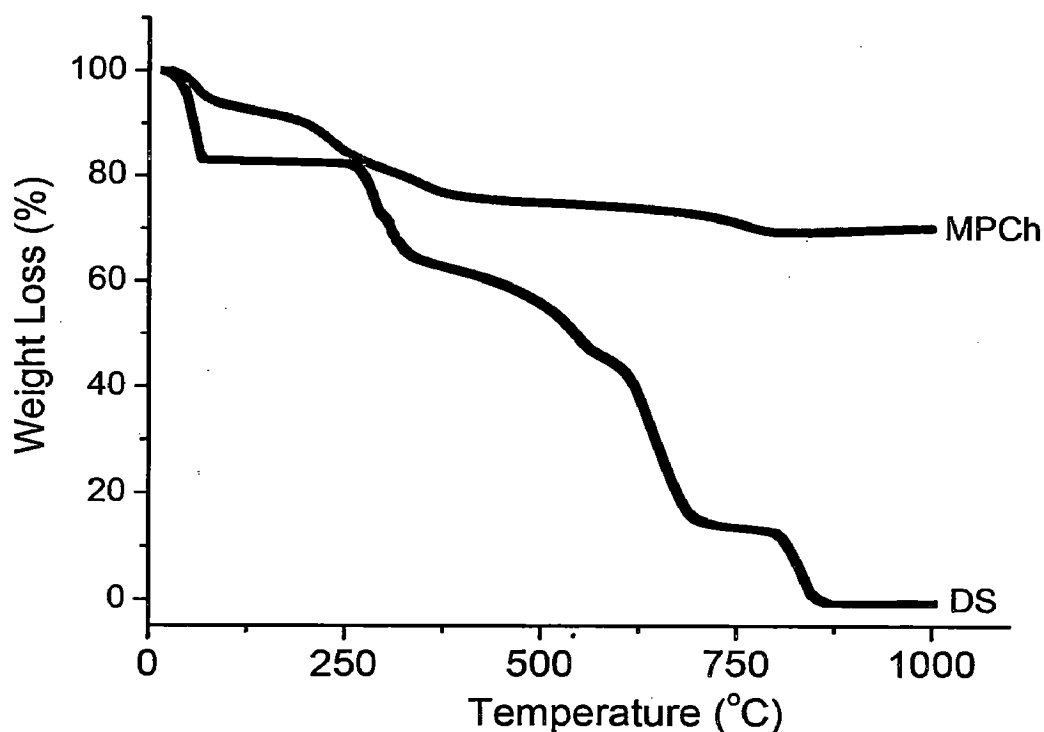


Fig. 4.7b. TGA plot of MPCh and diclofenac sodium (DS).

The thermal analysis of the batches MPCh-DS0.01 and MPCh-DS0.05 corresponding to diclofenac sodium drug loaded in the MPCh, also exhibited step wise mass loss. Similar to DS for the batch MPCh-DS0.01, initially about 2 % mass loss up to 80 °C followed by a 40 % rapid mass loss in the temperature range of 190 – 260 °C. This was followed by 21 % gradual mass loss in the temperature range between 260°C- 710 °C followed by another 11 % rapid mass loss in the temperature range between 710 -723 °C. Then about 2 % gradual mass loss was noted for this batch till it was heated to 1000 °C.

#### 4.3.6.1 Calculation of loaded drug from thermal analysis.

The weight loss for MPCh-DS0.01 was 72.0 % and that MPCh-DS0.05 was 75.8 %. Since drug decomposed completely as reflected from its thermal study, so the total weight losses in the MPCh-DS systems were due to loss of drug from the fabricated nanomaterials. The total drug loaded in the nanomaterials could be calculated from the thermal analysis as = total mass loss in MPCh-DS system – mass loss from MPCh system. In the case of MPCh-DS0.05, total mass loss = 75.8 % out of which 29.8 % loss is due to MPCh degradation i.e. 22.74 % loss is due to MPCh. So the mass loss due to drug in MPCh-DS0.05 = 75.8 – 22.7 = 53.1 % of fabricated MPCh-DS system. This was in good agreement with the drug loading as given in Table 4.1.

#### **4.3.7 Zeta potential measurement: mechanism of the formation of nanomaterial of MPCh-DS**

The zeta potential measurements (given in Table 4.3) offered an insight towards the formation of the nanomaterials of MPCh-DS0.05 as schematically represented in Fig. 4.8. The zeta potential of MNPs synthesized at pH~ 10 was measured as  $-41.8$  mV which confirmed synthesis of highly stable MNPs. These stable MNPs were conditioned at pH~ 4 and were mixed with pectin. At this pH, the zeta potential ( $\zeta$ ) of MNPs was found to be  $+17.7$  mV and that of pectin was  $-35.9$  mV. The negative zeta potential of pectin was due to polyanionic nature of pectin at pH~ 4. The zeta potentials of MNPs and pectin at pH~ 4 were thus favorable for electrostatic interaction of MNP and pectin. When DS was dispersed in chitosan and was subsequently mixed with pectin, the formation of spherical shaped MPCh-DS is persuasive due to electrostatic interaction between positively charged amino groups ( $\text{NH}_3^+$ ) of chitosan and anionic  $\text{COO}^-$  groups of pectin at pH~ 4. The similar reports were also found in the literature [14]. Furthermore, it has also been reported that the intramolecular H-bonding between the  $-\text{COOH}$  groups of pectin or  $-\text{NH}_2$  groups of chitosan and  $-\text{OH}$ ,  $-\text{OCH}_3$  or  $-\text{COOCH}_3$  groups elsewhere within the complex is also possible [14]. However, such interactions between pectin and chitosan are favored at low pH [15, 16], which could lead to the formation of more compact network structure. The formation of this network structure as well as the formation of spherical shape was due to minimum surface energy needed to attain stability in the MPCh-DS nanomaterials. Moreover, the spherical nanomaterials of MPCh-DS were likely to be due to cross linking of pectin with chitosan and not due to any chemical bonding by amide group formation. This was confirmed from the IR results which did not show any amide group. So the cross linking between pectin and chitosan could be persuaded due to electrostatic interaction as supported from the zeta potentials of chitosan and pectin as  $+117$  mV and  $-35.9$  mV respectively at pH ~4. Further the zeta potential of nanomaterial MPCh-DS0.05 was measured to be  $-18.6$  mV, indicating that the nanomaterials was reasonably stable [17].

The loading of the drug diclofenac sodium in the nanomaterials of MPCh was found to be successful only when the drug was first dispersed in chitosan and then mixed with pectin and not the other way. This could be explained on the basis of zeta potential data as given in Table 4.3. The zeta potential of DS was  $-110$  mV, which could electrostatically interact with chitosan ( $+114$  mV) (all measurements were at pH~ 4).

**Table 4.3.** Zeta potential measurements of magnetite nanoparticles (MNPs), pectin solution, chitosan solution, diclofenac sodium solution and nanomaterial MPCh-DS0.05.

| Samples           | Measured zeta potential value ( $\zeta$ ) in mV |
|-------------------|---|
| MNPs at pH ~10    | - 41.2  |
| MNPs at pH ~4     | + 17.1  |
| Pectin at pH~4    | - 35.7  |
| Chitosan at pH~4  | +114  |
| Diclofenac Sodium | - 110   |
| MPCh-DS0.05       | - 18.7  |

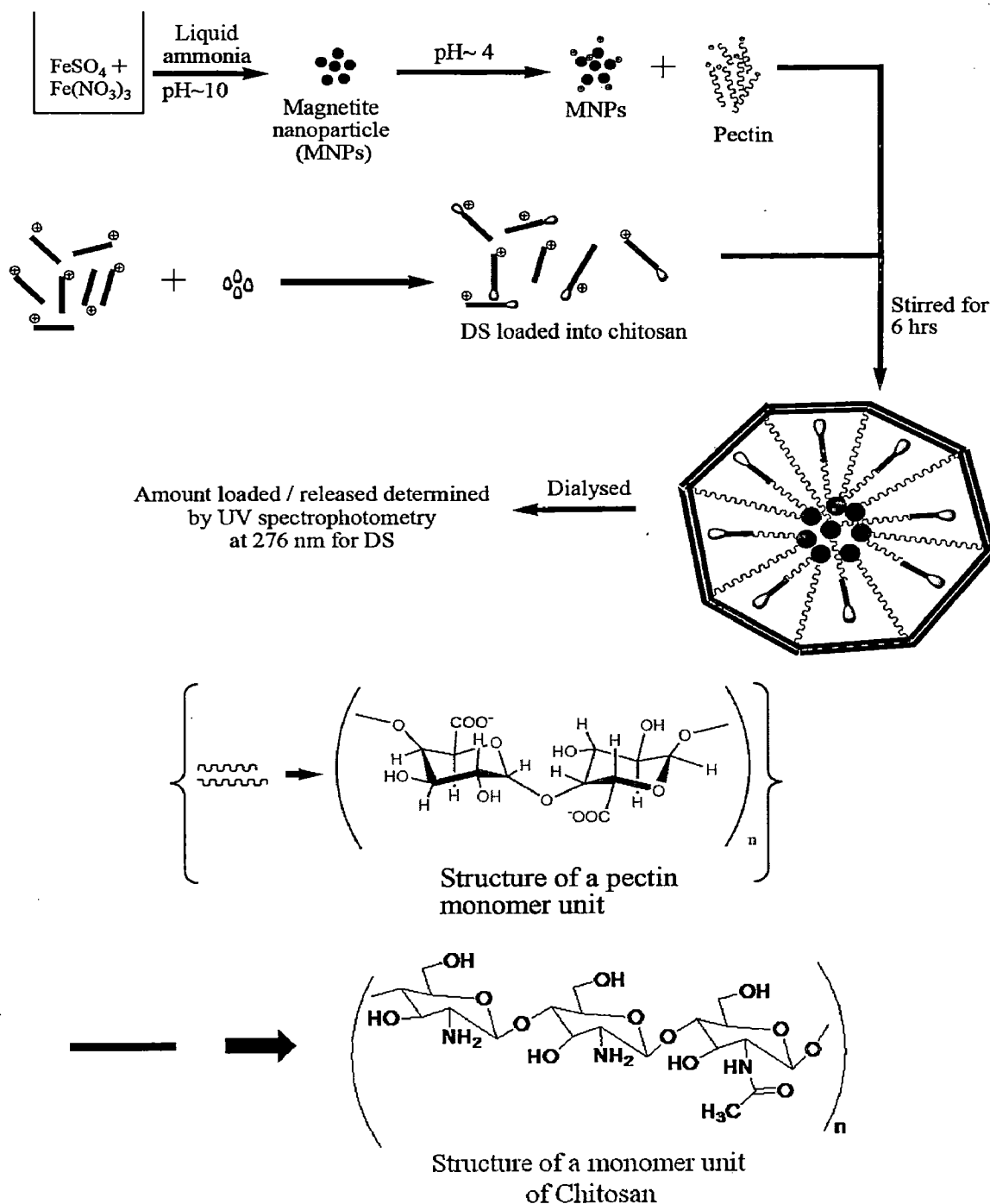


**Fig. 4.8.** Schematic representation of mechanism towards formation of the MPCh-DS nanomaterials.

#### 4.3.8 Magnetic studies

The magnetic property of the as synthesized batches of nanomaterials of MPCh-DS were studied by from the saturation magnetization ( $M_s$ ) from the M-H curves of these batches from VSM measurements recorded in the magnetic field scanned in the range of  $\pm 10$  kOe at room temperature. The  $M_s$  of the batches of MPCh-DS0.01 and MPCh-DS0.05 were compared with that of MPCh (without drug loading) and MNPs. It was noted that the magnetization curves (M-H) for all the batches were similar to that of the as-synthesized MNPs (Fig. 4.9), i.e., these batches exhibited negligible remanence magnetization and coercivity. In the case of MNPs, such magnetic properties were reported to be due to the phenomenon of superparamagnetism, usually exhibited by magnetite nanoparticles of sizes less than 20 nm [18]. Thus the phenomenon of superparamagnetism in the batches of MPCh-DS was attributable to the presence of magnetite nanoparticles, indicating the incorporation of magnetic properties in the as-synthesized batches of nanomaterials of MPCh-DS. However, the measured saturation magnetization ( $M_s$ ) was found to be lesser than the magnetite nanoparticles. Compared to the MNPs ( $M_s = 55.82$  emu/g) the saturation magnetization of nanomaterials of magnetite-pectin-chitosan, (i.e. the batch without drug loading - MPCh) was measured to be 44.15 emu/g, while that of the batches MPCh-DS0.01 and MPCh-DS0.05 were measured to be 36.63 emu/g and 34.40 emu/g respectively. The decrease in the saturation magnetization ( $M_s$ ) in these batches could be attributed either to the effect of small particle size owing to non-collinear spin arrangement at the surface, or due to the formation of magnetic dead layer by pectin and or chitosan at the domain boundary wall of MNPs [19, 20]. The particle size effect on reduction of  $M_s$  may be ruled out as the same batch of MNPs with uniform particle size distribution was used for synthesis of different batches of MPCh-DS. The magnetic moments could however be quenched due to the formation of magnetic dead layer of pectin cross linked with chitosan at the domain wall of MNPs. This could hinder the domain wall motion during application of the magnetic field, which might be responsible for the reduction in the saturation magnetization in these nanomaterials. It may therefore be inferred that the synthesis of magnetic nanomaterials of MPCh-DS resulted in polymer-MNP interface. It was interesting to note that the magnetization ( $M_s$ ) in these nanomaterials was lowered due to the increase in the concentration of the loaded diclofenac sodium (DS). Apparently the drug DS might be thought to contribute to the formation of magnetic dead layer. Overall, it may be surmised



that the as-synthesized nanomaterials of MPCh-DS exhibited magnetic behavior and could be used as magnetically transported system.

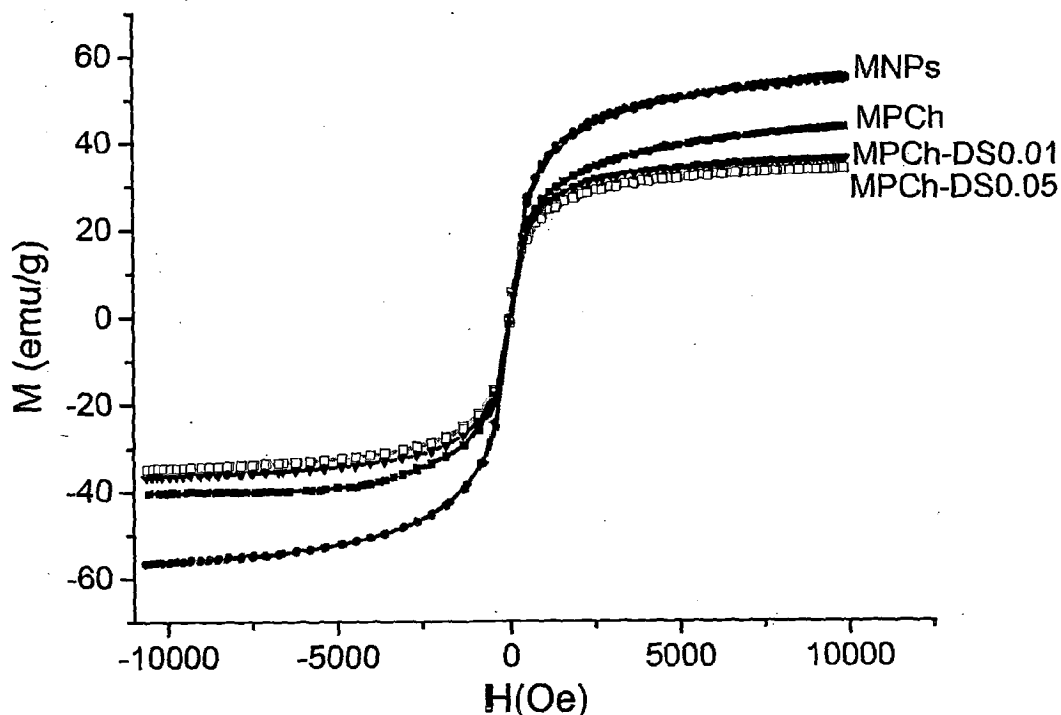


**Fig. 4.9.** Magnetization vs field (M-H) curve of MNPs, MPCh, MPCh-DS0.01 and MPCh-DS0.05 measured by VSM at room temperature.

In a magnetic material if the individual magnetic moments of the particles tend to orient randomly at room temperature, due to which the net magnetization becomes zero. At lower temperature, the flipping of the spins can be stopped which could result in finite magnetization. In certain cases, an applied magnetic field is required in addition to lowering of temperature for aligning the magnetic moments to give rise to a net magnetization. This phenomenon is known as superparamagnetism. This is typically observed for nanoscale magnetic materials. The phenomenon of superparamagnetism in the synthesized batches were studied using SQUID measurement by recording magnetization in the temperature range of 5 K and 300 K with and with the presence of an applied magnetic field (50 Oe), field cooled (FC) and zero field cooled (ZFC) conditions (Fig. 4.10).

The FC- ZFC curves were typically due to superparamagnetic MNPs of 2-8 nm size encapsulated in nanomaterials of MPCh-DS0.05. The curves diverged at 112 K, characterized as blocking temperature ( $T_B$ ), corresponded to the transition from ferromagnetic to superparamagnetic behavior. In the ZFC curve, without applied magnetic field, when the sample was cooled to 5 K the corresponding magnetization was very small

( $\sim 4.5$  emu/g). This may be attributed to the random orientation of the magnetic moments of individual particles. Now in the ZFC curve, as the temperature was increased, more particles reoriented their magnetic moment [21]. Due to this the magnetization increased till it reached a maximum value of 112 K (Fig. 4.10). Such a behavior was characteristic of superparamagnetism typically observed in small ferromagnetic or ferrimagnetic nanoparticles. Below  $T_B$ , the MPCh-DS0.05 nanoparticles exhibit ferromagnetic properties. When the temperature is above  $T_B$ , the thermal energy overcomes the anisotropy barrier and randomizes the magnetic moment, leading to the superparamagnetic behavior of the nanoparticles [21, 22]. On the other hand, the magnetization in the FC measurement recorded at 5 K temperature and 50 Oe magnetic field was 12.2 emu/g. Compared to ZFC measurement, the magnetization for FC measurement was higher due to the externally applied magnetic field which energetically favored the orientation of the individual magnetic moment and hence resulted in the observed magnetization along the direction of the applied field. Then the magnetization was nearly constant up to the temperature equivalent to  $T_B$ , at which its magnetization was similar to that recorded for ZFC measurement. At temperature higher than  $T_B$ , the magnetization in FC condition decreased as thermal energy was sufficient for overcoming the anisotropic barrier and led to randomization of the moments.

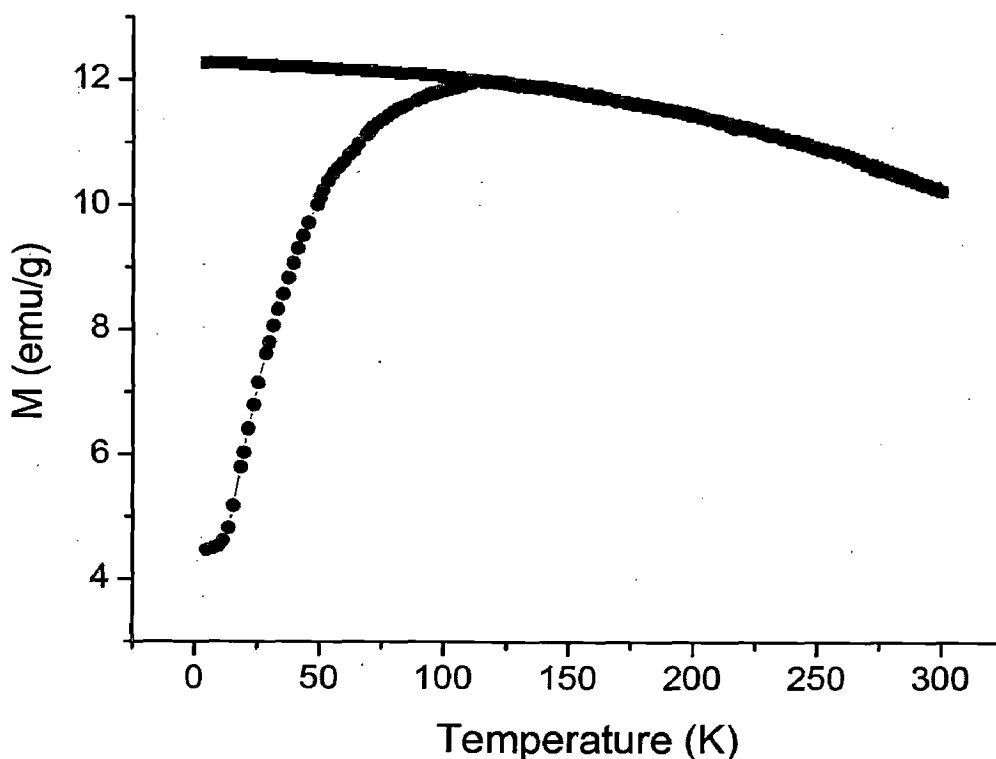


Fig. 4.10. ZFC and FC curve of MPCh-DS0.05 recorded at 50 Oe, measured by SQUID.

#### 4.3.9 *In vitro* release studies of MPCh-DS0.05 nanomaterial

As discussed in the chapter 3, DS a low molecular weight has a tendency to release from polysaccharide based matrices rapidly and can be referred to as burst release [12]. This is primarily due to high water contents in the polysaccharide based matrices which facilitates high drug solubility. However, sustained release property might be achieved by modifying the polysaccharide especially by cross-linking, so that the modified polysaccharide can hold back the drug in its network structure and assist in releasing the drug in a sustained manner. It may be remarked here that the trials of cross linking with  $\text{Ca}^{2+}$  in pectin-chitosan mixture was also carried out. But since no difference was observed with respect to the release of the DS from the system thus further trials were carried out without  $\text{Ca}^{2+}$  ions.

In the case of nanomaterials of MPCh-DS, the pectin was reinforced with chitosan by electrostatic interaction, which resulted in more than 99 % drug loading efficiency. The loading efficiency was much higher than that of magnetite-calcium pectinate nanomaterials where loading efficiency = 60.6 % and drug loading content was only 28.9 % (w/w), keeping pectin composition same) as discussed in the previous section. Here, the drug loading efficiency was calculated as the amount of drug loaded in the magnetite-pectin-chitosan nanomaterials with respect to the initial amount of drug taken for the loading. Notably, the concentration of the drug loaded in the MPCh-DS nanomaterial (~50% w/w) was also two folds higher than that of MP-DS (28.97% w/w). Therefore, to elucidate the potential applications of the nanomaterials of MPCh-DS for its ability for sustained release in colon specific site, an *in vitro* drug release study was carried out sequentially in simulated gastrointestinal fluid, e.g., in simulated gastric fluid (SGF) for 2 h, followed by simulated intestinal fluid (SIF) for 3 h and then in simulated colonic fluid (SCF) for 55 h to mimic the transportation to colon via gastrointestinal pathway. In addition, an *in vitro* release study of drug was also carried out in phosphate buffer at pH ~7.4 at 37°C for 48 h to mimic drug release in blood.

##### 4.3.9.1 *Sequential in vitro* release in gastrointestinal fluids

It was found that after 2 h interaction of MPCh-DS0.05 in SGF, negligible amount of DS (0.02 %) was released (showed in Fig. 4.11). This was similar to the poor release of DS from MPDS nanomaterials, as discussed in chapter 3. This was attributed to the poor solubility of DS in acidic medium as well as protonation of carboxyl groups of pectin and of amine group of chitosan as reported by George *et al.* [16] which causes slower

Ssahel  
13-07-2012

131  
13/7/12

release of DS. As the pH was increased, the concentration of negatively charged carboxylate groups in pectin was thought to be increased ( $pK_a$  of 2.9 - 4.1), which would however depend on the degree of esterification [23, 24]. However, 69 % of the loaded drug in MPCh-DS0.05 system was released during the 3 h of its interaction in simulated intestinal fluid. Notably, the pH in SIF was higher (pH 6.8) which might facilitate swelling of pectin-chitosan matrix and hence favored higher amount of drug release [12]. At this higher pH in SIF, it is persuasive that the electrostatic interaction between pectin and chitosan would become weaker and would result into formation of more porous material and hence increases the rate of drug release from the matrix. This could be explained on the basis  $pK_a$  value of chitosan, which is in the range of 6.3 and 7.0 [25]. It is reported that at pH 6.8, about 71.5 % of amino groups are not positively charged by an  $H^+$  ion [25]. Similarly, at pH 6.8, the swelling of pectin ( $pK_a = 2.9 - 4.1$ ) can be attributed to the increase in the concentrations of negatively charged carboxylate groups, which however would depend on the degree of esterification. This could lead to repulsion between pectin chains and thus result in swelling of pectin. Moreover, DS is a weak acid ( $pK_a = 4.0$ ), and is more soluble at neutral pH [26], thus at pH 6.8 it showed rapid release and soluble in intestinal fluid. The rate of drug release in SIF was slow in the beginning (Fig. 4.11), but increased after the first hour. Initially the rate of drug release was less which might be related to the slow rate of swelling of the pectin-chitosan structure. Besides, erosion of polymer (pectin) matrix due to the presence of pectinase enzyme in the SIF could also facilitate drug release. It may be surmised that both swelling effect and erosion effect were likely to be responsible for the rapid release of drug in the SIF. Because of the rapid drug release in intestine, the precise site specific drug delivery in the colon could be a challenge. After 3 h interaction with SIF, the MPCh-DS was treated with SCF, where the remaining drug (~ 30 %) was released over a span of 55 h. The rate of drug release was again slowed down in simulated colonic fluid (SCF) where the pH was at 5.5. Overall, a sustained release of drug was observed up to 60 h where significant release was observed in SIF (Fig 4.11).

Our results of the release of DS in SCF were similar to those reported for resveratrol loaded in microparticulates of pectin and chitosan cross linked with zinc ions [10]. This could be attributed to the sensitivity of the material to pectinase enzyme. Thus in SCF the release from the nanomaterials was due to potential degradation of the polymeric structure as well as due to the moderate solubility of DS at pH~5.5 which resulted into the drug release in a sustained manner. Our system also showed higher release of the drug DS in SIF

as compared to the release of resveratrol from zinc-pectinate-chitosan (0.5% w/v) microparticles where ~40% of the drug released in SIF after 5 h. In this reported work, 0.5 % w/v of chitosan was used as compared to only 0.025% chitosan in our method. The drug release pattern in zinc-pectinate-chitosan microparticles was though found to be more sustained which may be attributed to the higher concentration of the polymeric layer of the microparticles [27]. Overall, it was concluded that the system showed better sustained release than that reported for MP-DS in chapter 3.

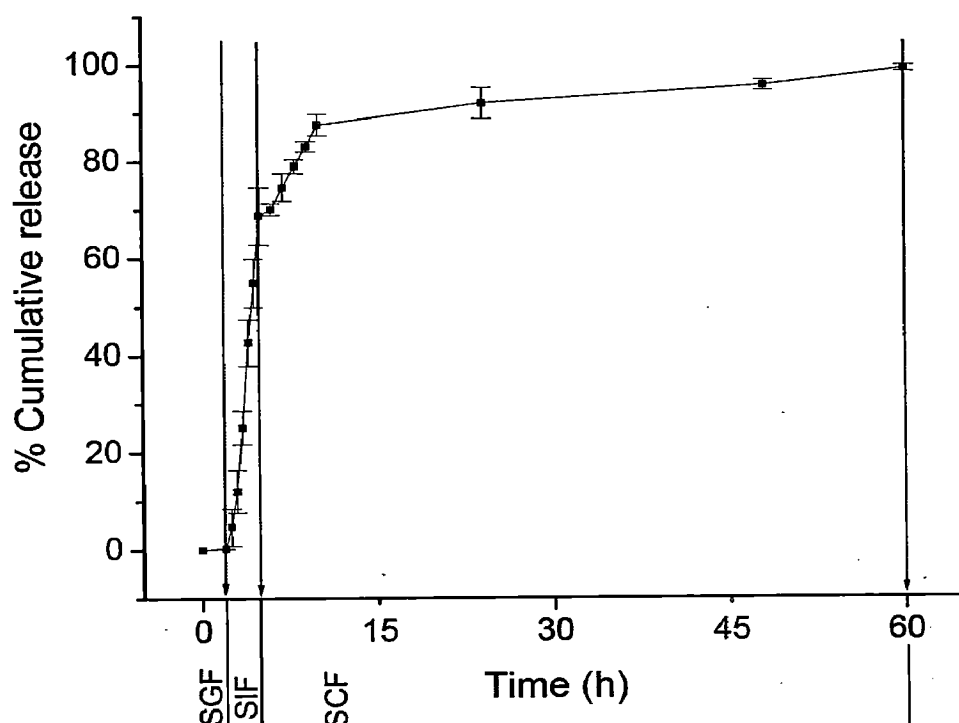


**Fig. 4.11.** Sequential *in vitro* release studies of DS from MPCh-DS0.05 in simulated gastric fluid (SGF pH 1.2) for 2 h, followed by simulated intestinal fluid (SIF pH 6.8) for 3 h and then in simulated colonic fluid (SCF pH 5.5) up to 60 h.

#### 4.3.9.2 *In vitro* release in phosphate buffer at pH 7.4

The *in vitro* release pattern of the drug DS in the phosphate buffer pH 7.4 was studied to mimic the drug release in blood, if the nanomaterials loaded with DS is injected intravenously. The *in vitro* release studies in phosphate buffer pH 7.4 reflected sustained release of DS where about 97% of release occurred within 12 hours (showed in Fig. 4.12). It may be noted that the release was more sustained at this pH as compared to that observed at pH~6.8. This was attributed to pH dependent swelling effect as discussed above. This sustained release from these magnetic nanomaterials could be due to a process which is

more complex than diffusion of the entrapped drug. Therefore to gain more insight into the mechanism of release of drug Korsmeyer- Peppas model was fitted.

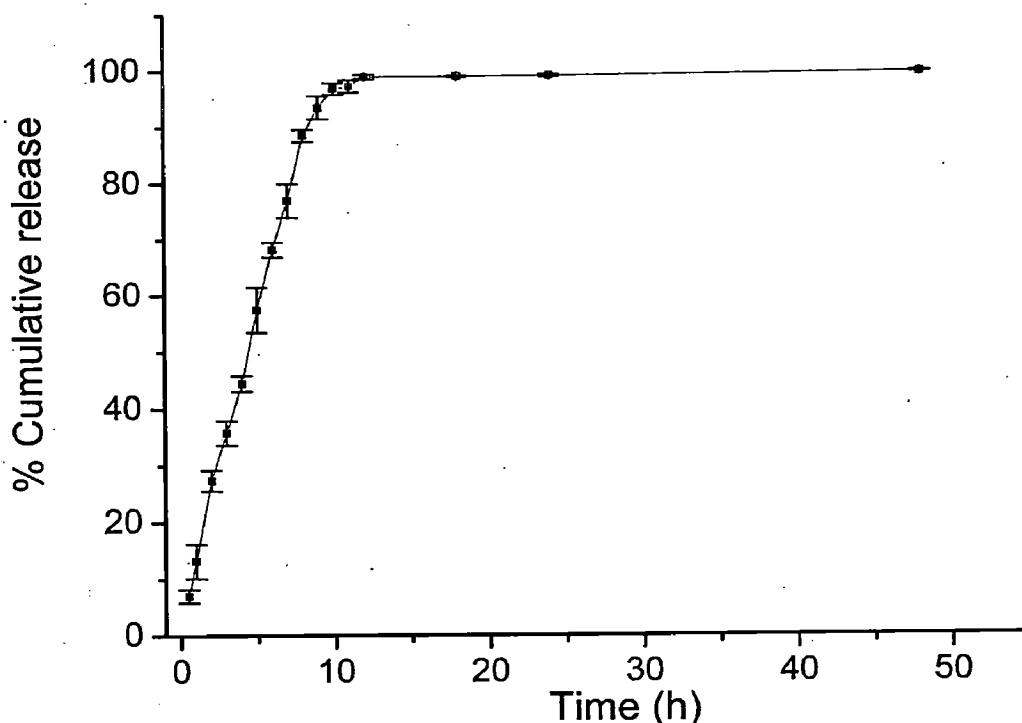
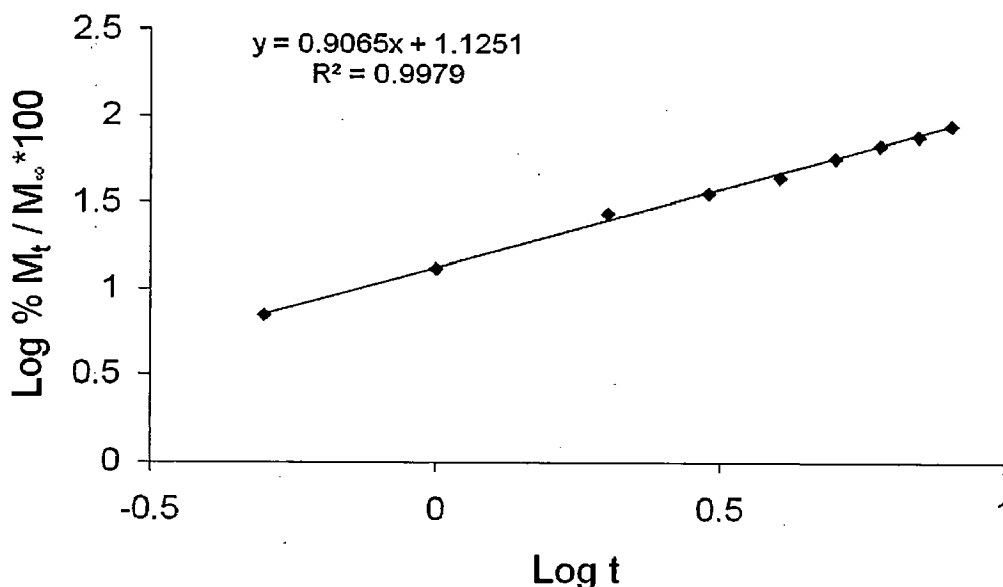


Fig. 4.12. In vitro release studies of DS from MPCh-DS0.05 in phosphate buffer at pH 7.4, for 48 h.

#### 4.3.9.3 Modeling of drug release

The release mechanism of DS from MPCh-DS0.05 nanomaterials was fitted using Korsmeyer - Peppas model as described in chapter 3 (Fig 4.13). The *in vitro* release data of DS from MPCh-DS0.05 in phosphate buffer pH 7.4 up to 8 h in log scale, exhibited a linear fit ( $R^2 = 0.997$ ). The  $n = 0.9065$  was observed which indicated non-Fickian transport, and was attributable to the swelling effect of the host material (pectin reinforced chitosan) in the aqueous medium [28, 29]. The value of  $k*100$  (where  $k$  is a constant related to the structural and geometric characteristic of the device) was found to be 13.33.



**Fig. 4.13.** Showing linear fit of *in vitro* release of DS up to 8 h from MPCh-DS0.05 in phosphate buffer solution (at pH 7.4), using Korsmeyer Peppas equation.

#### 4.4 CONCLUSION

A series of novel magnetite nanoparticles encapsulated in pectin reinforced with chitosan nanomaterials loaded with diclofenac sodium were fabricated. The formation of the batches of magnetic nanomaterials of MPCh-DS was evidenced by XRD, FTIR and was confirmed by TG analysis. The fabricated MPCh-DS nanomaterials were mostly uniform in size with a distribution in the range of 100-150 nm (in dried condition) as characterized by its SEM and TEM analysis. The superparamagnetic behavior was established by its FC-ZFC measurement at 50 Oe. The VSM measurement at room temperature and at  $\pm 10$  kOe showed its high saturation magnetization of 34.40 emu/g for MPCh-DS0.05. The *in vitro* release studies of DS from hybrid nanomaterial MPCh-DS system in gastrointestinal fluid was pH dependent. It exhibited poor release in gastric fluid, while about 70 % of the drug was released rapidly in simulated intestinal fluid, and ~30 % was released in simulated colonic fluid. The *in vitro* release study carried out at pH 7.4 (mimicking blood pH) exhibited sustained release which satisfied non-Fickian release based on Korsmeyer-Peppas model and corresponded to swelling controlled mechanism. This was attributed to swelling effect of pectin in aqueous medium, also supported by the dynamic light scattering (DLS) measurement which exhibited particle size ranging between 230 – 520 nm.

The sustained drug release at pH 7.4 corresponding to blood pH was encouraging for targeted drug delivery, especially via intravenous administration followed by magnetic guiding to inflammatory site where otherwise the direct drug administration is cumbersome,

e.g., knee joints, for its sustained release. This would also minimize the distribution of the drug to other undesirable parts of the body. However this proposal will be further augmented after in vivo studies of this formulation.



## REFERENCES

1. Ilium, L. Chitosan and its use as a pharmaceutical excipient. *Pharm. Res.* **1998**, *15*, 326–1331.
2. Bhise, K. S.; Dhumal, R. S.; Chauhan, B.; Paradkar, A.; Kadam, S. S. Effect of oppositely charged polymer and dissolution medium on swelling, erosion, and drug release from chitosan matrices. *AAPS Pharm. Sci. Tech.* **2007**, *8*, E1–E9.
3. Risbud, M. V.; Hardikar, A. A.; Bhat, S. V.; Bhonde, R. R. pH sensitive freeze-dried chitosan-polyvinyl pyrrolidone hydrogels as controlled release system for antibiotic delivery. *J. Control. Release*, **2000**, *68*, 23–30.
4. Chen, W. B.; Wang, L. F.; Chen, J. S.; Fan, S. Y. Characterization of polyelectrolyte complexes between chondroitin sulfate and chitosan in the solid state. *J. Biomed. Mater. Res.* **2005**, *75*, 128–137.
5. Dumitriu, S.; Chornet, E. *Polyionic hydrogels as supports for enzyme immobilization*. Muzzarelli, R. A. A., Ed. *Chitin enzymology: Italy*, **1996**; pp. 527–542.
6. Cooper S.L.Kataoka K.; Vert, M. *Polyelectrolyte complex composed of chitosan and sodium alginate for wound dressing application*. *Journal of Biomaterial Science. Polymer Edition*, Browse Brill's publications France, **1999**,
7. Wang, H. F.; Li, W. J.; Lu, Y. H. & Wang, Z. L. Studies on chitosan and poly(acrylic acid) interpolymer complex I. Preparation, structure, pH sensitive and salt sensitivity of complex forming poly (acrylic acid): Chitosan semi interpenetrating polymer network. *J. Appl. Polym. Sci.* **1997**, *65*, 1445–1450.
8. Yao, K. D.; Tu, H.; Cheng, F.; Zhang, J. W.; Liu, J. pH sensitive of the swelling of chitosan-pectin polyelectrolyte complex. *Die Angewandte Makromolekulare Chemie.* **1997**, *245*, 63–72.
9. Boonsongrit, Y.; Mitrevej, A.; Mueller, B. W. Chitosan drug binding by ionic interaction. *Eur. J. Pharm. Biopharm.* **2006**, *62*, 267–274.
10. Das, S.; Chaudhury A.; Ng, K. Y. Preparation and evaluation of zinc-pectin-chitosan composite particles for drug delivery to the colon: Role of chitosan in modifying in vitro and in vivo drug release. *Int. J. Pharm.* **2011**, *406*, 11-20.

11. Arias, J. L.; Gallardo, V.; Ruiz, M. A.; Delgado, A. V.; Magnetite/poly (alkylcyanoacrylate) (core/shell) nanoparticles as 5-Fluorouracil delivery systems for active targeting. *Eur. J. Pharm. Biopharm.* **2008**, *69*, 54-63.
12. Yu, C.Y.; Cao, H.; Zhang, X.C.; Zhou, F.Z.; Cheng, S.X.; Zhang, X.Z.; Zhuo, R.X. Hybrid nanospheres and vesicles based on pectin as drug carriers. *Langmuir*, **2009**, *25*, 11720-11726.
13. Sliverstein, R. M., Webster F.X. *Spectrometric identification of organic compounds*; John Wiley and Sons: Asia, **2002**.
14. Bigucci, F.; Luppi, B.; Cerchiara, T.; Sorrenti, M.; Bettinetti, G.; Rodriguez, L.; Zecchi, V. Chitosan/pectin polyelectrolyte complexes: selection of suitable preparative conditions for colon-specific delivery of vancomycin. *Eur. J. Pharm. Sci.* **2008**, *35*, 435-441.
15. Munjeri, O.; Collett, J.H.; Fell, J.T. Hydrogel beads based on amidated pectins for colonspecific drug delivery: The role of chitosan in modifying drug release. *J. Control. Release.* **1997**, *46*, 273-278.
16. George, M.; Abraham, T.E. Polyionic hydrocolloids for the intestinal delivery of protein drugs: Alginate and chitosan -- a review. *J. Control. Release.* **2006**, *114*, 1-14.
17. Cesaro, A.; Delben, F.; Paoletti, S. Thermodynamics of the proton dissociation of natural polyuronic acids. *Int. J. Biol. Macromol.* **1990**, *12*, 170-176.
18. Daou, T. J.; Pourroy, G.; Bégin, C. S.; Grenèche, J. M.; Ulhaq, B. C.; Legaré, P.; Bernhardt, P.; Leuvrey, C.; Rogez, G. Hydrothermal Synthesis of Monodisperse Magnetite Nanoparticles. *Chem. Mater.* **2006**, *18*, 4399- 4404.
19. Shafi, K. V. P. M.; Ulman, A.; Dyal, A.; Yan, X.; Yang, N. L.; Estournes, C.; Fournes, L.; Wattiaux, A.; White, H.; Rafailovich, M. Magnetic Enhancement of  $\gamma$ -Fe<sub>2</sub>O<sub>3</sub> Nanoparticles by Sonochemical Coating. *Chem. Mater.* **2002**, *14*, 1778-1787.
20. Morales, M. P.; Verdaguier, S. V.; Montero, M. I.; Sterna, C. J.; Roing, A.; Casas, L.; Martinez, B.; Sandiumenge, F. Surface and Internal Spin Canting in  $\gamma$ -Fe<sub>2</sub>O<sub>3</sub> Nanoparticles. *Chem. Mater.* **1999**, *11*, 3058-3064.
21. Si, S.; Kotal, A.; Mandal, T.K.; Giri, S.; Nakamura, H.; Kohara, T. Size-Controlled Synthesis of Magnetite Nanoparticles in the Presence of Polyelectrolytes *Chem. Mater.* **2004**, *16*, 3489-3496.

22. Hou, Y. L.; Yu, J. F.; Gao, S. J. Solvothermal reduction synthesis and characterization of superparamagnetic magnetite nanoparticles. *J. Mater. Chem.* **2003**, *13*, 1983-1987.
23. Ofori-Kwakye, K.; Fell, J. T. Biphasic drug release: the permeability of films containing pectin, chitosan and HPMC. *Int. J. Pharm.* **2001**, *28*, 139–145.
24. Ralet, M. C.; Dronnet, V.; Buchholt, H. C.; Thibault, J. F. Enzymatically and chemically de-esterified lime pectins: characterization, polyelectrolyte behavior and calcium binding properties. *Carbohydr. Res.* **2001**, *336*, 117–125.
25. Beppu, M. M.; Santana, C.C. PAA influence on chitosan membrane calcification. *Mater Sci Eng C.* **2003**, *23*, 651-658.
26. Llinas, A.; Burley, J.C.; Box, K.J.; Glen, R.C.; Goodman, J. M. Diclofenac solubility: independent determination of the intrinsic solubility of three crystal forms. *J. Med. Chem.* **2007**, *50*, 979-983.
27. Das, S.; Lin, H. S.; Ho, P. C.; Ng, K. Y. The impact of aqueous solubility and dose on the pharmacokinetic profiles of resveratrol. *Pharm. Res.* **2006**, *25*, 2593-2600.
28. Korsmeyer, R. W.; Gurny, R.; Doelker, E.; Buri, P.; Peppas, N. A. Mechanisms of solute release from porous hydrophilic polymers. *Int. J. Pharm.* **1983**, *15*, 25-35.
29. Wang, Q.; Zhang, J.; Wang, A. Preparation and characterization of a novel pH-sensitive chitosan-g-poly (acrylic acid)/attapulgit/sodium alginate composite hydrogel bead for controlled release of diclofenac sodium. *Carbohydr. Polym.* **2009**, *78*, 731–737.

***CHAPTER - 5***

***5-FLUOROURACIL LOADED IN  
NANOMATERIALS OF  
MAGNETITE – PECTIN***

## 5.1 INTRODUCTION

Compared to conventional chemotherapeutic methods, there has been an increasing demand of targeted delivery of anticancer drug with sustained/ controlled drug release property. This would restrict the distribution of anticancer drugs to undesirable location in the body and will minimize severe side effects of these drugs, as they exhibit cytotoxicity even to normal cells [1]. Here, it was envisaged that nanoscale drug delivery system could improve the therapeutic action due to their ease in transportation through finer capillaries and potentially overcome various biological barriers to reach any desired location for delivering the drug. Notably drug carriers of sizes of a few hundred nanometers have been reported to be capable of penetrating tumors due to enhanced penetration rate (EPR effect) of small particles [2]. As a result, nanoscale materials can be useful for site-specific anticancer therapeutic agent [2, 3].

It was noted from literature that the biopolymers like chitosan, pectin, alginate *etc.* were used for fabricating drug carrier of micro and nanospheres for loading and release of anticancer drugs e.g. 5-Fluorouracil (5-FU) [4-8]. The use of polysaccharide is advantageous due to biocompatibility, non-toxicity and adjustable controlled release properties as discussed earlier. In this regard nanospheres of pectin were reported to be an excellent nanoscale matrix for fabricating 5-FU loaded drug delivery system of [9]. The 5-FU has been extensively used in clinical chemotherapy for the treatment of metastatic carcinomas of breast, gastrointestinal tract, pancreas, liver, head, neck, and ovary [10-12].

However, this drug is rapidly absorbed as well as metabolized in the body with biological half-life ( $t_{1/2}$ ) = 10-20 min [13, 14]. Therefore in order to maintain a suitable concentration of the drug in serum for improved therapeutic activity, the drug is needed to be continuously administered by intravenous injection or infusion [14]. But above the minimum effective concentration in plasma it exhibits severe toxicity to normal tissue [1]. Therefore, there is a recognized need of a targeted drug delivery system (DDS) of nanoscale dimension with sustained and controlled release of 5-FU.

### 5.1.1. Objective of the study

It was noted that nanoscale targeted drug delivery system comprising of core/ shell type magnetite/ poly (alkylcyanoacrylate) loaded with 5-FU was successfully fabricated for active targeting [15]. However, the preparation suffered from some limitations, namely use of organic solvents. This would require removal of organic solvents as it reduces the

bioactivity of drug. Moreover, even a low-level exposure to residual organic solvents may lead to lasting toxic effects. It occurred to us that there is a need to develop a novel targeted drug delivery system in aqueous medium. In this regard we aimed at fabricating 5-FU loaded in nanomaterials of MNP encapsulated in pectin in aqueous medium as a magnetic responsive nanoscale drug carrier for potential cancer therapy. Importantly, this method did not involve any organic solvent and surfactant. This system is expected to improve the therapeutic index of like 5-FU (hydrophilic drug) which are reported to redistribute rapidly after their release from carrier. Subsequently, it enters the circulation and results in incrementally improved pharmacokinetics. Moreover, highly stable formulations are required to take full advantage of the EPR effect in treating solid tumors [2].

The present study reports about synthesis, characterization and *in vitro* release of 5-fluorouracil (5-FU) from hybrid nanomaterials comprising magnetite and pectin. These nanomaterials were characterized by XRD, SEM-EDAX, TEM, DLS, FT-IR, zeta potential, SQUID and VSM. The *in vitro* release of these nanomaterials was studied in simulated gastrointestinal fluid and in phosphate buffer solution.

## 5.2 MATERIALS AND METHODS

### 5.2.1 Materials

In addition to the materials needed for fabricating magnetite nanoparticles coated with pectin as discussed in Chapter 2, 5-Fluorouracil (5-FU) was procured from Sisco Research Laboratories Pvt. Ltd., India. Simulated gastric fluid (SGF), simulated intestinal fluid (SIF), simulated colonic fluid (SCF) and phosphate buffer solution were prepared as discussed in chapter 3.

The cytotoxicity study of 5-Fluorouracil (5-FU) loaded in the hybrid nanomaterials of magnetite and pectin was performed at ACTREC, Mumbai, a recognized laboratory for *in vitro* studies in cancer cell lines. The chemical and other materials needed for the study were provided by ACTREC.

#### 5.2.1.1 5-fluorouracil

##### *Physical and chemical properties*

The chemical structure of 5-Fluorouracil is given in Fig. 5.1. Its molecular weight is 130.08 g/mol. It is an odorless white / off-white colored powder which is crystalline in

nature. It is soluble in water but only partially soluble in cold water and methanol and is insoluble in diethyl ether.

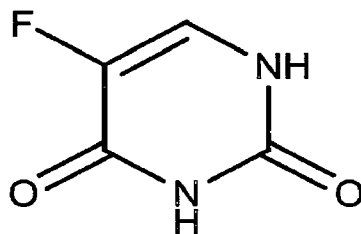


Fig. 5.1 Structure of 5-fluorouracil.

### Pharmacology

5-FU belongs to the family of drugs called antimetabolites, which are very similar to normal substances within the cell. When the cells incorporate these substances into the cellular metabolism, they are unable to divide. These antimetabolites are specific to any particular cell-cycle. They attack cells at very specific phases in the cycle like 5-FU is an S-phase specific drug and only active during particular cycles of the cell. Thus 5-FU is effective in rapidly dividing cells which extensively utilizes nucleotide synthesis machinery, such as cancer cells [16]. It has a broad spectrum of activity against various solid tumors including that of the gastrointestinal like rectum, colon, oesophageous, pancreas and stomach [16, 17]. Further it is also used for the treatment of cancers of liver (hepatoma cancer), basal cell cancer of the skin and actinic keratoses, head, and neck [16, 17]. Sometimes it is also used in the treatment of inflammatory breast cancer which is especially an aggressive form of breast cancer.

### Method of administration

5-Fluorouracil is poorly absorbed after oral administration, with erratic bioavailability [18]. Therefore, it is administered as an injection into the vein (intravenous or *i.v.*), or as an infusion (bolus or continuous infusion) which may be given over several hours to several weeks depending upon the protocol of the treatment. After the parenteral administration it is rapidly distributed as well as eliminated with an apparent terminal half-life of approximately 10 to 20 minutes [14]. The rapid elimination is primarily due to swift catabolism of the liver.

Based on the route of administration a variety of formulations are available for this drug in the national as well as international market. The name of the drug under separate categories is given below along with the name of the company that markets/ manufactures the particular dosage form of the drug:

- a) Topical ointment or cream or solution which is applied as a thin coating to the affected skin lesions twice a day, which may continue over several weeks. Topical solutions and cream of 5-FU often referred to by its trade names *Efudex*, *Carac* or *Fluoroplex*, *Adrucil*, *Cara*, *Efudex*, *Fluoroplex*, *Flonida* (Shalak Pharma India).
- b) It is available in form of injectables under the trade names of 5-Flucel {Celon (Vivilon)}, 5-FU-Korea {SG Pharma}, 5FU-CBC {Chandra Bhagat Pharma}, Flutas {Intas Pharmaceuticals}, Fivoflu {Dabur Pharmaceuticals}, Fivocil {Alkem Laboratories (Cytomed Division)}, Fludin inj. {Biological E.} with the strength of 250mg and 500mg.

### *Mechanism of action*

As it is a pyrimidine antagonist, the possible mechanism for cytotoxicity of 5-FU, could be attributable to its antimetabolite effect. Further it is a pyrimidine analogue due to its similar chemical structure with that of the uracil. Thus it inhibits RNA replication enzymes during the nucleic acid replication process which stops the growth of cancerous cells. Further the 5-FU interferes with thymidylate synthesis by acting as a thymidylate synthase inhibitor. The enzyme thymidylate synthase plays a role in the synthesis of thymidylate which is important for cell growth. This enzyme methylates deoxyuridine monophosphate (dUMP) into thymidine monophosphate (dTMP). Therefore the 5-FU by inhibition of thymidylate synthase, leads to shortage of dTMP which in turn inhibits the production of thymine. Without thymine the rapidly dividing cancerous cells undergo cell death [19].

### *Side effects*

The 5-FU is most effective in killing cells that divide rapidly. However, it is not able to differentiate between the cancerous cells and the normal cells. Therefore various normal cells like the blood cells, cells in mouth, stomach, bowel, and the hair follicles are affected. This results in low blood counts, mouth sores and ulcers, nausea, diarrhoea, and/or hair loss. The low blood counts especially the count of white, red blood cells and platelets decreases temporarily. This in turn reduces resistance to infection (neutropenia), anemia and/or bleeding. The anaemia also leads to tiredness and weakness. Other reported side effects are myelosuppression, mucositis, and dermatitis [17, 20].



The 5-FU can also cause a rash, which may be itchy. Due to 5-FU the nails may become brittle, chipped and ridged. It also leads to watery eyes (due to increased production of tears), gritty eyes and blurred vision but increases sensitivity to light (photophobia). Even the change in taste is also observed; particularly metallic taste in mouth is felt during infusion. It also shows the discoloration along the vein through which is administered. The darkening of the skin due to excess production of pigments is also observed.

When 5-FU is given continuously for a long time soreness and redness of palms of the hands and soles of the feet is observed. This is referred to as palmar plantar, or hand and foot syndrome. This syndrome is temporary and improves when the treatment finishes. In some cases chest pain, changes in ECG (electrocardiograph) and increase in cardiac enzymes is observed which indicates problems with the heart [21]. These symptoms are observed rarely but increased for patients with a prior history of heart disease.

Thus overall it may be concluded that 5-FU is an effective drug for the treatment of a variety of cancerous tumors but it also shows non-selective action against healthy cells. Further it has short biological half-life of ( $t_{1/2}$ ) 10–20 min in the body due to rapid metabolism by dihydropyrimidine dehydrogenase. The drug also shows incomplete and non-uniform oral absorption due to high variability in enzymatic degradation [18]. Further, only less than 20% of an injected dose undergoes enzymatic activation. Therefore there is necessity to prolong the circulation time of 5-FU and increase its efficacy. This may be achieved by suitable drug delivery system (DDS) with sustained release and/ or targeted delivery of 5-FU.

### ***5.2.2 Method for fabrication of nanomaterials of magnetite-pectin cross linked with $Ca^{2+}$ ions loaded with 5-FU***

Three protocols were developed for synthesizing nanomaterials of magnetite-pectin-5FU.

#### ***5.2.2.1 Protocol I***

5-FU was mixed with 25 mL of 0.4 % and 1.0 % w/v pectin solution and stirred continuously at 55 °C for 24 h. The temperature of 55 °C was needed to achieve higher solubility of 5-FU [9]. To these batches 25 mL of freshly prepared MNP dispersion at pH ~ 4 was added and stirred for 1 h.  $CaCl_2$  solution was slowly added to the above dispersion to facilitate cross linking pectin with  $Ca^{2+}$  to form a complex network structure of calcium pectinate. The whole mixture was stirred for 6 h at 55 °C and then cooled rapidly to 10 °C in

cold water circulating bath. Notably the MNP dispersion was synthesized by co-precipitation method as discussed in chapter 2. Three different concentrations of 5-FU, e.g. 0.1 M, 0.05 M and 0.025 M were used in this study for fabricating magnetite-pectin-5FU nanomaterials.

#### 5.2.2.2 Protocol II

The objective of developing this alternate protocol for fabricating magnetite-pectin-5FU nanomaterials was to reduce the processing time of fabrication. One of the key parameters in the fabrication step was proper mixing of pectin and 5-FU, which required 24 h of magnetic stirring at 55 °C as discussed in protocol 1. Here the mixing was performed by probe sonication (Sonics vibra cell VCX-750, 20 kHz) with the probe temperature of 55 °C. The probe sonication method was optimized by varying the time of sonication i.e. 30 min, 60 min and 90 min and the drug loading efficiency was assayed for different initial drug concentration i.e. 0.025 M, 0.05 M and 0.1 M. After probe sonication the mix of 5-FU and pectin were added to the dispersion of MNPs maintained at pH ~ 4. This was followed by slow addition of 0.8 % solution of CaCl<sub>2</sub> to the mixture and stirred continuously at 55°C by magnetic stirrer for 6 h for cross linking with pectin to form magnetite-pectin-5FU nanomaterial. This mixture was then cooled rapidly to 10 °C in cold water circulating bath.

#### 5.2.2.3 Protocol III

Here probe sonication was replaced with ultrasonication. The other parameters were same as described above. However, here the sonication was carried out at ambient condition for 1 h at 55 °C. After ultra-sonication the mix of 5-FU and pectin were added to the dispersion of MNPs maintained at pH ~ 4. This was followed by slow addition of 0.8 % solution of CaCl<sub>2</sub> to the mixture and stirred continuously by magnetic stirrer for 6 h at 55 °C for cross linking with pectin to form magnetite-pectin-5FU nanomaterial. This mixture was then cooled rapidly to 10 °C in cold water circulating bath.

The conditions for fabrication with their corresponding % drug encapsulation efficiencies and drug loading content (wt %) in magnetite-pectin-5FU are as given in Table 5.1 (protocol I), Table 5.2a and 5.2b (protocol II) and Table 5.3 (protocol III) respectively. It may be noted here that magnetite-pectin-5FU prepared by protocol II with 0.4 % pectin, 0.8 % CaCl<sub>2</sub> and 0.025 M 5-FU with 1 h sonication time will now be referred to as MP-5FU.

In addition to the above nanomaterials, 5-FU loaded in magnetite encapsulated in pectin reinforced with chitosan was fabricated but it showed poor drug encapsulation efficiency (i.e. ~4 %). Due to this further studies of MPCh-5FU were not performed.

**Table 5.1.** Parameters for fabrication of magnetite-pectin-5FU nanomaterials with fixed concentration of MNPs (Protocol I)

| Concentration of 5-FU | Pectin (% w/v) | CaCl <sub>2</sub> (% w/v) | % Encapsulation efficiency | Drug loading content (wt %) |
|-----------------------|----------------|---------------------------|----------------------------|-----------------------------|
| 0.1 M                 | 1.0 %          | 2.0 %                     | 17.30 ± 2.2                | 12.5 ± 1.9                  |
| 0.05 M                | 1.0 %          | 2.0%                      | 18.36 ± 2.5                | 11.1 ± 1.8                  |
| 0.05 M                | 0.4 %          | 0.8 %                     | 17.28 ± 1.6                | 10.0 ± 1.6                  |
| 0.025 M               | 0.4 %          | 0.8 %                     | 16.90 ± 1.3                | 9.8 ± 1.5                   |

**Table 5.2a** Optimization of the probe sonication time for fabrication of magnetite-pectin-5FU with 0.1 M 5-FU using different probe sonication time (Protocol II)

| Sonication Time | Pectin (% w/v) | CaCl <sub>2</sub> (% w/v) | Encapsulation efficiency (%) | Drug loading content (wt %) |
|-----------------|----------------|---------------------------|------------------------------|-----------------------------|
| 30 min          | 0.4 %          | 0.8 %                     | 11.08 ± 1.6                  | 4.0 ± 0.9                   |
| 60 min          | 0.4 %          | 0.8 %                     | 33.23 ± 2.5                  | 18.15 ± 1.1                 |
| 90 min          | 0.4 %          | 0.8 %                     | 34.20 ± 3.3                  | 19.5 ± 2.2                  |

**Table 5.2b** Parameters for fabricating magnetite-pectin-5FU with different concentrations of 5-FU and fixed probe sonication time of 60 min (Protocol II)

| Concentration of 5-FU | Pectin (% w/v) | CaCl <sub>2</sub> (% w/v) | Encapsulation efficiency (%) | Drug loading content (wt %) |
|-----------------------|----------------|---------------------------|------------------------------|-----------------------------|
| 0.1 M                 | 0.4 %          | 0.8 %                     | 33.23 ± 2.5                  | 17.51 ± 1.1                 |
| 0.05 M                | 0.4 %          | 0.8 %                     | 31.10 ± 1.3                  | 17.20 ± 1.8                 |
| 0.025 M               | 0.4 %          | 0.8 %                     | 29.80 ± 2.1                  | 16.97 ± 1.9                 |

**Table 5.3** Parameters for fabricating magnetite-pectin-5FU with fixed concentration of MNPs and fixed ultra sonication time of 1 h (Protocol III)

| Concentration of 5-FU | Pectin (% w/v) | CaCl <sub>2</sub> (% w/v) | Encapsulation efficiency (%) | Drug loading content (wt%) |
|-----------------------|----------------|---------------------------|------------------------------|----------------------------|
| 0.05M                 | 0.4%           | 0.8%                      | 13.50± 2.9                   | 7.1 ± 2.1                  |
| 0.025M                | 0.4%           | 0.8%                      | 11.20±1.8                    | 6.5 ± 2.6                  |

### 5.2.3 Methodology for drug loading analysis

As mentioned in the drug loading protocols, the mixture obtained after rapidly cooling to 10 °C comprised free dissolved drug and drug loaded in nanomaterials. The drug loaded in the nanomaterials would therefore be difference of total drug taken for fabrication and amount of the free dissolved drug in the dispersion i.e.

Amount of loaded drug = Initial amount of the drug taken – amount of free dissolved drug.

The concentration of free dissolved drug in the dispersion was determined by the bulk equilibrium reverse dialysis at 10 °C, as discussed in chapter 3. The concentration of the drug from the dialysis bag was measured by UV visible spectrophotometry at  $\lambda_{\text{max}} = 266$  nm. The detail of drug analysis is discussed in section 5.2.6.

The drug loading content (wt %) in magnetite-pectin-5FU nanomaterial was calculated as:

$$\text{Drug loading content (wt \%)} = (a/b) * 100$$

a = amount of the drug loaded in magnetite-pectin nanomaterials loaded with 5FU.

b = weight of fabricated magnetite-pectin nanomaterials loaded with 5FU.

Drug incorporation into magnetite-pectin nanomaterial was expressed in terms of % encapsulation efficiency of 5-FU, which is given as:

$$\% \text{ Encapsulation efficiency} = (a / t) * 100$$

a = amount of the drug loaded in magnetite-pectin nanomaterials loaded with 5-FU.

t = Initial amount of the drug taken.

It may be noted here that, the magnetite pectin nanomaterials cross linked with calcium which were fabricated using fixed concentration of the dispersion of MNPs, 0.4 % pectin and 0.8 % CaCl<sub>2</sub> as discussed in chapter 2, without 5-FU will now be referred to as MP (magnetite nanoparticles: pectin cross linked with Ca<sup>2+</sup>).

#### 5.2.4 Characterization

The fabricated MP-5FU nanomaterials were characterized for their structure, morphology and magnetic properties of MP-5FU by XRD, FT-IR, DLS, SEM-EDAX, TEM, SQUID, and VSM; the details of the methods used are discussed in chapters 2 and 3.

#### 5.2.5 *In vitro* drug release and analysis

*In vitro* release studies the MP-5FU nanomaterials fabricated by probe sonication (protocol –II) for 60 min using 0.025 M 5-FU by protocol II, were performed by dialysis bag diffusion technique in simulated gastrointestinal fluid and in phosphate buffer solution at pH 7.4. This was referred to as donor compartment. For gastrointestinal release studies, the MP-5FU was treated sequentially in SGF for 2 h followed by 3 h in SIF and 43 h in SCF.

The drug analysis was performed by measuring absorbance of 5-FU in Millipore water, SGF, SIF (without pancreatin), SCF and phosphate buffer solution (pH 7.4). The  $\lambda_{\text{max}}$  of 5-FU dissolved in Millipore water was measured at 266 nm.

Similar to that discussed in chapter 3 about 1.5 mL of an aliquot was withdrawn from the receptor compartment of the respective fluid at each specified time intervals and was replaced with equal volume of fresh medium to mimic the sink conditions of the human body. The aliquot was centrifuged at 15000 rpm for 15 minutes and the supernatant liquid consisting of released drug was estimated with Shimadzu 1600 UV visible spectrophotometer against appropriate blank.

### 5.2.6 Drug analysis

The concentration of the drug was measured by UV-visible absorption spectra in different media, namely, in Millipore water, SGF, SIF (without pancreatin), SCF and phosphate buffer solution.

Stock solution of 100  $\mu\text{g}/\text{mL}$  of 5-FU in Millipore water, SGF, SIF (without pancreatin), SCF and phosphate buffer solution were prepared by transferring 10 mg of accurately weighed 5-Fluorouracil to 100 mL volumetric flasks (sufficient quantity of Millipore water/ SGF without pepsin / SIF without pancreatin/ SCF without pectinase was added to dissolve it). The volume was made up to 100 mL with the respective medium. From this stock solution, 1 mL aliquot was taken and diluted to 10 mL. This solution was scanned between 230 to 350 nm on a Shimadzu 1600 double beam UV-Visible spectrometer. The UV spectra showed  $\lambda_{\text{max}}$  at 266 nm in all four media and agreed well with the reported values [7]. All measurements were thus carried out at  $\lambda_{\text{max}} = 266$  nm in triplicate, for estimation of the concentration of 5-fluorouracil in these media.

#### 5.2.6.1 Calibration curve for estimation of 5-fluorouracil in Millipore water

The calibration curve was prepared by recording absorbance at  $\lambda_{\text{max}} = 266$  nm. The mean value and the standard deviations from triplicate analysis were calculated. The calibration curve was obtained by plotting mean values of the absorbance against the respective concentration of 5-FU ranging between 5 and 25  $\mu\text{g}/\text{mL}$  (Fig. 5.2). The experimental data were fitted linearly ( $R^2 = 0.998$ ), from which the concentration of the drug was calculated.

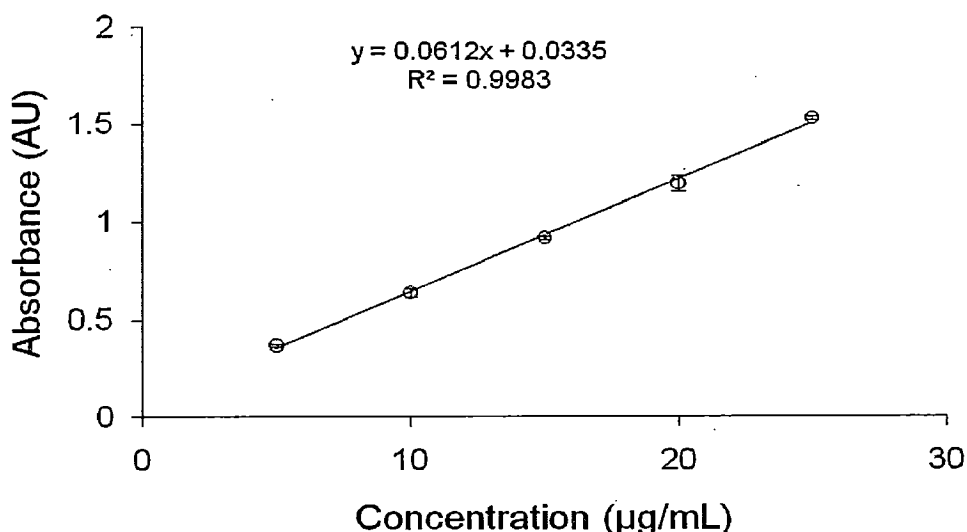


**Fig. 5.2.** Calibration curve for estimation of 5-fluorouracil in Millipore water at  $\lambda_{\text{max}} = 266$  nm. (Results are given as mean  $\pm$  standard deviation, calculated from triplicate analysis)

#### 5.2.6.2 Calibration curve for estimation of 5-fluorouracil in simulated gastric fluid (SGF)

The aliquots from the stock solution of 100  $\mu\text{g/mL}$  were taken and dilutions made with SGF (without pepsin) to prepare sample for calibration in the concentration range of 5 to 25  $\mu\text{g/mL}$ . The absorbance of dilutions was measured in triplicate by UV-Visible spectrometry at  $\lambda_{\text{max}} = 266$  nm against SGF as blank and the calibration curve was plotted (Fig. 5.3). Linear fit of the calibration curve was obtained ( $R^2 = 0.999$ ). Analysis of *in vitro* drug release in SGF medium was performed in this concentration range accordingly.

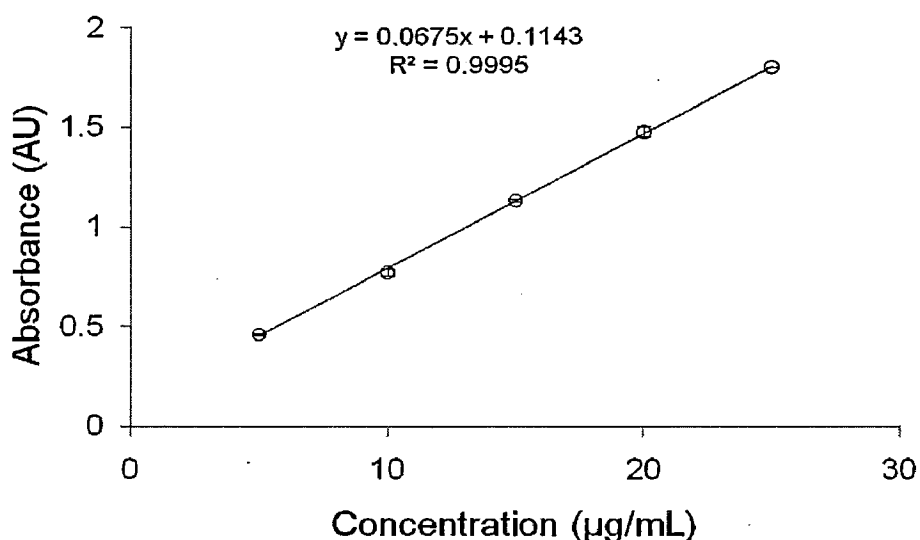


**Fig. 5.3.** Calibration curve for estimation of 5-fluorouracil in SGF without pepsin at  $\lambda_{\text{max}} = 266$  nm (Results are given as mean  $\pm$  standard deviation, calculated from triplicate analysis).

### 5.2.6.3 Calibration curve for estimation of 5-fluorouracil in simulated intestinal fluid (SIF) at 266 nm

The aliquots from the stock solution of 100  $\mu\text{g/mL}$  were taken and dilutions were made with SIF (without pancreatin) to prepare sample for calibration in concentration range of 5 to 25  $\mu\text{g/mL}$ . The absorbance of dilutions was measured in triplicate by UV-Visible spectrometry at  $\lambda_{\text{max}} = 266$  nm against SIF (without pancreatin) as blank and the calibration curve was plotted (Fig. 5.4). A linear fit of the calibration curve was obtained ( $R^2 = 0.999$ ).

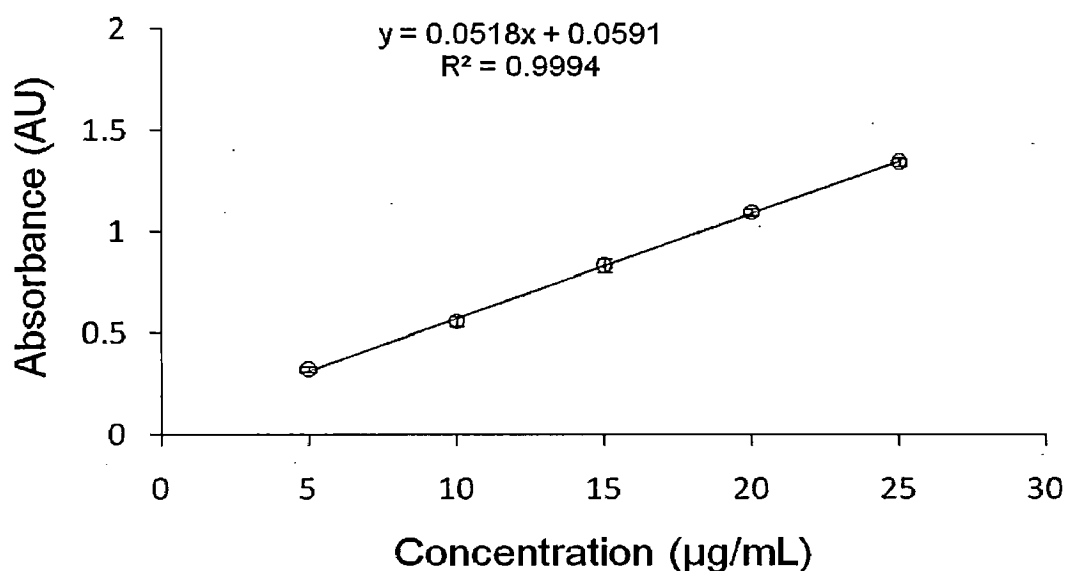


**Fig. 5.4.** Calibration curve for estimation of 5-fluorouracil in SIF without pancreatin at  $\lambda_{\text{max}} = 266$  nm (Results are given as mean  $\pm$  standard deviation, calculated from triplicate analysis).

### 5.2.6.4 Calibration curve for estimation of 5-fluorouracil in simulated colonic fluid (SCF)

The aliquots from the stock solution of 100  $\mu\text{g/mL}$  were taken and dilutions were made with SCF (without pectinase) to prepare sample for calibration in the concentration range of 2.5 to 25  $\mu\text{g/mL}$ . The absorbance of dilutions was measured by UV-Visible spectrometer at  $\lambda_{\text{max}} = 266$  nm against SCF without pectinase as blank and the calibration curve was plotted (Fig. 5.5). A linear fit of the calibration curve ( $R^2 = 0.998$ ) was obtained.

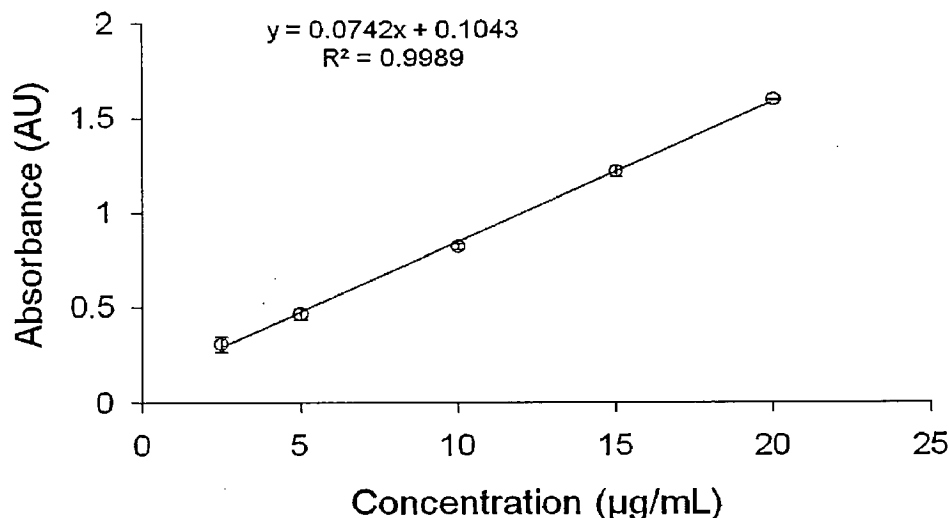


Fig. 5.5. Calibration curve for estimation of 5-fluorouracil in SCF without pectinase at  $\lambda_{\text{max}} = 266$  nm (Results are given as mean  $\pm$  standard deviation, calculated from triplicate analysis).

#### 5.2.6.5 Calibration curve for estimation of 5-fluorouracil in phosphate buffer pH 7.4

The aliquots from the stock solution of 100  $\mu\text{g/mL}$  were taken and dilutions were made with phosphate buffer pH 7.4 to prepare sample for calibration in the concentration range of 5 to 25  $\mu\text{g/mL}$ . The absorbance of the dilutions was measured by UV-Visible spectrometry at  $\lambda_{\text{max}} = 266$  nm against phosphate buffer as blank and the calibration curve was plotted (Fig. 5.6). A linear fit of the calibration curve ( $R^2 = 0.999$ ) was obtained

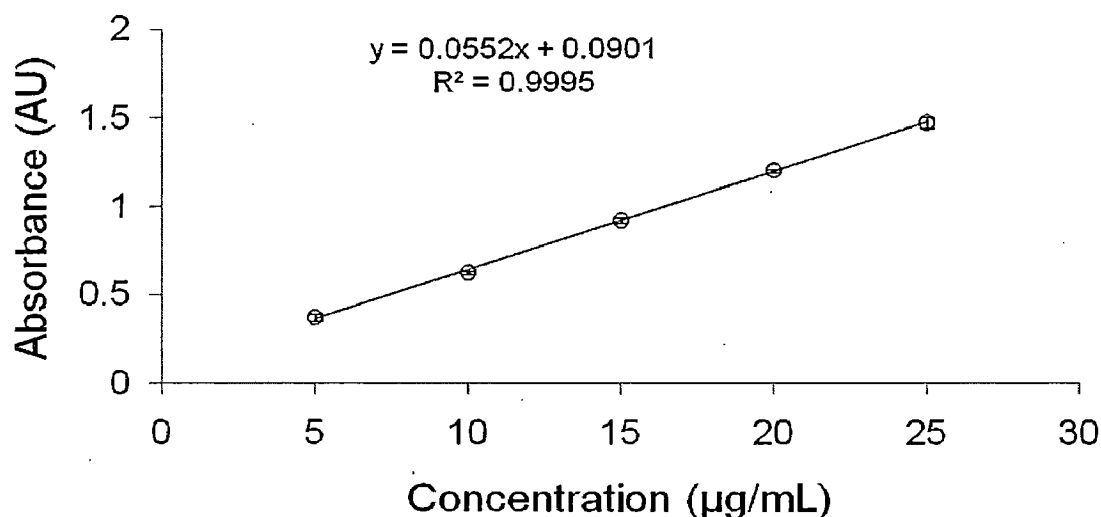


Fig. 5.6. Calibration curve for estimation of 5-fluorouracil in phosphate buffer (pH 7.4) at  $\lambda_{\text{max}} = 266$  nm (results are given as mean  $\pm$  standard deviation, calculated from triplicate analysis).

#### 5.2.7 Experimental procedure for SRB assay

Cell viability was evaluated using the sulforhodamine B (SRB) dye assay [22, 23]. The cell lines were grown in RPMI 1640 medium containing 10% fetal bovine serum and 2



mM L-glutamine. For present screening experiment, cells were inoculated into 96 well microtiter plates in 100  $\mu$ L depending on the doubling time of individual cell lines. After cell inoculation, the microtiter plates were incubated at 37 °C, 5 % CO<sub>2</sub>, 95 % air and 100 % relative humidity for 24 h prior to addition of experimental drugs/ nanomaterials. The experiments were performed in the authorized cancer research institute at Tata Memorial Centre, Advanced Centre for Treatment Research and Education in Cancer (ACTREC) Mumbai (India).

After 24 h, one 96 well plate containing  $5 \times 10^3$  cells/ well was fixed *in situ* with TCA (Trichloro acetic acid), to represent a measurement of the cell population at the time of drug addition (T<sub>2</sub>). Experimental sample (MP-5FU) of concentration in the range of 1 - 5 mg/mL was dispersed in phosphate buffer pH ~ 7.4. 10  $\mu$ l of this dispersion was added to the microtiter wells already containing 90  $\mu$ l of medium. Similarly, 10  $\mu$ l solution of 5-FU of 800  $\mu$ g/mL was treated to respective cell line [22, 23].

#### 5.2.7.1 Endpoint measurement

After the addition, plates were incubated at standard conditions for 48 hours and the assay was terminated by the addition of cold TCA (Trichloro acetic acid). Cells were fixed *in situ* by the gentle addition of 50  $\mu$ l of cold 30 % (w/v) TCA (final concentration, 10 % TCA) and incubated for 60 min at 4 °C. The supernatant was discarded; the plates were washed five times with tap water and air dried. Sulforhodamine B (SRB) solution (50  $\mu$ l) at 0.4 % (w/v) in 1 % acetic acid was added to each of the wells, and plates were incubated for 20 minutes at room temperature. After staining, unbound dye was recovered and the residual dye was removed by washing five times with 1 % acetic acid. The plates were air dried. Bound stain was subsequently eluted with 10 mM trizma base, and the absorbance was read on a plate reader at a wavelength of 540 nm with 690 nm reference wavelength. These experiments were performed in triplicate and the cell viability as mean  $\pm$  standard deviation of triplicate analysis.

Percent growth was calculated on a plate-by-plate basis for test wells relative to control wells. Percent growth was expressed as the ratio of average absorbance of the test well to the average absorbance of the control wells \* 100.

Using the six absorbance measurements [time zero (T<sub>2</sub>), control growth (C), and test growth in the presence of drug at the four concentration levels (T<sub>i</sub>)], the percentage growth was calculated at each of the drug concentration levels. Percentage growth inhibition was

calculated as:

$[(T_i - T_z)/(C - T_z)] \times 100$  for concentrations for which  $T_i \geq T_z$  ( $T_i - T_z$ ) positive or zero

$[(T_i - T_z)/T_z] \times 100$  for concentrations for which  $T_i < T_z$ . ( $T_i - T_z$ ) negative

Growth inhibition of 50 % ( $GI_{50}$ ) was calculated from the drug concentration resulting in a 50% reduction in the net protein increase (as measured by SRB staining) in control cells during the drug incubation. This value was determined for each drug, MP and nanomaterials of MP-5FU using the dose dependent curves.

Values of  $GI_{50}$  were calculated for each of cell lines if the level of activity was reached; however, if the effect was not reached or was exceeded, the values for that parameter were expressed as greater or lesser than the maximum or minimum concentration tested.

Growth inhibition of 50 % ( $GI_{50}$ ) calculated from  $[(T_i - T_z)/(C - T_z)] \times 100 = 50$ , drug concentration resulting in a 50 % reduction in the net protein increase.

### 5.3. RESULTS AND DISCUSSION

#### 5.3.1 Evaluation of drug loading

It may be noted from Table-5.1 that the batches of magnetite-pectin -5FU nanomaterials synthesized using pectin concentrations of 0.4 % followed by loading with 5-FU with the concentrations ranging from 0.1M to 0.025 M using the protocol I, resulted in ~ 17 % w/v drug encapsulation, with ~ 11 % of drug loaded content (wt %). However, 1.0 % (w/v) pectin is not suitable for fabrication process as it results in to formation of a viscous polymeric matrix. On the other hand, the batch synthesized using 0.4 % pectin with the concentrations of 5 FU ranging from 0.1 M to 0.025 M by probe sonication (protocol II) showed higher % drug loading efficiency (~ 31 % w/v) and the corresponding % drug loaded content in the fabricated nanomaterials also increased to 17 – 18 %. It was noted that by increasing the initial drug concentration, did not affect % encapsulation of the drug or the % drug content in the fabricated nanomaterials of MNPs- calcium pectinate loaded with 5-FU. So we surmised that 0.025 M concentration of 5-FU was optimum for fabrication of 5-FU loaded in nanomaterials of MNP-calcium pectinate. It was also be noted from the Table 5.2a that maximum encapsulation of 5-FU was observed for 60 min ( $18.15 \pm 1.1$ ) and 90 min ( $19.5 \pm 2.2$ ) probe sonication. However the batch prepared by 30 minutes of probe sonication resulted in very low drug encapsulation efficiency of only  $4.0 \pm 0.9$  (Table 5.2a). Further initial drug of 0.025 M concentration was found to be sufficient for loading drugs, as higher

initial concentration of drugs also exhibited similar % encapsulation efficiency (Table 5.2b). Furthermore, trials with bath sonication showed poor drug entrapment of ~ 11% for 0.025 M (Table 5.3).

This indicated that this method may not be suitable to achieve a homogenous dispersion of the 5-FU after 1 h. From the above results, it was noted that the optimized conditions needed for preparing hybrid nanomaterials of magnetite-pectin-5-fluorouracil were 0.4% w/v pectin, 0.8% w/v of  $\text{CaCl}_2$  and 0.025M of 5-FU with 1 h probe sonication at 70 °C. This batch will now be referred as MP-5FU.

### 5.3.2 X-ray diffraction studies

The fabrication of MP-5FU nanomaterial was characterized by using various techniques. The X-ray diffraction pattern of MP-5FU matched with that of pure MNPs exhibiting peaks at 220, 311, 400, 511 and 440 planes, corresponding to cubic magnetite structure as reported in JCPDS 01-11111 data (Fig. 5.7). This indicated the incorporation of MNPs in MP-5FU batch.

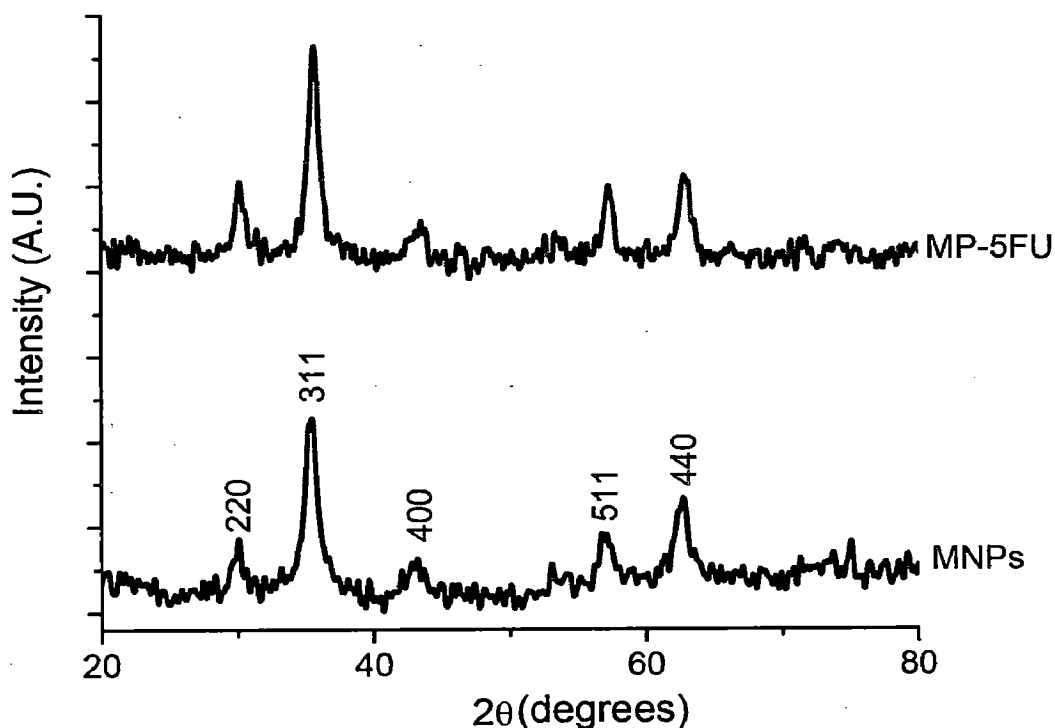


Fig. 5.7. XRD of the fabricated MP-5FU nanomaterials and the as-synthesized MNPs

### 5.3.3 Morphological studies

The SEM study revealed that the MP-5FU nanomaterial were mostly spherical in shape with size distribution in the range of 100 – 150 nm, in dry condition (Fig. 5.8). The

formation of MP-5FU was evident from the EDAX analysis of a selected area of a representative spherical nanomaterial of MP-5FU displayed characteristic X-ray peaks of Fe, F and Ca corresponding to MNPs, 5-FU and calcium pectinate respectively (Fig. 5.8).

Further, the TEM analysis of the MP-5FU illustrated formation of nanomaterials of 100 – 150 nm size (Fig. 5.9a, 5.9 b, 5.9c), and corroborated well with the SEM results. Its SAED pattern was more complex than those observed for MNP coated with calcium pectinate (MP) as shown in Chapter 2. This indicated the presence of more than one types of crystalline material, attributed due to presence of MNPs and 5-FU (Fig. 5.9a, 5.9b, 5.9c).

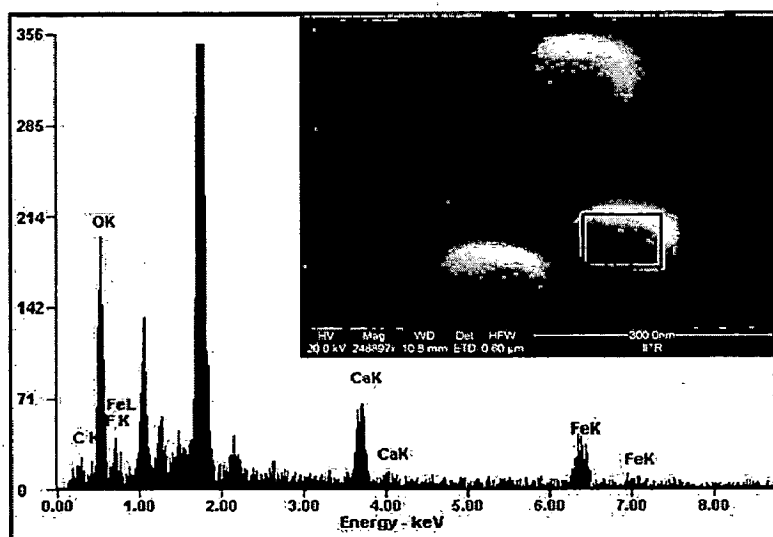


**Fig. 5.8.** Morphology and elemental composition of the 100 nm sized MP-5FU by SEM and EDAX. The X-ray spectrum corresponded to the marked area in the inset.

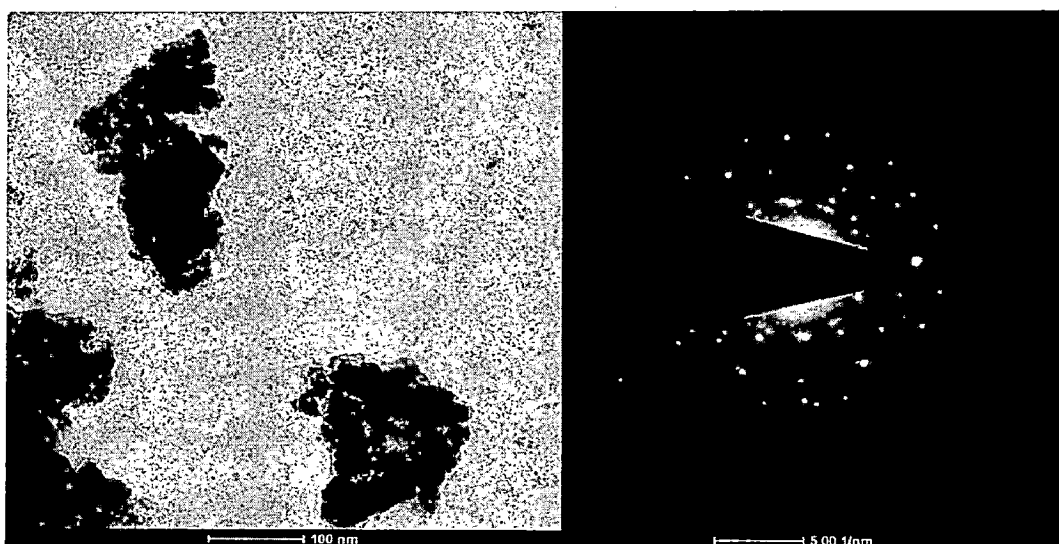


**Fig. 5.9a.** Transmission electron microscopy (TEM) of MP-5FU showing structure of 100-150 nm, its corresponding SAED image exhibits crystalline nature of the material.

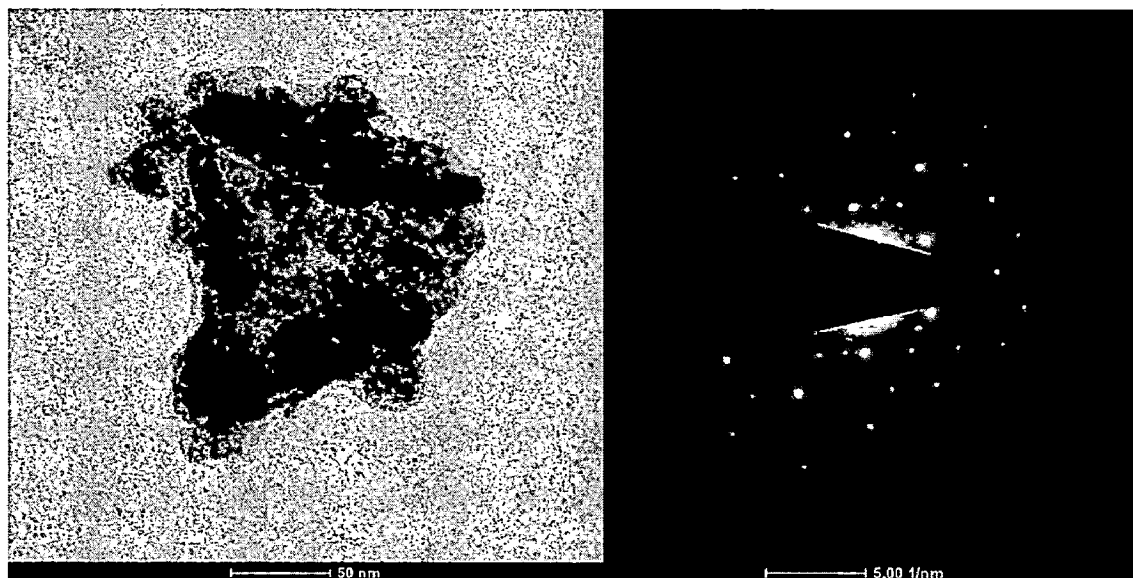


**Fig. 5.9b.** A detailed transmission electron microscopy (TEM) and corresponding selected area electron diffraction (SAED) of the MP-5FU nanomaterial of about 100 -150 nm.

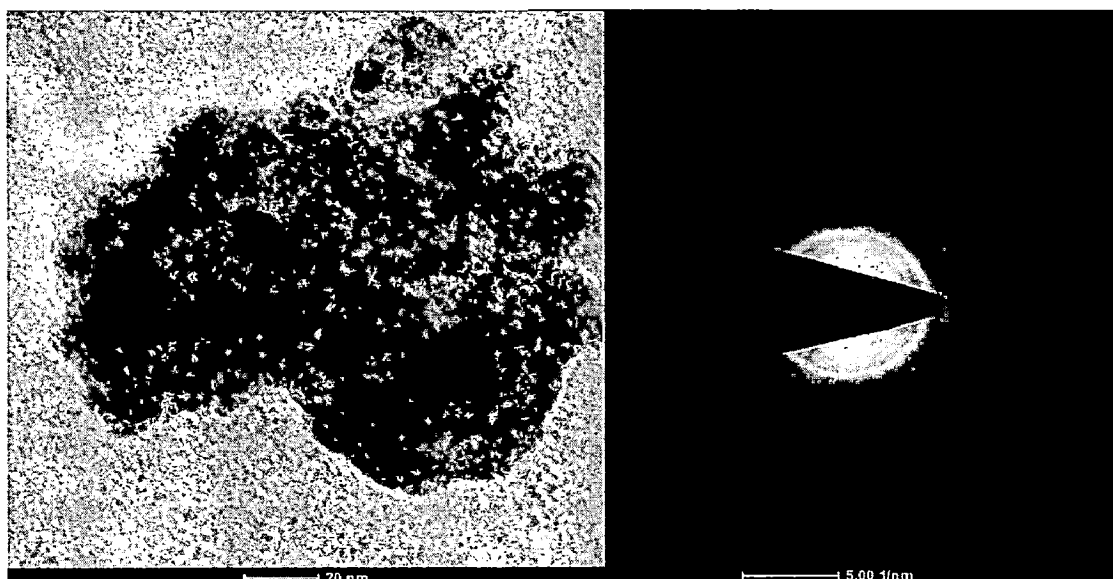


**Fig. 5.9c.** Higher resolution transmission electron microscopy (TEM) of about 100 -150 nm MP-5FU and its corresponding selected area electron diffraction (SAED) showing polycrystalline MNPs.

The size distribution of the MP-5FU was also measured by dynamic light scattering (DLS) measurement, where the nanomaterials were dispersed in aqueous solution at pH ~4. The DLS measurement exhibited unimodal size distribution in the range of 190 – 430 nm with maximum intensity at ~ 300 nm (Fig. 5.10), indicating that the method of synthesis of these nanomaterials offered a good control over their sizes. However, the size distribution obtained from DLS measurements were two folds higher than that measured by SEM and TEM studies. This discrepancy can be attributed due to swelling effect of calcium pectinate in aqueous medium [9].

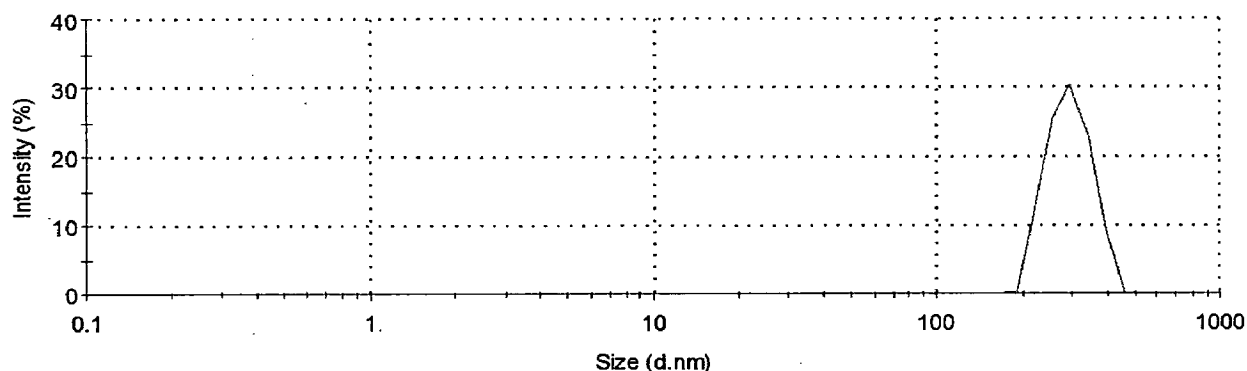


**Fig. 5.10.** Dynamic Light Scattering (DLS) measurement of MP-5FU nanomaterials in aqueous solution at pH~ 4.

### 5.3.4 FT-IR analysis

The formation of MP-5FU system was confirmed by FT-IR studies. Broadly, it was observed that the absorption bands in the IR spectrum recorded for MP-5FU nanomaterials matched with the bands recorded for pure drug to a large extent. The corresponding IR peaks of these groups were identified from literature [24, 25].

5-FU consists of various functional groups, notably, N – H and C=O, substituted ring and C-F. The IR of 5-FU was quite similar to that of MP-5FU. The peaks due to stretching of N-H group of 5-FU observed at  $3165\text{ cm}^{-1}$  and  $3065\text{ cm}^{-1}$  were overlapped by a broad peak of pectinate structure in the range of  $3100$  to  $3600\text{ cm}^{-1}$  in MP-5FU due to the presence of O-H group (Fig. 5.11). The peak observed at  $1735\text{ cm}^{-1}$  in MP-5FU and 5-FU was attributable to stretching frequency of C=O group. The characteristic ring structure of 5-FU was evident from the corresponding peak at  $1235\text{ cm}^{-1}$  and a medium strong peak at  $1000\text{ cm}^{-1}$  corresponding to ring of 5-FU confirmed the entrapment of 5-FU in MP-5FU. Further the peaks at  $1630\text{ cm}^{-1}$  observed in MP was attributable to the presence of carboxylate group in calcium pectinate, while the peak at  $1650\text{ cm}^{-1}$  corresponded to ring structure of 5-FU was observed [25].

Further the peaks recorded at  $745$ ,  $665$  and  $550\text{ cm}^{-1}$  in the IR spectrum of 5-FU corresponded to its ring structures. However these peaks were found to overlap in MP-5FU, which also comprised of a strong peak at  $580\text{ cm}^{-1}$  due to Fe-O vibration as observed in MP. So from IR studies it was conclusive that nanomaterials of 5-FU loaded in MNP coated with calcium pectinate was formed.

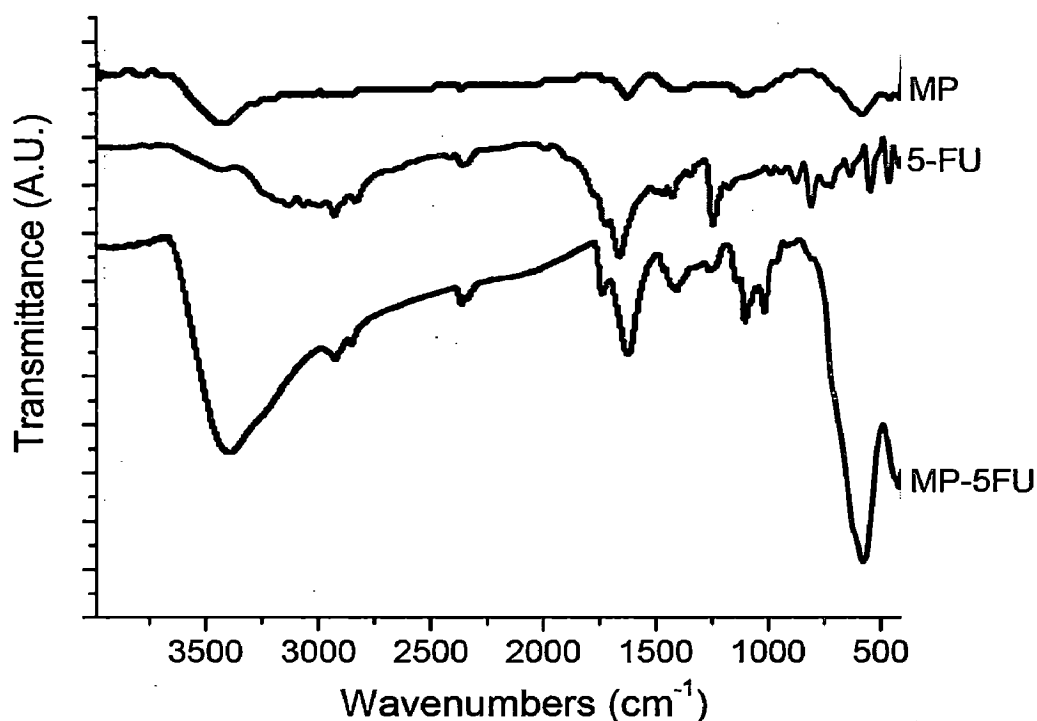


Fig. 5.11. FT-IR spectra of MP, 5-FU and fabricated MP-5FU nanomaterials.

### 5.3.5 Zeta potential measurement: mechanism of the formation of nanomaterial of MP-5FU nanomaterials

MNPs, MP and pectin showed zeta potential of + 17.4 mV at pH~ 4, - 17.8 mV and -35.9 mV at pH~ 4, as discussed in chapter 2. However the zeta potential of MP-5FU was measured as - 40.5 mV which indicated the fabricated system was very stable as zeta potentials more that  $\pm 25$  mV are considered to be stable [26] (Table 5.4). The negative zeta potential in MP-5FU could be attributed to polyanionic nature of pectin. In view of the results obtained from various studies a mechanism towards formation of the MP-5FU nanomaterials is proposed as shown in Fig. 5.12.

**Table 5.4.** Zeta potential measurements of magnetite nanoparticles at pH 4, nanomaterials of magnetite-pectin (MP) at pH ~ 4, magnetite nanoparticles encapsulated in calcium pectinate nanomaterials loaded with 5-FU (MP-5FU) at pH 4 and 5-FU.

| Samples       | Measured zeta potential value ( $\zeta$ ) in mV |
|---------------|---|
| MNPs (pH~4)   | +17.4   |
| Pectin (pH~4) | -35.9   |
| MP (pH~4)     | -17.8   |
| 5- FU         | - 36.0  |
| MP-5FU        | - 40.5  |

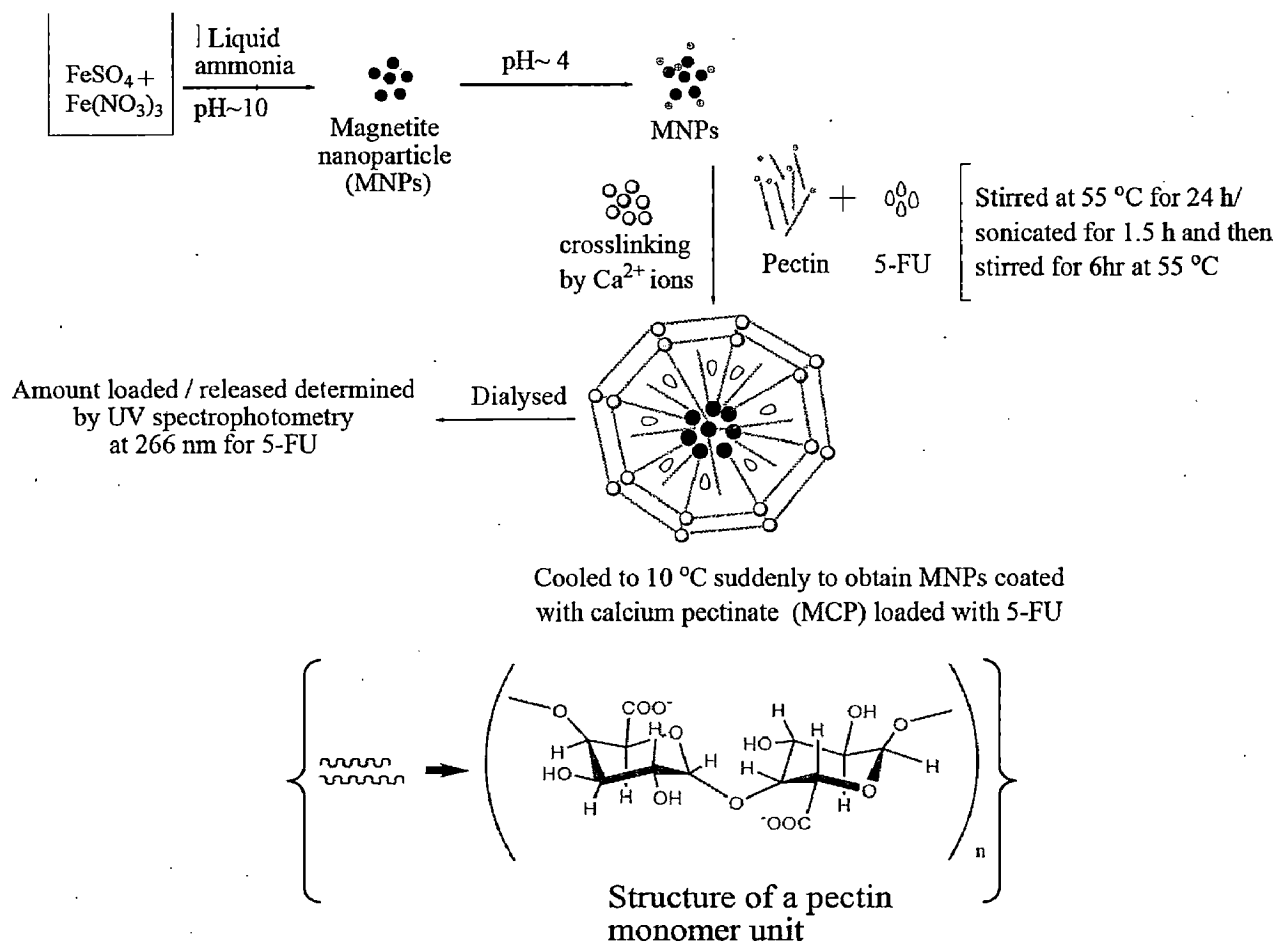


Fig. 5.12 Schematic representation of mechanism towards formation of the MP-5FU nanomaterials.

Since 5-FU and pectin both exhibit negative zeta potential so it is unlikely that there could be any electrostatic interaction between them during mixing. So during formation of MP-5FU by cross linking of pectin with  $\text{Ca}^{2+}$  ions, apparently 5-FU was entrapped in the nanomaterial. Probably due to absence of any electrostatic binding or affinity of 5-FU with pectin, the loading efficiency was less.

### 5.3.6 Magnetic properties of MP-5FU nanomaterials

The nanomaterials of MP-5FU were magnetic in nature, as evident from the Fig 5.13, which were attracted to an external magnet placed adjacent to the sample vial containing MP-5FU.



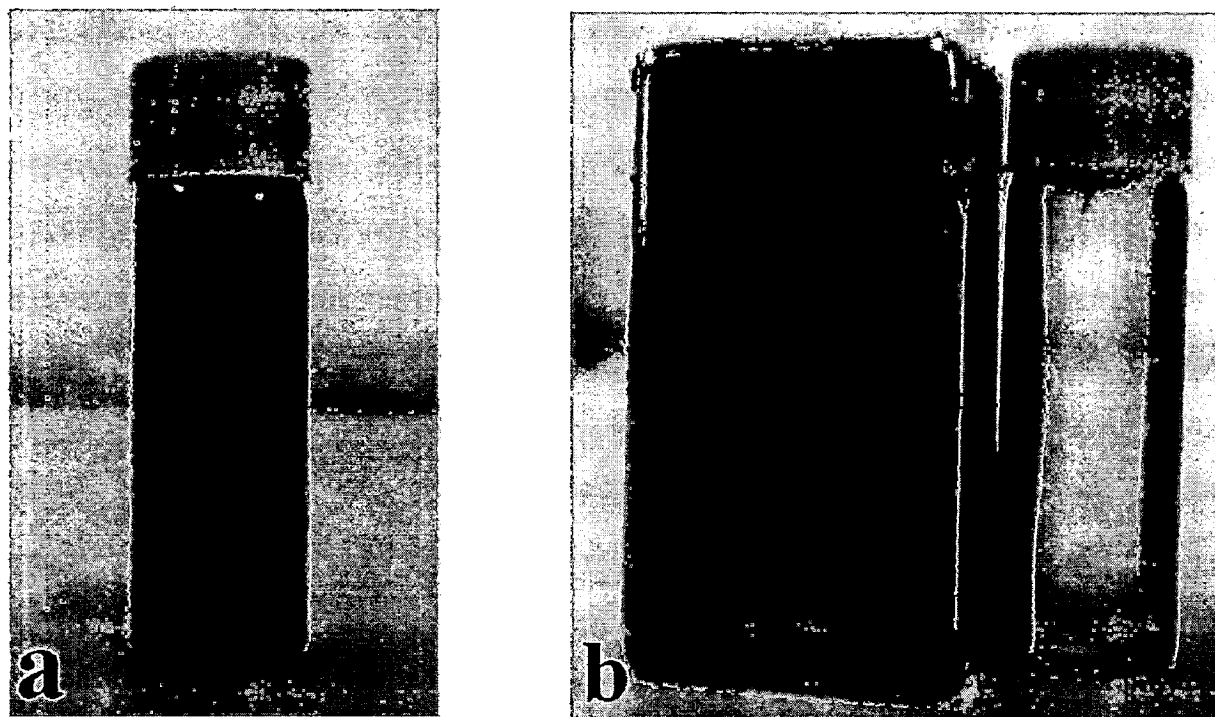


**Fig. 5.13.** a) Dispersion of freshly prepared MP-5FU b) showing MP-5FU nanomaterials attracted to the external magnet placed adjacent to sample vial, indicating its magnetic properties.

The magnetic behavior of MP-5FU was studied by recording magnetization curve (M-H curve) at room temperature from VSM measurements. The M-H curve for MP-5FU exhibited negligible coercivity and remanence magnetization which was found to be similar to that of the as-synthesized MNPs and MP (Fig. 5.14). This phenomenon was typically due to superparamagnetism, attributable to nanoparticles of magnetite. The saturation magnetization measured ( $M_s$ ) measured at room temperature between  $\pm 10$  kOe were 55.53 emu/g, 47.07 emu/g and 43.15 emu/g for as-synthesized MNPs, MP and MP-5FU respectively. The decrease in the saturation magnetization in the nanomaterials loaded with 5-FU (MP-5FU) could be attributed either due to the effects of small particle size owing to non-collinear spin arrangement at the surface [27, 28], or due to the formation of magnetic dead layer by nonmagnetic material at the domain boundary wall of MNPs [29, 30]. The particle size effect on reduction of  $M_s$  may be ruled out as the same batch of MNPs with uniform particle size distribution was used for synthesis of different MP compositions, as discussed in the chapter 2 and chapter 3. The magnetic moments could be quenched due to the formation of magnetic dead layer at the domain wall of MNPs. In the case of MP-5FU, pectin and 5-FU are non magnetic material, which are likely to form magnetic dead layer. This could hinder the domain wall motion during application of the magnetic field, which

might be responsible for the reduction in the saturation magnetization in these synthesized hybrid nanomaterials.

The superparamagnetic behaviour of MP-5FU was studied from SQUID measurement by recording field cooled (FC) and zero field cooled (ZFC) magnetization (in emu/g) at 50 Oe and 500 Oe in a temperature range of between 5 K and 300 K (Fig. 5.15a, 5.15b). The magnetization of the sample at 5 K was measured to be 6.05 emu/g. Such lower magnetization could be attributed to the random orientation of the magnetic moments of individual particles due to particles less than 20 nm sizes [31]. As the temperature was increased more particles reoriented their magnetic moment (magnetization) along the external applied field. Due to this the magnetization increased till it reached a maximum value (8.78 emu/g) at 80.4 K as shown in the ZFC curve. Further increasing the temperature resulted in decrease in magnetization. Thus the transition temperature was at 80.4 K, corresponding to the transition from ferromagnetic to superparamagnetic behaviour. On the other hand, the magnetization was measured to be 11.66 emu/g at 5 K in the FC condition in the presence of applied external magnetic field of 50 Oe. The externally applied magnetic field energetically favoured the reorientation of the individual magnetic moment which resulted in the increase in magnetization along the direction of the applied field. Such a behavior was characteristic of superparamagnetism typically observed for small ferromagnetic or ferrimagnetic nanoparticles. Below  $T_B$ , the MP-5FU nanoparticles exhibit ferromagnetic properties. When the temperature is above  $T_B$ , the thermal energy overcomes the anisotropy barrier and randomizes the magnetic moment, leading to the superparamagnetic behavior of the nanoparticles [32]. Notably, at higher applied field of 500 Oe, the blocking temperature expectedly occurred at lower temperature (70.8 K). In the case of the batch measured at 50 Oe, the FC curve showed gradual decrease in the magnetization up to 104.4 K after which the decrease in the magnetization was less pronounced and is typically due to superparamagnetic nature of very smaller particles as discussed above. However, in the case of the batch recorded at 500 Oe external field, the decrease in the magnetization was sharp after the blocking temperature. Moreover the magnetization was higher than that recorded for the batch measured at 50 Oe. Keeping in mind that the MNPs were same, the higher magnetization observed for higher external applied field was likely to be due to alignment of magnetic moments [33].

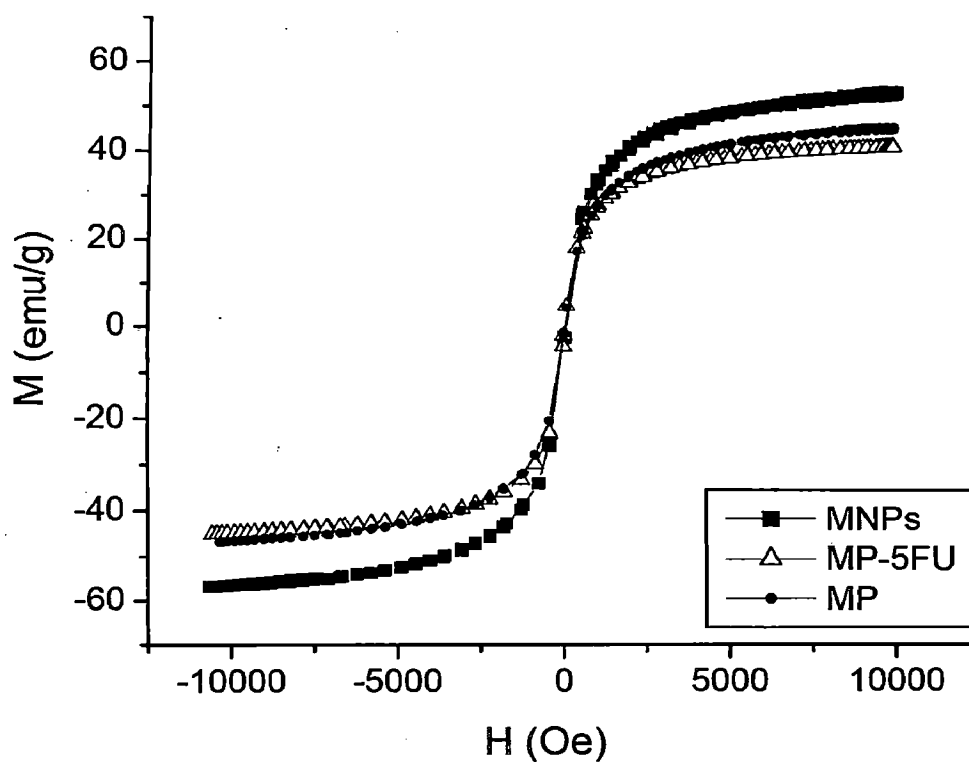


Fig. 5.14. Magnetization vs field (M-H) curve of MNPs and MP-5FU measured by VSM at room temperature.

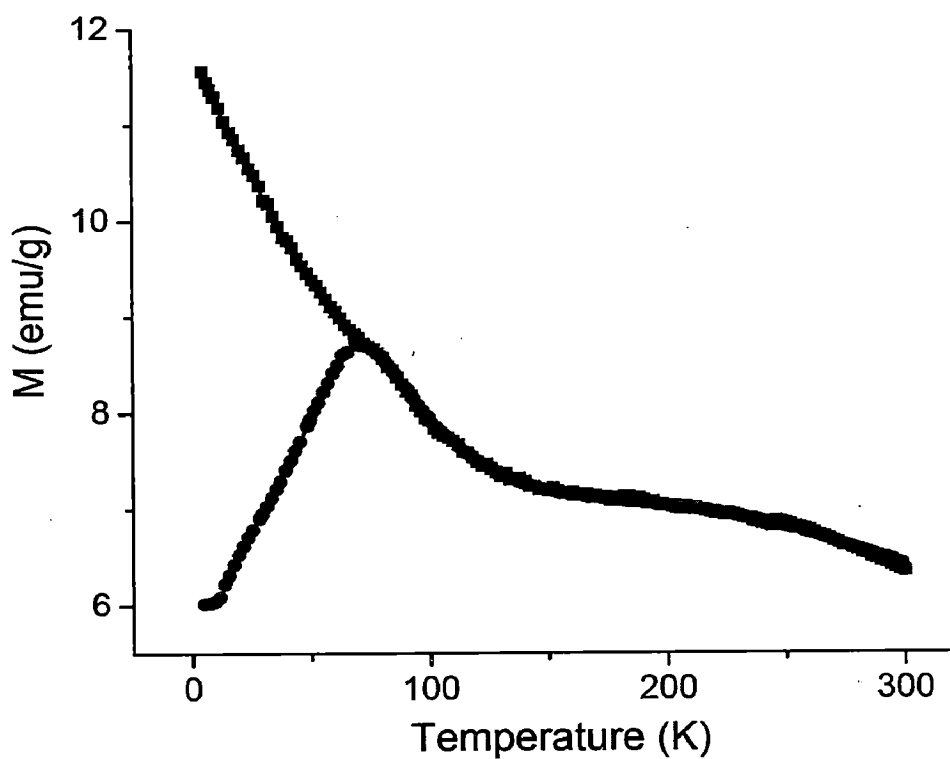


Fig. 5.15a. ZFC and FC curves of MP-5FU nanomaterials recorded at 50 Oe, measured by SQUID.

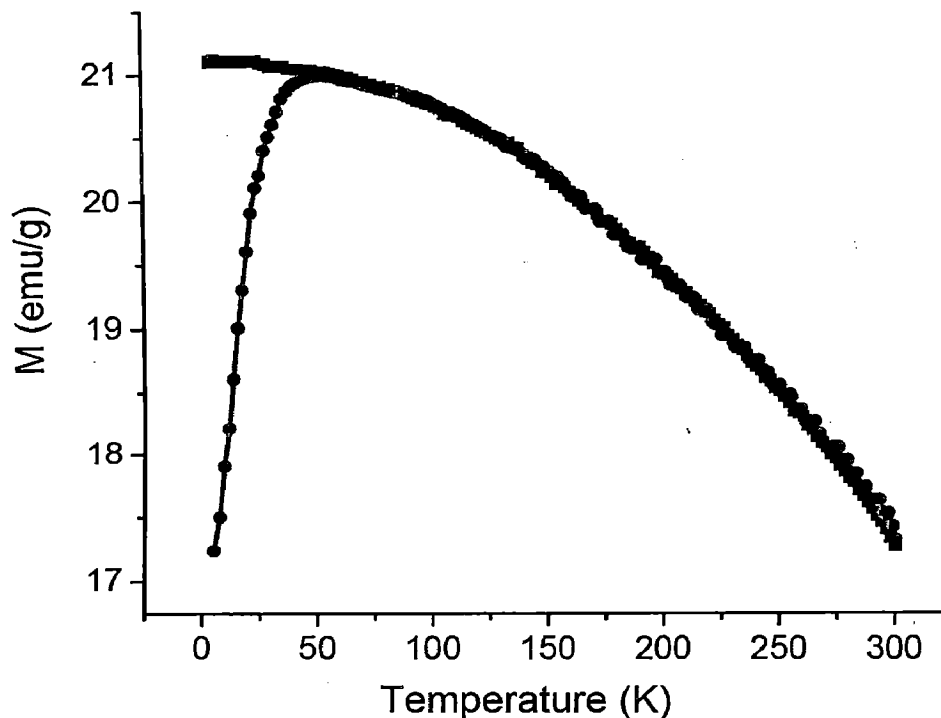


Fig. 5.15b. ZFC and FC curves of MP-5FU nanomaterials recorded at 500 Oe, measured by SQUID.

### 5.3.7 *In vitro* drug release studies from MP-5FU nanomaterials

As discussed earlier, that the sustained or controlled release of low molecular weight drugs from polysaccharide-based matrices are not trivial, attributable to higher drug solubility due to high water contents in the polysaccharide based matrices. The release rate of drugs from the polysaccharide-based matrices is generally very fast and can be referred to as burst release [9]. Sustained release might be achieved by modifying the polysaccharide especially by cross-linking in order to hold back the drug in its network structure for sustaining its release. In the case of MP-5FU nanomaterials, the pectin was cross-linked with  $\text{Ca}^{2+}$  ions and the nature of release of the drug 5-FU was studied by *in vitro* method by treating MP-5FU sequentially in simulated gastric fluid (SGF) followed by simulated intestinal fluid (SIF) and then in simulated colonic fluid (SCF) to mimic the gastrointestinal digestion pathway. In addition, the *in vitro* release study was also carried out in phosphate buffer at pH 7.4 at 37°C for 48 h to mimic drug release in blood. The release of drug from a matrix is mostly governed by pH and in certain cases by specific enzymes.

#### 5.3.7.1 Sequential *in vitro* release in gastrointestinal fluids

It was found that after treating MP-5FU for 2 h in SGF the drug release was only 11.78 % (showed in Fig. 5.16). The drug release of this order in SGF indicated significant

shielding of the drug by calcium pectinate. This is in good agreement to our previous study discussed in chapter 2, where we showed the stability of calcium pectinate in acidic gastric condition. However, the 11.78 % release of FU from MP-5FU in gastric medium was much higher than that discussed for DS release in chapter 3 and 4. This can be explained on the basis of higher solubility of 5-FU in acidic conditions [34] It may be envisaged that the SGF (pH 1.2) might diffuse in to the MP-5FU nanomaterials and led to dissolution of the encapsulated drug (5-FU). The dissolved drug could be released from the nanomaterial by diffusion mechanism. In the case of MP-DS and MPCh-DS the release of DS was insignificant as the drug is insoluble in acidic medium

On the other hand, the *in vitro* release of the drug in SIF at pH 6.8 for 3 h was rapid but sustained, which could be attributed to weakening of calcium pectinate network structure at higher pH (Fig. 5.16) leading to swelling. In fact, it was noted that 21% of the drug was released during the first 2 h in SIF medium, while 19 % of the drug was released during the 3<sup>rd</sup> hour in SIF medium. The rapid release of the drug in SIF observed in this study was in consistence with the literature reports [7], which could be attributed to swelling effect of calcium pectinate as demonstrated in the DLS measurement. The swelling of calcium pectinate can be attributed to increase in the concentrations of negatively charged carboxylate groups in pectin at higher pH ( $pK_a = 2.9-4.1$ ), which however would depend on the degree of esterification [35, 36]. This could lead to repulsion between pectin chains and thus resulted in swelling of pectin. Compared to DS release from MP-DS and MPCh-DS nanomaterials (discussed in Chapters 3 and 4), the release of 5-FU from MP-5FU was less (~ 40%). The swelling effect of the polymer coating in all these batches was supposed to be similar. Thus the reduced FU release from MP-5FU in SIF may be attributed to its lower solubility as compared to DS at pH 6.8 [37].

Further, the rate of drug release was slowed down in simulated colonic fluid (SCF) where ~40% of release was observed in a pH ~5.5 over the rest of 48 h. Overall the system exhibited sustained drug release for about 48 h where almost all the encapsulated drug was released. This may be probably attributable to the *in-vitro* release studies in the presence of enzymes. From these studies, it may be surmised that the MP-5FU nanomaterial is very effective for sustained release of the drug 5-FU in gastrointestinal tract.

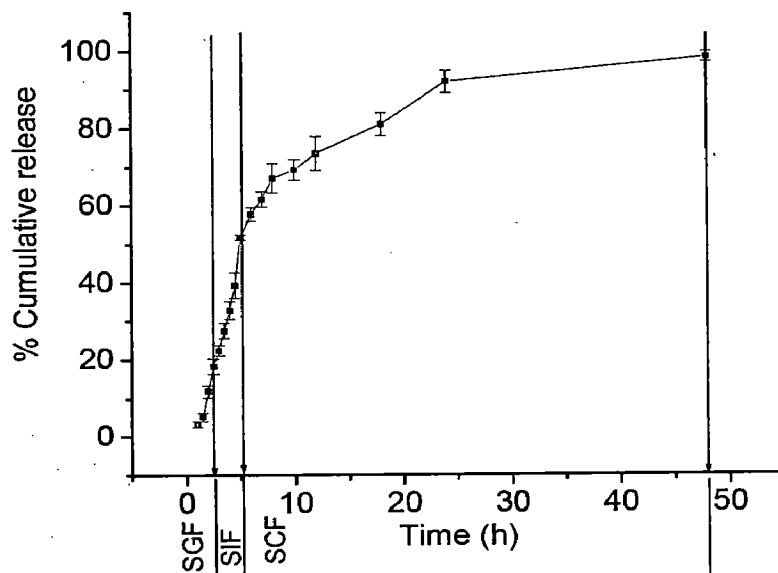


**Fig. 5.16.** Sequential *in vitro* release of 5-FU from MP-5FU nanomaterials in simulated gastric fluid (SGF pH 1.2) for 2 h, followed by simulated intestinal fluid (SIF pH 6.8) for 3 h and simulated colonic fluid (SCF pH 5.5) up to 48 h.

#### 5.3.7.2 *In vitro* release in phosphate buffer at pH 7.4

The *in vitro* release studies of 5-FU from MP-5FU formulation in phosphate buffer solution at pH 7.4 at 37 °C exhibited sustained cumulative release (Fig. 5.17). About 83 % of the loaded drug was released in 24 h after which the rate of release was less. In 48 h, 95 % cumulative release was observed. Our *in vitro* release study was in good agreement with that of Yu *et al.* [9], who reported *in vitro* release from pectin nanospheres (without magnetic material).

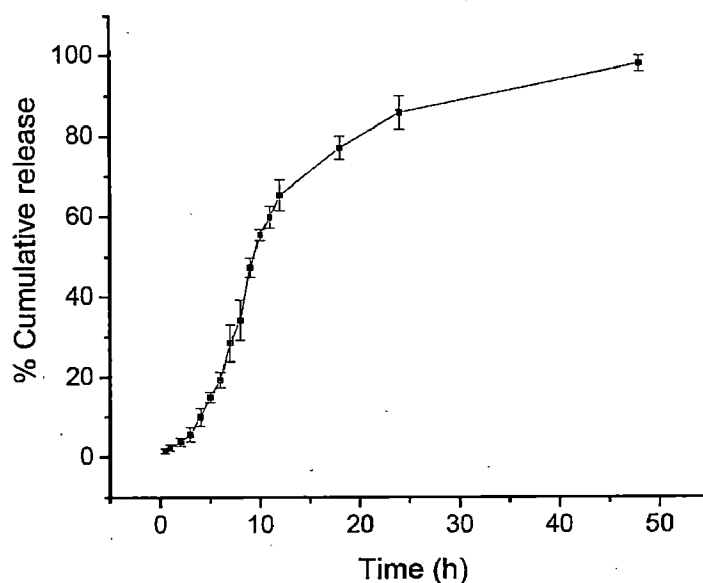


**Fig. 5.17.** *In vitro* sustained release studies of the drug 5-FU for 48 h from MP-5FU nanomaterials in phosphate buffer solution (pH 7.4)

### 5.3.7.3 Modeling of drug release

The release mechanism of 5-FU from MP-5FU nanomaterials was fitted using Korsmeyer - Peppas model as described in chapter 3 (Fig 5.18). The *in vitro* release data of 5-FU from MP-5FU in phosphate buffer pH 7.4 up to 12 h (corresponding to 65.23 %) in log scale, exhibited a linear fit ( $R^2 = 0.968$ ).

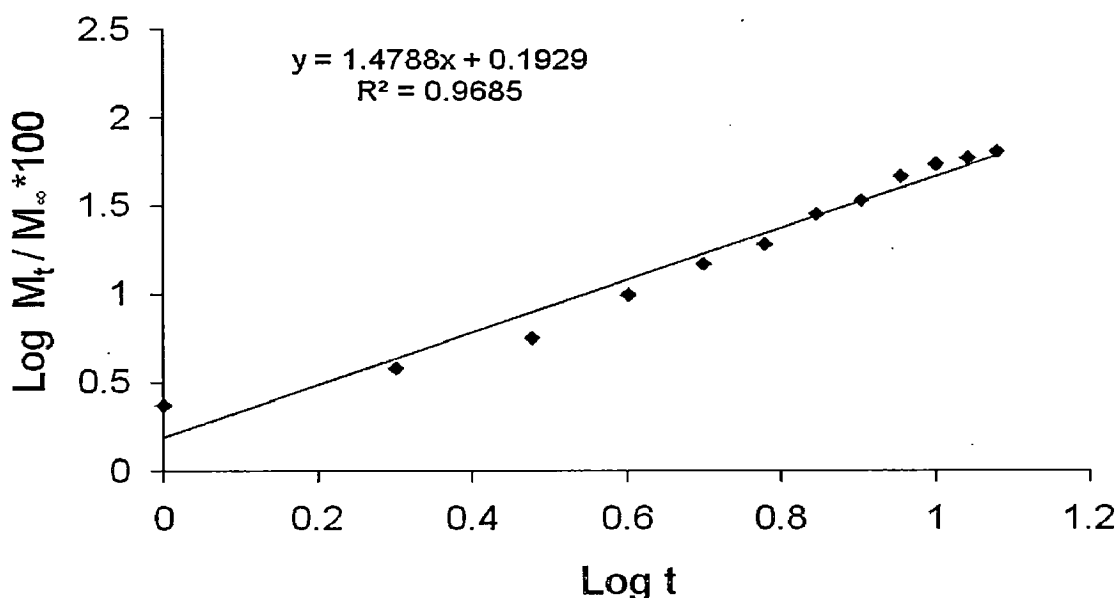


**Fig. 5.18.** Showing linear fit of *in vitro* release of 5-FU up to 12 h from MP-5FU nanomaterials in phosphate buffer solution (at pH 7.4), using Korsmeyer Peppas equation in log scale.

From the slope of the plot  $n$  was found to be 1.4788 which clearly indicated swelling controlled drug release [38]. The swelling of the calcium pectinate was explained from DLS measurements. The value of  $k*100$  (constant related to the structural and geometric characteristic of the device) was found to be 1.5. The  $n$  and  $k$  values were in good agreement with that reported by Wang et al [39].

It may be highlighted that even though the nanomaterial system reported by Yu *et al.* [9] exhibited sustained drug release for a longer period of time, but our system is more functional as it consists of magnetic property and provides an opportunity to improve its overall efficacy in the in-vivo system as magnetic targeted drug delivery. Further, the sustained drug release at pH  $\sim 7.4$  corresponding to blood pH was encouraging for targeted drug delivery, especially via intravenous administration followed by magnetic guiding to tumor site where otherwise the direct drug administration could be cumbersome, e.g., pancreatic tumor, hepatic tumor *etc.* for its sustained release. This would also minimize the distribution of the drug to other undesirable parts of the body. Thus to elucidate the cytotoxic effect of the system so developed we have carried out the in-vitro cytotoxicity

studies in HT29 (colon), HEPG2 (liver), MIA-PA-CA-2 (pancreas) cancer cell lines by SRB assay after 48 h.

### 5.3.8 *In vitro* cytotoxic activity profiles of MP-5FU nanomaterials

The % cell viability due to interaction of MP-5FU nanomaterials in the concentration range of 1 to 5 mg/mL for 48 h is given in Fig. 5.19a, Fig. 5.19b and Fig. 5.19c. The % cell viability of the pure drug was also studied. It was noted that the % cell viability decreased with increasing concentrations of MP-5FU dispersions. The cell viability of 5 mg/mL of MP-5FU was found to be  $60.9 \pm 3.3$  % for HT-29 and  $68.2 \pm 16.1$  % for HEPG2 cancer cell lines (Fig. 5.19a, and 5.19b respectively). In both the cases the  $GI_{50}$  was more than 5 mg/mL. Strikingly, the cell viability for 5 mg/mL of MP-5FU in MIA-PA-CA-2 pancreatic cancer cell line was only  $23.9 \pm 5.1$  % (Fig. 5.19c) and the corresponding  $GI_{50}$  was found to be 3.7 mg/mL. Similar results were found in the reports for the free drug doxorubicin and the doxorubicin encapsulated in nanoparticles [40]. It was important to note that the nanomaterial of MNP coated with calcium pectinate (MP), did not indicate any antiproliferative effect. Therefore decrease in cell viability for MP-5FU was due to release of the anticancer drug 5-FU from these nanomaterials. These results indicated the successful fabrication of magnetic nanomaterials of pectin for potential delivery of 5-FU.

The batch studied for cytotoxicity comprised ~ 17% drug loading content. From our *in vitro* release study in pH 7.4 condition, it was found that ~ 95 % of the drug was released in 48 h. So for the batch of 5 mg/mL MP-5FU, about 800  $\mu$ g/mL of the drug could be released in 48 h in phosphate buffer. In order to compare the cytotoxicity effect of the released drug from MP-5FU nanomaterials, we conducted cell viability studies using 800  $\mu$ g/mL of pure 5-FU in the said cancer cell lines. The cell viability was found to be  $23.6 \pm 1.2$ ,  $48.8 \pm 2.3$  and  $1.5 \pm 0.1$  % respectively in HT-29, HEPG2 and MIA-PA-CA-2 cancer cell lines (Fig 5.19a, 5.19b and 5.19c respectively). The corresponding % cell viability for pure 5-FU (800  $\mu$ g/mL were 18.61 % for HT-29, – 20.78% in HEPG2 and 1.2 % in MIA-PA-CA-2 cancer cell lines. It was noted that the % cell viabilities of MP-5FU were significantly less than those of the pure drug. This could be attributed due to sustained release of drug from MP-5FU while entire amount of the pure drug was available after its treatment on these cell lines. Similar cytotoxic effects were reported for doxorubicin loaded in SPION based nanomaterials [40] and in the liposomal formulation of 5-fluorocytosine (5-FC), as compared to their respective free drugs in cancer cell lines [41].



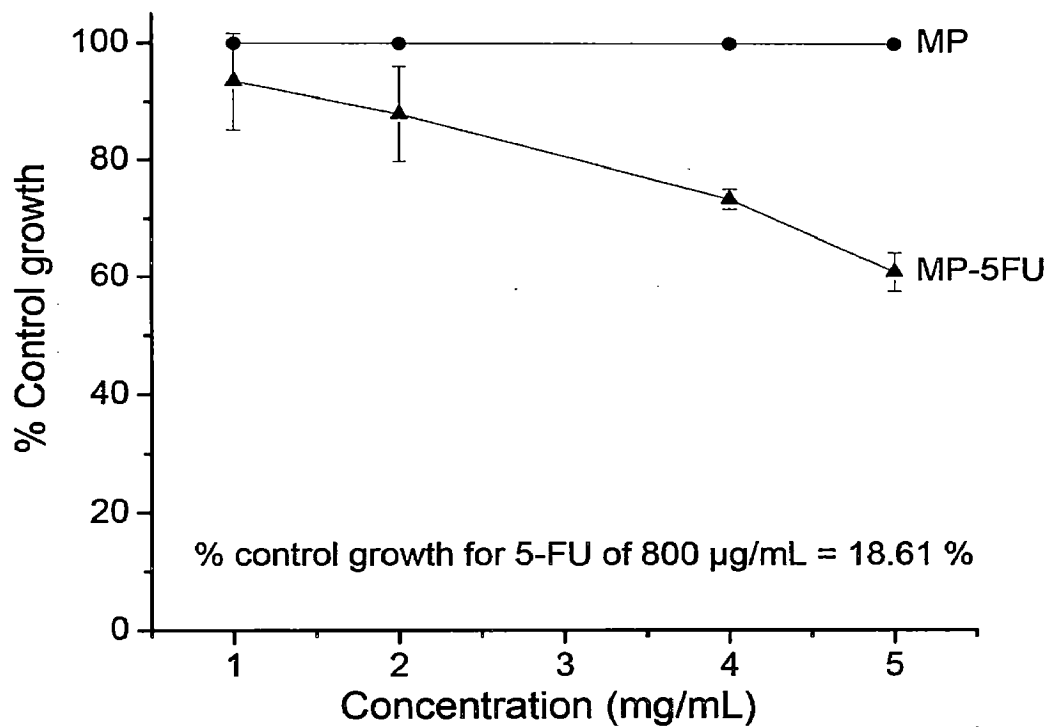


**Fig. 5.19a.** *In vitro* cytotoxic activity profiles of MP-5FU nanomaterials and MP on HT-29 (colon) cancer cell line after 48 h.

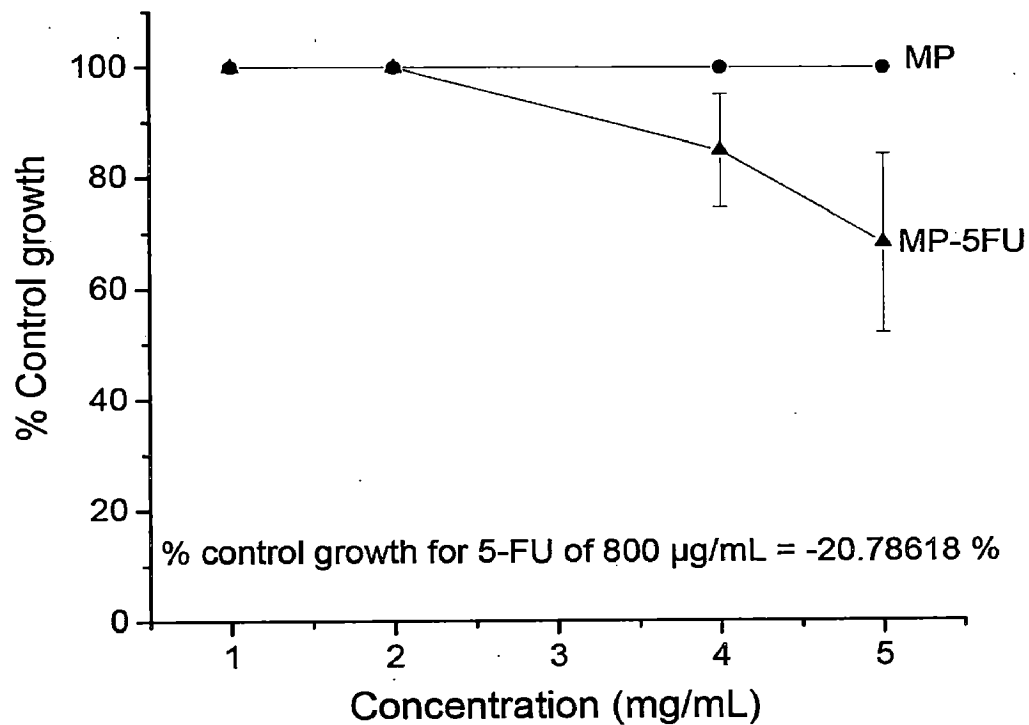


**Fig.5.19b.** *In vitro* cytotoxic activity profiles of MP-5FU nanomaterials on HEPG2 (liver) cancer cell line after 48 h.

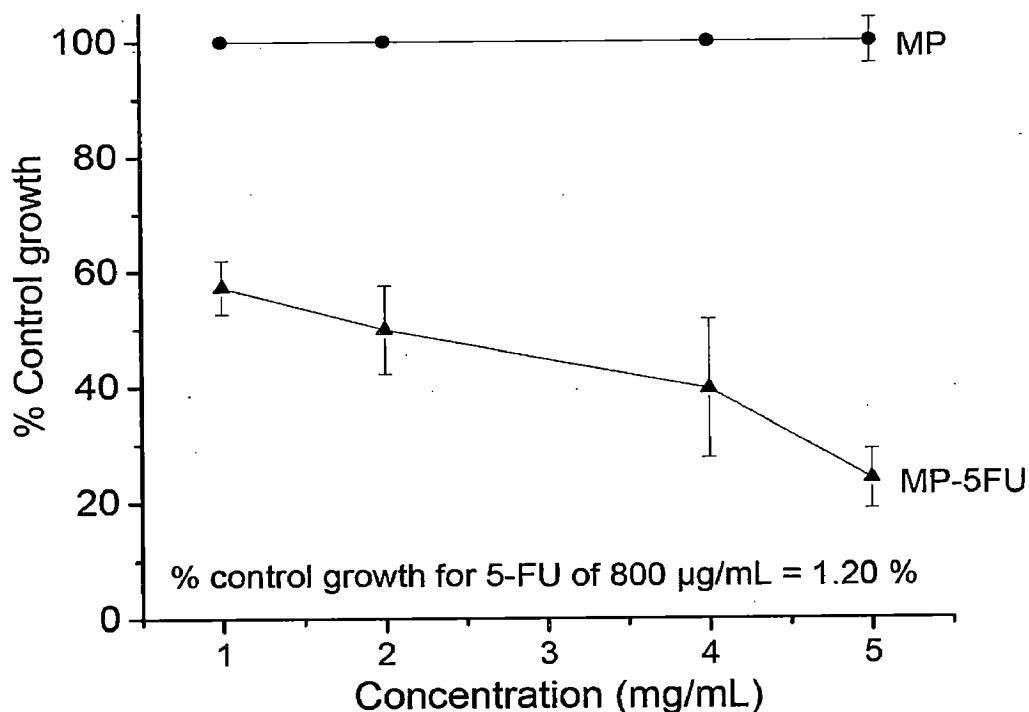


**Fig. 5.19c.** *In vitro* cytotoxic activity profiles of MP-5FU nanomaterials and MP on MIA-PA-CA-2 (pancreas) cancer cell line after 48 h.

#### 5.4 CONCLUSION

A series of novel MNP coated with calcium pectinate nanomaterials loaded with different concentrations of 5-FU were fabricated. The method of mixing drug and pectin was found to be a key parameter. Mixing by magnetic stirring was not only time consuming (24 h) but was apparently not efficient. It was found that the mixing by probe sonication not only reduced the mixing time from 24 h to 1 h, but the % encapsulation efficiency was also enhanced from to  $16.90 \pm 1.3$  % to  $29.80 \pm 2.1$  %. Further the drug loading content (wt %) in the nanomaterials also increased by nearly two folds from  $9.8 \pm 1.5$  to  $16.97 \pm 1.9$ .

The formation of magnetic nanomaterials of MP-5FU of 100-150 nm was characterized by its SEM and TEM analysis, XRD, and FT-IR analysis. The FC-ZFC measurement at 50 Oe confirmed superparamagnetic property of MP-5FU. The VSM measurement at room temperature and 10 kOe showed its high saturation magnetization of 43.15 emu/g which was 20 % less than MPNs. The *in vitro* release studies of MP-5FU formulation in simulated gastrointestinal fluid was studied by treating the nanomaterial sequentially in respective enzyme based simulated gastric fluid at pH 1.2, simulated intestinal fluid at pH 6.8 and simulated colonic fluid at pH 5.5. A sustained release was observed where maximum release occurred in simulated intestinal fluid. Similarly, the *in vitro* release of 5-FU from MP-5FU nanomaterial was studied in phosphate buffer at pH 7.4

which demonstrated sustained release of the drug. The cumulative release of drug was fitted with Korsmeyer Papas model which reflected swelling controlled drug release. The swelling behavior of the polymer was also confirmed by dynamic light scattering measurement which showed larger particle size ranging between 190-430 nm as compared to its dried material measured by SEM and TEM. The sustained drug release at pH 7.4 corresponding to blood pH was encouraging for targeted drug delivery, especially via intravenous administration followed by magnetic guiding to a potential tumor site where otherwise the direct drug administration is cumbersome, e.g., pancreatic tumor, hepatic tumor *etc.* for its sustained release. This would also minimize the distribution of the drug to other undesirable parts of the body. The cytotoxicity studies of the novel fabricated MP-5FU nanomaterial was studied by measuring cell viability of concentration dependent MP-5FU nanomaterials in different cancer cell lines namely, HT-29, HEPG2 and MIA-PA-CA-2 cancer cell lines. The  $GI_{50}$  of MP-5FU was more than 5 mg/mL in HT-29 and HEPG2, while it was 3.7 mg/mL MIA-PA-CA-2 cancer cell line. Compared to the equivalent concentration of pure drug (800  $\mu$ g/mL), the corresponding cytotoxicity of 5 mg/mL of MP-5FU was less, indicating sustained release phenomenon of the drug from the nanomaterial. Thus it was concluded that the nanomaterials of MP-5FU was successfully fabricated which exhibited sustained release and was effective in antiproliferative action in cancer cells.

## REFERENCES

1. Blagosklonny, M. V. Carcinogenesis, cancer therapy and chemoprevention. *Cell Death and Differentiation*. **2005**, *12*, 592–602.
2. Acharya, S.; Sahoo, K.S. PLGA nanoparticles containing various anticancer agents and tumour delivery by EPR effect. *Adv. Drug Delivery Rev.* **2011**, *63*, 170–183.
3. Arias, J. L.; López-Viota, M.; Delgado, A. V.; Ruiz, A.M. Iron/ethylcellulose (core/shell) nanoplatform loaded with for cancer targeting. *Colloids and Surfaces B: Biointerfaces*. **2010**, *77*, 111-116.
4. Babu, V. R.; Sairam, M.; Hosamani, K. M.; Aminabhavi, T. M. Development of 5- fluorouracil loaded poly(acrylamide-co-methylmethacrylate) novel core-shell microspheres: in vitro release studies. *Int. J. Pharm.* **2006**, *325*, 55–62.
5. Lamprecht, A.; Yamamoto, H.; Takeuchi, H.; Kawashima, Y. Microsphere design for the colonic delivery of 5-fluorouracil. *J. Control. Release*. **2003**, *90*, 313–322.
6. Lo, C. L.; Lin, K. M.; Hsiue, G. H. Preparation and characterization of intelligent core-shell nanoparticles based on poly (D,L-lactide)-g-poly(N-isopropyl acrylamide-co-methacrylic acid). *J. Control. Release*. **2005**, *104*, 477–488.
7. Lai, L. F.; Guo, H. X. Preparation of new 5-fluorouracil-loaded zein nanoparticles for liver targeting. *Int. J. Pharm.* **2011**, *404*, 317–323.
8. Zhang, C.; Cheng, Y.; Qu, G. W.; Wu, X. L.; Ding, Y.; Cheng, Z. H.; Yu, L. L.; Ping, Q. N. Preparation and characterization of galactosylated chitosan coated BSA microspheres containing 5-fluorouracil. *Carbohydr. Polym.* **2008**, *72*, 390–397.
9. Yu, C. Y.; Cao, H.; Zhang, X. C.; Zhou, F. Z.; Cheng, S. X.; Zhang, X. Z.; Zhuo, R. X. Hybrid nanospheres and vesicles based on pectin as drug carriers. *Langmuir*, **2009**, *25*, 11720-11726.
10. Garcia, O.; Blanco, M. D.; Martin, J. A.; Teijon, J. M. 5-Fluorouracil trapping in poly (2-hydroxyethyl methacrylate-co-acrylamide) hydrogels: in vitro drug delivery studies. *Eur. Polym. J.* **2000**, *36*, 111–122.

11. Muzzalupo, R.; Nicoletta, F. P.; Trombino, S.; Cassano, R.; Iemma, F.; Picci, N. A new crown ether as vesicular carrier for 5-fluorouracil: synthesis, characterization and drug delivery evaluation. *Colloids Surf. B.* **2007**, *58*, 197–202.
12. Singh, B.; Chauhan, N. Preliminary evaluation of molecular imprinting of fluorouracil within hydrogels for use as drug delivery systems. *Acta Biomater.* **2008**, *4*, 1244–1254.
13. Rejinold, N. S.; Muthunarayanan, M.; Chennazhi, K. P.; Nair, S. V.; Jayakumar, R. 5-Fluorouracil loaded fibrinogen nanoparticles for cancer drug delivery applications. *Int. J. Biol. Macromol.* **2011**, *48*, 98–105.
14. Tanaka, F.; Fukuse, T.; Wada, H.; Fukushima, M. The history, mechanism and clinical use of oral 5-fluorouracil derivative chemotherapeutic agents. *Curr. Pharm. Biotech.* **2000**, *1*, 137–164.
15. Arias, J. L.; Gallardo, V.; Ruiz, M. A.; Delgado, A. V. Magnetite/poly(alkylcyanoacrylate) (core/shell) nanoparticles as 5-Fluorouracil delivery systems for active targeting. *Eur. J. Pharmaceut. Biopharmaceut.* **2008**, *69*, 54–63.
16. Jasmin, C., Capanna, R. *Textbook of bone metastases*; John Wiley and Sons: **2005**.
17. Tripathi, K. D. *Essentials of Medical Pharmacology*, 6<sup>th</sup> Edi.; **2008**.
18. Grem, J. L.; *Fluorinated pyrimidines. Cancer Chemotherapy: Principles and Practice*, Lippincott Company: Philadelphia, **1990**; pp 180–224.
19. Longley D.B.; Harkin D.P.; Johnston P.G. 5-fluorouracil; mechanism of action and clinical strategies. *Nat. Rev. Cancer.* **2003**, *3*, 330–338.
20. Sarg, M.; Gross, A. D., Altman, R. *The cancer dictionary*, III edition.; **2007**.
21. McGlinchey, P.G.; Webb, S.T.; Campbell, N.P.S. 5-Fluorouracil-induced cardiotoxicity mimicking myocardial infarction: a case report. *BMC Cardiovasc Disord.* **2001**, 1–3.
22. Vichai, V.; Kirtikara, K. Sulforhodamine B colorimetric assay for cytotoxicity screening. *Nature Protocols.* **2006**, *1*, 1112 – 1116.
23. Skehn, P.; Storeng, R.; Scudiero, A.; Monks, J.; McMohan, D.; Vistica, D.; Jonathan, T. W.; Bokesch, H.; Kenney, S.; Boyd, M. R. New colorimetric

- cytotoxicity assay for anticancer drug screening. *J. Natl. Cancer Inst.* **1990**, *82*, 1107.
24. Sliverstein, R. M., Webster F. X. *Spectrometric identification of organic compounds*; John Wiley and Sons: Asia, **2002**.
  25. Singh J. S. FTIR and Raman Spectra and Fundamental Frequencies of 5-halosubstituted uracils: 5-X-uracil (X= F, Cl, Br & I), *Spectrochimica Acta Part A: Molecular and Biomolecular Spectroscopy*. **2010**, *2012*, *87*, 106–111
  26. Cesaro, A.; Delben, F.; Paoletti, S. Thermodynamics of the proton dissociation of natural polyuronic acids. *Int. J. Biol. Macromol.* **1990**, *12*, 170-176.
  27. George, M.; John, A. M.; Nair, S. S.; Joy, P. A.; Anantharaman, M. R. Finite size effects on the structural and magnetic properties of sol-gel synthesized NiFe<sub>2</sub>O<sub>4</sub> powders. *J. Magn. Magn. Mater.* **2006**, *302*, 190–195.
  28. Haneda, K.; Morrish, A. H. The formation of magnetic dead layer by nonmagnetic material at the domain boundary wall of MNPs. *J. Appl. Phys.* **1988**, *63*, 4258-4260.
  29. Shafi, K. V. P. M.; Ulman, A.; Dyal, A.; Yan, X.; Yang, N. L.; Estournes, C.; Fournes, L.; Wattiaux, A.; White, H.; Rafailovich, M. Magnetic Enhancement of  $\gamma$ -Fe<sub>2</sub>O<sub>3</sub> Nanoparticles by Sonochemical Coating. *Chem. Mater.* **2002**, *14*, 1778-1787.
  30. Morales, M. P.; Verdaguer, S. V.; Montero, M. I.; Sterna, C. J.; Roing, A.; Casas, L.; Martinez, B.; Sandiumenge, F. Surface and internal spin canting in  $\gamma$ -Fe<sub>2</sub>O<sub>3</sub> nanoparticles. *Chem. Mater.* **1999**, *11*, 3058-3064.
  31. Daou, T. J.; Pourroy, G.; Bégin, C. S.; Grenèche, J. M.; Ulhaq, B. C.; Legaré, P.; Bernhardt, P.; Leuvrey, C.; Rogez, G. Hydrothermal Synthesis of Monodisperse Magnetite Nanoparticles. *Chem. Mater.* **2006**, *18*, 4399–4404.
  32. Hou, Y. L.; Yu, J. F.; Gao, S. J. Solvothermal reduction synthesis and characterization of superparamagnetic magnetite nanoparticles. *J. Mater. Chem.* **2003**, *13*, 1983-1987.
  33. Guardia, P.; Batlle-Brugal, B.; Roca, A. G.; Iglesias, O.; Morales, M. P.; Serna, C. J.; Labarta, A.; Batlle, X. Surfactant effects in monodisperse magnetite nanoparticles of controlled size. *J. Magn. Magn. Mater.* **2007**, *316*, 756–759.
  34. Rudy, B.C.; Senkowski, B.Z. Fluorouracil In: Florey, K. (Ed.), Analytical profiles of drug substances. Academic Press. **1973**, 221–244.

35. Ofori-Kwakye, K.; Fell, J.T. Biphasic drug release: the permeability of films containing pectin, chitosan and HPMC. *Int. J. Pharm.* **2001**, *226*, 139-145.
36. Ralet, M. C.; Dronnet, V.; Buchholt, H. C.; Thibault, J. F. Enzymatically and chemically de-esterified lime pectins: characterization, polyelectrolyte behavior and calcium binding properties. *Carbohydr. Res.* **2001**, *336*, 117–125.
37. Rudy, B.C.; Senkowski, B.Z. Fluorouracil In: Florey, K. (Ed.), *Analytical Profiles of Drug Substances*. Academic Press. **1973**, 221–244.
38. Siepmann, J.; Peppas, N. A. Modeling of drug release from delivery systems based on hydroxypropyl methylcellulose (HPMC). *Adv. Drug Delivery Rev.* **2001**, *48*, 139–157.
39. Wang, Qin.; Zhang, J.; Wang, A. Preparation and characterization of a novel pH-sensitive chitosan-g-poly (acrylic acid)/attapulgate/sodium alginate composite hydrogel bead for controlled release of diclofenac sodium. *Carbohydr. Polym.* **2009**, *78*, 731–737.
40. Jain, T.; Marco, A. K.; Sahoo, S. K.; Leslie-Pelecky, D, L.; Labhasetwar, V Iron oxide nanoparticles for sustained delivery of anticancer agents, *Mol. Pharmaceut.* **2005**, *2* (3), 194-205.
41. Chaszczewska-Markowska M.; Stebelska K.; Sikorski A.; Madej J.; Opolski A.; Ugorski M. Liposomal formulation of 5-fluorocytosine in suicide gene therapy with cytosine deaminase – for colorectal cancer. *Cancer Lett.* **2008**, *262*, 164–172.

***CHAPTER - 6***  
***OXALIPLATIN LOADED***  
***IN NOVEL MAGNETIC***  
***POLYMERIC NANOMATERIALS***



## 6.1 INTRODUCTION

Cis-oxalato (trans-1-1-2-diaminocyclohexane) platinum (II) and its optical enantiomer cis-oxalato(trans-d-1,2-diaminocyclohexane) platinum (II) and any mixture of these two enantiomers is referred to as oxaliplatin, which is a third generation platinum based anti-cancer drug [1]. It is denoted as L-OHP or OHP, which shows better *in vitro* and *in vivo* efficacy against many tumor cell lines which are even resistant to the most common platinum containing anticancer drugs, namely, cisplatin (first generation) and carboplatin (second generation) [2]. The presence of bulky 1, 2-diaminocyclohexane (DACH) carrier ligand in oxaliplatin is reported to form platinum - DNA adducts, which blocks DNA replication more effectively. These adducts are more cytotoxic than those formed by cisplatin. The cyclohexyldiamine group of oxaliplatin improves antitumor activity and the oxalato bidentate ligand renders water solubility. Thus better solubility and a decreased likelihood of development of resistance makes oxaliplatin a good candidate for first-line therapy. Further in the blood plasma it rapidly undergoes non-enzymatic transformation into reactive compounds because of displacement of the oxalate group. This process complicates its pharmacokinetic profile. Though most of the metabolites do not exhibit pharmacological activity, but dichloro(1,2-diaminocyclohexane) platinum(II) complexes enters the cell and display cytotoxicity [1]. However, like other anticancer drugs it is also associated with a range of side-effects like acute dysesthesias, cumulative peripheral distal neurotoxicity [3–5] that limits the range of usable doses. Further this drug also shows high *in vivo* partitioning to erythrocytes [5]. Therefore to improve the efficacy and reduce its side effects, different approaches are reported, which includes encapsulation of drug in microspheres, liposomes, micelles and nanoparticles [6–12].

The main advantages associated with the encapsulation of the drug substance within nanomaterials includes the possibility of decreasing the toxicity of the drug, prolongation of the plasma half-life of the drug which is ~ 14.1 minutes, targeting to specific molecules or structures in the body or having a triggered drug release induced by acid, light, heat or enzymes [13-15]. The site specific targeting and delivery of drug, especially at tumor sites has been a major challenge in the cancer therapy. In this regard, several approaches are being evaluated including the concept of engineered magnetic nanocarriers. The drug loaded in the magnetic nanocarriers can be magnetically guided to the tumor site and delivered locally for efficient therapy. This will provide therapeutic concentrations while minimizing toxicity by non specific biodistribution at normal tissues. It is important to note that this

drug does not result in nephrotoxicity as it exhibits higher urinary excretion as compared to cisplatin and carboplatin [3, 4]. The pharmacokinetic profile of oxaliplatin showed high clearance rates, high volume of distribution and faster elimination of this drug as compared to cisplatin. Further, it has also been reported that ~ 85 % of oxaliplatin present in plasma binds to proteins and ~ 37 % of the oxaliplatin administered is sequestered in the erythrocytes within 2 - 5 hours. In this regard a targeted drug delivery system of this drug would not only improve its therapeutic action but also minimize its toxicity towards normal cells.

### 6.1.1 Objective of our work

Superparamagnetic iron oxide nanoparticles coated with polysaccharide is found to be efficient recipe for fabrication of magnetic responsive nanomaterial based targeted drug delivery system.

(1) It occurred to us that fabrication of oxaliplatin (OHP) loaded in nanomaterials of calcium pectinate with encapsulated magnetite nanoparticles could be useful for developing efficient nanomaterials of platinum based targeted drug delivery system for cancer therapy. In addition, magnetite nanoparticle encapsulated in nanomaterials of pectin re-inforced with chitosan, which showed improved drug loading efficiency for diclofenac sodium (as discussed in chapter 4), was used for OHP loading and evaluated for drug for potential drug delivery system.

(2) Characterization of these two types of novel nanomaterials by XRD, SEM, TEM, DLS, Zeta potential, VSM and SQUID magnetometry. To elucidate their applicability towards potential targeted drug delivery these nanomaterials were studied for their *in vitro* drug release in phosphate buffer with pH 5.5 and 7.4. Furthermore, their *in vitro* cytotoxicity in cancer cell lines was assayed.

## 6.2 MATERIALS AND METHODS

### 6.2.1 Materials

In addition to the materials required for fabricating magnetite nanoparticles coated with pectin as discussed in Chapter 2, Oxaliplatin was procured from Sigma-Aldrich GmbH, Germany. The calcium hydroxide used for fabrication of nanomaterials and platinum standard used for the calibration of ICPMS were procured from Merck, India. All other materials required in this study were similar to those as discussed in the previous chapters.

The phosphate buffer solution pH 5.5 and phosphate buffer solution pH 7.4 were prepared as discussed in chapter 3. Further, the cytotoxicity study was performed at ACTREC, Mumbai, a recognized laboratory for in vitro studies in cancer cell lines. The chemical and other materials needed for the study were provided by ACTREC.

### 6.2.1.1 Oxaliplatin

#### *Physical and chemical properties*

The chemical structure of oxaliplatin is given in Fig. 6.1. Its molecular weight is 397.3 g/mol. It is an odorless white crystalline powder with the Pt content of 48.0 - 50.0%. Its solubility in water is reported to be ~6 mg/mL (at 20 °C), ~20 mg/mL in DMSO at 20 °C [16]. It exhibits poor solubility in methanol, almost insoluble in ethanol and acetone.

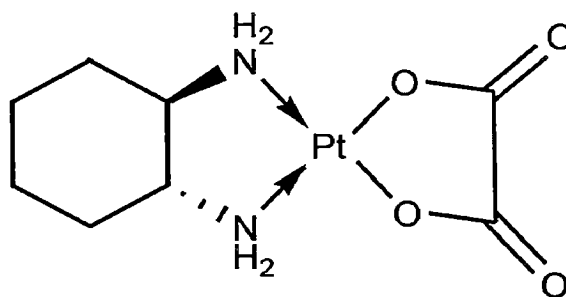


Fig. 6.1 Structure of oxaliplatin

#### *Pharmacology*

Oxaliplatin is an antineoplastic drug belonging to a new generation of platinum-based compounds, which contains a platinum atom complexed with oxalate and 1,2-diaminocyclohexane. Unlike other platinum-based agents, oxaliplatin shows clinical activity in colorectal cancer and for metastatic pancreatic cancer [17].

#### *Mechanism of action*

The cytotoxicity of oxaliplatin is in general based on apoptosis mechanism. Its anticancer activity as reported in pancreas cancer cell line, can be attributed to DNA damage similar to those reported for other platinum-based compounds [1]. Apoptosis may occur due to formation of DNA lesions, arrest of DNA synthesis, inhibition of RNA synthesis, and triggering of immunologic reactions [1]. Further the formation and aquation of Dichloro (1,2-diaminocyclohexane) platinum(II) complexes compounds takes place at intracellular physiological concentrations of  $\text{HCO}_3^-$  and  $\text{H}_2\text{PO}_4^-$  ions. This compound then enters the cell nucleus, with a peculiar tropism for sites rich in guanine-

cytosine. It is reported to bind with the seventh nitrogen atom of guanine which leads to the formation of DNA monoadducts, and then diadducts [18]. These adducts which are formed in nucleosomes can also inhibit the cell division. The drug can induce 3 types of cross links with DNA, namely DNA intra-strand cross links, DNA inter-strand cross links and DNA-protein cross links. But the intra-strand cross links is probably the main mechanism of action in the induction of DNA lesions (DNA damage and repair), with binding of two guanine (Gs) or less frequently, a guanine-adenine (G–A) base pair [18].

#### *Method of administration*

The drug oxaliplatin is administered by the *i.v.* (intravenous) route. The various marketed product of oxaliplatin are:

- a) Eloxatin<sup>®</sup> marketed by Sanofi Synthelabo (France) under the given trademark. The Eloxatin<sup>®</sup> is available as:
  - I. Eloxatin powder, for solution for intravenous use.
  - II. Eloxatin injection, solution, concentration for intravenous use.
- b) Oxaliplatin Pliva (Pliva Croatia Ltd., Republic of Croatia) powder for solution for infusion, is a white freeze-dried powder. It is a sterile lyophilized product marketed in two presentations, 50 mg/vial and 100 mg/vial. Oxaliplatin Pliva is reconstituted with 10 mL or 20 mL solvent (water for injection or 5 % glucose) to obtain 5 mg/mL of oxaliplatin.

Further a Folfox regimen is also reported for a combination of oxaliplatin-5 Fluorouracil-folinic acid which is used for the treatment of colorectal cancer.

#### *Side effects*

Oxaliplatin causes adverse reactions that narrow its therapeutic index. The target organs are mainly the hematopoietic system, the peripheral nerves, and the gastrointestinal (GI) system. Oxaliplatin is moderately myelotoxic [1]. Commonly it leads to grades 3 and 4 neutropenia, but the incidence of neutropenic fever is only ~ 4 % [19]. The hemolytic anemia and secondary immune thrombocytopenia are observed but usually it is not severe. Sometimes it also leads to secondary acute leukemia. Its prominent toxic effect is acute or chronic peripheral neuropathy of the characteristics of peripheral sensory nerve lesions. It is associated with oral around the upper respiratory (usually laryngeal) and digestive tract spasms and sensory dysfunction. Mild to moderate nonspecific toxic

effects of oxaliplatin on the rapidly dividing cells of the GI tract are also observed. This leads to nausea, vomiting, and diarrhoea.

### **6.2.2 Method for fabrication of nanomaterials of magnetite-pectin cross linked with $\text{Ca}^{2+}$ loaded with OHP and magnetite-pectin reinforced with chitosan loaded with OHP**

Two types of OHP loaded nanomaterials were fabricated based on the selection of polysaccharide as a coating agent e.g. pectin and pectin reinforced with chitosan.

#### **6.2.2.1 Method for fabrication of nanomaterials of magnetite-pectin cross linked with $\text{Ca}^{2+}$ ions loaded with OHP**

5 mg of oxaliplatin (OHP) was mixed with 2.5 mL of Millipore water to prepare 2.0 mg/mL stock solution of OHP. 250  $\mu\text{L}$  of this stock solution was mixed with 5 mL of 0.4 % w/v pectin solution and stirred for 1 h. To this mixture, 5 mL of as-synthesized dispersion of MNPs, conditioned at pH  $\sim$  4 was added and stirred for 1 h. The acidic pH was maintained by adding dilute  $\text{H}_2\text{SO}_4$ . Here dilute HCl was not used as oxaliplatin in presence of chloride ions ( $\text{Cl}^-$ ) form an inactive precipitate of 1, 2-diaminocyclohexane platinum(II) [20]. For the same reason calcium chloride ( $\text{CaCl}_2$ ) solution was not used for cross linking with pectin, instead it was cross linked by 0.8 % w/v solution of calcium hydroxide  $\text{Ca}(\text{OH})_2$  as reported by Yu *et al.* [21]. The whole mixture was stirred for 6 h. This nanomaterial will be referred to as MP-OHP (Table 6.1).

#### **6.2.2.2 Method for fabrication of nanomaterials of magnetite-pectin reinforced with chitosan loaded with OHP**

The fabrication of MPCh-OHP was performed using the optimum condition as discussed for synthesizing MPCh-DS in chapter 4. A 250  $\mu\text{L}$  of stock solution of oxaliplatin (OHP) was mixed in 5 mL of 0.025 % w/v chitosan solution, where chitosan was dissolved in dilute acetic acid. To this solution, 5 mL 0.4 % pectin solution mixed with MNPs at pH  $\sim$  4 was added. The mixture was stirred for 6 h to facilitate cross linking of pectin with chitosan. This nanomaterial will be referred to as MPCh-OHP (Table 6.1).

**Table 6.1.** % Encapsulation efficiency (mean  $\pm$  SD; SD = standard deviation) measured from triplicate analysis in MP-OHP and MPCh-OHP.

| Batch code | Pectin (% w/v) | Ca(OH) <sub>2</sub> (% w/v) | Chitosan (% w/v) | % Encapsulation Efficiency |
|------------|----------------|-----------------------------|------------------|----------------------------|
| MP-OHP     | 0.4%           | 0.8%                        | Nil              | 55.20 $\pm$ 1.23           |
| MPCh-OHP   | 0.4%           | Nil                         | 0.025%           | 50.92 $\pm$ 1.52           |

*Note: The volume of magnetite dispersion was kept constant for all the batches.*

### 6.2.3 Methodology for drug loading analysis

As mentioned in the drug loading protocols, the dispersion obtained after the synthesis of MP-OHP and MPCh-OHP comprised free dissolved drug and drug loaded in nanomaterials. The drug loaded in the nanomaterials would therefore be difference of total drug taken for fabrication and the amount of free dissolved drug in the dispersion i.e.

Loaded drug content = Initial amount of the drug taken – amount of free dissolved drug.

(Notably, initial amount of drug taken was 500  $\mu$ g)

The concentration of free dissolved drug in the dispersion was determined by the bulk equilibrium reverse dialysis as discussed in chapter 3. The concentration of the drug present inside the dialysis bag was measured by ICPMS. The detail of drug analysis is discussed in section 6.2.6.

The drug loading content (wt %) in MP-OHP and MPCh-OHP nanomaterials was calculated as:

$$\text{Drug loading content (wt \%)} = (a / b) * 100$$

a = amount of the drug loaded in MP-OHP or MPCh-OHP nanomaterial.

b = weight of fabricated MP-OHP or MPCh-OHP nanomaterial.

Drug incorporation was expressed in terms of % encapsulation efficiency of OHP, which is given as:

$$\% \text{ Encapsulation efficiency} = (a / t) * 100$$

a = amount of the drug loaded in MP-OHP or MPCh-OHP nanomaterial.

t = Initial amount of the drug taken.

It may be noted here that, in the similar manner as discussed in chapter 2, the magnetite pectin nanomaterials cross linked with calcium which were fabricated using fixed concentration of the dispersion of MNPs, 0.4 % pectin and 0.8 % Ca(OH)<sub>2</sub>, without OHP will now be referred to as MP (magnetite nanoparticles: pectin cross linked with Ca<sup>2+</sup>). Further similar to that discussed in chapter 4, the magnetite pectin nanomaterials reinforced with chitosan which were fabricated using fixed concentration of the dispersion of MNPs,

0.4 % pectin, 0.025 % chitosan without OHP will now be referred to as MPCh (magnetite nanoparticles: pectin reinforced with chitosan).

#### 6.2.4 Characterization

The fabricated nanomaterials, MP-OHP and MPCh-OHP were characterized by an array of techniques, namely, XRD, SEM-EDAX, TEM, DLS, SQUID and VSM. The details of these are discussed in chapter 2 and 3.

#### 6.2.5 Methodology for *in vitro* drug release

The *in vitro* drug release study was based on the dialysis bag diffusion technique as discussed in chapter 3. Briefly, the *in vitro* release of OHP from the respective batches of MP-OHP and MPCh-OHP nanomaterials were performed by transferring these nanomaterials in respective dialysis bags containing 5 mL of freshly prepared phosphate buffer at pH 5.5 (without enzymes). This is referred to as donor compartment. This bag with its contents was then transferred to a beaker containing 20 mL of the buffer solution at pH 5.5 without enzymes (referred as receptor compartment) and gently stirred at 100 rpm for 40 h at  $37.0 \pm 0.1$  °C in an incubator shaker. The pH 5.5 was selected as it has been reported that the extracellular pH is slightly acidic in the vicinity of tumor tissues [22]. Further the pH of the proximal colon is also slightly acidic (pH 5.5 – 5.7) where this drug has been reported to be effective [23]. In the similar manner these studies were performed in phosphate buffer, at pH 7.4, without enzyme for 48 h to mimic the drug release from MP-OHP and MPCh-OHP in blood.

About 1.5 mL of an aliquot was withdrawn from the respective receptor compartments at each specified time periods and was replaced with equal volume of fresh medium to mimic the sink conditions of the human body. The aliquot was centrifuged at 15000 rpm for 15 minutes and the supernatant liquid consisting of released drug was analyzed.

#### 6.2.6 Drug analysis

As the drug oxaliplatin contains platinum (Pt), the drug analysis was performed by measuring corresponding Pt concentration in the drug. The Pt concentration was determined by inductively coupled plasma mass spectrometry (ICPMS, Perkin Elmer Sciex, Elan DRC-e). It is highly sensitive method for detecting inorganic elements of the order of ng/mL

(parts per billion). This method is based on ionization of analyte by plasma and subsequent determination of ionic species in terms of  $m/z$  ratio using mass spectrometry technique. In the plasma, almost all the positive ions are singly charged, thus  $m/z$  ratio essentially represent the mass of the singly ionized atoms. Unlike atomic absorption spectrometry, matrix effect in ICPMS is less. The drug concentration was determined from calibrating plot of Pt concentrations against different drug concentrations.

#### 6.2.6.1 Preparation of calibration curve for estimation of oxaliplatin

First the analysis of platinum concentration was calibrated by measuring 50, 100, 250, 500 and 750 ng/mL of standard platinum solution (Merck). The calibration curve showed a linear relation between standard Pt concentrations (ng/mL) and measured intensities (Fig. 6.2a;  $R^2 = 0.999$ ), indicated the suitability of measuring Pt by ICPMS method.

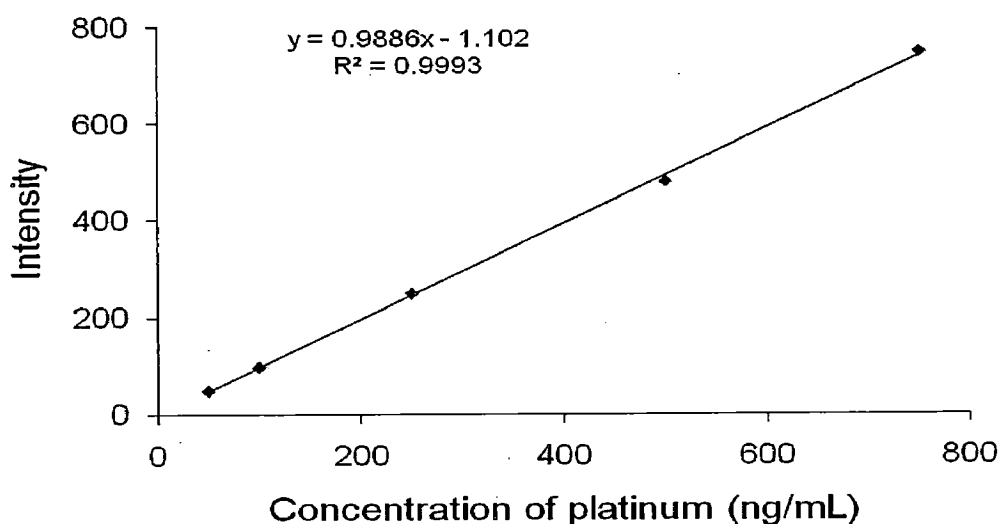


**Fig. 6.2a.** Calibration curve showing linear correlation between concentration of oxaliplatin (at pH 7.4) and Pt concentration measured by ICPMS analysis. The results are given as mean  $\pm$  SD; (SD = standard deviation calculated from triplicate measurements).

Further, a calibration curve for estimating drug concentration was plotted by measuring Pt concentration by ICPMS against known drug concentrations (Fig. 6.2b). A linear fit with  $R^2 = 0.993$  indicated the validity of the method for measuring drug concentration. All the experiments were performed in triplicate and results are given as mean  $\pm$  SD (SD= standard deviation).

The calibration plots for drug analysis were obtained in solutions (without any enzyme) at pH 5.5 and 7.4 and Millipore water. Stock solution of 10  $\mu\text{g/mL}$  of OHP in



phosphate buffer solution at pH 5.5 and 7.4 were prepared from the stock solution (2 mg/mL) by transferring 50  $\mu$ L of OHP solution to 10 mL volumetric flasks. The volume was made up to 10 mL with the phosphate buffer pH 5.5 and pH 7.4 respectively. From this stock solution, aliquots were taken and diluted to obtain OHP concentration of 200 ng/mL, 350 ng/mL, 500 ng/mL, 750 ng/mL and 1000 ng/mL. The calibration curve was prepared by recording the respective concentration of platinum in these solutions by ICPMS. The mean value and the standard deviations from triplicate analysis were calculated. The mean values of Pt concentrations were plotted against the respective concentration of OHP in pH 7.4 ranging between 200 and 1000 ng/mL to obtain a calibration curve (Fig. 6.2). Linear fit of the calibration curve ( $R^2 = 0.993$ ) was obtained. The calibration plot was used for estimating drug released in the in vitro condition from MP-OHP and MP-Ch-OHP at pH 7.4. In the similar manner calibration curve for estimating OHP in pH 5.5 was prepared. Linear fit of the calibration curve ( $R^2 = 0.998$ ) was obtained with the corresponding equation of  $y = 0.3842x - 42.26$ , which was used for estimating in vitro drug release at pH 5.5. Similarly calibration curve for estimating OHP in Millipore water was prepared. Linear fit of the calibration plot ( $R^2 = 0.999$ ) was obtained with the corresponding equation of  $y = 0.3747x - 37.40$ , which was used for estimating drug loading efficiency.

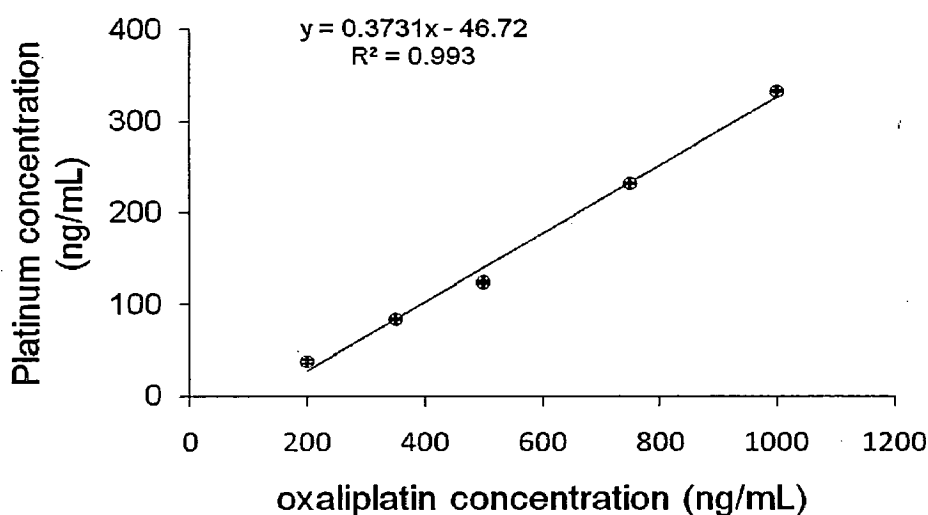


**Fig. 6.2b** Calibration curve showing linear correlation between concentration of oxaliplatin (in pH 7.4) and Pt concentration measured by ICPMS analysis. The results are given as mean  $\pm$  SD; (SD = standard deviation calculated from triplicate measurements).

### 6.2.7 SRB assay for cytotoxicity studies in cancer cell lines

The cytotoxicity of the MP-OHP was evaluated using the sulforhodamine B (SRB) dye assay on the cancer cell lines of HT-29 (colon) and MIA-PA-CA-2 (pancreas) as discussed in chapter 5.

## 6.3 RESULTS AND DISCUSSION

### 6.3.1 Drug loading efficiency

It was noted from Table 6.1 that the batches of MP-OHP synthesized using pectin solution of 0.4 % w/v and 0.8 % w/v  $\text{Ca}(\text{OH})_2$  with 500  $\mu\text{g}$  of initial amount of drug resulted in  $\sim 55.20 \pm 1.23$  % encapsulation efficiency. On the other hand, the batch synthesized using 0.4 % w/v pectin solution cross linked with 0.025 % w/v chitosan solution exhibited  $\sim 50.92 \pm 1.52\%$  encapsulation efficiency. Though the % encapsulation efficiency is quite high as compared to those discussed with MP-5FU yet very low drug content was present ( $\sim 1.0$  % w/w).

### 6.3.2 X-ray diffraction study

The formation of as-synthesized stable MNPs were confirmed by recording the position and relative intensities of diffraction patterns at 220, 311, 400, 511 and 440 planes (Fig. 6.3) which corroborated well with those of cubic magnetite ( $\text{Fe}_3\text{O}_4$ ) structures as reported in JCPDS 01-11111. These characteristic XRD peaks were also observed in the X-ray diffractogram of MP-OHP and MPCh-OHP, which confirmed the incorporation of magnetite nanoparticles (MNPs) in these batches.

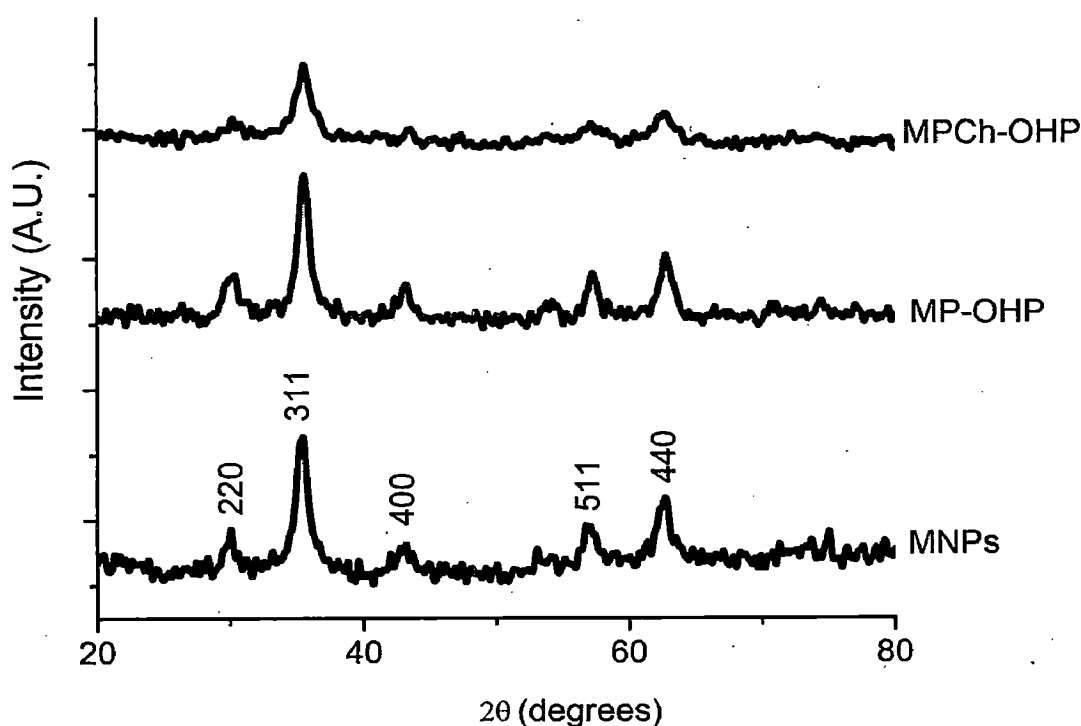


**Fig. 6.3.** XRD of the MNPs synthesized by coprecipitation method, MP-OHP and MPCh-OHP nanomaterials.

### 6.3.3 Morphological studies

The morphology of these nanomaterials of MP-OHP and MPCh-OHP were studied by SEM-EDAX and TEM. A representative SEM image of MP-OHP showed formation of large number of spherical nanomaterials, with size distribution in the range of 100 - 200 nm (Fig. 6.4a). The energy dispersive X-ray analysis (EDAX) of a nanomaterial (marked in the Fig 6.4b) clearly showed the characteristic X-ray peaks of Fe, indicating that the magnetite nanoparticles were present in the nanomaterials. The corresponding X-ray peaks of Pt were not observed in the X-ray spectrum from EDAX study due to very low concentration of Pt in these nanomaterials which were much below the detection limits of EDAX. However, the characteristic K X-ray peaks of Fe (6.39 keV) and Ca (3.63 keV) confirmed that the MNPs were encapsulated in these nanomaterials. Similarly the SEM analysis of MPCh-OHP also revealed spherical shaped nanomaterials of 100-200 nm size (Fig. 6.5). The TEM image of MP-OHP (Fig. 6.6) and MPCh-OHP (Fig. 6.7) were reasonably similar, which revealed spherical shape of the nanomaterials. The sizes of these nanomaterials in dry condition was about 100 – 200 nm, which were similar to those of MP-5FU discussed in the previous chapter. The TEM image of MP-OHP and MPCh-OHP (Fig. 6.6 and Fig. 6.7 respectively) also revealed 100 – 150 nm spherical shaped nanomaterials and corroborated with the SEM results. The corresponding SAED image confirmed the presence of polycrystalline MNPs encapsulated in the MP-OHP (Fig. 6.6) and MPCh-OHP (Fig 6.7) nanomaterials respectively.

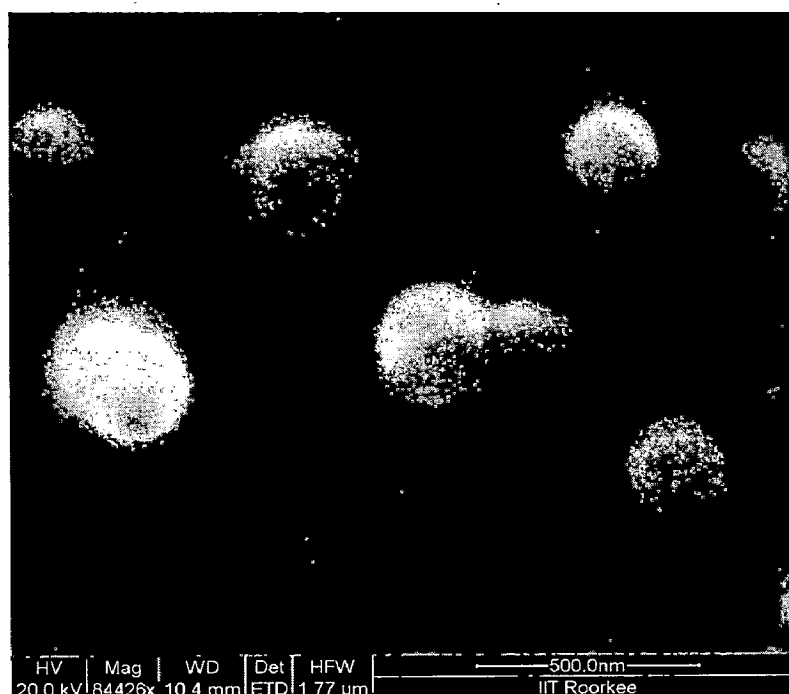


Fig. 6.4a. Scanning electron microscopy of MP-OHP nanomaterials.

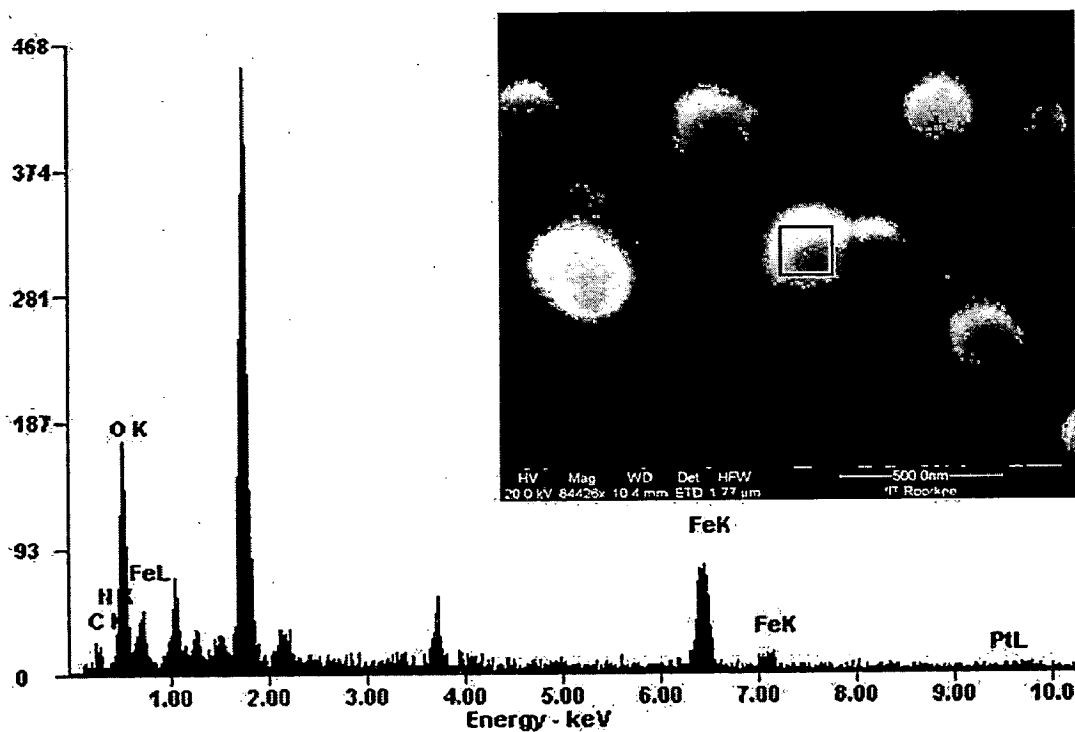


Fig. 6.4b. Scanning electron microscopy energy dispersive X-ray analysis (EDAX) of the marked nanomaterial showing the occurrence of magnetite nanoparticles in MP-OHP nanomaterials.

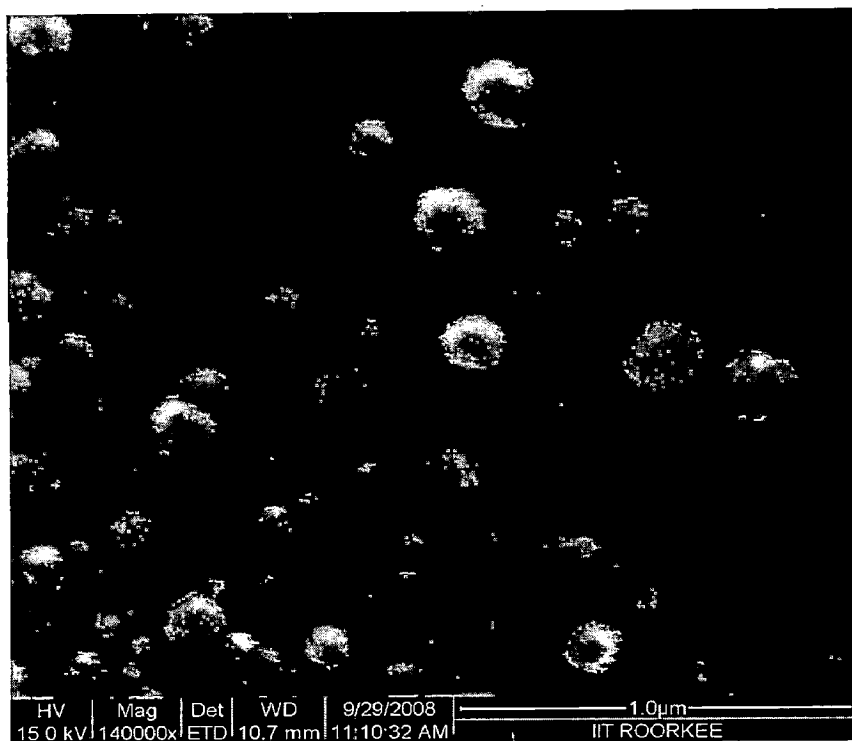
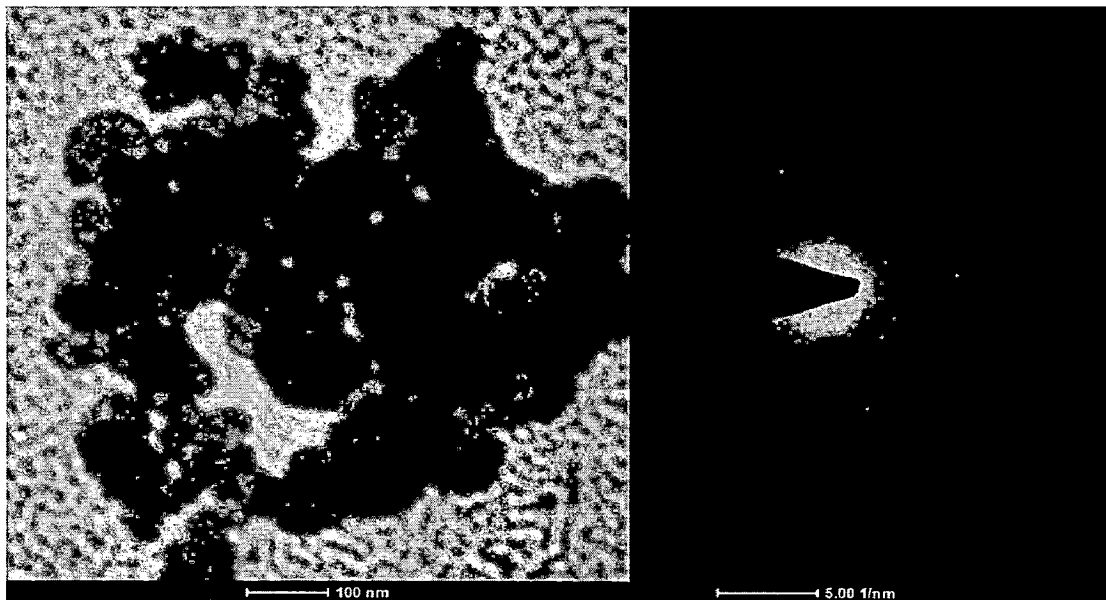
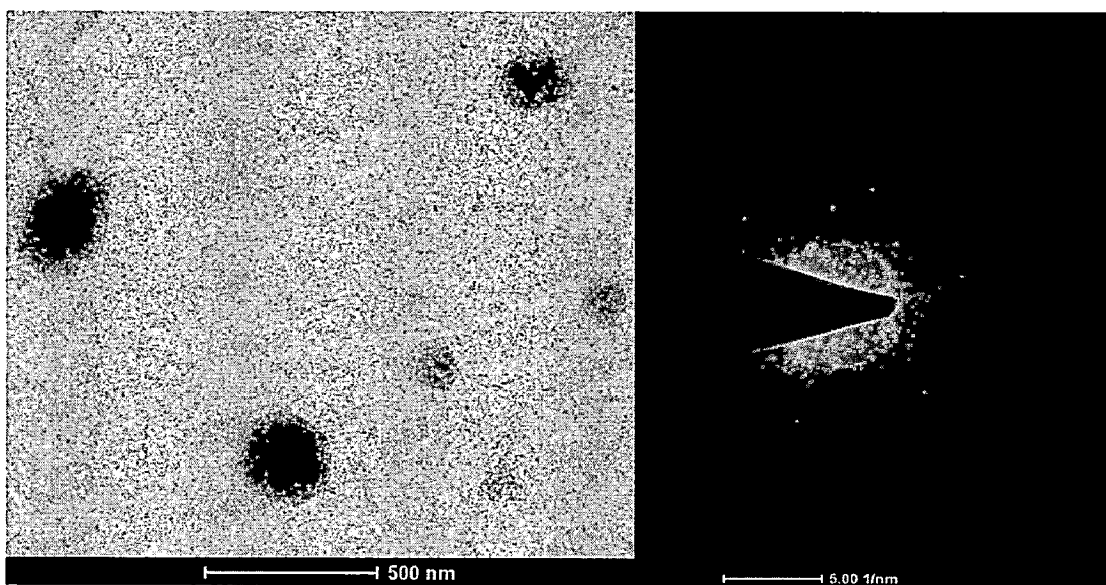


Fig. 6.5. Scanning electron microscopy of MPCh-OHP nanomaterials.



**Fig. 6.6.** TEM of MP-OHP nanomaterials and selected area electron diffraction (SAED) image of MP-OHP showing the presence of polycrystalline MNPs and OHP.



**Fig. 6.7.** TEM of MPCh-OHP nanomaterials and selected area electron diffraction (SAED) image of MPCh-OHP showing the presence of polycrystalline MNPs and OHP.

The size distribution of the MP-OHP and MPCh-OHP was also measured by dynamic light scattering (DLS) measurement, where the nanomaterials were dispersed in aqueous solution at pH  $\sim$  4. The DLS measurement exhibited unimodal size distribution with an average size of  $\sim$  320 - 350 nm for both MP-OHP and MPCh-OHP (Fig. 6.8 and 6.9 respectively), indicating that the method of synthesis of these nanomaterials offered a good control over their sizes. However, the size distribution obtained from DLS measurements were nearly two folds higher than that measured by SEM and TEM studies. The increase in

the sizes of MP-OHP as well as MPCh-OHP nanomaterials could be attributed to the swelling effect of pectin in aqueous medium [21].

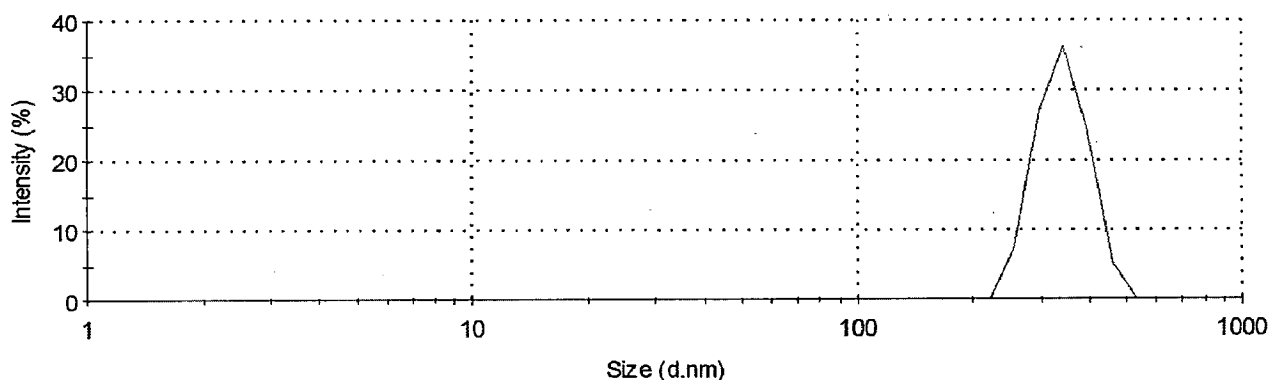


Fig. 6.8. DLS measurement of MP-OHP nanomaterials in aqueous solution at pH ~ 4.

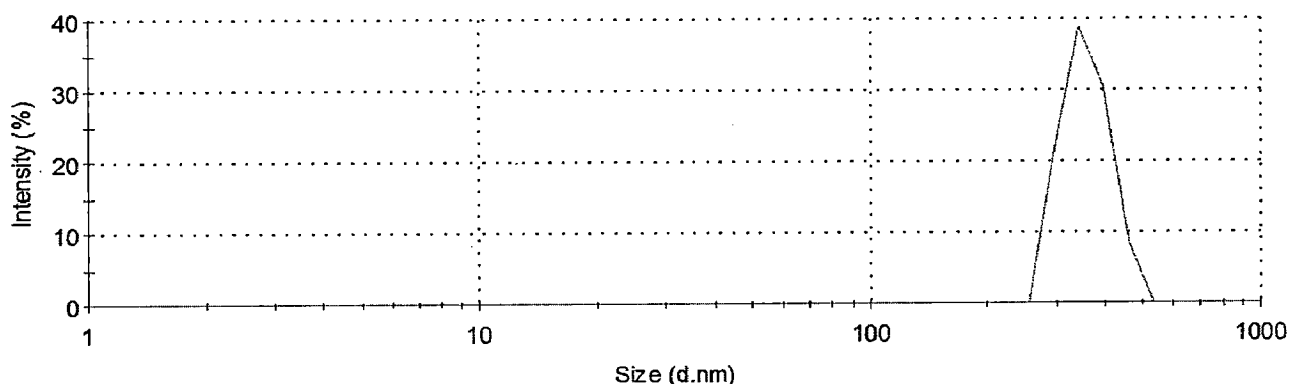


Fig. 6.9. DLS measurement of MPCh-OHP nanomaterials in aqueous solution at pH ~ 4.

### 6.3.4 Zeta potential measurements

The zeta ( $\xi$ ) potential of the as-synthesised MNPs at pH ~ 10 and at pH ~ 4 was measured to be -40.7 mV and +17.6 mV respectively, which were similar to the zeta potential measurements discussed in chapter 2. Pectin at pH ~ 4 was -36.1 mV, chitosan at pH ~ 4 was +113.8 mV and that of the OHP was -35.2 mV at pH ~ 4. Further the MP-OHP system showed zeta values of -30.5 mV which indicated that the fabricated nanomaterials were stable (Table 6.2) as zeta potentials more than  $\pm 25$  mV are considered to be stable [24]. Similarly, MPCh-OHP showed zeta potential of -22.8 mV and can also be considered to be stable. It may be envisaged that, at pH ~ 4, OHP ( $\xi = -35.2 \pm 1.2$ ) would interact electrostatically with chitosan ( $\xi = +113.8 \pm 1.5$ ) and with pectin reinforced with chitosan, and the polymer can subsequently be cross linked to form a complex network structure carrying drug.

**Table 6.2.** Zeta potential measurements of oxaliplatin (OHP), magnetite pectin cross lined with Ca<sup>2+</sup> loaded with OHP (MP-OHP) and magnetite pectin reinforced with chitosan loaded with OHP (MPCh-OHP).

| Batches           | Measured zeta potential value ( $\zeta$ ) in mV |
|-------------------|---|
| MNPs (pH ~ 10)    | - 40.7  |
| MNPs (pH ~ 4)     | +17.6   |
| Pectin (pH ~ 4)   | - 36.1  |
| Chitosan (pH ~ 4) | +113.8  |
| OHP               | - 35.2  |
| MP-OHP            | - 30.5  |
| MPCh-OHP          | - 22.8  |

### 6.3.5 Magnetic studies

The magnetic behavior of the MP-OHP and MPCh-OHP nanomaterial was studied by recording its magnetization curve (M-H curve) from VSM measurement recorded at room temperature. The M-H curves for MP-OHP and MPCh-OHP exhibited negligible coercivity as well as negligible remanence magnetization (as given in Fig. 6.10 and Fig. 6.11 respectively), which were similar to that of the as-synthesized MNPs. This phenomenon was attributed to superparamagnetic behaviour of MNPs. The saturation magnetization ( $M_s$ ) measured at room temperature between  $\pm 10$  kOe for MNPs, MP and MP-OHP were 55.69 emu/g, 47.64 emu/g and 45.65 emu/g respectively (Fig. 6.10). Similarly in the case of MPCh-OHP and MPCh the saturation magnetization ( $M_s$ ) measured at room temperature between  $\pm 10$  kOe was 42.46 emu/g and 45.51 emu/gm respectively (Fig. 6.11). The decrease in the saturation magnetization in the OHP loaded batches (MP-OHP and MPCh-OHP) was attributable to the formation of magnetic dead layer by nonmagnetic material at the domain boundary wall of MNPs [25, 26] in the fabricated MP-OHP and MPCh-OHP nanomaterials. These non magnetic components are calcium pectinate and pectin reinforced with chitosan respectively for MP-OHP and MPCh-OHP nanomaterial. This could hinder the domain wall motion during application of the magnetic field, which might be responsible for the reduction in the saturation magnetization in these formulations.

Further the superparamagnetic magnetic behavior of the MP-OHP nanomaterials was ensured from the FC-ZFC measurements recorded between 5 and 300 K using zero-field cooling (ZFC) and field cooling (FC) in an applied magnetic field of 100 Oe (Fig. 6.12). The

curves diverged at 78.20 K, characterized as blocking ( $T_B$ ) temperature, which corresponded to the transition from ferromagnetic to superparamagnetic behavior

In the ZFC curve, without applied magnetic field, when the sample was cooled to 5 K the total magnetization was  $\sim 4.97$  emu/g (Fig. 6.12). Such lower magnetization may be attributed to the random orientation of the magnetic moments of individual particles due to particles of sizes less than 20 nm sizes [27]. As the temperature was increased more particles reoriented their magnetic moment (magnetization). Due to this the magnetization increased till it reached a maximum value of 78.20 K as shown in the ZFC curve. On the other hand, the magnetization measured at 5 K and in the presence of 100 Oe in the FC curve was 15.74 emu/g. The externally applied magnetic field energetically favored the reorientation of the individual magnetic moment which resulted in the increase in magnetization along the direction of the applied field. Such a behavior was characteristic of superparamagnetism typically observed in small ferromagnetic or ferrimagnetic nanoparticles. Below  $T_B$ , the MP-OHP nanoparticles exhibit ferromagnetic properties. When the temperature is above  $T_B$ , the thermal energy overcomes the anisotropy barrier and randomizes the magnetic moment, leading to the superparamagnetic behavior of the nanoparticles [28].

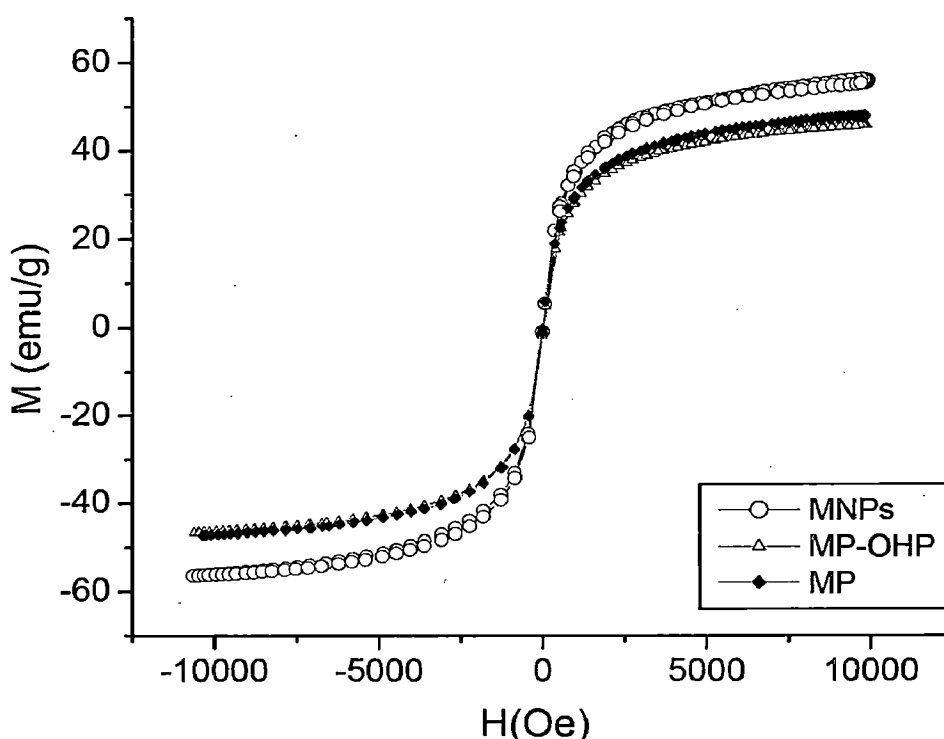


**Fig. 6.10.** Magnetization vs field (M-H) curve of MNPs, MP (without drug) and MP-OHP nanomaterials measured by VSM at room temperature.



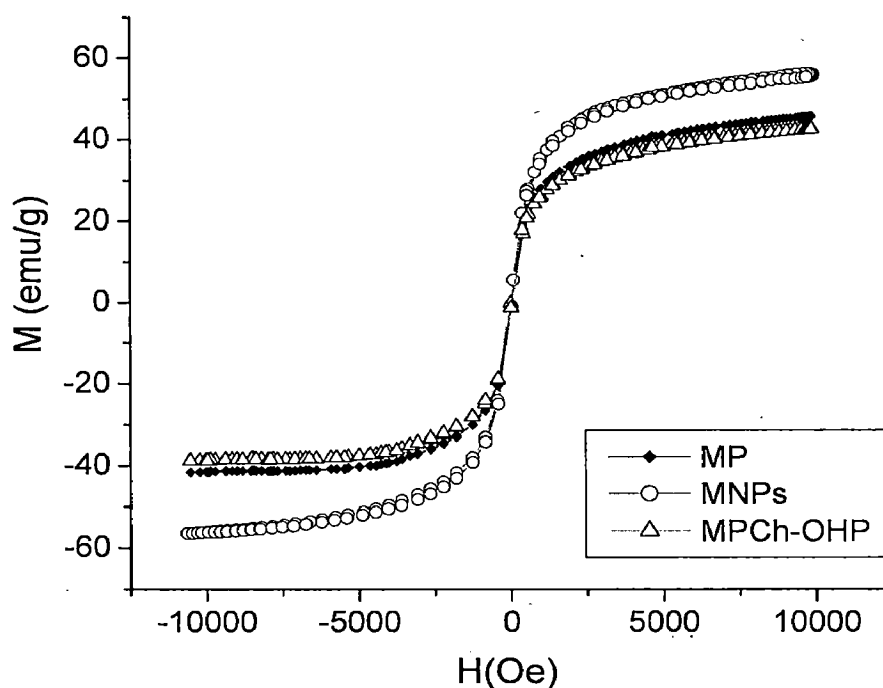


**Fig. 6.11.** Magnetization vs field (M-H) curve of MNPs, MP (without drug) and MPCh-OHP nanomaterials measured by VSM at room temperature.

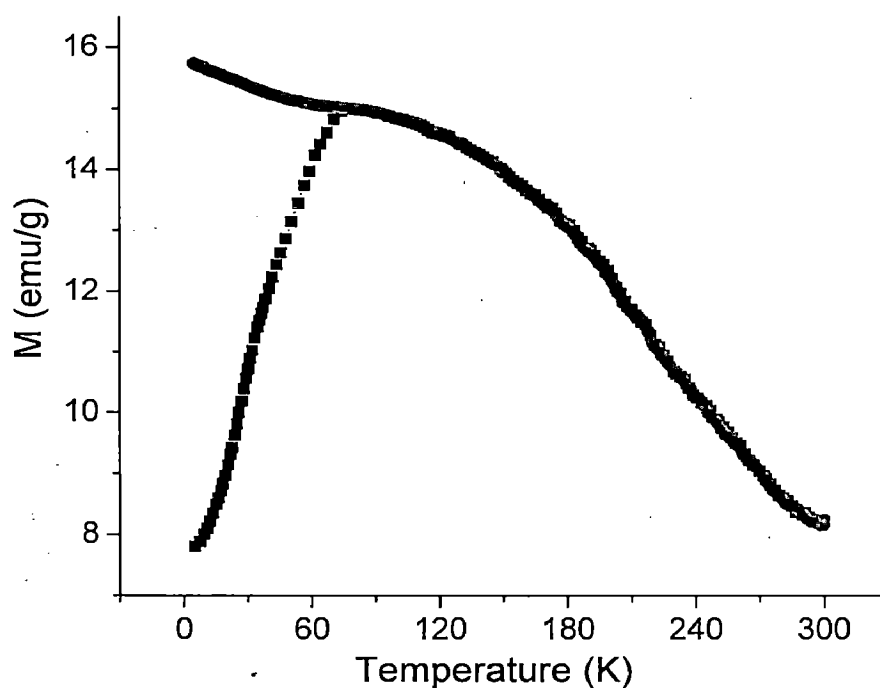


**Fig. 6.12.** ZFC and FC curve of MP-OHP nanomaterials recorded at 100 Oe, measured by SQUID.

### 6.3.6 *In vitro* release studies of MP-OHP and MPCh-OHP

Though polysaccharides are preferred matrices for loading drug, but low molecular weight drugs loaded in polysaccharides have burst release tendency [21]. This is primarily due to high water contents in the polysaccharide based matrices which facilitates high drug

solubility. However, it is envisaged that a sustained release property could be achieved by modifying the polysaccharide especially by cross linking, so that the modified polysaccharide can hold – back the drug in its network structure and assist in releasing the drug in a sustained manner. In the case of MPCh-OHP nanomaterial, the pectin was reinforced with chitosan, which showed ~ 51 % of drug encapsulation efficiency (Table 6.1). Similarly the loading efficiency of OHP in magnetite-calcium pectinate nanomaterial was ~55 % (where pectin composition was same as in the batch of MPCh-OHP). In order to elucidate the potential applications of these drug loaded nanomaterials (MPCh-OHP and MP-OHP) for its sustained release ability in colon or near to the tumor after injecting the nanomaterial dispersion injected intravenously, an *in vitro* drug release study was performed for 48 h at 37 °C in phosphate buffer solutions at pH 5.5 and pH 7.4 respectively.

A time dependent cumulative release of OHP from MPCh-OHP and MP-OHP was observed at pH 5.5 (Fig. 6.13 and 6.14 respectively). Notably, ~49 % and 23 % of OHP was released from MP-OHP and MPCh-OHP respectively, after 1 h interaction in phosphate buffer solution at pH 5.5 (Fig. 6.13 and Fig. 6.14 respectively). At this pH, 90 % of the total loaded OHP was released in 7 h from MPCh-OHP. While for the same release condition, only 65 % of the loaded OHP was released from MP-OHP system. However, in 24 h about 85 % of OHP loaded in MP-OHP nanomaterial was released. So from our studies, it was surmised that MP-OHP nanomaterials exhibited better sustained release of OHP at pH 5.5.

At pH 7.4 the *in vitro* release of OHP from MPCh-OHP and MP-OHP nanomaterials (Fig. 6.15 and 6.16 respectively) after 1 h interaction showed 32 % and 19 % cumulative release of OHP respectively. These values were significantly lesser than those observed for the release studies at pH 5.5. Further after 7 h of interaction cumulative release of OHP from MPCh-OHP nanomaterials was ~ 72 % and that from MP-OHP nanomaterials was ~60 %. The remaining amount of OHP was released over a period of 48 h. Therefore it was noted that pH 7.4 offered better sustained release of OHP. *In vitro* release studies from MP-OHP system was found to be similar to the release studies of cis-platin from PLGA-PEG nanoparticles as reported by Dhar *et al.* [29].

The higher release of OHP at pH 5.5 was attributable to its higher solubility at this pH, which could facilitate diffusion based release of OHP from these nanomaterials [20]. The higher release condition observed for MPCh-OHP nanomaterial at pH 5.5 was due to the tendency of higher solubility of chitosan in acidic medium [30]. As a result the network structure of pectin reinforced with chitosan might tend to loosen and caused higher release.

Ssahul  
13-07-2012

194  
13/7/12

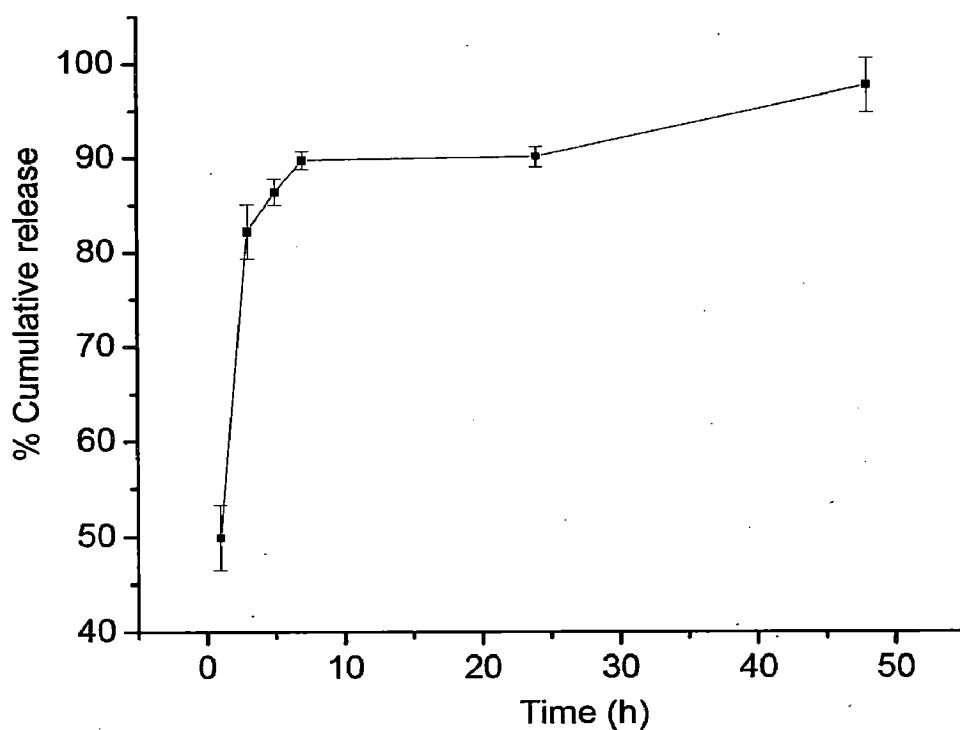


**Fig. 6.13.** In vitro release studies of the drug OHP for 48 h from MPCCh-OHP nanomaterials in phosphate buffer solution (pH 5.5)

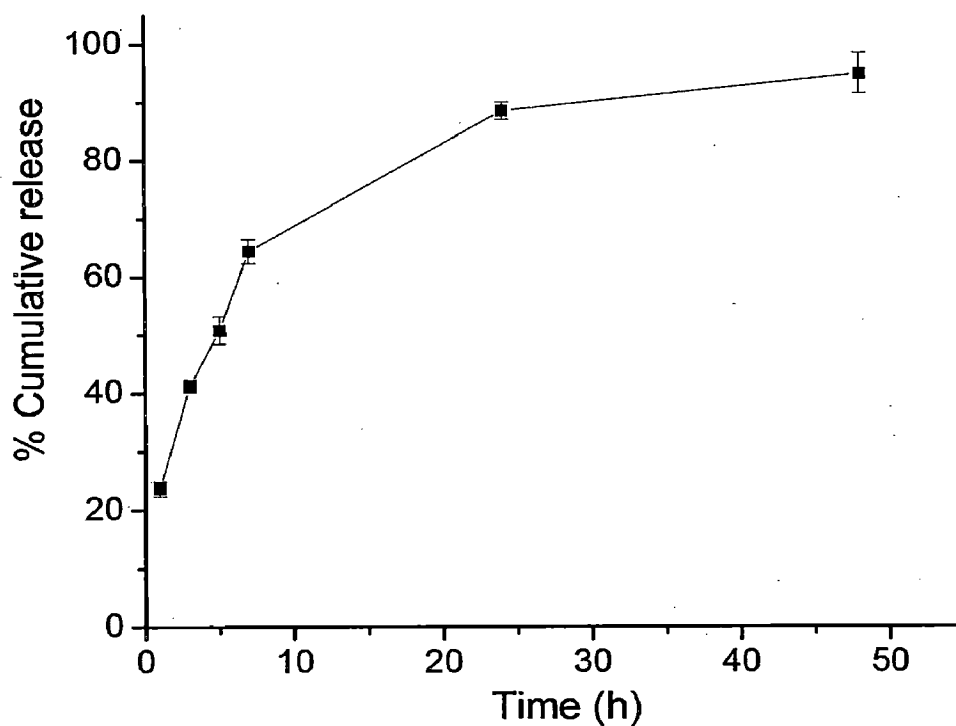


**Fig. 6.14.** In vitro release studies of the drug OHP for 48 h from MP-OHP nanomaterials in phosphate buffer solution (pH 5.5)

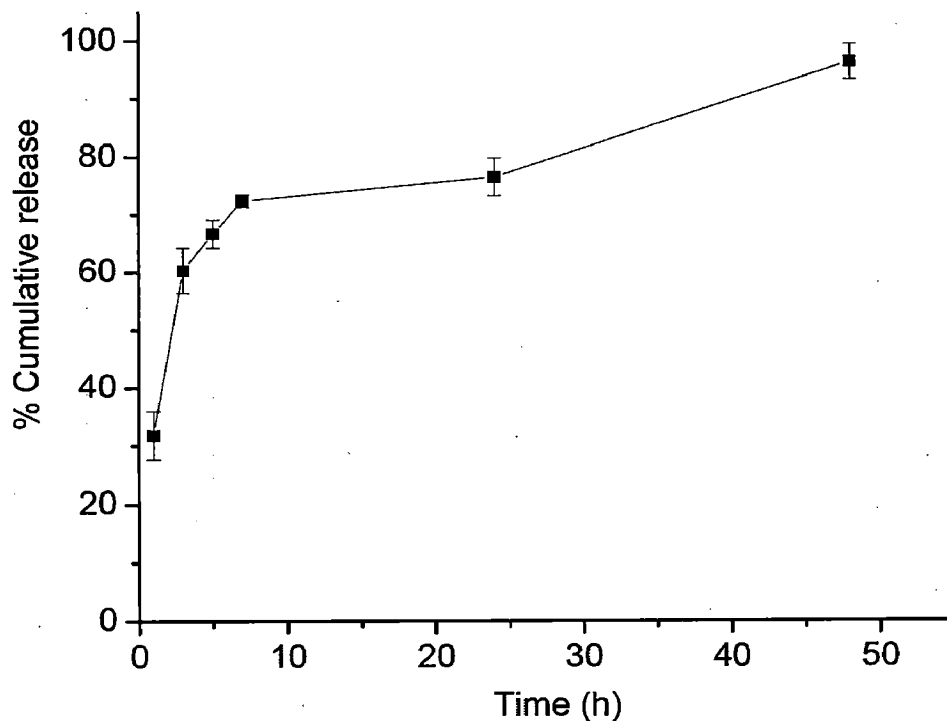


**Fig. 6.15.** In vitro release studies of the drug OHP for 48 h from MPCh-OHP nanomaterials in phosphate buffer solution (pH ~7.4)

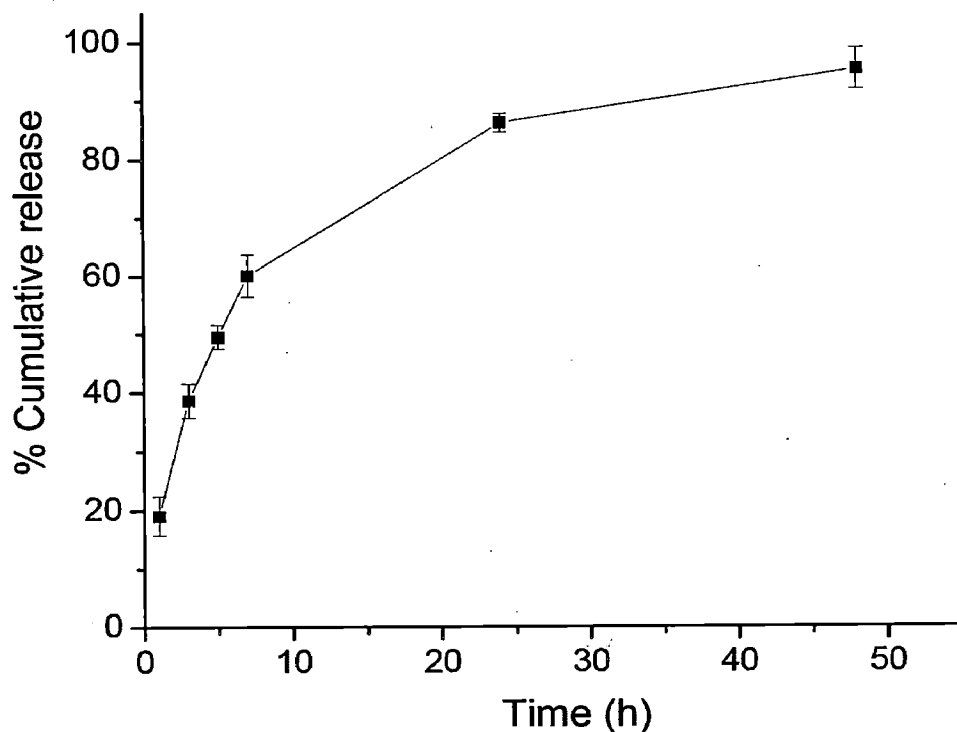


**Fig. 6.16.** In vitro release studies of the drug OHP for 48 h from MP-OHP nanomaterials in phosphate buffer solution (pH ~7.4)

### 6.3.6.1 Modeling of drug release

The *in vitro* release data obtained from the above studies were fitted using Korsmeyer - Peppas model as described in chapter 3, to establish the time dependent release mechanism of OHP.

The *in vitro* release data of OHP from MPCh-OHP in phosphate buffer at pH 7.4 up to 7 h (corresponding to 72 %) in log scale, exhibited a linear fit ( $R^2 = 0.951$ ) (Fig. 6.17). Here, the  $n = 0.4288$  which corresponded to diffusion based release mechanism according to Fickian transport [31]. The Fickian transport may be attributed to very low concentration of the encapsulated drug. In this case the value of  $k^*100$  (constant related to the structural and geometric characteristic of the device) was found to be 33.51.

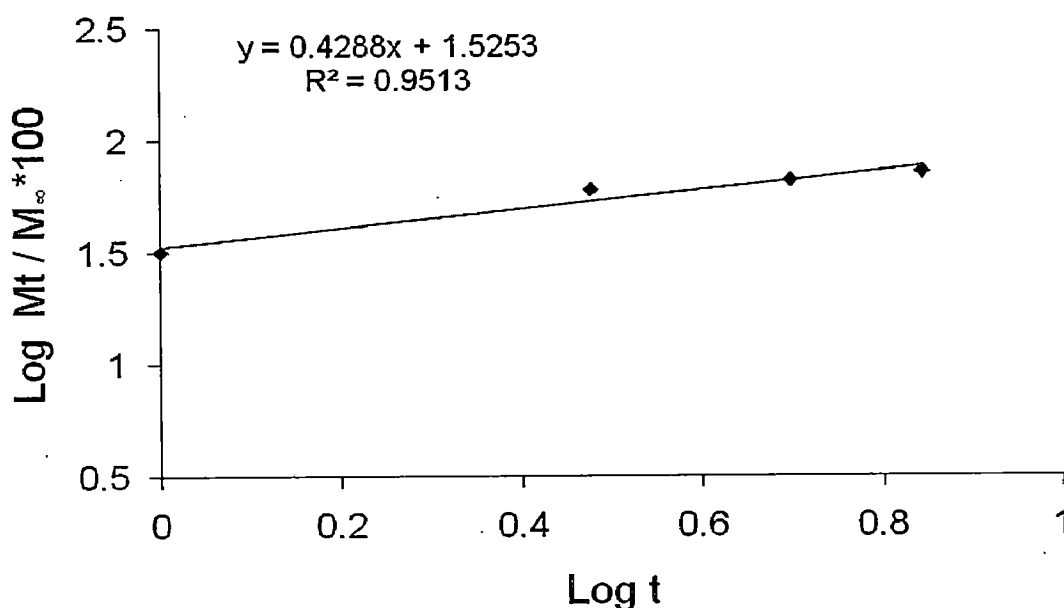


**Fig. 6.17.** Showing linear fit of *in vitro* release of OHP up to 7 h from MPCh-OHP in phosphate buffer solution (at pH 7.4), using Korsmeyer - Peppas equation in log scale.

On the other hand, the linear fit was not possible for the data obtained from the *in vitro* release of OHP from MPCh-OHP nanomaterials in phosphate buffer pH 5.5 up to 7 h (Fig 6.18). This was probably due to burst release of the drug.

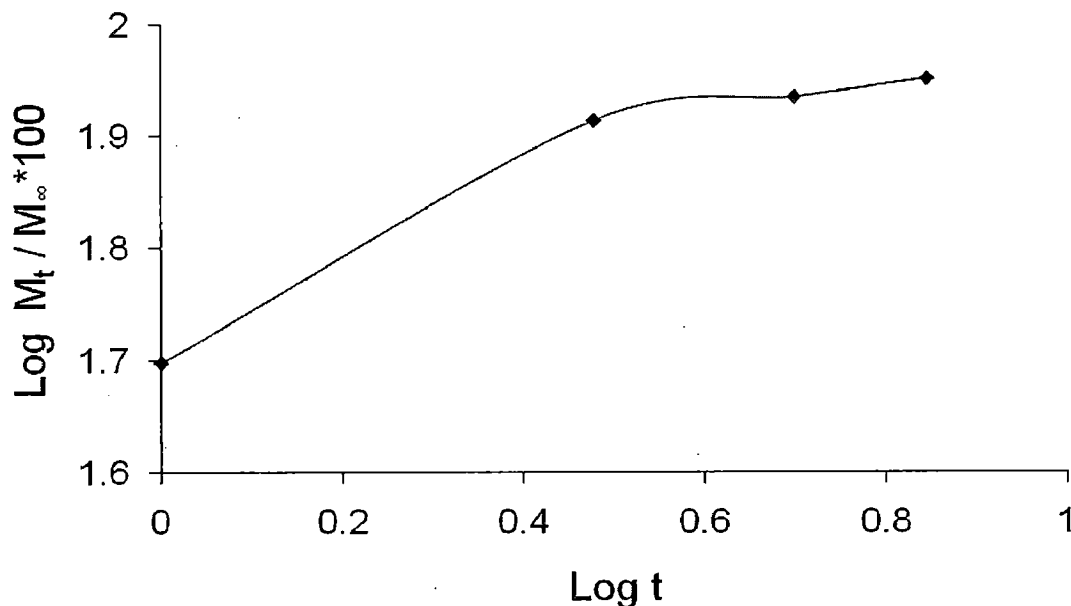


**Fig. 6.18.** The in vitro release of OHP up to 7 h from MPCh-OHP in phosphate buffer solution (at pH 5.5), using Korsmeyer - Peppas equation in log scale.

In the case of MP-OHP nanomaterials, the data obtained from the in vitro release of OHP in phosphate buffer pH 7.4 up to 7 h showed a linear fit with  $R^2 = 0.9967$  (Fig 6.19). The factor  $n$  was found to be 0.5886 which indicated non-Fickian transport [31]. This is an indication of both diffusion as well as swelling controlled drug release. Here, the value of  $k*100$  was found to be 19.39.

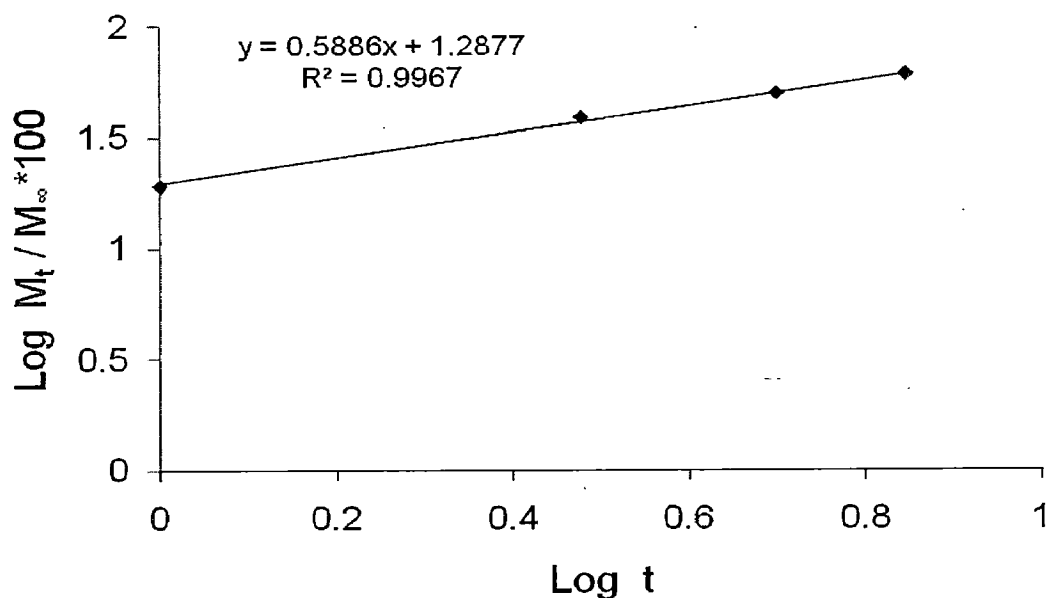


**Fig. 6.19.** Showing linear fit of in vitro release of OHP up to 7 h from MP-OHP in phosphate buffer solution (at pH 7.4), using Korsmeyer - Peppas equation in log scale.

The data obtained from the in vitro release of OHP from MP-OHP nanomaterials in phosphate buffer pH 5.5 up to 7 h showed a linear fit with  $R^2 = 0.995$  (Fig 6.20). Here, the factor  $n$  was found to be 0.5018 which indicated non-Fickian transport where the release of the drug was based on diffusion as well as swelling of the polymer. In this case the value of  $k*100$  was found to be 23.58.

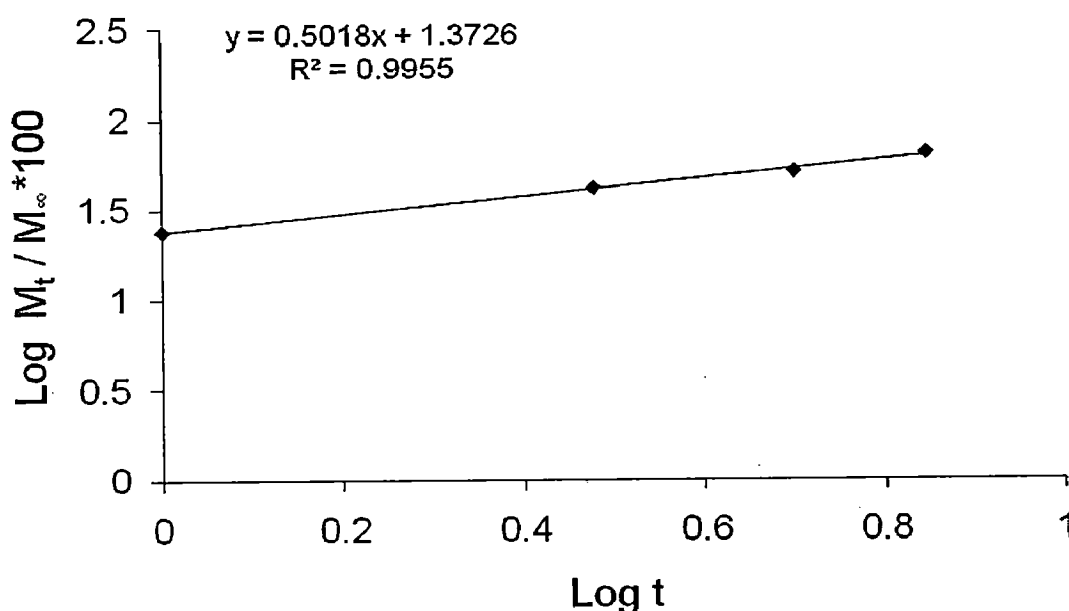


**Fig. 6.20.** Showing linear fit of in vitro release of OHP up to 7 h from MP-OHP in phosphate buffer solution (at pH 5.5), using Korsmeyer - Peppas equation in log scale.

### 6.3.7 In vitro cytotoxic activity profiles of MP-OHP

Based on our in vitro release studies, which showed better sustained release patterns for MP-OHP nanomaterials, their cytotoxicity studies were performed by the SRB assay by recording cell viabilities. On the basis of the reported pharmacological actions of oxaliplatin [17], two cancer cell lines, namely HT-29 (Colon) and MIA-PA-GA-2 (Pancreas) were selected to assess the cytotoxicity profiles of MP-OHP. Equivalent concentration of pure OHP were treated i.e. 1 mg/mL of MP-OHP containing about  $\sim 10 \mu\text{g/mL}$  of the OHP. Pure drug OHP of this concentration was treated. Similarly for other concentrations of MP-OHP, an equivalent concentration of the OHP was used.

The cytotoxicity of MP-OHP in the HT-29 cell lines was not found to be significant for MP-OHP nanomaterials, when different concentrations of MP-OHP nanomaterials (1, 2, 4 and 5 mg/mL) in phosphate buffer solution at pH 7.4 was studied for 48 h (Fig. 6.21a). Here only  $\sim 5\%$  of the growth inhibition was observed for the batch of 5 mg/mL concentration of MP-OHP. On the other hand, the pure drug of the concentrations of 10 – 50

$\mu\text{g/mL}$  showed growth inhibition up to 24 % (Fig. 6.21b). Though above 95% of drug release was expected in phosphate buffer solution at pH 7.4, but the growth inhibition was negligible, which probably indicated that the drug loading contents in the nanomaterials were less. Our results were similar to those reported for the liposomal formulation of 5-fluorocytosine (5-FC), when compared to free drug on MC38/7 cells [32] and similar to the reports of the SPIONs based drug delivery system of doxorubicin [33].

However in the case of the MIA-PA-GA-2 (Pancreas), the cell viability decreased as the concentration of MP-OHP was increased from 1 mg/mL to 5 mg/mL (Fig. 6.22a). The batch of 5 mg/mL exhibited 39.7 % growth inhibition. It was noted that the pure drug of concentration of 50  $\mu\text{g/mL}$  exhibited 40.9% growth inhibition which was almost similar to that of the 5 mg/mL MP-OHP batch (Fig. 6.22b). The  $\text{GI}_{50}$  value for MP-OHP in this pancreatic cancer cell line was more than 5 mg/mL. Further it may be noted here that the magnetite nanoparticles coated with calcium pectinate (MP) of similar concentration (1 – 5 mg/mL) did not exhibit any decrease in the cancer cell growth, indicating that the MP nanocarriers did not result in the decrease in the cell viability for MP-OHP system. In other words, it was confirmed that the antiproliferative effect was due to the release of the OHP from MP-OHP. This was in good agreement with literature reports on other types of drugs loaded in different nanomaterials [34-36]. These results indicated the successful fabrication of magnetic nanomaterial of pectin for potential delivery of OHP.

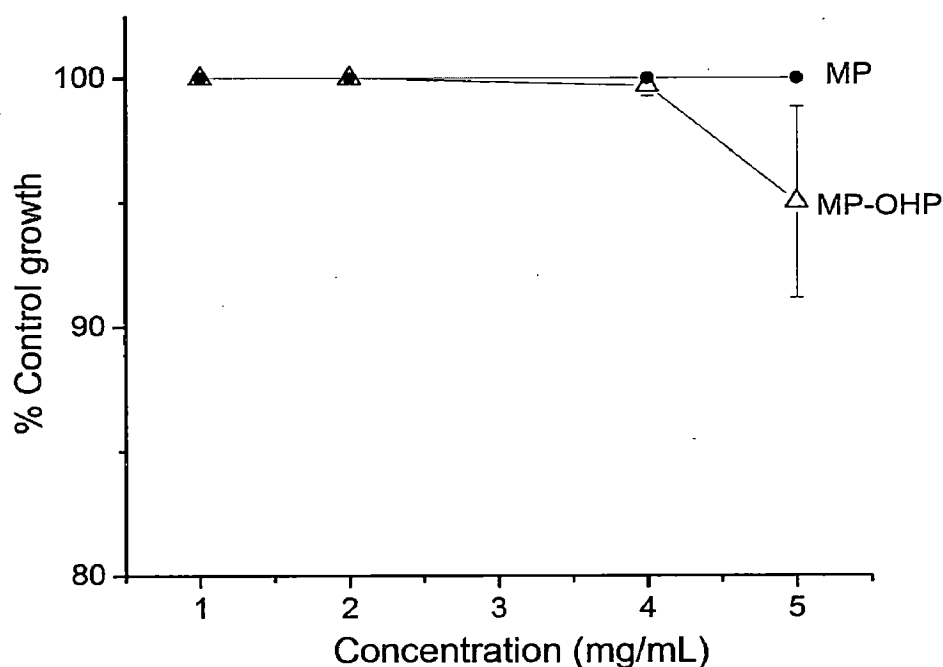


**Fig. 6.21a.** *In vitro* cytotoxic activity profiles of MP-OHP and MP nanomaterials on HT-29 (colon) cancer cell line after 48 h.



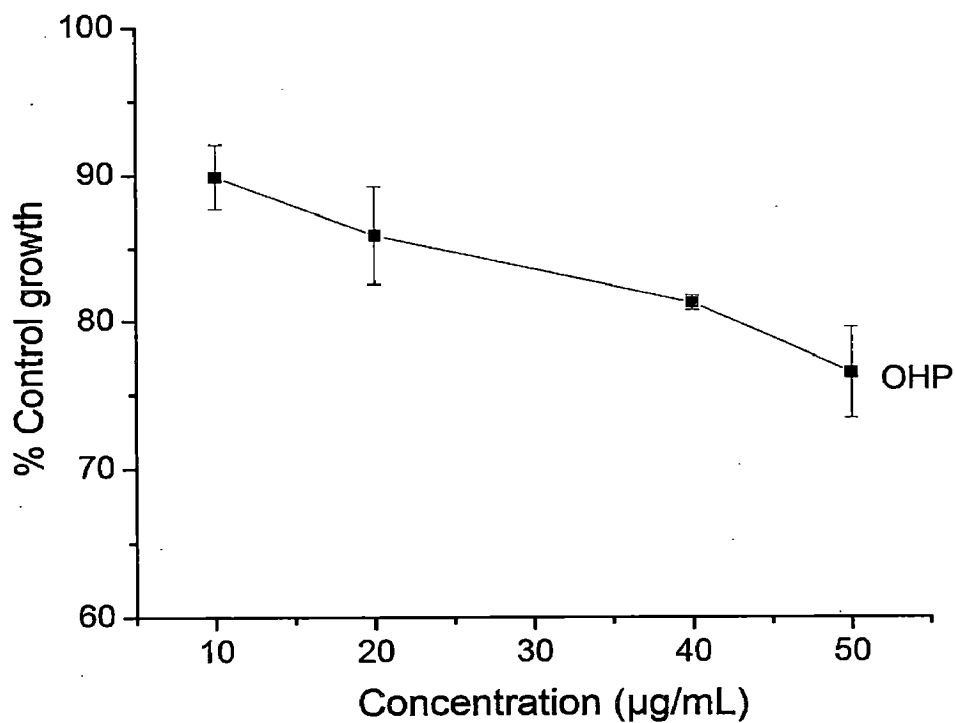


Fig. 6.21b. *In vitro* cytotoxic activity profiles of OHP on HT-29 (colon) cancer cell line after 48 h.

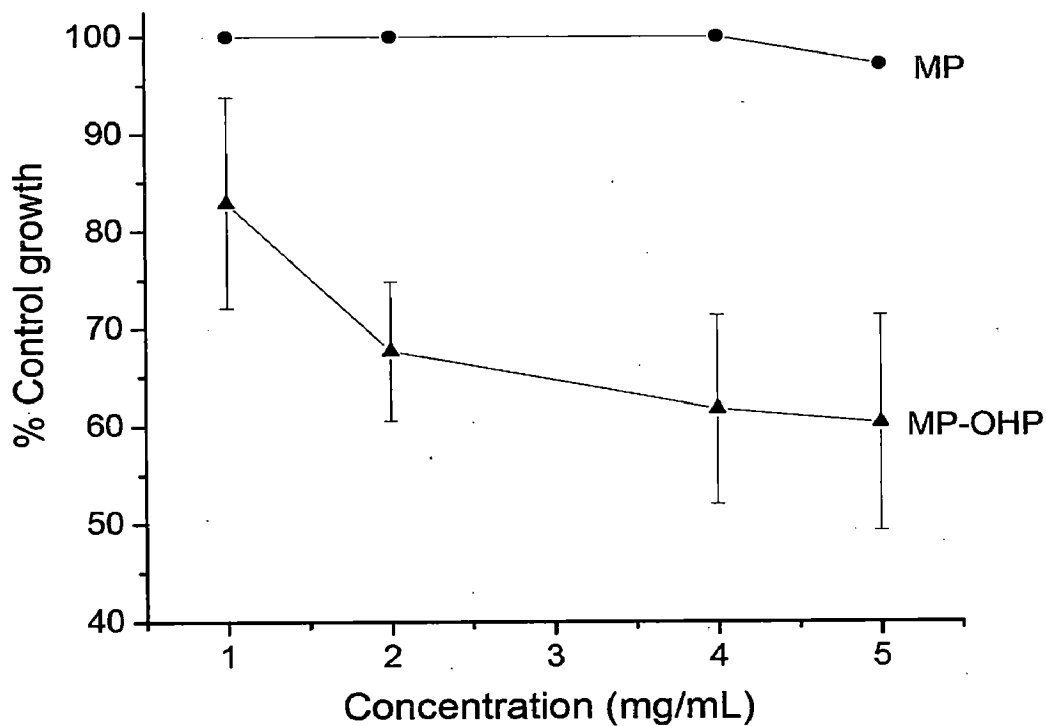
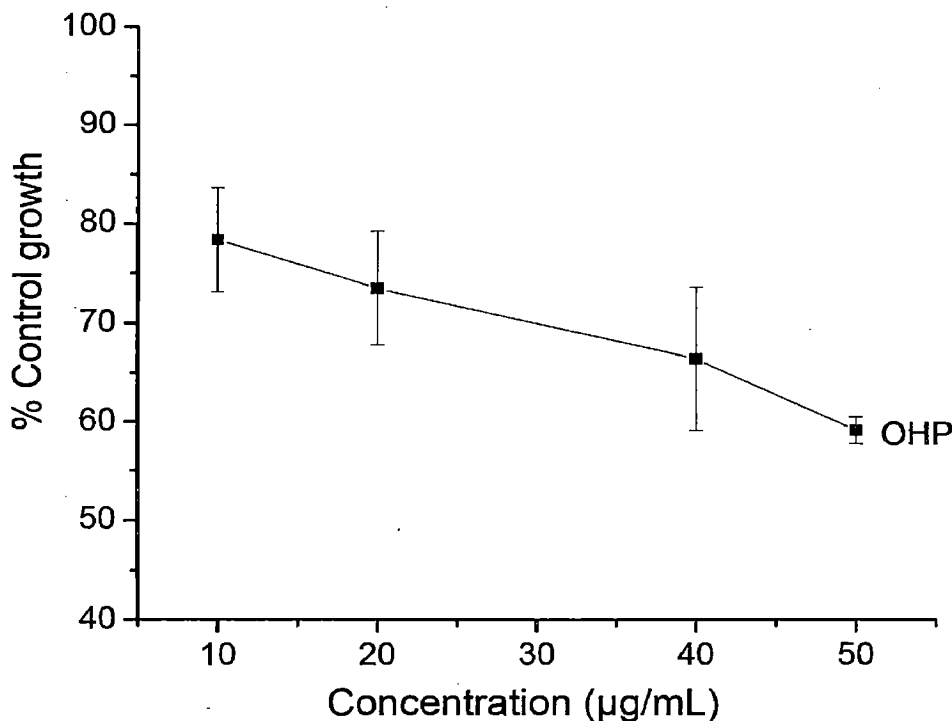


Fig. 6.22a. *In vitro* cytotoxic activity profiles of MP-OHP and MP nanomaterials on MIA-PA-CA-2 cancer cell line after 48 h.



**Fig. 6.22b.** *In vitro* cytotoxic activity profiles of OHP on MIA-PA-CA-2 cancer cell line after 48 h.

#### 6.4 CONCLUSION

Fabrication of a simple, reproducible and novel targeted drug delivery system of 100-150 nm size (measured by SEM and TEM) comprising of MNPs, pectin cross linked with calcium ions and loaded with oxaliplatin (MP-OHP) as well as MNPs, pectin reinforced with chitosan and oxaliplatin (MPCh-OHP) has been achieved. The loading efficiencies in MP and MPCh systems were  $55.20 \pm 1.23$  and  $50.92 \pm 1.52$  respectively. However, the drug loading content was very small (less than 1 %) as the starting drug concentration was less. These nanomaterials (MP-OHP and MPCh-OHP) showed superparamagnetic behavior with saturation magnetization of 45.51 emu/g and 42.46 emu/g respectively. The SQUID and VSM studies of MP-DS system confirmed its superparamagnetic nature. The high  $\zeta$ -potential ( $-30.5 \pm 1.3$  mV) in case of the MP-OHP and  $-22.8 \pm 2.1$  in case of MPCh-OHP indicated the stability of the synthesized drug delivery system.

The *in vitro* drug release from MPCh system at pH 5.5 and 7.4 corresponded to burst release, while the release of OHP from MP-OHP system showed better sustained release both at pH 5.5 and at pH 7.4. This was attributed to solubility of the OHP and its less concentration which also enhances its diffusion (a process dependent of the concentration) from the polymeric structure. The swelling effect of pectin in aqueous medium was also supported by the dynamic light scattering (DLS) measurement which showed average particle size  $\sim 300$  nm. The released data of OHP from MPCh-OHP fitted with Korsmeyer-

Peppas equation satisfied Fickian transport and was diffusion controlled release, while the release of OHP from MP-OHP satisfied non-Fickian diffusion transport and the release was based on diffusion and swelling. Further cytotoxicity studies of MP-OHP were performed in cancer cell lines e.g., MIA-PA-GA-2 and HT-29. Notably, the MP-OHP showed 39.7 % reduction in the growth of MIA-PA-GA-2 (pancreas) cancer cells at a concentration of 5 mg/mL of the nanomaterial. Such reduction of growth matched with the 50 (g/mL of pure OHP. From this result, it was concluded that MP-OHP magnetic nanomaterial system could be potentially effective as anticancer therapy in pancreas.

## REFERENCES

1. Alcindor, T.; Beauger, N. Oxaliplatin: a review in the era of molecularly targeted therapy. *Curr. Oncol.* **2011**, *18*, 18-25.
2. Di Francesco, A.M.; Ruggiero, A.; Ruggieroc, R. Cellular and molecular aspects of drugs of the future: oxaliplatin. *Cell. Mol. Life Sci.* **2002**, *59*, 1914–1927.
3. Grothey A. Oxaliplatin-safety profile: neurotoxicity. *Semin. Oncol.* **2003**, *30*, 5–13.
4. Pietrangeli, A.; Leandri M. ; Terzoli E. ; Jandolo B. ; Garufi C. Persistence of high-dose Oxaliplatin-induced neuropathy at long-term follow-up. *Eur. Neurol.* **2006**, *56*, 13-16.
5. Pendyala, L.; Creaven, P. J. In vitro cytotoxicity, protein binding, red blood cell partitioning and biotransformation of oxaliplatin. *Cancer Res.* **1993**, *53*, 5970–5976.
6. Lagarce, F.; Cruaud, O; Deuschel, C; Bayssas, M; Griffon-Etienne, G; Benoit, J. oxaliplatin loaded PLGA microspheres: design of specific release profiles. *Int. J. Pharm.* **2002**, *242*, 243–246.
7. Abu Lila, A. S.; Kizuki S.; Doi, Y.; Suzuki, T.; Ishida, T.; Kiwada, H. Oxaliplatin encapsulated in PEG-coated cationic liposomes induces significant tumor growth suppression via a dual-targeting approach in a murine solid tumor model. *J. Control. Release.* **2009**, *137*, 8–14.
8. Suzuki R.; Takizawa, T.; Kuwata, Y.; Mutoh, M.; Ishiguro, N.; Utoguchi, N.; Shinohara, A.; Eriguchi, M.; Yanagie, H.; Maruyama, K. Effective anti-tumor activity of oxaliplatin encapsulated in transferrin-PEG-liposome. *Int. J. Pharm.* **2008**, *346*, 143–150.
9. Stathopoulos, G.P.; Boulikas, T.; Kourvetaris, A.; Stathopoulos, J. Liposomal oxaliplatin in the treatment of advanced cancer: a phase I study. *Anticancer. Res.* **2006**, *26*, 1489–1493.
10. Cabral, H.; Nishiyama, N.; Kataoka, K. Optimization of (1,2-diamino-cyclohexane) platinum(II)-loaded polymeric micelles directed to improved tumor targeting and enhanced antitumor activity. *J. Control. Release.* **2007**, *121*, 146–155.
11. Xu, Y.Y.; Du, Y.Z.; Yuan, H.; Liu, L.N.; Niu, Y.P.; Hu, F. Q. Improved cytotoxicity and multidrug resistance reversal of chitosan based polymeric micelles encapsulating oxaliplatin. *J. Drug Target.* **2011**, *19(5)*, 344-353.

12. Anekant, J.; Sanjay, K. J.; Ganesh, N.; Jaya, B.; Beg, A. M. Design and development of ligand-appended polysaccharidic nanoparticles for the delivery of oxaliplatin in colorectal cancer. *Nanomedicine (NBM)*, **2010**, *6*, 179–190.
13. Metselaar, J.M.; Mastrobattista, E.; Storm, G. Liposomes for intravenous drug targeting: design and applications. *Med. Chem.* **2002**, *2*, 319–329.
14. Torchilin, V.P. Recent advances with liposomes as pharmaceutical carriers. *Nat. Rev. Drug Discov.* **2005**, *4*, 145–160.
15. Andresen, T.L.; Jensen, S.S.; Jorgensen, K. Advanced strategies in liposomal cancer therapy: problems and prospects of active and tumor specific drug release. *Prog. Lipid Res.* **2005**, *44* 68–97.
16. British Pharmacopoeia commission office (BP 2009). Published by the stationary office on behalf of the medicines and healthcare products regulatory agency (MHRA); London., **2009**.
17. Oettle, H.; Pelzer, U.; Stieler, J.; Hilbig, A.; Roll, L.; Schwaner, I.; Adler, M.; Detken, S.; Dörken, B.; Riess, H. Oxaliplatin/folinic acid/5- fluorouracil [24h] (OFF) plus best supportive care versus best supportive care alone (BSC) in second-line therapy of gemcitabine- refractory advanced pancreatic cancer (CONKO 003). *J. Clin.Oncol. ASCO Annual Meeting Proceedings.***2005**, *23*. 4031.
18. Faivre, S.; Chan, D.; Salinas, R.; Woynarowska, B.; Woynarowski, J. M. DNA strand breaks and apoptosis induced by oxaliplatin in cancer cells. *Biochem. Pharmacol.* **2003**, *66*,225–37.
19. Tournigand, C.; André, T; Achille, E; Lledo, G; Flesh, M.; Mery-Mignard, D.; Quinaux, E.; Couteau, C.; Buyse, M.; Ganem, G.; Landi, B.; Colin, P.; Louvet, C.; de Gramont, A. FOLFIRI followed by FOLFOX6 or the reverse sequence in advanced colorectal cancer: a randomized GERCOR study. *J. Clin.Oncol.***2004**, *22*, 229–237.
20. Edgar S.; Bernd M.; Stefan Peter,G. US Patent Application 20060063720,Oxaliplatin solution concentrate. Filed on September 22, **2004**. Published on March 23,**2006**
21. Yu, C.Y.; Cao, H.; Zhang, X.C.; Zhou, F.Z.; Cheng, S.X.; Zhang, X.Z.; Zhuo, R.X. Hybrid nanospheres and vesicles based on pectin as drug carriers. *Langmuir* **2009**, *25*, 11720-11726.

22. Fukamachi, T.; Chiba Y.; Wanga Xin.; Saito H.; Tagawa M.; Kobayashi H. Tumor specific low pH environments enhance the cytotoxicity of lovastatin and cantharidin. *Cancer Lett.* **2010**, *297*, 182–189.
23. Liu, L.; Fishman, M.L.; Kost, J.; Hicks, K.B. Pectin-based systems for colon specific drug delivery via oral route. *Biomaterials.* **2003**, *24*, 3333–3343.
24. Cesaro, A.; Delben, F.; Paoletti, S. Thermodynamics of the proton dissociation of natural polyuronic acids. *Int. J. Biol. Macromol.* **1990**, *12* (3), 170–176.
25. Shafi, K.V.P.M.; Ulman, A.; Dyal, A.; Yan, X.; Yang, N.L.; Estournes, C.; Fournes, L.; Wattiaux, A.; White, H. Magnetic enhancement of  $\gamma$ -Fe<sub>2</sub>O<sub>3</sub> nanoparticles by sonochemical coating. *Chem. Mater.* **2002**, *14*, 1778–1787.
26. Morales, M.P.; Verdaguer, S.V.; Montero, M.I.; Sterna, C.J.; Roing, A.; Casas, L.; Martinez, B.; Sandiumenge, F. Surface and internal spin canting in  $\gamma$ -Fe<sub>2</sub>O<sub>3</sub> nanoparticles. *Chem. Mater.* **1999**, *11*, 3058-3064.
27. Daou, T. J.; Pourroy. G.; Bégin, C. S.; Grenèche, J. M.; Ulhaq, B. C.; Legaré, P.; Bernhardt, P.; Leuvrey, C.; Rogez, G.; Hydrothermal Synthesis of Monodisperse Magnetite Nanoparticles. *Chem. Mater.* **2006**, *18*, 4399–4404.
28. Hou, Y. L.; Yu, J. F.; Gao, S. J.; Solvothermal reduction synthesis and characterization of superparamagnetic magnetite nanoparticles. *J. Mater. Chem.* **2003**, *13*, 1983-1987.
29. S, Dhar.; Gu, F. X.; Langer, R.; Farokhzad, O. C. ; Lippard, S. J. Targeted delivery of cisplatin to prostate cancer cells by aptamer functionalized Pt(IV) prodrug-PLGA-PEG nanoparticles. *PNAS*, **2008**, *105*(45), 17356–17361.
30. Risbud, M. V.; Hardikar, A. A.; Bhat, S. V.; & Bhonde, R. R. pH sensitive freeze-dried chitosan-polyvinyl pyrrolidone hydrogels as controlled release system for antibiotic delivery. *J. Controlled Release*, **2000**, *68*, 23–30.
31. Siepmann, J.; Peppas, N. A. Modeling of drug release from delivery systems based on hydroxypropyl methylcellulose (HPMC). *Adv. Drug Delivery Rev.* **2001**, *48*, 139–157.
32. Monika, C.; Stebelska, K.; Sikorski, A.; Madej, J.; Opolski, A.; Ugorski, M. Liposomal formulation of 5-fluorocytosine in suicide gene therapy with cytosine deaminase – for colorectal cancer. *Cancer Lett.* **2008**, *262*, 164–172.

33. Tapan, K. J.; Marco, A. M.; Sanjeeb, K. S.; Diandra, L. L.; Vinod, L. Iron Oxide Nanoparticles for Sustained Delivery of Anticancer Agents. *Mol. Pharm.* **2005**, *2*, 194-205.
34. Mahmoudi, M.; Simchi, A.; Imani, M.; Shokrgozar, M. A.; Milani, A. S.; Hafeli, U. O. Stroeve, P. A new approach for the in vitro identification of the cytotoxicity of superparamagnetic iron oxide nanoparticles. *Colloids Surf. B.* **2010**, *75*, 300–309.
35. Mahmoudi, M.; Simchi, A.; Milani, A. S.; Stroeve, P. Cell toxicity of superparamagnetic iron oxide nanoparticles. *J. Colloid. Interface. Sci.* **2009**, *336*, 510–518.
36. Muller, K.; Skepper J. N.; Posfai, M.; Trivedi, R.; Howarth, S.; Corot, C.; Lancelot, E.; Thompson, P. W.; Brown, A. P.; Gillard, J. H. Effect of ultra small superparamagnetic iron oxide nanoparticles (Ferumoxtran- 10) on human monocyte-macrophages in vitro. *Biomaterials.* **2007**, *28*, 1629–1642.

# ***SUMMARY***



Nanomaterial based drug delivery system has drawn significant scientific attention due to its ease in transportation through biological barriers. Primarily, nanomaterials of different types of biodegradable polymers have been evaluated by different research groups across the globe, but development of polysaccharide based nanomaterials have been of prime interest as most of these materials are proven to be excellent bulk matrix for conventional drug formulation. In this study we have chosen pectin as the polysaccharide for developing its nanomaterial for targeted drug delivery. Notably, pectin nanomaterials were developed prior to the start of this project which exhibited successful loading of insulin (discussed in Chapter 2). But these materials lack targeting ability. So we started developing a novel hybrid nanomaterial where magnetic nanoparticles were encapsulated in pectin and loaded drug in it, for fabricating of magnetic responsive nanomaterials for potential targeted drug delivery.

The magnetic nanoparticles were synthesized as  $\text{Fe}_3\text{O}_4$  (magnetite) by co-precipitation method and were characterized by XRD,  $^{57}\text{Fe}$  Mössbauer spectroscopy. The synthesized MNPs were highly stable as evident from high zeta potential ( $-41.2$  mV). The room temperature Mössbauer spectrum of the as synthesized magnetite showed highly relaxed sextet signature owing to superparamagnetism, which was due to particles of sizes less than 20 nm. The magnetite phase was confirmed from the low temperature Mössbauer studies (at 5 K) in the presence of an external field of 5 Tesla, which exhibited two sextets corresponding to tetrahedral  $\text{Fe}^{3+}$  site and octahedral  $\text{Fe}^{2+/3+}$  site. The oxidation states of iron were corroborated from the isomer shift, while the cubic structure of magnetite phase was reflected from low quadrupole splitting measured for 5 K and 5 T conditions. The intrinsic magnetic field ( $B_{hf}$ ) was found to be 59.0 T corresponding to tetrahedral sites and 50.77 T corresponding to octahedral sites of magnetite at 5 K and 5 T. The shapes and sizes of the as synthesized magnetite nanoparticles (MNPs) were determined from scanning electron microscopy (SEM) and transmission electron microscopy (TEM). The TEM studies showed particles of 2 – 8 nm sizes, which supported the superparamagnetic behavior exhibited (corroborated) by Mössbauer spectroscopy. The magnetic properties of the MNPs were further determined from SQUID measurements. The saturation magnetization of the MNPs was found to be 53.9 emu/g.

These MNPs were encapsulated in pectin. The pectin was cross linked with  $\text{Ca}^{2+}$ ,  $\text{Mg}^{2+}$ ,  $\text{Mn}^{2+}$  and  $\text{Zn}^{2+}$  ions out of which cross linking with  $\text{Ca}^{2+}$  showed excellent results and the method of cross linking with  $\text{Ca}^{2+}$  ions was continued for further studies. The

nanomaterials comprising MNPs encapsulated with calcium pectinate is abbreviated as MP. The magnetite phase in the MP was confirmed from XRD and  $^{57}\text{Fe}$  Mössbauer spectroscopy. The synthesized MPs were spherical in shape with sizes ranging mostly between 100-150 nm in dry condition as evidenced by TEM and SEM. The DLS measurement of representative MP-0.4 nanomaterials showed unimodal size distribution, signifying that the method of synthesizing MPs offered a good control over the size of these nanomaterials. However, the average size of MPs in aqueous solution at pH~ 4 was about 300 - 400 nm which was due to the swelling of the pectin. The stability of MNPs was confirmed from its zeta potential measurement. The coating of the as-synthesized MNPs with pectin and formation of MNP-pectin interface was proposed on the basis of their electrostatic interaction at pH~ 4, as supported from their respective zeta potentials. Eventually, the MP nanomaterials were achieved by cross linking the carboxylic group of the pectin with  $\text{Ca}^{2+}$  ions to form rigid calcium pectinate structure at the periphery of MP. This was confirmed from reduction of zeta potential of pectin attributed to shielding of its higher charge density by  $\text{Ca}^{2+}$ . The formation of MP nanomaterials was further corroborated by FT-IR, TGA, XPS and its dissolution in SGF. According to our proposed mechanism, most of the MNPs were completely encapsulated within the MP nanomaterials. This was verified from the measurement of total Fe content ( $43.3 \pm 2.1$  %) in MP-0.4 by instrumental neutron activation analysis, which corresponded to  $59.6 \pm 2.9$  % of MNPs in MP-0.4. Further, dissolution study of MP-0.4 in SGF revealed negligible loss of Fe (1.9%) from the MP-0.4 which correlated well with the surface Fe composition as measured by XPS. The superparamagnetic nature of the MP-0.4 was confirmed by measuring ZFC-FC profile at an applied field of 200 Oe whose blocking temperature was found to be 93.3 K. Its saturated magnetization was 46.21 emu/g measured at an applied field of 2.5 T, which was lower than that of as-synthesized MNPs (53.9 emu/g at 2.5 T) and it decreased with increasing concentration of the precursor pectin. This property was explained on the basis of magnetic quenching phenomena due to the formation of magnetic dead layer by pectin at the domain boundary wall of the MNPs which restricted its motion to orient the magnetic moments during externally applied magnetic field. Further, the as synthesized system was found to be reasonably stable over a time of 6 months as supported from XRD, Mössbauer studies of the aged samples.

The fabricated nanomaterial of magnetite encapsulated by calcium pectinate was studied for its loading of diclofenac sodium (DS), 5-fluorouracil (5-FU) and oxaliplatin

(OHP). The drug loaded nanomaterials were characterized by array of techniques. They were mainly spherical shaped of about 100 – 150 nm in dried condition as corroborated from SEM and TEM studies. The encapsulated iron oxide phase was magnetite as confirmed from XRD and  $^{57}\text{Fe}$  Mössbauer spectroscopy. The loading of the drugs were indicated from the weight loss studies by thermogravimetry analysis and FT-IR spectroscopy. In the case of diclofenac sodium loaded in magnetic calcium pectinate (MP-DS), The drug loading efficiency was  $60.6 \pm 1.1$  % for the batch synthesized using 0.4 % pectin and the corresponding drug loading content was only  $28.9 \pm 1.2$  (wt %).

The *in vitro* release of the drug from MP-DS nanomaterials was studied in simulated gastrointestinal fluid by sequentially treating the drug loaded nanomaterials in simulated gastric fluid (SGF) containing pepsin for 2 h, followed by treating with simulated intestinal fluid (SIF) containing pancreatin for 3 h and then in simulated colonic fluid (SCF) containing pectinase for remaining of the 48 h, in sink conditions. A time dependent % cumulative drug release was observed which indicated sustained release properties of the drug from MP-DS system. The drug release in the SGF was insignificant which was due to poor solubility of the DS in acidic conditions. In SIF, about 88 % of the drug was released from MP-DS nanomaterials. Such rapid release was attributed to swelling of calcium pectinate. Since the solubility of the drug was high at pH 6.8, so the swelling effect of pectin facilitated the diffusion of the drug from the nanomaterials. The remaining of the drug was released in the SCF. On the other hand, the release of the drug DS from MP-DS in phosphate buffer solution was more sustained, as 88 % of the drug was released in 8 h. The drug release profile was modeled using Korsmeyer - Peppas equation, where the the transport of solute, i.e., drug was non-Fickian type and was found to be swelling controlled. It was interesting to note that when pectin was mixed with chitosan, the loading efficiency of the drug DS increased appreciably (above 99 %), and the drug loading content in the polymeric nanomaterial was 46 – 50 % which of course was dependent on the initial concentration of the drug used. Such a nanomaterial was referred to as magnetite nanoparticle encapsulated in pectin reinforced with chitosan (MPCh). Notably, the chitosan concentration was only 0.025 % as compared to 0.4 % pectin. The fabricated drug loaded nanomaterials were spherical shaped of 100 – 150 nm and exhibited superparamagnetism with saturation magnetization of 36.63 emu/g and 34.40 emu/g respectively for 0.01 and 0.05 M concentration of drug used for loading. The release profile of the drug in simulated gastrointestinal fluid corresponded to sustain release of drug from MPCh nanomaterials. The

release was negligible in SGF while about 70 % of the drug was released in SIF for 3 h and the remaining 30 % of the drug was released in SCF over a period of 60 h. A better sustained release was noted in phosphate buffer solution. The drug release profile was fitted with Korsmeyer - Peppas equation, which satisfied swelling controlled non-Fickian transport condition.

It was evident that the sustained release of DS in simulated gastrointestinal fluid was better for pectin-reinforced with chitosan system, while the sustained release of DS in phosphate buffer was similar for MP-DS and MPCh-DS systems. The magnetic properties were also similar for both types of nanomaterials. However, the drug loading in MPCh nanomaterials was more, due to which MPCh-DS nanomaterials were considered to be more suitable for magnetically targeted drug delivery system.

The loading of 5-FU in magnetite-calcium pectinate nanomaterials was studied for developing potential targeted drug delivery for cancer therapy. The loading of 5-FU in calcium pectinate coated magnetite nanomaterials was low (~ 10.0 % by wt), which was attributed to poor mixing of the drug with pectin by magnetic stirring. Notably, the mixing of pectin with 5-FU by magnetic stirring was carried out for 24 h. In contrast, it was found that probe sonication for 1 h led to two fold higher drug loading efficiency as well as drug loading content. The drug loading efficiency was about 33 % and the drug loading content in the MP-5FU was 18.15 %. The enhanced drug loading efficiency and drug loading content was attributable to better mixing by probe sonication. The MP-5FU exhibited superparamagnetism with reasonably large saturation magnetization (43.15 emu/g) and thus could be referred to as magnetic nanomaterials for drug delivery.

The *in vitro* release of 5-FU from MP-5FU nanomaterials were studied in simulated gastrointestinal fluid and in phosphate buffer solution. The time dependent % cumulative release of drug was observed where the release in SGF was 11.78 % of the loaded drug. Higher release of 5-FU in SGF than that of DS was due to higher solubility of 5-FU in acidic condition. About 50 % of the loaded drug was released in SIF for 3h followed by the remaining 35 % release in SCF. Higher release in SIF and SCF was attributed to pH effect. In addition to that the enzyme pectinase in SCF could also contribute to the release of the drug by polymeric degradation. The *in-vitro* release of 5-FU in phosphate buffer also showed a time dependent sustained release. The released drug in phosphate buffer solution at pH 7.4 was modeled using Korsmeyer - Peppas equation, which satisfied swelling controlled non-Fickian transport condition.

The cytotoxicity studies of the novel fabricated MP-5FU nanomaterial was studied by measuring cell viability of concentration dependent MP-5FU nanomaterials in different cancer cell lines namely, HT-29, HEPG2 and MIA-PA-CA-2 cancer cell lines. The  $GI_{50}$  of MP-5FU was more than 5 mg/mL in HT-29 and HEPG2, while it was 3.7 mg/mL in MIA-PA-CA-2 cancer cell line. Compared to the equivalent concentration of pure drug (800  $\mu$ g/mL), the corresponding cytotoxicity of 5 mg/mL of MP-5FU was less, indicating sustained release phenomenon of the drug from the nanomaterial. Thus it was concluded that the nanomaterials of MP-5FU was fabricated successfully which exhibited sustained release and was effective in antiproliferative action in cancer cells.

The loading of oxaliplatin, a third generation platinum based anticancer drug, in magnetite nanoparticles coated with calcium pectinate and magnetite nanoparticles coated with pectinate reinforced with chitosan were studied. The drug loading efficiencies in MP and MPCh systems were  $55.20 \pm 1.23$  % and  $50.92 \pm 1.52$  % respectively. However, the drug loading content was very small ( $\sim 1$  %) as the starting drug concentration was less. The morphology and magnetic properties of these drug loaded nanomaterials were quite similar to those discussed for MP-5FU and other systems. But the *in vitro* drug release was different from the earlier cases. Burst release was observed for from MPCh system at pH 5.5, while the release of OHP from MP-OHP system showed better sustained release both at pH 5.5 and at pH 7.4. Contrastingly, the OHP released from MPCh-OHP fitted with Korsmeyer-Peppas equation satisfied Fickian transport and was diffusion controlled release which that for MP-OHP the release of OHP was non-Fickian and was diffusion and swelling controlled. The cytotoxicity studies of MP-OHP were performed in cancer cell lines e.g., MIA-PA-GA-2 and HT-29. Notably, the MP-OHP showed 39.7 % reduction in the growth of MIA-PA-GA-2 (pancreas) cancer cells at a concentration of 5 mg/mL of the nanomaterial. Such reduction of growth matched with the 50  $\mu$ g/mL of pure OHP. From this result, it was concluded that MP-OHP magnetic nanomaterial system could be potentially effective for anticancer therapy in pancreas.

From this extensive study, we have shown the possibility of fabricating magnetic polymeric nanomaterials suitable for drug loading, especially for cancer therapy. The incorporation of magnetic materials in the nanomaterials has provided an additional as well as important functionality for targeted drug delivery. It may be assumed that the drug delivered by intravenous mode may be guided to the tumour site and due to its reduced size it would be expected to exhibit enhanced penetration rate (EPR effect) for improved therapy.

## **FUTURE SCOPE OF THE WORK**

There is a scope for improving drug loading efficiency of 5-FU. The polymer could be modified to achieve better loading. In addition, attention needs to be paid for better loading of OHP in such polysaccharide based nanomaterials. The release was very rapid which could to be controlled for better efficacy against cancer therapy. Furthermore, these drug loaded nanomaterials could be tested in animal model for a better understanding of release of the loaded drug and their effects in the *in vivo* conditions.

## **LIST OF PAPERS PUBLISHED/ ACCEPTEED/ SUBMITTED FOR PUBLICATION**

1. Novel hybrid nanostructured materials of magnetite nanoparticles and pectin by S. Sahu, R. K. Dutta, Journal of magnetism and magnetic materials. **2011**, 323(7), 980-987.
2. Synthesis, characterization and in vitro release of diclofenac sodium from hybrid nanostructured magnetite-calcium pectinate by R.K. Dutta, Saurabh Sahu, V.R. Reddy, Submitted.
3. Hybrid magnetic nanomaterials of pectin reinforced with chitosan as drug carriers by Saurabh Sahu, R.K. Dutta, Submitted.
4. Fabrication, characterisation and in vitro evaluation of 5-FU loaded in magnetite calcium pectinate nanomaterial by Saurabh Sahu, R.K. Dutta, Submitted.
5. Novel magnetic nanomaterial for potential targeted drug delivery of oxaliplatin, under preparation.

## LIST OF PAPERS PRESENTED AT NATIONAL/ INTERNATIONAL CONFERENCES

1. Synthesis and characterisation of pectin and chitosan coated iron oxide nanoparticles for developing magnetically targeted drug delivery, International Conference on Nanomaterials and Devices Processing and Applications (NADPA) 2007, Organised by IIT Roorkee, Roorkee, India.
2. Spectrophotometric assay of loading and release of diclofenac sodium and catechin from calcium pectinate-magnetite hybrid nanostructured material, by Saurabh Sahu, Debashish Bhowmik, R. K. Dutta, Forth National Conference on Recent Trends in Instrumental Methods of Analysis, 18-20 February 2011, organized by Department of Chemistry, IIT Roorkee, Roorkee, India.
3. Magnetic studies of as-synthesized pectin coated magnetite nanoparticles by  $^{57}\text{Fe}$  Mössbauer spectroscopy, by Saurabh Sahu, V. R. Reddy, R. K. Dutta, Nuclear and radiochemistry symposium (NUCAR, 2011), held at GITAM Institute of science, Vishakhapatnam, India, February 22-26, organised by Board of Research in Nuclear Science (BRNS), Department of Atomic Energy, p.p. 595-596.



## APPENDIX I

The drug loaded NPs were placed in a dialysis bag, along with the 5 mL of buffer containing simulated gastric fluid at pH 1.2 mixed with pepsin enzyme. The dialysis bag was then immersed in a buffer solution maintained at similar condition but without the enzyme. After 2 h release studies in SGF, the medium was withdrawn from the dialysis bag and replaced by simulated intestinal fluid at pH 6.8 and pancreatin enzyme. The dialysis bag containing the above mixture was then immersed in a medium at pH 6.8 and the release study was monitored for 3 h. Similarly the release study was conducted in simulated colonic fluid at pH 5.5 for 48 h.

Sgahul  
13-07-2012

Reda  
13/7/12

## APPENDIX II

The differential thermal analysis (DTA) of the pure drug (DS) did not match with those of the drug in MP-DS. The DTA of pure drug (DS) reflected a major exothermic event at 650 °C, which was associated with heat release of 2.53 J/mg (Chapter 3 p 98, Fig. 3.11b) and corresponded to a weight loss due to thermal degradation of the material (Chapter 3 p-97, Fig. 3.11a). However in the case of MP-DS batch, the exothermic event was recorded at 395 °C, and the measured heat release was 1.69 J/mg (Chapter 3 p 98, Fig. 3.11b). Such a shift of thermal event towards the lower temperature could be due to the increase in thermal conductivity of materials attributed to phonon properties in nanomaterials of sizes less than 100 nm (Ju 2005; Nika et al. 2009). In addition, the presence of MNPs with large heat capacity (Cornell and Schwertmann 2003) could stimulate thermal wave propagation to the encapsulated drug in MP-DS nanostructure, resulting in degradation of drug at lower temperature. This phenomenon would be more relevant if the drug DS interacts with the MNPs. Such interaction was favourable in MP-DS as the measured zeta potentials of DS and MNPs at working pH ~4 were  $-110.0 \pm 3.0$  mV and  $+17.4 \pm 1.4$  mV (Chapter 3, p 98, Table 3.2) respectively and favored electrostatic interaction. Furthermore, the lack of thermal signatures of the drug corresponding to its bulk property in the thermal analysis of MP-DS also confirmed that there was no drug content on the periphery of the nanostructured MP-DS and all the drug content in it was mostly encapsulated in the MP-DS nanostructure.

### References:

1. Ju YS (2005) Phonon Heat Transport in Silicon Nanostructures. App Phys Lett 87: 153106-1-3
2. Cornell RM, Schwertmann U (2003) The Iron Oxides: Structure, Properties, Reactions, Occurrences and Uses, 2<sup>nd</sup> edn, Wiley-VCH Verlag GmbH & Co. KGaA, Weinheim, p-189.

Ssahu  
13-07-2012

Rosult  
13/7/12